Synthesis and Aggregation Behavior of Nature-Inspired Amphiphiles

Maria Bastian

university of groningen / faculty of mathematics and natural sciences / stratingh institute for chemistry

The work reported in this thesis was performed at the Stratingh Institute for Chemistry of the University of Groningen, The Netherlands and financially supported by the Netherlands Organization for Scientific Research (NWO).

Printed by: Ipskamp Drukkers, Enschede, The Netherlands

ISBN: 978-90-367-7689-9 (Printed Version)
ISBN: 978-90-367-7688-2 (Electronic Version)

university of groningen

Synthesis and Aggregation Behavior of Nature-Inspired Amphiphiles

PhD thesis

to obtain the degree of PhD at the
University of Groningen
on the authority of the
Rector Magnificus Prof. E. Sterken
and in accordance with
the decision by the College of Deans.

This thesis will be defended in public on

Monday 30 March 2015 at 16.15 hours

by

Maria Bastian

born on 18 April 1984
in Duschanbe, Rusland

Supervisor

Prof. B.L. Feringa

Prof. A.J. Minnaard

Assessment committee

Prof. B. Poolman

Prof. S. Otto

Prof. E.J.R. Sudhölter

For my family

Table of Contents

Chapter 1

Introduction

During evolution, nature has developed an intriguing variety of complex organisms containing a broad variety of molecular structures. One major class of components allowing the existence of life are lipids. Several interesting molecular entities in lipids play thereby a crucial role allowing the survival of organisms under harsh conditions like extreme temperatures and pressure. Also, the viability in toxic environment is enabled through increased density and decreased permeability of the membrane provided by the constituting lipids. Nowadays, synthetic lipids are applied for the understanding and mimicking of the naturally developed systems allowing the creation of artificial membranes with impressive properties. Moreover, those amphiphilic structures are applied for medical purposes as well.

1.1 Composition and Physiological Properties of Bio-Membranes

1.1.1 Lipid: Properties and Classification

The formation of compartments, namely cells and organelles, through bio-membranes is required to enable the existence of living organisms. This compartmentalization allows the formation of concentration gradients, protection of the interior and can result in enrichment and active transport.[1] As shown in Figure 1.1.1a, the major components forming the membrane are proteins and lipids. Thereby, the latter compounds enable the stability and high flexibility at the same time. To fulfill these requirements, noncovalent interactions between membrane constituents are present. The chemical architecture of lipids comprises a hydrophilic head group and a hydrophobic tail resulting in the amphiphilic character (Figure 1.1.1b).[2] Whereas the head group is pointing towards the aqueous medium, the hydrophobic tail undergoes clustering by hydrophobic interactions.[2] As a result of those interactions lipid bilayers can be formed (Figure 1.1.1a).

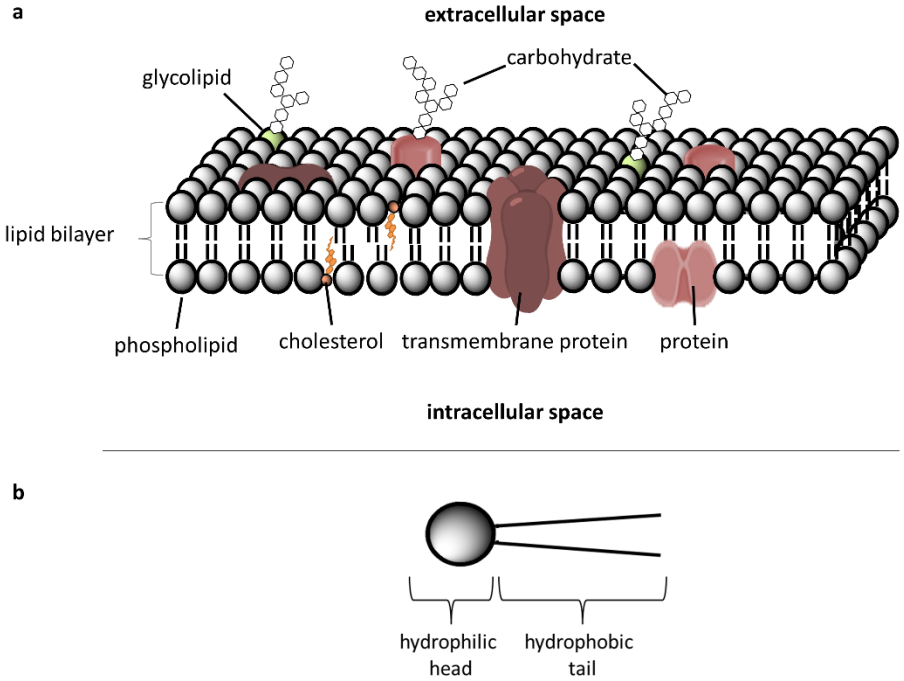

Figure 1.1.1: (a) Schematic representation of the bio-membrane. (b) Schematic representation of a lipid.

Lipids can be divided in three major classes.[3,4] The first kind of lipids is represented by phospholipids which contain a phosphate ester unit. As shown in Figure 1.1.2, this lipid class has two members exhibiting different lipid backbones: glycerophospholipids carrying glycerol and sphingophospholipids carrying a sphingosine moiety.[3,5] These molecular entities serve as connection between the aliphatic tail and the polar phosphate ester group. Furthermore, additional polar residues at the phosphate unit are increasing the hydrophilic property of the head group. Common substituents are serine, ethanolamine and choline which are charged

under physiological pH (pH = 7.4) (Figure 1.1.2).[3,5] The hydrophobic tail consists mainly of long hydrocarbon chains which can carry a variety of highly interesting moieties (see Chapter 1.1.2). Furthermore, dependent on the organism two different chemical connections have been observed tying the aliphatic chain on the lipid backbone, namely ester or ether groups.[6] The more common esters are mainly found in eukaryotes and bacteria. In contrast, ether bonds are typically present in archaeal membranes.

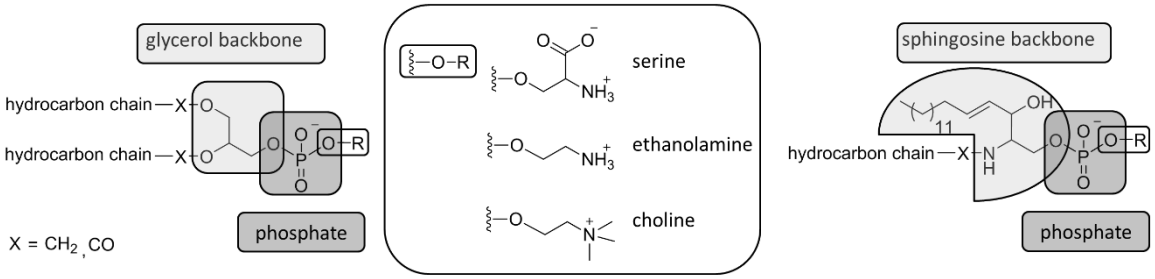

Figure 1.1.2: Chemical structure of phospholipids.

The second class of lipids is represented by glycolipids. These sugar-containing lipids possess mono- or oligo-saccharides as hydrophilic head group which are directly connected to the lipid backbone.[3,4] As shown in Figure 1.1.3, one distinguishes between glyceroglycolipids and sphingoglycolipids. These amphiphiles are generally located at the outer surface of the cell membrane reaching into the extracellular fluid with the carbohydrate unit (Figure 1.1.1a).

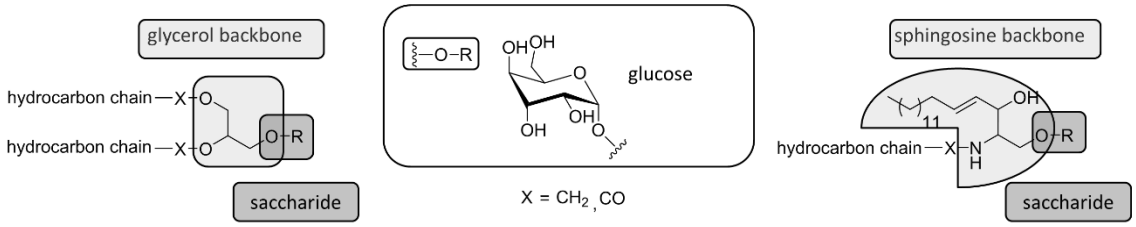

Figure 1.1.3: Chemical structure of glycolipids carrying glucose as representative head group moiety.

The third lipid class is represented by sterol derivatives which incorporate several cycloalkane moieties.[3,4] These lipids are present to a large extend in eukaryotic membranes (20 to 40%), whereas they are absent in prokaryotes.[7] The structure of the most common amphiphilic sterols are shown in Figure 1.1.4. It should be noted that cholesterol **1** is present in animals, ergosterol **2** is found in fungi and β-sitosterol **3** in plants.[7]

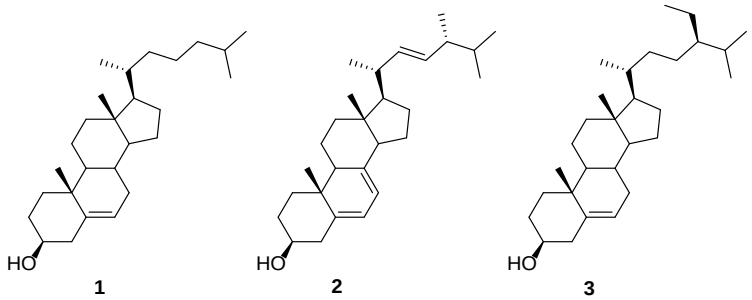

Figure 1.1.4: Chemical structure of cholesterol **1**, ergosterol **2** and β-sitosterol **3**.

1.1.2 Intriguing Aliphatic Acids and Alcohols in Nature

In nature the hydrophobic moiety of lipids is mostly represented by aliphatic alcohols or acids. The most common fatty acids contain an aliphatic chain consisting of an even number of 14 to 24 carbon atoms (Figure 1.1.5).[3] Thereby, unsaturation occurs resulting in up to four double bonds per chain. These mostly *cis*-configured bonds result in a bended tail as shown for stearic acid in Figure 1.1.5.

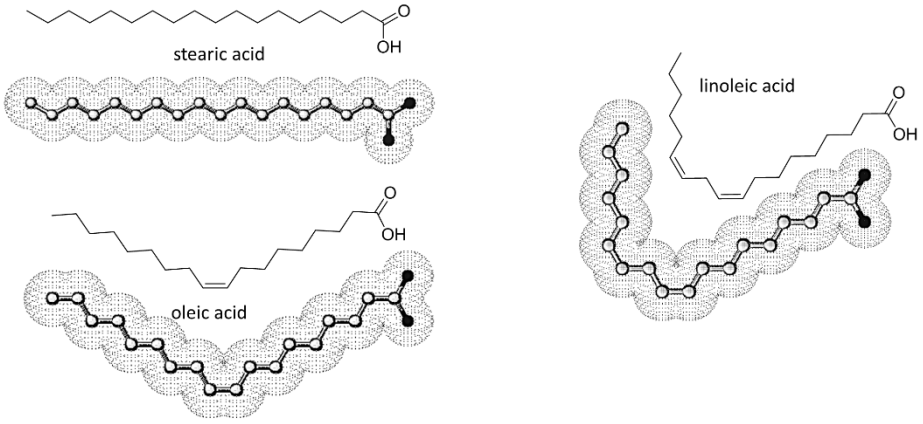

Figure 1.1.5: Molecular structures and space filling molecular models of three C_{18}-fatty acids, namely stearic acid (18:0), oleic acid (18:1) and linoleic acid (18:2). (Number of carbon atoms: number of double bonds).

The most common aliphatic alcohols present in the archaeal lipids contain 20, 25 or 40 carbon atoms. In contrast to fatty acids, no double bonds are present in those aliphatic compounds. Instead methyl branched chains in repetitive units are common (Figure 1.1.6).[6]

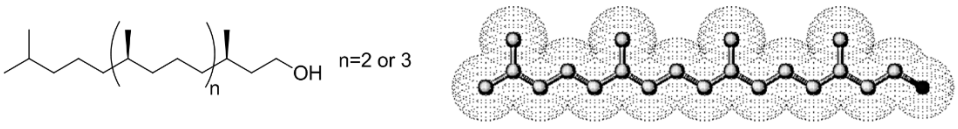

Figure 1.1.6: Molecular structure and space filling molecular model of common archaeal aliphatic alcohols.

It was suggested that the molecular structure of the hydrophobic tail can influence significantly the stability and permeability of bio-membrane. Archaea which incorporate a high degree of methyl branched lipids and the more stable ether linkage can survive at extreme temperatures without showing significant increase in membrane permeability.[8] In contrast, the membrane permeability of eukaryotes and bacteria is often strongly influenced by temperature changes.[8] However, to enable bacteria to survive harsh conditions, e.g. high temperatures, low pH and high salt concentration, different modifications of the fatty acids occurred during evolution.
In this regard, in 1929 *Anderson et al.* isolated the methyl branched fatty acids tuberculostearic acid **4** (10-methylstearic acid, Figure 1.1.7a) from *Mycobacterium tuberculosis*.[9] The structure of this acid was established in 1934 by *Spielman* followed by determination of the absolute configuration in 1948 by *Prout et al.*[10,11] First approaches studying the biosynthetic pathway revealed that the methylation of the double bond of oleic

acid resulted in fatty acid **4**.[12,13,14] Further studies showed that an enzymatic reaction mechanism which is involved in a variety of double bond modifications catalyzes methylation, cyclopropanation and double bond migration.[15,16] During the following decades a large variety of fatty acids carrying not only non-polar methyl branched moieties but also polar methoxy- and ketone units were isolated from Mycobacteria.[15,17] Fatty acids with those polar functionalities are known as mycolic acids **5** and some representative compounds are shown in Figure 1.1.7b and c.

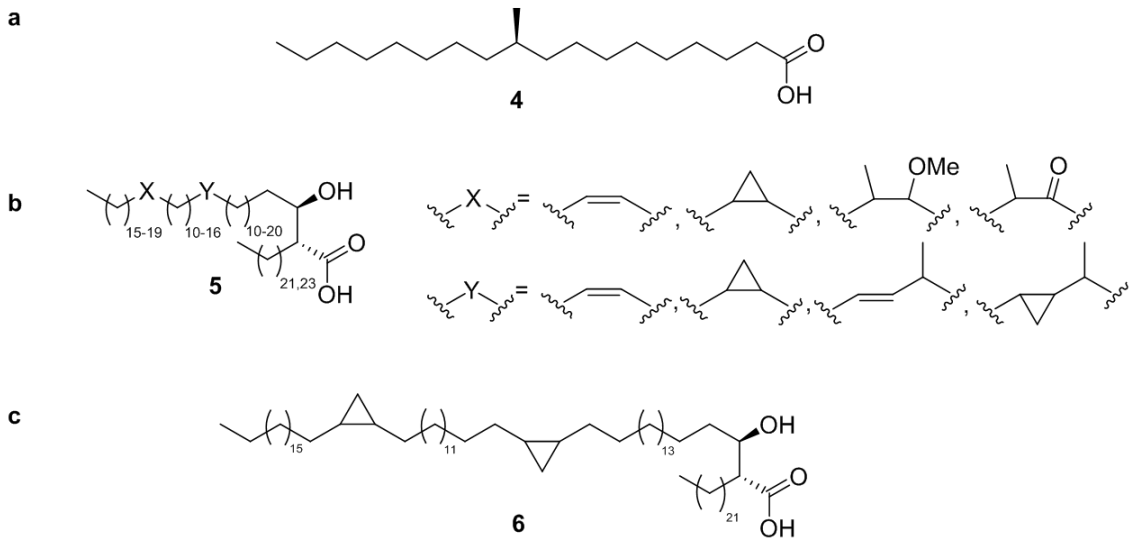

Figure 1.1.7: (a) Molecular structure of tuberculostearic acid **4**. (b) General molecular structure of mycolic acids **5**. (c) Molecular structure of an α-mycolic acid **6**.

After the discovery of cyclopropane moieties in mycolic acids **5** more naturally occurring *cis*- and *trans*-cyclopropane-containing fatty acids (CFAs) have been found. One representative of the more common *cis*-isomer is lactobacillic acid **7**, which was discovered in 1950 by *Hofmann et al.* (Figure 1.1.8).[18] Also the *trans*-cyclopropane ring was found in several fatty acids like lyngbyoic acid **8**, grenadadiene **9** and majusculoic acid **10**, which were isolated from cyanobacteria. The latter one was isolated by *MacMillan et al.* revealing the presence of a cyclopropane moiety and a brominated olefinic moiety (Figure 1.1.8).[19,20,21]

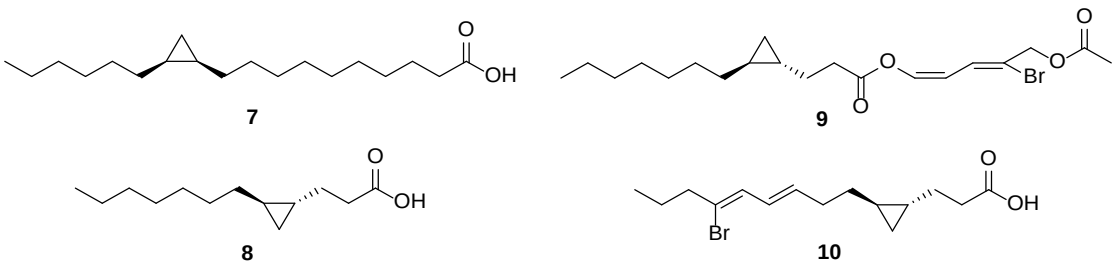

Figure 1.1.8: Molecular structures of lactobacillic acid **7**, lyngbyoic acid **8**, grenadadiene **9** and majusculoic acid **10**.

Other molecular architectures like modifications carrying cycloalkane moieties have been found in several membrane components. Unique examples are the ladderane lipids

(Figure 1.1.9). In 2002 *Sinninghe Damsté et al.* discovered these lipids which are carrying three to five linear fused cyclobutane rings at the hydrophobic tail of the fatty acid.[22] As shown in Figure 1.1.9, ladderane lipids incorporating a cyclohexane ring were described as well.[22] At this point it is noticeable that not only the for bacteria common ester bonds are present in ladderane lipids. Instead many aliphatic alcohols are incorporated resulting into ether linkages.[23]

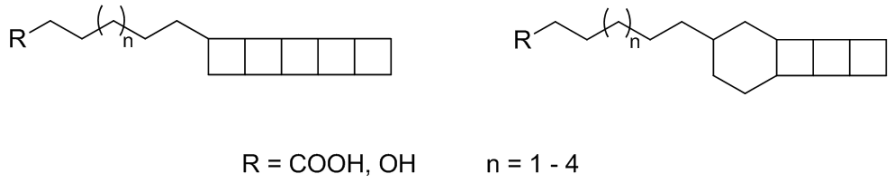

Figure 1.1.9: Molecular structures of fatty acids and alcohols containing ladderane units.

Furthermore, it needs to be mentioned that cycloalkane moieties are also found in aliphatic alcohols that are present in archaeal membranes.[6] As shown in Figure 1.1.10, several cyclopentane and occasionally also cyclohexane moieties can be present.[24]

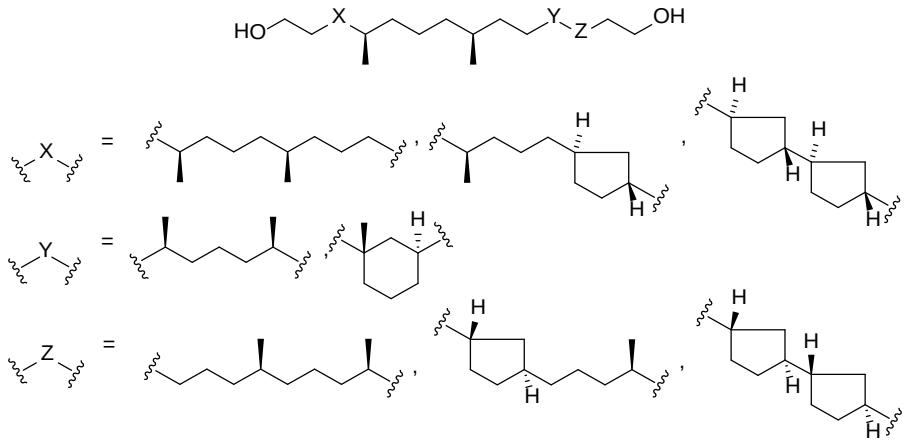

Figure 1.1.10: Molecular structures of aliphatic alcohols occurring in archaeal membranes.

1.1.3 Lipids: The Key for Survival

The above discussed broad range of lipids has been found in several organisms like bacteria, eukaryotes and archaea. These organisms have in common that they are able to survive under extreme conditions. Thereby, even direct adaptation to environmental changes has been observed.

The multiplicity of modifications has a direct influence on the physiological properties of the membrane and the phase transition states, permeability, molecular packing, fluidity and density of the membrane can be varied. This response to the environment can result in higher chemical tolerance and stability of the organism.

For example, some bacteria developed the ability of double bond isomerization.[25] Studies demonstrated that the amount of *trans*-unsaturated lipids increases under influence of organic

solvents or higher temperatures resulting in lower fluidity of the membrane.[26,27] Other modifications are important to influence the packing behavior resulting in an change of lipid density and the dependent permeability.[22] Also, it was shown that modifications can lead to an increase of the chemical stability of the membrane without influencing the physiological properties considerable.[28,29]

A representative example are mycolic acids **5** (Figure 1.1.7, page 6) which are able to influence the membrane properties. For instance, the presence of fatty acids **5** in the cell wall of mycobacteria reduces the permeability for small hydrophilic compounds up to 10.000-fold in comparison to *Escherichia coli*.[30] Hence, cell walls containing mycolic acids **5** represent a great barrier against antibiotics like β-lactams and aminoglycosides. Furthermore, it reduces the vulnerability by chemicals.[31]

Additionally, it has to be emphasized that the composition of the cell wall, in particular the degree of *cis*/*trans* isomerization, is directly influenced by the increasing temperature resulting in a direct adjustment of the affiliated fluidity.[32] The same correlation was shown for other bacteria like *Pseudomonas*.[25] The thermal adaptation is required to maintain the viscosity at low temperature and simultaneously increasing the stability at higher temperatures by controlling the *cis*/*trans* ratio of double bonds and cyclopropyl moieties.[33]

Furthermore, it has been shown that not only the temperature can influence the membrane composition. In 1965, *Knivett et al.* demonstrated already that changes in pH, temperature, carbon source, salt concentration and air composition can influence the amount of cyclopropane fatty acids (CFA) in the membrane.[34] Also, it was reported that cell cultures growing at low pH, high temperatures and in presence of an oxygen rich environment incorporate a larger amount of CFAs.[34] Several studies trying to understand the role of cyclopropane units in lipids report contradictory results.[14] However, it was clearly shown that the cyclopropyl unit exhibits lower reactivity compared to olefinic moieties resulting in higher stability of the membrane.[28] In this regard, it was shown that cyclopropanes are chemically inert against oxidation reagents like hydrogen peroxide and ozonolysis.[29,35] Hence, through the presence of cyclopropyl moieties an increased chemical tolerance is observed without changing the physiological properties of the membrane. Furthermore, it was reported that the presence of organic solvents like toluene results in a change of the degree of cyclopropanation.[36]

A further unique modification of membranes is the incorporation of ladderane fatty acids exhibiting several linear fused cycloalkane moieties. It is suggested that the presence of these molecular entities results in an increase of the density of the bio-membrane.[22] The increased density prevents diffusion of small molecules through the membrane and therefore, enables the surviving of the organism in a toxic environment.

Despite that the reason for the presence of the large variety of molecular moieties is not fully understood, studies clearly reveal a relation between the degree of the change of membrane composition and changes of the environment.

1.2 Lipid Aggregation in Aqueous Media

The ability of amphiphilic compounds, such as like lipids, to aggregate in aqueous media driven by non-covalent interactions has been studied intensively during the last forty years. First attempts to understand the parameters that effect aggregation and to find general rules predicting the resulting aggregate have been published by *Israelachvili et al.* and *Tanford*.[2,37,38] *Tanford* considered mainly hydrophobic effects, repulsive interactions and thermodynamic factors which all together result in micelle formation and a lower chemical potential for the amphiphile incorporated in the assembly, in comparison to the free amphiphile in solution.[2,38] In this regard, the formation of spherical micelles is energetically preferred in comparison to aggregates like vesicles and sheets. At around the same time *Israelachvili et al.* demonstrated the relationship between the molecular structure, size and shape of the amphiphile as well as non-covalent interactions.[37] To explain the existence of thermodynamic disfavored aggregates he introduced a simple concept defining a packing parameter based on geometric and mathematic relations. As shown in Figure 1.2.1, the packing parameter (P) is dependent of the length (l_c), volume (v) of the hydrophobic tail and the surface area (a_0). Thereby, P is defined as $v/a_0 l_c$.[37] It has to be emphasized that the surface area a_0 is strongly depended on charge repulsion effects, resulting in an effective area larger than the physical size of the head group.

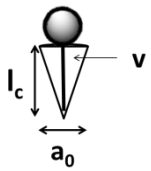

Figure 1.2.1: Schematic representation of an amphiphile and its parameters: length l_c, surface area a_0 and volume v.

In order to assign values for the packing parameter *Israelachvili et al.* treated different aggregates as simple geometrical structures like sphere, cylinder and cuboid for micelles, wormlike micelles and bilayer, respectively.[37] However, further assumptions were necessary to apply basic mathematic relations. Therefore, the total volume V of an aggregate was introduced and was defined by the volume v of one amphiphile multiplied with the number of amphiphilic molecules N present in an assembly (equation 1). The same relation was assumed for the total surface area A (equation 1). Furthermore, the radius r of an aggregate has to be smaller or equal to the total length of the unfolded hydrocarbon chain l_c of one amphiphile (equation 2).[37] Combining equation 1 and 2 with the above mentioned definition of the packing parameter P result in equation 3 allowing the determination of P (Figure 1.2.3).

equation 1: $V/v = A/a_0 = N$

equation 2: $r \leq l_c$

equation 3: $P=v/a_0 l_c \leq V/Ar$

Additionally, as shown in Figure 1.2.2 the total surface area *A* can be further simplified, since it is highly dominated by the larger surfaces of the assembly. As examples the simplified surface *A* of sheets and wormlike micelles are shown in Figure 1.2.2.

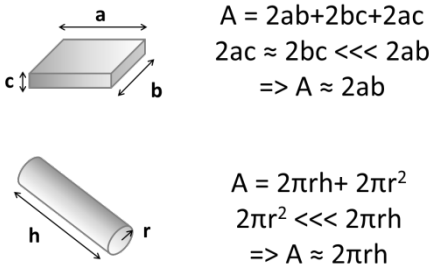

Figure 1.2.2: Simplified equation to determine the surface area *A* of a thin cuboid and a long cylinder.

Having in mind equation 1, the packing parameter of aggregates can be calculated for each individual amphiphilic molecule. Hence, now a relation between amphiphile shape, packing parameter and assembly can be drawn. As shown in Figure 1.2.3, different aggregates can be expected dependent of the shape of the molecule.

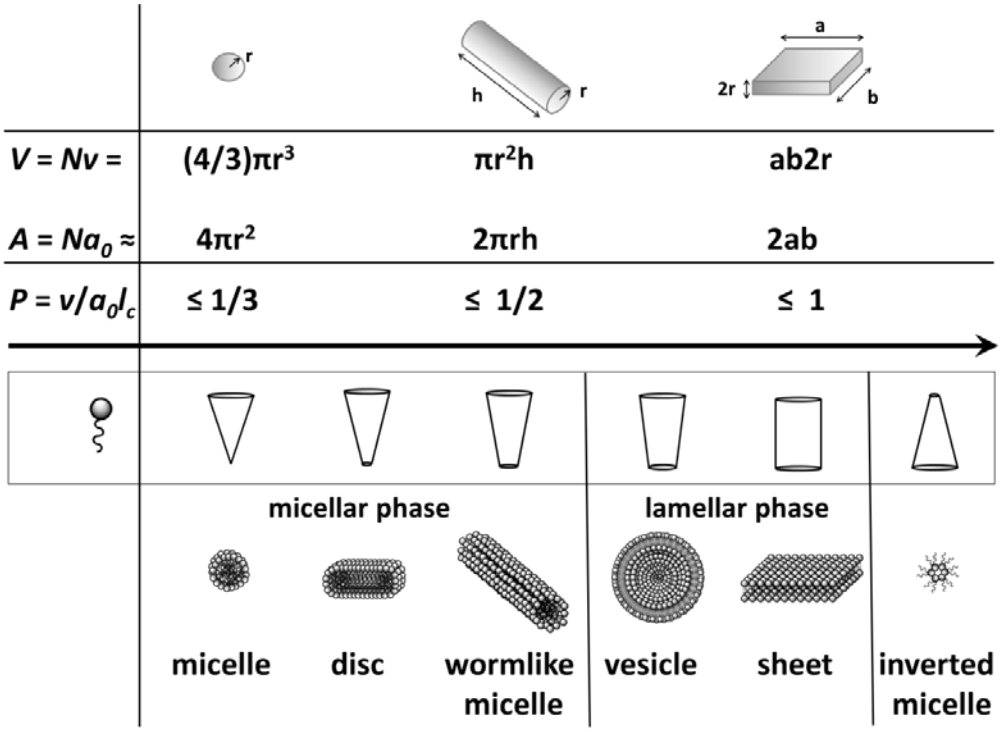

Figure 1.2.3: Illustration of the relationship between geometrical structures, calculated packing parameter, amphiphile shape and aggregates. Figure adapted from literature.[37,39]

Micellar phases are dominantly formed by single tailed amphiphiles and lamellar phases are preferably consisting of double tailed compounds. However, parameters like temperature, salt concentration and chain composition have a large influence on the observed aggregates. For instance, with increasing temperature more flexibility is expected for the hydrophobic tail

which would result in an increased packing parameter. In contrast, an extension of the chain would result in higher transition temperatures reducing *P*. Also, the addition of counter ions could lead to a variety of results. An example is the presence of positively charged ions like Ca^{2+} which can have a reducing effect on the charge repulsion of negatively charged head groups.
It can be concluded that the above described packing parameters have to be used with caution. Certainly, they can give an estimation which aggregate is to be expected, but packing parameters do not include surrounding influences.

1.3 Application of Amphiphilic Compounds during Everyday Life

The knowledge obtained studying the phenomena observed in nature can be applied for a variety of different materials. Thereby, fatty acids can be found during daily life for example in cleaning reagents, cosmetic products, food supplements and drugs.[40-43]
The amphiphilic character of fatty acids results after mixing with aqueous media to a decrease of the surface tension of water and an increase of the solubility of hydrophobic compounds.[44] These advantages were already recognized and used by ancient cultures like Babylonians and Egyptians.[41] Simple recipes mixing animal fat or vegetable oil with alkaline salt in water resulted in soap-like mixtures which were used for cleaning, medical and cosmetic purposes. The first known scientific literature mentioning acid-soaps was published in 1823 by *Chevreul*.[45] During the following decades *Ekwall et al.* and *McBain et al.* studied the acid-soaps described by *Chevreul* proving their existence and analyzing the stoichiometric ion composition.[46]
Furthermore, it was observed that solutions incorporating surfactants are able to form foams in the presence of gas. Thereby, gas bubbles are surrounded by surfactant aggregates which are stabilized through noncovalent interactions. As shown in Figure 1.3.1, an orientation of the amphiphilic compound takes place wherein the hydrophilic head group is pointing to the polar aqueous phase and the hydrophobic tail is facing towards the apolar gas phase.[47] This behavior is widely observed for different amphiphiles. Some well known examples observed in everyday life are soap foam, beer foam and fire extinguisher foam.

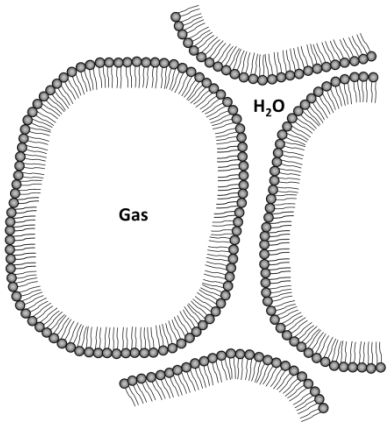

Figure 1.3.1: Schematic representation of foam composition in surfactant containing solutions. Figure adapted from reference 47.

Another industrial application is the use of surfactant in emulsions. Here, amphiphiles are employed to increase the miscibility of hydrophobic material with water and hydrophilic compounds in oil. As shown in Figure 1.3.2, the minor compound is encapsulated by the surfactants resulting in an emulsion.[48] This principle is widely applied in paint-, cosmetic-, food- and pharmaceutical-industry.[48,49]

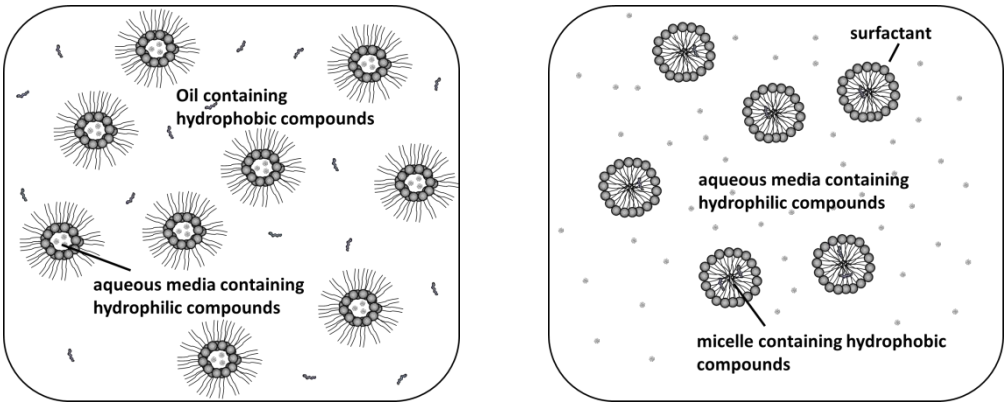

Figure 1.3.2: Schematic representation of an emulsion of water in oil (left) and of oil in water (right).

For most applications simple saturated and unsaturated fatty acids are sufficient whereas fatty acids, carrying a variety of modifications, are often applied during drug development. Studies using artificial membranes which incorporate molecules based on natural occurring fatty acids can lead to drug systems that overcome chemical resistance, increase stability and decrease–permeability. Also they might results in controlled release mechanisms, allow influencing the circulation life times and give access to higher target selectivity. Thereby, the amphiphilic character of fatty acids enables their application as transport systems in aqueous media.[50,51] An example are DNA carrier systems in which an aggregate complex (lipoplex, Figure 1.3.3a) between the negatively charged DNA phosphate backbone and a positively charged surfactant is allowing efficient transportation of DNA molecules into a broad range of eukaryotic cells (Figure 1.3.3b).[52] Thereby, the lipoplex is preventing the DNA from degradation through nucleases and increases the half-time of DNA in vivo.

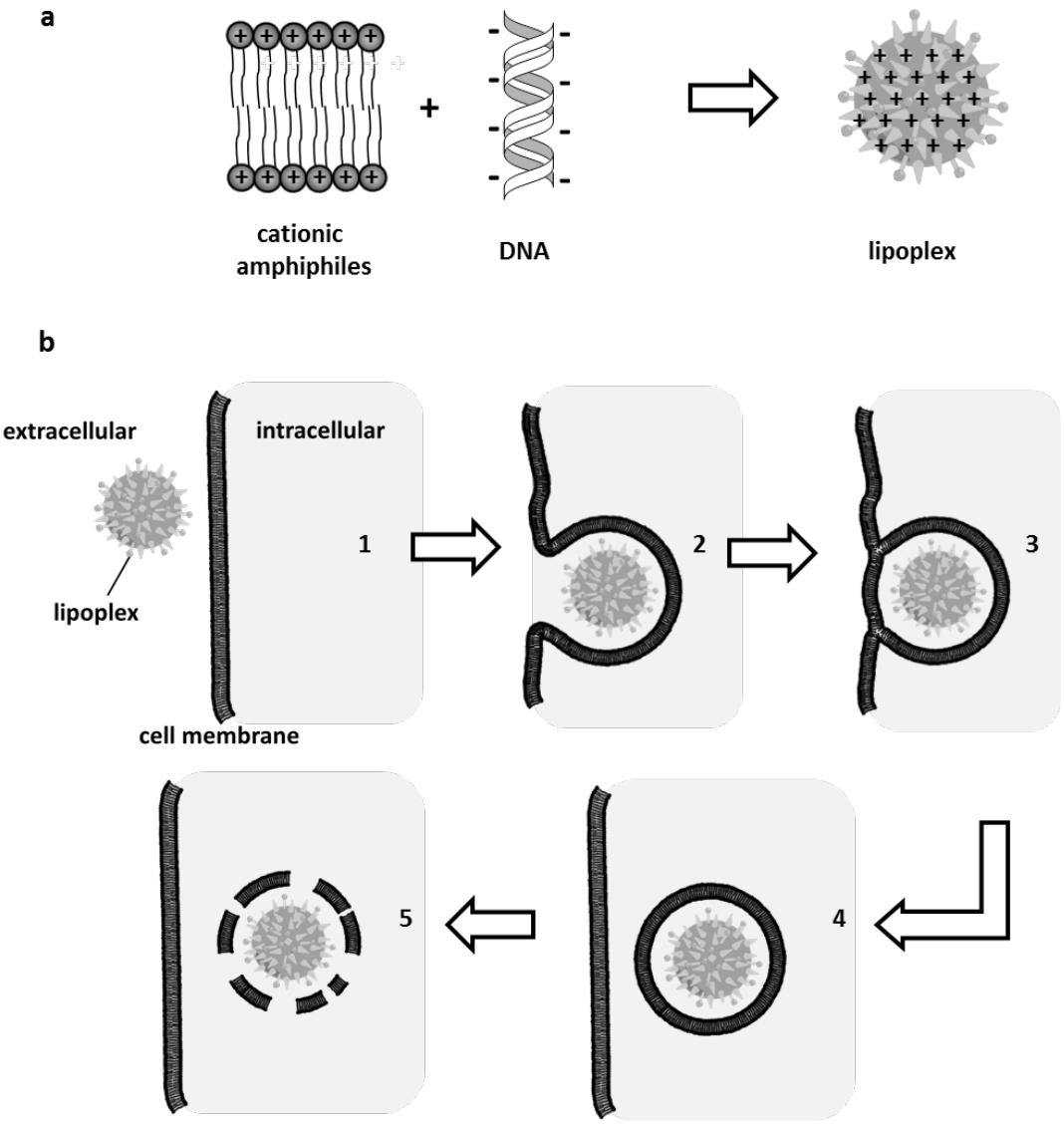

Figure 1.3.3: (a) Schematic representation of the lipoplex formation stabilized by electrostatic interactions. (b) Schematic representation of DNA transfer through endocytosis using an lipoplex as DNA-carrier. 1) Interaction of liposome with bio-membrane 2) Invagination of membrane 3) Endosome formation 4) Encapsulation of endosome carrying a liposome 5) Degradation of endosome. Figure adapted from literature.[52]

1.4 Outline of this Thesis

The above mentioned unique features of amphiphiles allow the survival of different organisms under extreme conditions and in the presence of toxic chemicals. However, the low availability of most of these amphiphilic compounds isolated from natural sources and the often complicated cultivation process makes organic synthesis to an irreplaceable tool giving not only access to the desired molecule but also to a variety of derivatives.
Therefore, the first part of my thesis is focusing on the synthesis of natural fatty acids and their derivatives. In Chapter **II** and **III**, the synthesis of fatty acids carrying a hydrophobic tail containing linear fused cyclobutane rings is described. The in Chapter **II** via [2+2] photocycloaddition obtained building blocks are used in Chapter **III** giving access to ladderane fatty acids. Furthermore, a brominated, unsaturated fatty acid carrying a cyclopropane moiety, namely majusculoic acid, is synthesized in Chapter **IV**. The synthesis described in this thesis is the first successful total synthesis of majusculoic acid. Key steps applied in this synthesis are selective reduction and isomerization of double bonds, ozonolysis and asymmetric cyclopropanation.

In the second part of this thesis a simplified lipid system containing only naturally occurring building blocks is reported. First, the optimized synthesis of *N*-phosphoamino acids composed of just three synthetic steps is reported in Chapter **V**. This efficient three-step synthesis is applied to obtain a collection of more than 15 amphiphilic acids. Subsequently, these amphiphilic compounds are used in Chapter **VI** for aggregation and biocompatibility studies. Finally, further modifications at the hydrophilic head group of *N*-phosphoamino acids is performed and their influence on the aggregation and biocompatibility is demonstrated in Chapter **VII**.

1.5 References

1) K. Simons, J. L. Sampaio. Membrane Organization and Lipid Rafts. *Cold Spring Harb. Perspect. Biol*., **3**, 1-17 (2011).
2) C. Tanford. The Hydrophobic Effect and the Organization of Living Matter. *Science*, **200**, 1012-1018 (1978).
3) B. S. Brown. Biological Membranes. *The Biochemical Society*. London (1996).
4) A. A. Spector, M. A. Yorek. Membrane Lipid-Composition and Cellular Function. *J. Lipid Res.*, **26**, 1015-1035 (1985).
5) M. Seewald, H. M. Eichinger. Separation of major phospholipid classes by high-performance liquid chromatography and subsequent analysis of phospholipid-bound fatty acids using gas chromatography. *J. Chrom. A*, **469**, 271-280 (1989).
6) M. De Rosa, A. Gambacorta, A. Gliozzi. Structure, biosynthesis, and physicochemical properties of archaebacterial lipids. *Microbiol. Rev.*, **50**, 70-80 (1986).
7) O. G. Mouritsen, M. J. Zuckermann. What's So Special About Cholesterol? *Lipids*, **39**, 1101-1113 (2004).
8) K. Yamauchi, K. Doi, Y. Yoshida, M. Kinoshita. Archaebacterial lipids: highly proton-impermeable membranes from 1,2-diphytanyl-*sn*-glycero-3-phosphocholine. *Biochimica Biophysica Acta*, **1146**, 178-182 (1993).
9) J. Anderson, E. Chargaff. The Chemistry of the Lipoids of Tubercle Bacilli: VI. Concerning Tuberculostearic Acid and Phthioic Acid from the Acetone-Soluble Fat. *J. Biol. Chem*., **85**, 77-88 (1929).
10) M. A. Spielman. The Chemistry of the Lipoids of Tubercle Bacilli: XXXIX. The Constitution of Tuberculostearic Acid. *J. Biol. Chem*., **106**, 87-96 (1934).
11) F. S. Prout, J. Cason, A. W. Ingersoll. Branched-Chain Fatty Acids. V. The Synthesis of Optically Active 10-Methyloctadecanoic Acid. *J. Am. Chem. Soc*., **70**, 298-305 (1948).
12) W. J. Lennarz, G. Scheuerbrandt, K. Bloch. The Biosynthesis of Oleic and 10-Methylstearic Acid in *Mycobacterium phlei*. *J. Biol. Chem*., **237**, 664-671 (1962).
13) E. Lederer. The Origin and Function of Some Methyl Groups in Branched-chain Fatty Acids, Plant Sterols and Quinones. *Biochem. J.*, **93**, 449-468 (1964).
14) D. W. Grogan, J. E. Cronan Jr. Cyclopropane Ring Formation in Membrane Lipids of Bacteria. *Microbiol. Mol. Biol. Rev.*, **61**, 429-441 (1997).
15) C. E. Barry 3rd, R. E. Lee, K. Mdluli, A. E. Sampson, B. G. Schroeder, R. A. Slayden, Y. Yuan. Mycolic Acids: Structure, Biosynthesis and Physiological Functions. *Prog. Lipid Res*., **37**, 143-179 (1998).
16) M. Fontecave, M. Atta, E. Mulliez. *S*-Adenosylmethionine: Nothing Goes to Waste. *Trends Biochem. Sci*., **29**, 243-249 (2004).
17) F. Laval, M. A. Lanéelle, C. Déon, B. Monsarrat, M. Daffé. Accurate Molecular Mass Determination of Mycolic Acids by MALDI-TOF Mass Spectrometry. *Anal. Chem*., 73, 4537-4544 (2001).

18) K. Hofmann, R. A. Lucas. The Chemical Nature of a Unique Fatty Acid. *J. Am. Chem. Soc*., **72**, 4328-4329 (1950).
19) J. C. Kwan, T. Meickle, D. Ladwa, M. Teplitski, V. Paul, H. Luesch. Lyngbyoic Acid, a "Tagged" Fatty Acid from a Marine Cyanobacterium, Disrupts Quorum Sensing in *Pseudomonas aeruginosa*. *Mol. BioSyst.*, **7**, 1205-1216 (2011).
20) N. Sitachitta, W. H. Gerwick. Grenadadiene and Grenadamide, Cyclopropyl-Containing Fatty Acid Metabolites from the Marine Cyanobacterium *Lyngbya majuscule*. *J. Nat. Prod.*, **61**, 681-684 (1998).
21) J. B. MacMillan, T. F. Molinski. Majusculoic Acid, a Brominated Cyclopropyl Fatty Acid from a Marine Cyanobacterial Mat Assemblage. *J. Nat. Prod*., **68**, 604-606 (2005).
22) J. S. Sinninghe Damsté, M. Strous, W. I. C. Rijpstra, E. C. Hopmans, J. A. J. Geenevasen, A. C. T. van Duin, L. A. van Niftrik, M. S. M. Jetten. Linearly concatenated cyclobutane lipids form a dense bacterial membrane. *Nature*, **419**, 708-712 (2002).
23) I. Lanekoff, R. Karlsson. Analysis on intact ladderane phospholipids, originating from viable anammox bacteria, using RP-LC-ESI-MS. *Anal. Bioanal. Chem*., **397**, 3543-3551 (2010).
24) J. S. Sinninghe Damsté, S. Schouten, E. C. Hopmans, A. C. T. van Duin, J. A. J. Geenevasen. Crenarchaeol: The Characteristic Core Glycerol Dibiphytanyl Glycerol Tetraether Membrane Lipid of Cosmopolitan Pelagic Crenarchaeota. *J. Lipid Res*., **43**, 1641-1651 (2002).
25) M. D. Kiran, S. Annapoorni, I. Suzuki, N. Murata, S. Shivaji. *Cis-trans* Isomerase Gene in Psychrophilic *Pseudomonas Syringae* is Constitutively Expressed during Growth and under Conditions of Temperature and Solvent Stress. *Extremophiles*. **9**, 117-125 (2005).
26) R. Diefenbach, H.-J. Heipieper, H. Keweloh. The Conversion of *Cis* into *Trans* Unsaturated Fatty Acids in *Pseudomonas Putida* P8: Evidence for a Role in the Regulation of Membrane Fluidity. *Appl. Microbiol. Biotechnol*., **38**, 382-387 (1992).
27) H. Okuyama, N. Okajima, S. Sasaki, S. Higashi, N. Murata. The *cis*/*trans* Isomerization of the Double Bond of a Fatty Acid as a Strategy for Adaptation to Changes in Ambient Temperature in the Psychrophilic Bacterium, *Vibrio* sp. Strain ABE-1. *Biochim. Biophys. Acta*, **1084**, 13-20. (1991).
28) J. H. Law. Biosynthesis of Cyclopropane Rings. *Acc. Chem. Res*., **4**, 199-203 (1971).
29) F. D. Gunstone. Topics in Lipid Chemistry. *John Wiley & Sons, Inc*., New York, N.Y (1970).
30) H. F. Chambers, D. Moreau, D. Yajko, C. Miick, C. Wagner, C. Hackbarth, S. Kocagoz, E. Rosenberg, W. K. Hadley, H. Nikaido. Can Penicillins and Other Beta-Lactam Antibiotics be Used to Treat Tuberculosis? *Antimicrob. Agents Chemother*., **39**, 2620-2624 (1995).
31) M. B. Goren, M. Cernich, O. Brokl. Some Observations on Mycobacterial Acid-Fastness. *Am. Rev. Respir. Dis*., **118**, 151-154 (1978).
32) I. Tomiyasu. Mycolic Acid Composition and Thermally Adaptative Changes in Nocardia asteroids. *J. Bacteriol*., **151**, 828-837 (1982).

33) M. D. Kiran, J. S. S. Prakash, S. Annapoorni, S. Dube, T. Kusano, H. Okuyama, N. Murata, S. Shivaji. Psychrophilic *Pseudomonas Syringae* Requires *Trans*-Monounsaturated Fatty Acid for Growth at Higher Temperature. *Extremophiles*, **8**, 401-410 (2004).
34) V. A. Knivett, J. Cullen. Some Factors Affecting Cyclopropane Acid Formation in Escherichia coli. *Biochem. J*., **96**, 771-776 (1965).
35) Y. Yuan, R. E. Lee, G. S. Besra, J. T. Belisle, C. E. Barry 3rd. Identification of a Gene Involved in the Biosynthesis of Cyclopropanated Mycolic Acids in *Mycobacterium tuberculosis*. *Proc. Natl. Acad. Sci.* USA, **92**, 6630-6634 (1995).
36) J. L. Ramos, E. Duque, J.-J. Rodríguez-Herva, P. Godoy, A. Haïdour, F. Reyes, A. Fernández-Barrero. Mechanisms for Solvent Tolerance in Bacteria. *J. Biol. Chem*., **272**, 3887-3890 (1997).
37) J. N. Israelachvili, D. J. Mitchell, B. W. Ninham. Theory of Self-Assembly of Hydrocarbon Amphiphiles into Micelles and Bilayers. *J. Chem. Soc., Faraday Trans. 2*, **72**, 1525-1568 (1976).
38) C. Tanford. The Hydrophobic Effect. *John Wiley & Sons*, New York (1973).
39) R. Nagarajan. Molecular Packing Parameter and Surfactant Self-Assembly: The Neglected Role of the Surfactant Tail. *Langmuir*, **18**, 31-38 (2002).
40) A. Cooper, M. W. Kennedy. Biofoams and Natural Protein Surfactants. *Biophys Chem.*, **151**, 96–104 (2010).
41) J. Toedt, D. Koza, K. Van Cleef-Toedt. Chemical Composition of Everyday Products. *Greenwood Press*, London (2005).
42) R. Wolf, D. Wolf, B. Tüzün, Y. Tüzün. Soaps, Shampoos and Detergents. *Clin. Dermatol*., **19**, 393-397 (2001).
43) L. L. Schramm, E. N. Stasiuk, D. G. Marangoni. Surfactants and their Applications. *Annu. Rep. Prog. Chem., Sect. C: Phys. Chem*., **99**, 3-48 (2003).
44) M. J. Rosen. Surfactants and Interfacial Phenomena, 3rd ed. *Wiley-Interscience, John Wiley & Sons*, Hoboken, NJ (2004).
45) M. E. Chevreul. *Recherche Chimique Sur les Corps Gras d'Origine Animal.* Paris (1823).
46) M. L. Lynch. Acid-Soaps. *Curr. Op. Coll. Int. Sci*., **2**, 495-500 (1997).
47) L. L. Schramm, F. Wassmuth. Foams: Fundamentals and Applications in the Petroleum Industry. *Am. Chem. Soc*., Washington, DC (1994).
48) B. Guy. The Perfect Mix: Recent Progress in Adjuvant Research. *Nature Rev. Microbiol*., **5**, 505-517 (2007).
49) A.-C. Hellgren, P. Weissenborn, K. Holmberg. Surfactants in water-borne paints. *Prog. Org. Coat*., **35**, 79-87 (1999).
50) A. Sharma, U. S. Sharma. Liposomes in Drug Delivery: Progress and Limitations. *Int. J. Pharm*., **154**, 123-140 (1997).
51) T. Lian, R. J. Y. Ho. Trends and Developments in Liposome Drug Delivery Systems. *J. Pharm. Sci*., **90**, 667-680 (2001).
52) S. Bhattacharya, A. Bajaj. Advances in Gene Delivery through Molecular Design of Cationic Lipids. *Chem. Commun*., **2009**, 4632-4656 (2009).

Chapter 2

Synthesis of Ladderane Structures Applying Inter- and Intramolecular [2+2] Photocycloaddition

Naturally occurring compounds carrying several fused cyclobutane moieties, named a ladderane unit, have been isolated from natural sources. However, the synthesis of those natural products bearing ladderane structures is challenging. Therefore, in this chapter we apply inter- and intra-molecular [2+2] photocycloaddition reactions to give access to a diversity of compounds carrying up to three linear fused cycloalkanes.

2.1 Introduction

One efficient way to synthesize the in chapter 1 introduced fatty acids carrying linear fused cyclobutane rings is the [2+2] photocycloaddition (Scheme 2.1.1a). This reaction was observed in 1908 for the first time by *Ciamician et al.* when carvone **1** was exposed for one year to direct sunlight.[1] The structure of the formed product carvone camphor **2** was confirmed in 1957 revealing an intramolecular reaction between two alkene moieties of carvone **1** (Scheme 2.1.1b).[2] This discovery represented the starting point of light induced cycloadditions. Due to the diversity and complexity of the obtained products a growing interest for [2+2] photocycloadditions was observed leading to the total synthesis of several natural and non-natural products.[3] Notable examples for the application of intramolecular [2+2] photocycloaddition are the synthesis of cubane **3** in 1964 by *Eaton et al.*[4] and (+)-Lactiflorin **4** in 2012 by *Lu et al.* (Scheme 2.1.1c).[5] Examples applying an intermolecular photoreaction are the synthesis of cyclobutane derivate **5** published in 2013 by *Coote et al.*[6] and the total synthesis of (+)-Lineatin **6** reported by *Racamonde et al.* in 2008 (Scheme 2.1.1c).[7]

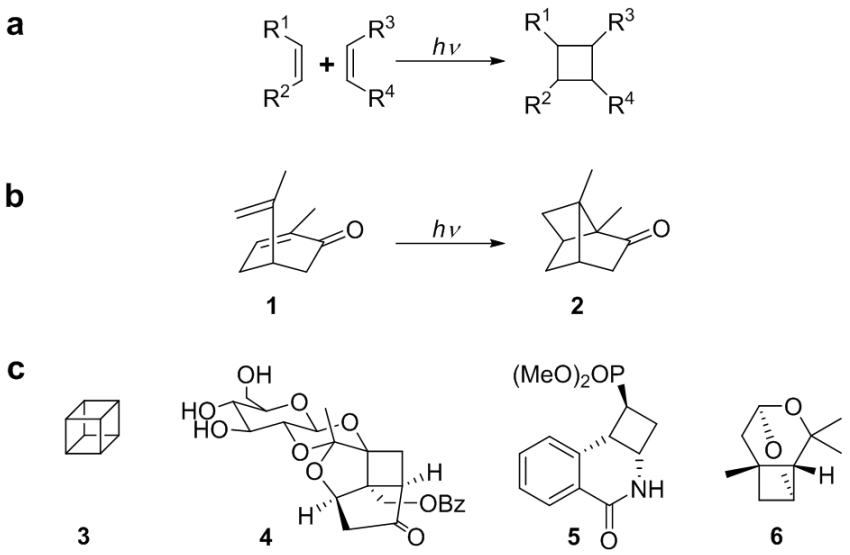

Scheme 2.1.1: (a) Photo induced [2+2] cycloaddition. (b) Intramolecular cycloaddition of carvone **1** resulting in carvone camphor **2**. (c) Molecular structure of natural and non-natural compounds synthesized via intramolecular (**3** and **4**) and intermolecular (**5** and **6**) [2+2] photocycloaddition.

The [2+2] photocycloaddition is a thermodynamically forbidden process. As shown in figure 2.1.1a the **l**owest **u**noccupied **m**olecular **o**rbital (LUMO) and the **h**ighest **o**ccupied **m**olecular **o**rbital (HOMO) of alkenes involved in the reaction cannot overlap. Conclusively, the σ-bonds between the alkenes cannot be formed. Therefore, an excitation of the electronic ground state is necessary to allow a reaction. The resulting orbital occupation of the excited state is shown in figure 2.1.1b allowing a photochemical induced [2+2] cycloaddition.

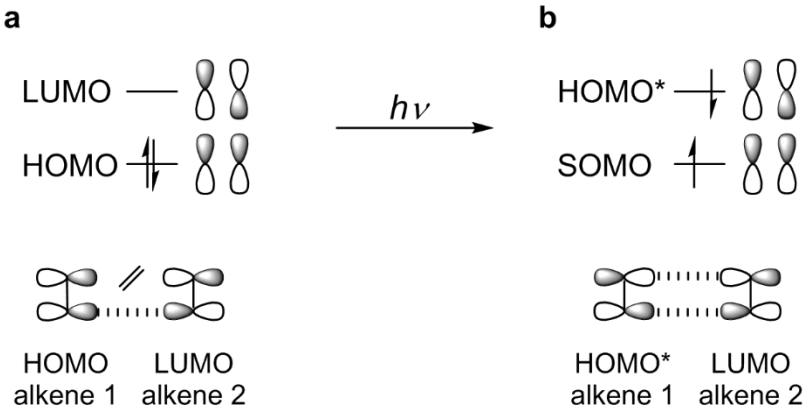

Figure 2.1.1: Occupation of molecular orbitals during the thermodynamically (a) forbidden and photo chemically (b) allowed [2+2] cycloaddition. SOMO stands for **s**ingle **o**ccupied **m**olecular **o**rbital.

Every molecule has a multiple number of energetic states and the energy needed to cross the barrier between these states can be obtained through photon absorption (*hν*). The resulting excited state is higher in energy than the ground state and can undergo several processes to obtain a low energetic state.[8] Hence, as demonstrated in a *Jablonski* diagram vibration, **i**nternal **c**onversion (IC), **i**nter**s**ystem **c**rossing (ISC) and emission (fluorescence and phosphorescence) are competitive processes to the [2+2] photocycloaddition (Figure 2.1.2a).[9] The excitation of an alkene in solution takes about 10^{-15} s, IC (10^{-6} to 10^{-12} s) and fluorescence (10^{-5} to 10^{-9} s) represent the fastest way for the molecule to return to the energetic ground state.[8] Therefore, photochemical reactions are limited to a timeframe given by the fluorescence life time of the molecule. The processes via ISC (10 to 10^{-11} s) and phosphorescence (10^{2} to 10^{-4} s) which involve a change in spin multiplicity (Figure 2.1.2b) are comparable slow.[8]

To enable a fast intermolecular photoreaction a high collision frequency between both molecules in solution is necessary and therefore, high concentrations of reactants are required. In contrast, low alkene concentrations are applied for intramolecular cycloaddition to prevent an intermolecular reaction.

Intermolecular cycloaddition has been successfully employed for the synthesis of natural products such as pentacycloanammoxic acid **7** (Scheme 2.1.2). The natural occurring fatty acid **7** was isolated in 2002 by *Sinninghe Damsté et al.* from *Candidatus Brocadia anammoxidans*, an **an**aerobic **amm**onium **ox**idizing (anammox) bacteria.[10] In 2004, *Mascitti* and *Corey* successfully synthesized the natural compound **7**[11] and published a revised synthetic pathway in 2006.[12] As shown in Scheme 2.1.2, both synthetic pathways contain an intermolecular [2+2] photocycloaddition between a cyclobutene derivative **8a-c** and cyclopentenone **9** resulting in a ladderane structure **10a-c** carrying two, three and four cyclobutane moieties, respectively. The cycloaddition is a crucial synthetic step in the total synthesis of the fatty acid **7**.

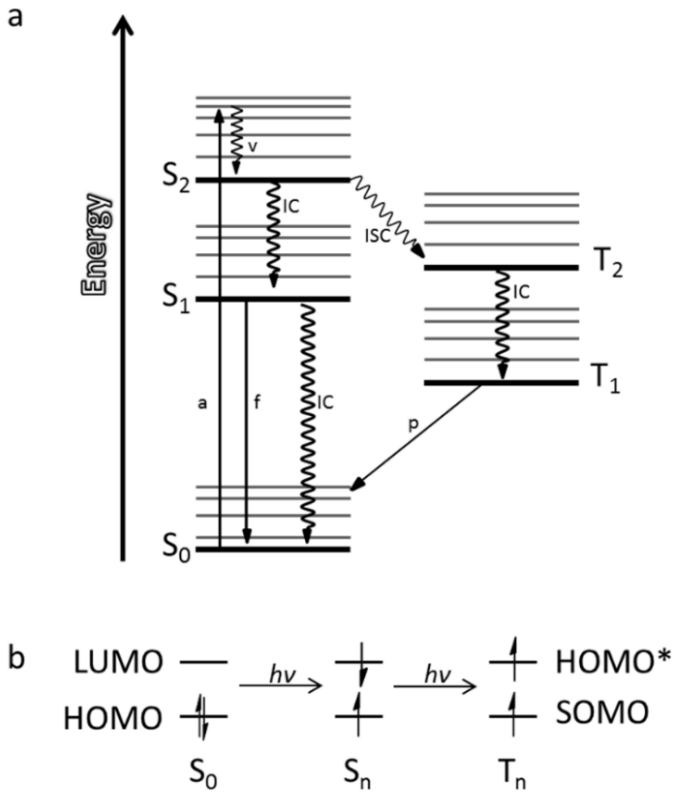

Figure 2.1.2: (a) *Jablonski* energy diagram showing different energetic states and energy transfer processes. (b) Change in spin multiplicity caused by ISC. (a: absorbance, f: fluorescence, p: phosphorescence, v: vibration, ISC: intersystem crossing, IC: internal conversion, S_0: ground state, S_n: singlet state, T_n: triplet state). Figure adapted from the *Jablonski* diagram reported in reference 8.

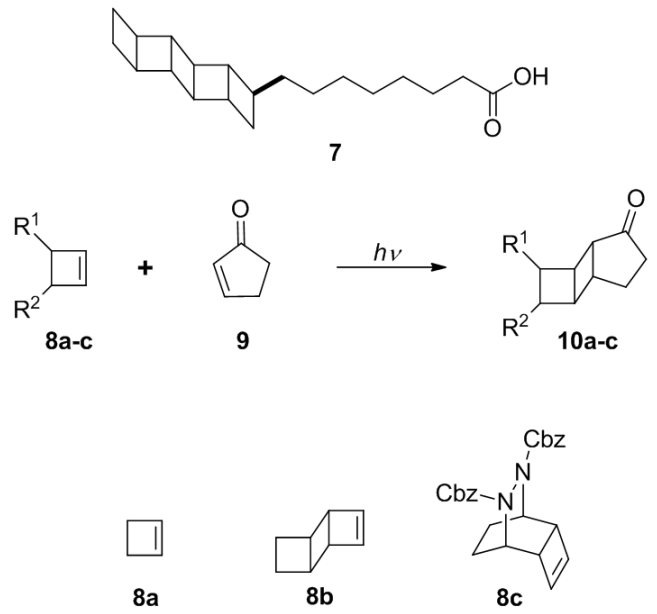

Scheme 2.1.2: Molecular structure of pentacycloanammoxic acid **7** and [2+2] photocycloaddition used as key step in the synthesis of **7** performed by *Mascitti* and *Corey*.[11,12]

A second approach to synthesize molecules exhibiting a ladderane structure is the intramolecular [2+2] photocycloaddition. Due to the fact that the reactive alkene groups are present in the same molecule they can be in close proximity. In this case the photo-induced cycloaddition can be faster and can result in higher yields. In 2005 *Hopf et al.* reported the application of intramolecular photoreactions for the synthesis of ladderane structures with up to five linear fused cyclobutane rings (Scheme 2.1.3a).[13] In this regard, a disubstituted paracyclophane **11** with two alkene chains was used giving access to the cyclobutane derivative **12**. As shown in scheme 2.1.3b, using the same approach *Zitt et al.* demonstrated in 2002 the use of unsaturated acid chlorides **13** and a pseudo-geminally substituted paracyclophane **14** during a [2+2] photocycloaddition.[14] After amide bond formation the resulting compound **15** can undergo a intramolecular photocycloaddition yielding the cyclobutane derivative **16**. In this strategy paracyclophane **14** acts as spacer that can be recovered by hydrolysis of the product **16** giving access to the ladderane compound **17** at the same time.

Compared to the intermolecular cycloaddition (*vide supra*) the synthesis of ladderane structures employing the reusable spacer **14** for the intramolecular photoreaction resulted in lower yield and longer reaction time.[14]

Furthermore, during the last decade several studies were published demonstrating the application of various templates **19** which can form multiple non-covalent interactions, such as H-bonding, to the substrate **18** (Scheme 2.1.3c).[15-17] It was shown that alkenes **18** can be arranged *via* template **19** in a complex **20** that can undergo an 'intramolecular' type photocycloaddition resulting in product **21** (Scheme 2.1.3c). The desired product **22** exhibiting one cyclobutane moiety could be obtained by breaking the non-covalent interactions in **21**. In this way template **19** could be recovered and reused for the next reaction cycle.

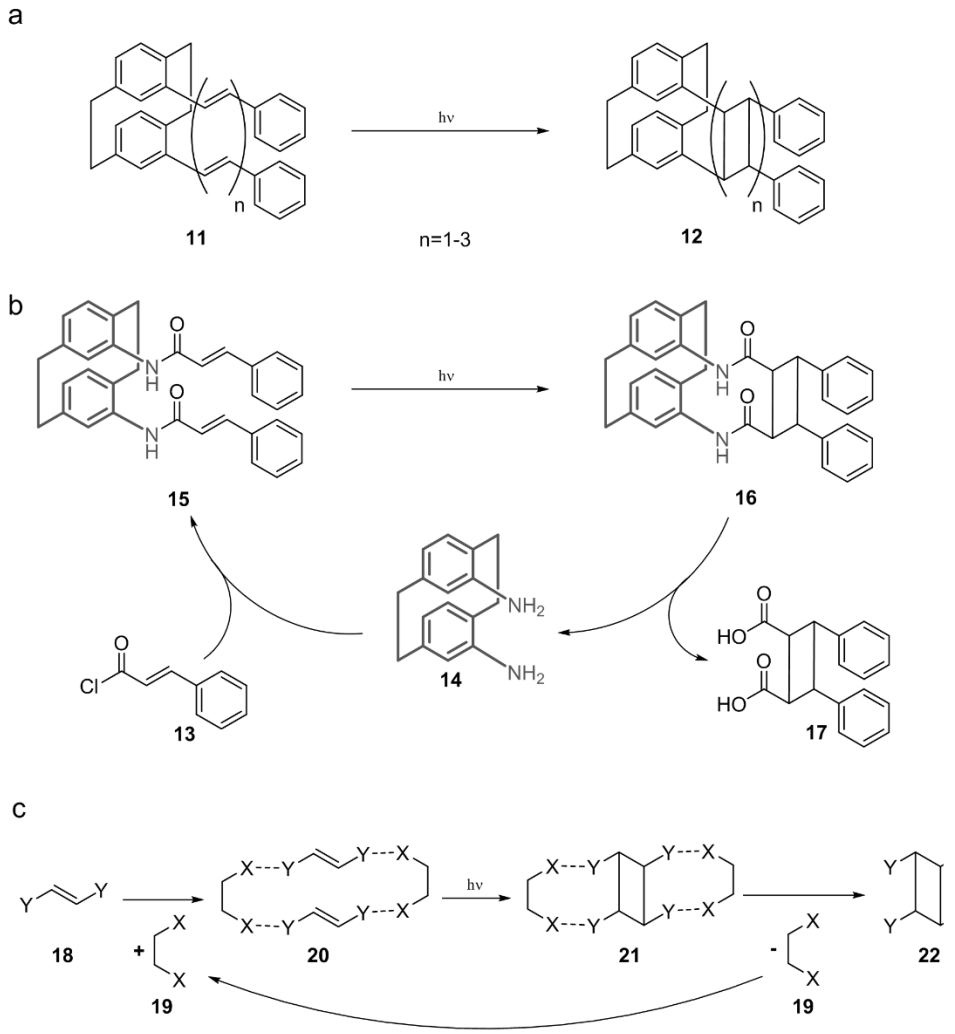

Scheme 2.1.3: Template supported [2+2] photocycloaddition: Covalent approach: by *Hopf et al.* in 2005 (a),[13] by *Zitt et al.* in 2002 (b)[14] and non-covalent approach: via non-covalent interactions (c).[15-17]

It needs to be mentioned that the synthesis of compounds exhibiting up to five fused cyclobutane rings has been successfully achieved using a single intramolecular cycloaddition.[13] In our studies, we employed both of the above mentioned strategies, i.e. intra- and intermolecular cycloaddition, to synthesize ladderane molecules with up to three fused cyclobutane moieties.

2.2 Results and Discussion

2.2.1 Intermolecular [2+2] Photocycloaddition

In this chapter two different approaches were applied with the aim to obtain ladderane structures with up to three fused cycloalkane moieties. The first synthetic strategy we applied was based on the synthesis of pentacycloanammoxic acid **7** reported by *Mascitti et al.*[12] in 2006. As shown in Scheme 2.2.1, an intermolecular [2+2] photocycloaddition between a cyclic enone **9** and a variety of cyclic alkenes **8a**, **8d**, **8e** was performed.

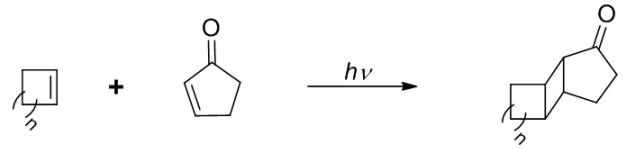

8a n=1
8d n=2
8e n=3

9

10a n=1
10d n=2
10e n=3

Scheme 2.2.1: Intermolecular [2+2] photocycloaddition of a cyclic enone **9** and the cyclic alkenes **8a**, **8d**, **8e**.

The employed cyclic alkenes **8d** (n = 2) and **8e** (n = 3) are commercially available. In contrast, the highly volatile cyclobutane **8a** had to be prepared in three synthetic steps. As shown in Scheme 2.2.2, the synthesis of alkene **8a** starts with mesylation of the commercial available cyclopropylmethanol **23** followed by a ring expansion of the cyclopropane **24** resulting in the cyclobutyl methanesulfonate **25**.[12,18] During the latter step the formation of an olefinic side product **26** was observed, which was formed *via* a ring opening reaction. Cyclobutane derivative **25** could be separated from the product mixture by an oxidation of **26** using potassium permanganate. Thereby, the in **26** incorporated terminal olefinic bond undergoes at 2 °C an oxidation whereas **25** is relatively stable under the applied low temperature conditions. The oxidation is followed by extraction giving **25** with an isolated yield of 71%. Finally, to obtain the desired cyclobutene **8a** an elimination of methanesulfonic acid applying potassium *tert*-butanolate in DMSO (**di**-**m**ethyl **s**ulf**o**xide) was carried out.[18] No additional purification of cyclobutene **8a** was necessary, since the reaction was performed at 70 °C leading to an instantaneous distillation of the product **8a** (boiling point 2 °C) to a precooled flask (-70 °C).

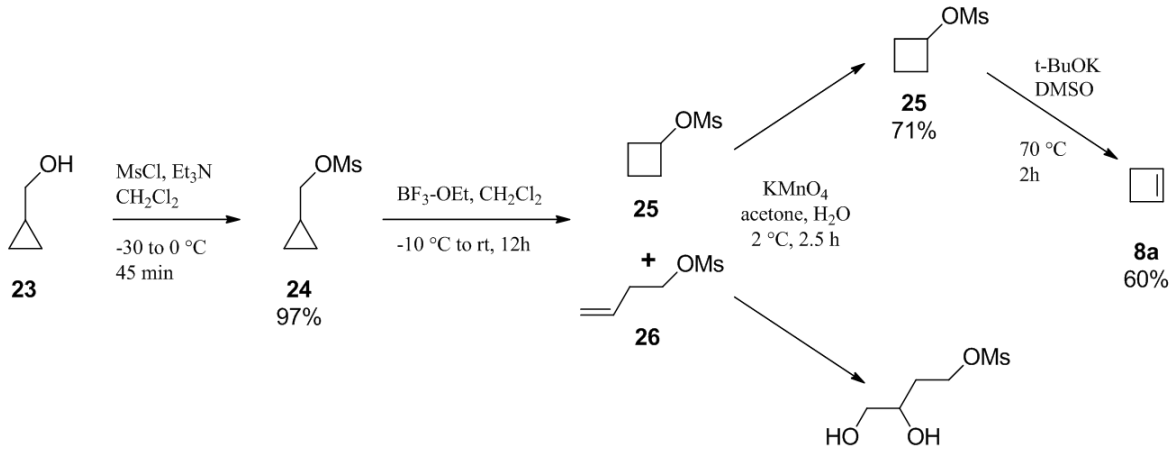

Scheme 2.2.2: Synthesis of cyclobutene **8a** from cyclopropylmethanol **23**.

After successful synthesis of **8a** the photochemical cycloaddition between alkenes **8a** and **9** was performed (Scheme 2.2.3). Here, two equivalents of the commercially available cyclopentanone **9** were dissolved in a degassed UV grade solvent and cooled to -30 °C. Cycloalkene **8a** was added and the resulting reaction mixture was irradiated for several hours *via* a medium pressure mercury lamp using a cooling mantel made of *Pyrex* glass. As shown in Scheme 2.2.3, employing an irradiation time of 30 hours resulted exclusively in diketones **27a** and **27b** formed by homo-dimerization of **9**. Isomers **27a** and **27b** were obtained in a ratio of 2 to 9 with a total yield of 62%. Both isomers could be separated by column chromatography or extraction of the isomer mixture with diethyl ether. However, formation of the desired product **10a** was not observed employing the above described reaction conditions.

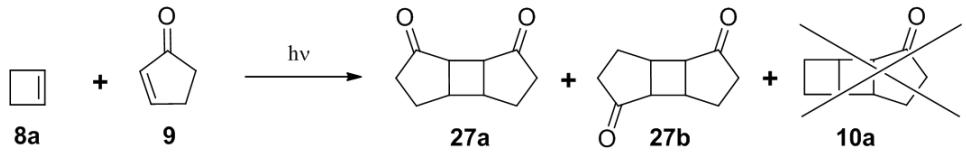

Scheme 2.2.3: Intermolecular [2+2] photocycloaddition.

In contrast, employing a reverse alkene ratio, i.e. cyclopentenone **9** and cyclobutene **8a** in a ratio of 1 to 2, resulted in the formation of the desired ketone **10a** as main product reaching an isolated yield of 54% (Table 2.2.1). Furthermore, different solvents were tested and the best result was obtained using acetone as reaction media. It needs to be mentioned that the optimized conditions shown in Table 2.2.1 allow shorter reaction time (4 hours).

Table 2.2.1: Optimized reaction conditions for intermolecular [2+2] photocycloaddition between cyclopentenone **9** and cyclobutene **8a**.

	Literature-conditions*	**Optimized conditions**
solvent	acetonitrile UV-Sol	acetone UV-Sol
Reaction time	~30 h	4 h
ratio	cyclobutene: cyclopentenone 1 : 2	cyclobutene: cyclopentenone 2 : 1
temperature	between -30 °C and -10 °C	add cyclobutene at -30 °C reaction temperature: -10 °C
products	**27a** and **27b**	**10a**, **27a** and **27b**

*Published in reference 12.

The above presented optimized conditions were also successfully applied for [2+2] cycloaddition using cyclopentene **8d** with ketone **9** (Scheme 2.2.1, page 27) yielding the corresponding photoproduct **10d** with an isolated yield of 62%. However, employing cyclohexene **8e** for the photoreaction resulted in a mixture of different structure isomers and the loss of the ladderane configuration giving a total yield of 57% (Scheme 2.2.4). This observation can be explained with the photoisomerization of the double bond of **8e** which is a known side reaction for cycloalkenes containing more than five carbons.[19]

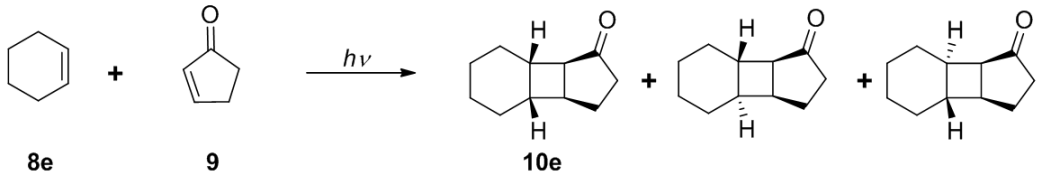

Scheme 2.2.4: Intermolecular [2+2] photocycloaddition between cyclohexene **8e** and ketone **9**.

To confirm the *exo*-configuration of compound **10a** and **10d** the synthesis of dinitrophenylhydrazone **29a** and **29d** was performed since their crystals can be applied directly for X-ray crystallography (Scheme 2.2.5). Thereby, a condensation under strong acidic conditions with dinitrophenylhydrazine **28** yielded orange crystals of hydrazone **29a** and **29d**. In Figure 2.2.1 the crystal structure of **29a** and **29d** are shown proving the *exo*-configuration of both hydrazones and their corresponding ketones **10a** and **10d**.

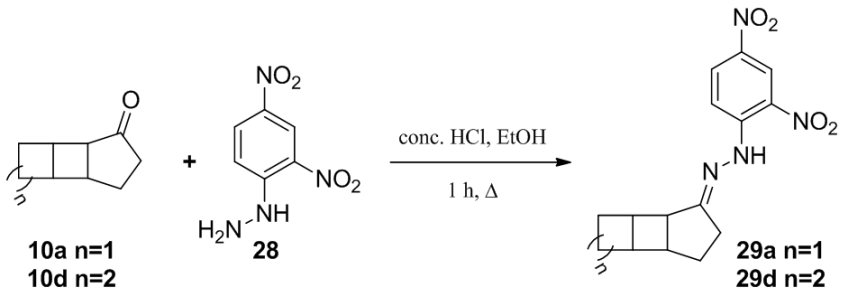

Scheme 2.2.5: Synthesis of dinitrophenylhydrazone **29a** and **29d**.

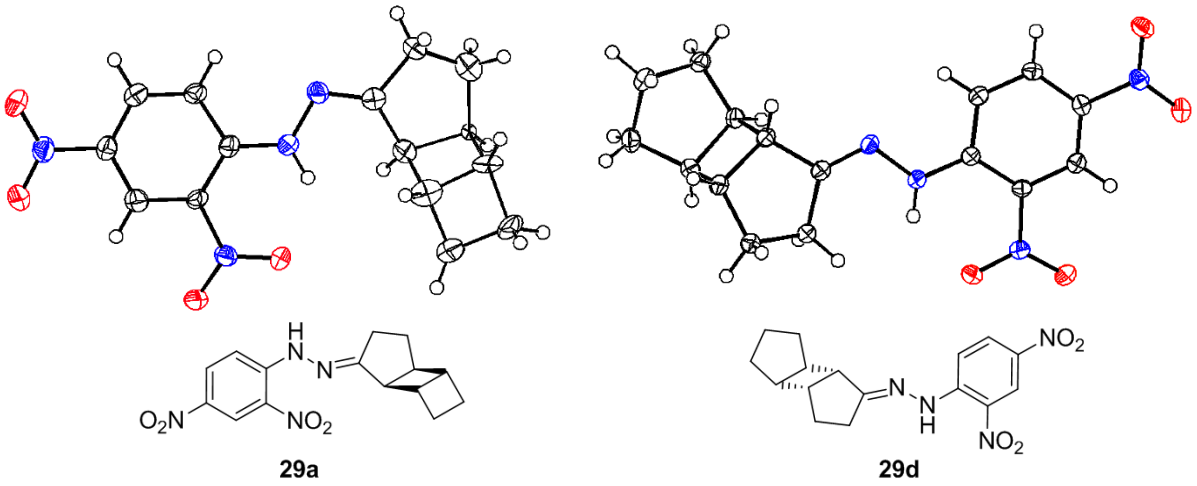

Figure 2.2.1: Molecular structure based on X-ray analysis of **29a** and **29b** revealing their *exo*-configuration. Color code: red, oxygen; blue, nitrogen; white, carbon or hydrogen.

2.2.2 Intramolecular [2+2] Photocycloaddition

Our second approach to obtain fused cycloalkenes is based on the work of *Zitt et al.* in 2002.[14] This group reported an intramolecular photoreaction using a reusable spacer **14** based on a pseudo-geminally substituted paracyclophane to synthesize a cyclobutane derivative **17** carrying two terminal phenyl moieties (Scheme 2.1.3b, p. 26). Inspired by this work, in our present study we evaluated if this intramolecular cycloaddition using a paracyclophane-based diamine spacer (blue in **30**, Scheme 2.2.6) can be performed, employing an extended conjugated system (red in **30**, Scheme 2.2.6) of the starting material **30**, giving access to the ladderane molecule **31** carrying three fused cyclobutane-rings (Scheme 2.2.6).

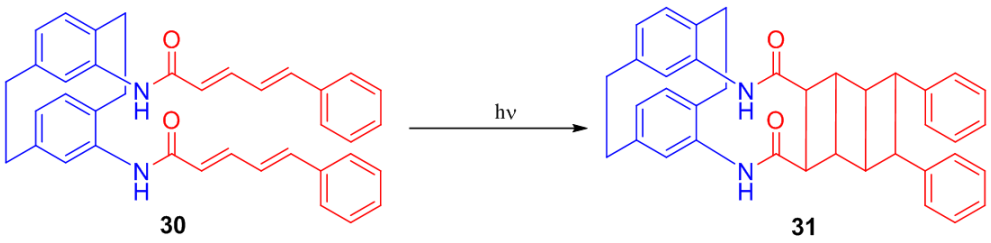

Scheme 2.2.6: Intramolecular [2+2] photocycloaddition of spacer (blue) - conjugated alkene (red) construct **30** yielding ladderane **31** in a single photoreaction.

The spacer **14**, namely 4,15-diamino[2.2] paracyclophane, was synthesized employing the route described by *Zitt et al.* in 2002.[14] As shown in Scheme 2.2.7, the synthesis of **14** starts with the functionalization of one phenyl moiety of the commercial available [2,2] paracyclophane **32** using oxalyl chloride and aluminum trichloride.[20] The obtained keto acid chloride **33** was heated in the subsequent step resulting in a decarbonylation and the formation of the acid chloride **34**.[20]

Esterification of **34** in methanol resulted in the corresponding methyl ester **35**.[20] In the next step a functionalization of the second phenyl moiety of the paracyclophane derivative **35** took place. Using α,α-dichloromethyl methylether and titaniumtetrachloride an aldehyde functionality was introduced yielding the aldehyde **36**. In the subsequent step, both incorporated functionalities, namely the methyl ester and the aldehyde, in **35** were transformed into carboxylic acids *via* hydrolysis with potassium hydroxide and oxidation with hydrogen peroxide, respectively. The resulting bis-acid **37** was further modified by heating at reflux in thionylchloride over 24 hours yielding the bis-acyl chloride **38** which was used for the formation of the bis-acyl azide **39** employing sodium azide. Subsequently, heating of compound **39** resulted in a twofold *Curtius* rearrangement providing bis-isocyanate **40**.[21] Finally, the isocyanate **40** was transferred during a one pot procedure to the bis-amine **14** using ethanol to form the corresponding bis-carbamate followed by a hydrolysis with potassium hydroxide resulting in a decarboxylation.

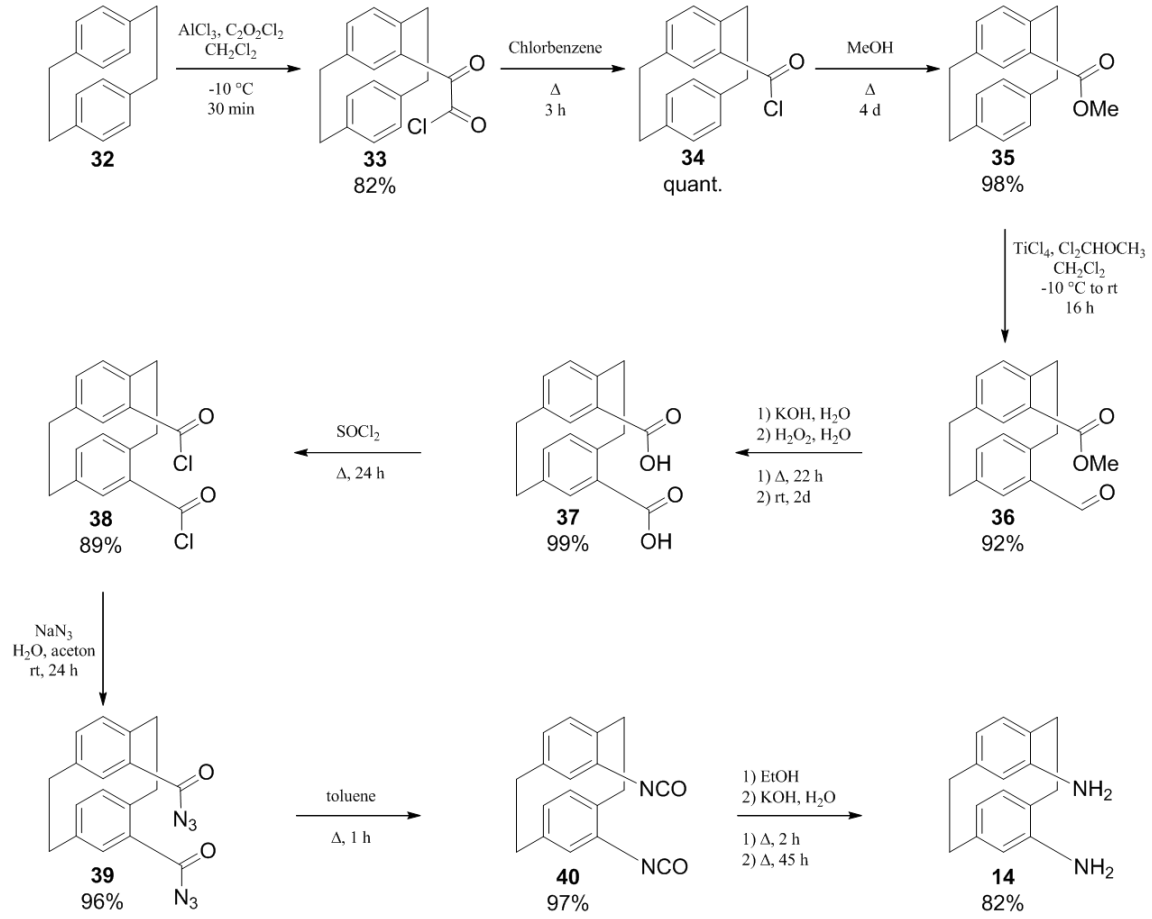

Scheme 2.2.7: Synthesis of 4,15-diamino[2.2] paracyclophane **14**.[14,20]

After the successful synthesis of spacer 4,15-diamino[2.2] paracyclophane **14** in nine steps with an overall yield of 50% the synthesis of the actual substrate **44** was performed (Scheme 2.2.8). First, a HWE (***H**orner-**W**adsworth-**E**mmons*) olefination of the commercially available *trans*-cinnamaldehyde **41** with 2-(diethoxyphosphoryl)acetic acid **42** was employed to obtain bis-alkene **43** (Scheme 2.2.8).[22] Subsequently, as shown in scheme 2.2.8, the treatment of the acid moiety of compound **43** with thionylchloride resulted in the acyl chloride **44** carrying two double bonds in *trans*-configuration.

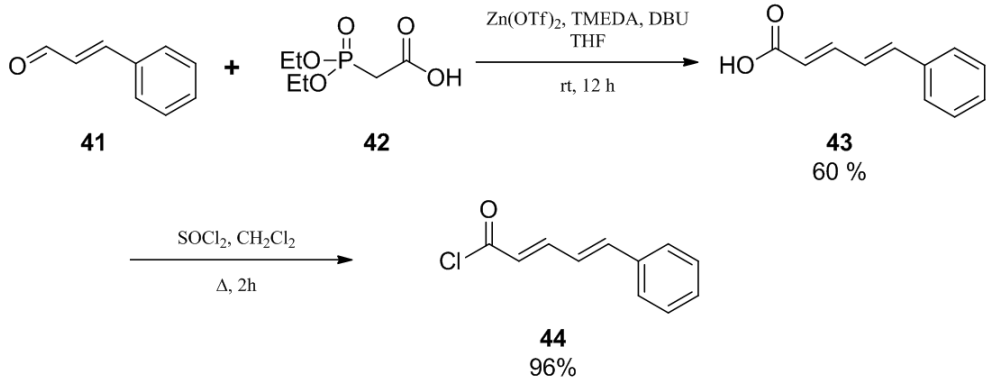

41 **42** **43** 60 % **44** 96%

Scheme 2.2.8: Synthesis of (2E,4E)-5-phenylpenta-2,4-dienoyl chloride **44**.

Finally as shown in scheme 2.2.9, the reusable spacer **14** and the substrate **44** were connected *via* an amide bond formation leading to the starting material **30** for an intramolecular [2+2] photocycloaddition.

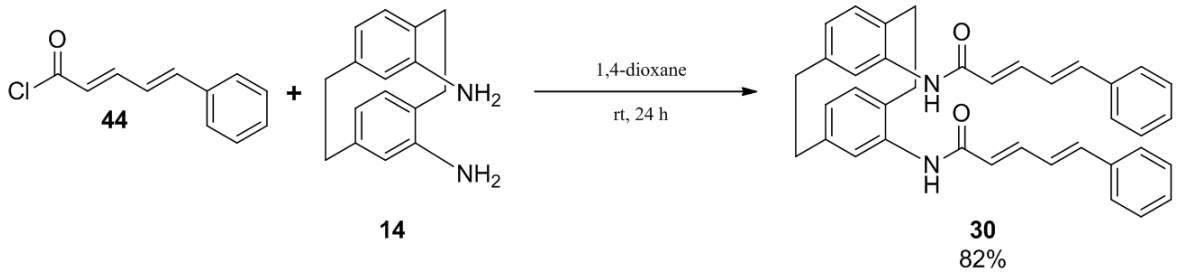

44 **14** **30** 82%

Scheme 2.2.9: Amide bond formation using acyl chloride **44** and spacer **14** resulting in substrate **30**.

Having compound **30** in hand the intramolecular cycloaddition was tested (Scheme 2.2.6, p. 31). However, in a first attempt employing the spacer - conjugated system construct **30** the photocycloaddition resulted in a mixture of several inseparable compounds, which was studied by NMR spectroscopy. Thereby, the complete disappearance of the staring material **30** could be observed (no proton signal between 6.5 and 7 ppm remains). Furthermore, this investigation revealed a photoisomerization and/or the formation of new olefinic moieties (increased proton signals between 6 and 6.5 ppm) as well as the formation of saturated alkane moieties (increased proton signals with ppm lower than 4.5) were detected. Based on these preliminary attempts and the in reference 23 described reactions for similar systems, we suggest that a mixture of photoproducts **45-47** was formed carrying alkenes and cyclic moieties (Figure 2.2.2). This result is in agreement with the literature observation when performing intramolecular

cycloaddition on molecular structures containing several conjugated double bonds.[23] In the work of *Maddipatla et al.* it was described that alkene photoisomerization as well as photodimerization between the unsaturated chains can take place resulting in a variety of products including a cyclooctadiene derivative.

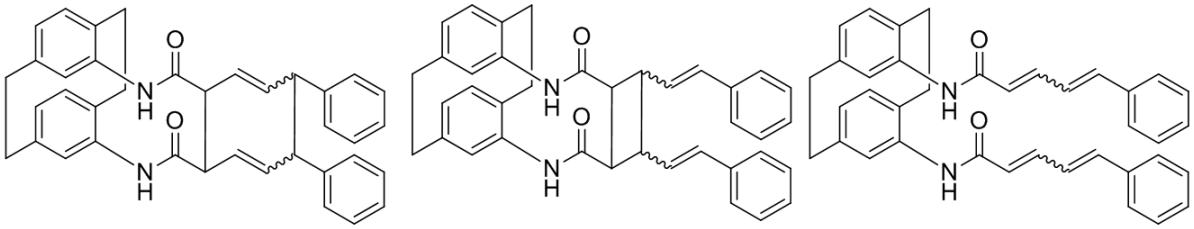

45 **46** **47**

Figure 2.2.2: Suggested composition of the product mixture **45-47** formed during the intramolecular photoreaction of **30**.

Nevertheless, the application of the successfully synthesized compound **30** for the suggested cycloaddition shown in Scheme 2.2.6 (p. 31) needs to be investigated in more detail during future studies to simplify the accessibility of ladderane moieties.

2.3 Conclusion

Summarized, in this chapter inter- and intramolecular [2+2] photochemical cycloadditions were employed as a tool to obtain molecular structures with linear fused cyclobutane rings, known as ladderane units.

For the intermolecular photoreaction first the starting material cyclobutene **8a** was successfully synthesized employing three synthetic steps reaching an overall yield of 41%. In the next step of this study, cycloalkene **8a** was employed in the photochemical intermolecular reaction with cyclopentenone **9** to obtain two fused cyclobutane rings. In the optimization process of the intermolecular cycloaddition it was found that alkenes **8a** and **9** need to be used in a ratio of 2 to 1, respectively, to minimize homo-dimerization of the cyclic enone **9**. Employing the suitable conditions the desired photoproduct **10a** exhibiting two fused cyclobutene rings and one cyclopentanone ring was obtained with a yield of 54%. The very same conditions were also employed successfully for the reaction of enone **9** with cyclopentene **8d** resulting in the desired cycloaddition product **10d** reaching a yield of 62%.

Furthermore, employing X-ray crystallography we demonstrated that both photochemical products **10a** and **10d** with three fused cycloalkane rings exhibit the *exo*-configuration.

It needs to be emphasized that the obtained products **10a** and **10d** are representing the starting point for the synthesis of the ladderane fatty acids shown in Chapter 3.

In the second part of the chapter, we investigated the applicability of the intramolecular cycloaddition using a reusable spacer to obtain ladderane units with three linear fused cyclobutane rings in only one synthetic step. For this purpose the starting material **44** exhibiting two alkene units and a spacer **14**, i.e. a pseudo-geminally substituted paracyclophane, needed to be synthesized. First, spacer 4,15-diamino[2.2]paracyclophane **14** was successfully synthesized employing nine synthetic steps reaching an overall yield of 50%. Further, the alkene unit exhibiting three conjugated *trans*-double bonds, i.e. 5-phenylpenta-2,4-dienoyl chloride **44**, was obtain in two synthetic steps with an overall yield of 58%. Finally, the acyl chloride **44** was attached to the spacer **14** in an amidation reaction yielding the starting material **30** for the intramolecular cycloaddition.

Initial attempts to use construct **30** in the photochemical reaction resulted in the formation of a product mixture instead of the desired ladderane units with three cyclobutane rings. Nevertheless, these results suggest that the synthesized spacer **14** is applicable for intramolecular cycloaddition. Further optimization of the intramolecular cycloaddition in the future might give access to the desired ladderane unit.

2.4 Experimental Section

2.4.1 Materials and Methods

All chemicals and reagents were purchased from commercial suppliers (*Acros* and *Sigma-Aldrich*) and used without further purification. Dry solvents were taken from an *MBraun* solvent purification system (SPS-800). Thin layer chromatographic (TLC) analysis was performed on Merck silicagel 60/Kieselguhr F254, 0.25 mm TLC plates and visualized by UV and staining with *Seebach's* reagent. Column chromatography was performed using silica gel (P60, 230 – 400 mesh).

^{1}H-NMR-, ^{13}C-NMR-, ^{31}P-NMR-, heteronuclear single-quantum correlation- (HSQC) spectra, Nuclear *Overhauser* effect spectroscopy (NOESY) and correlation spectroscopy (COESY) were recorded on a *Agilent 400* (400 MHz for ^{1}H-NMR, 100.59 MHz for ^{13}C-NMR) using $CDCl_3$ ($CDCl_3$: δ 7.26 for ^{1}H-NMR, δ 77.16 for ^{13}C-NMR). Data are reported as follows: chemical shifts, multiplicity (s= singlet, d= doublet, t= triplet, q= quartet, br= broad, m= multiplet), coupling constants *J* (Hz) and integration.

High resolution mass spectrometry (HRMS) was carried out on a LTQ ORBITRAP XL spectrometer (*Thermo Scientific*) employing **e**lectro**s**pray **i**onization (ESI) in positive ion mode (EI+) and negative ion mode (EI-).

X-ray data were collected using a Bruker SMART APEX CCD diffractometer. The diffractometer was equipped with a 4K CCD detector set 60.0 mm from the crystal and the crystal, which was obtained through slow crystallization in CH_2Cl_2/Pentane was cooled to 100 K using the Bruker KRYOFLEX low-temperature device.

2.4.2 General Procedure

[2+2] photocycloaddition:
Setup: A photo reactor with a total volume of 110 ml was equipped with a medium pressure mercury lamp (450W Hanovia® UV lamp). The lamp was cooled using absolute ethanol and was separate from the reaction mixture *via* a Pyrex® cooling jacked.
A solution of 2-cyclopenten-1-one **9** (1 equiv) in anhydrous, degassed acetone (100 mL) was placed in the photo reactor and cooled to -30 °C using an external bath. The cycloalkene **8** (2 equiv) was added as a cold solution in anhydrous, degassed acetone (5 mL) and the irradiation started. After 30 min of irradiation the temperature of the external bath was slowly increased to -5 °C over 2 h. Additional irradiation for 2 to 6 h completed the reaction and the mixture was warmed to room temperature, concentrated under reduced pressure and purified by flash column chromatography (pentane/Et_2O : 9/1).

Dinitrophenylhydrazone synthesis:
The ketone **10** (1 equiv) and DNPH (1.2 equiv) **28** were dissolved in ethanol. The resulting mixture was heated at reflux for 5 min and afterwards slightly cooled below the boiling point of ethanol. Subsequently concentrated HCl (0.1 equiv) was added and the reaction mixture was heated at reflux for an additional 30 min. Finally, cooling of the solution to room temperature and filtration yielded orange crystals of **29**. Repetitive recrystallization (3x) in ethanol gave access to highly pure material for X-Ray studies.

2.4.3 Synthesis and Characterization

Cyclopropylmethyl methanesulfonate (24): Methanesulfonyl chloride (1.5 equiv) was added at -30 °C to a stirred solution of cyclopropanemethanol **23** (1 equiv) in CH_2Cl_2 (0.5 mL/ mmol). Freshly distilled Et_3N (1.6 equiv) was added dropwise to the reaction mixture without allowing the internal temperature to rise above -20 °C. Subsequently, the temperature of the stirred solution was allowed to rise during the next 45 min to 0 °C. Finally, the reaction was quenched by adding dropwise a cold aqueous solution of HCl (3M, 0.1 mL/ mmol) and cold brine (50 mL, 0.1 mL/ mmol). The layers were separated and the aqueous layer was diluted using cold brine (0.5 mL/ mmol). After the extraction of the aqueous phase with CH_2Cl_2 (2 x 0.5 mL/ mmol), the combined organic extracts were washed with cold brine (0.5 mL/ mmol), dried over $MgSO_4$ and carefully concentrated under reduced pressure. The cyclopropylmethyl methanesulfonate **24** was obtained with a yield of 97% and used without further purification in the next step.

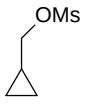

[0.38 mol scale, 97 % yield, yellow oil]
^{1}H NMR (400 MHz, $CDCl_3$); δ (ppm): 4.05 (dd, J=10 Hz, 1.2 Hz, 2H), 3.01 (d, J=1.6 Hz, 3H), 1.22 (m, 1H), 0.66 (dt, J=10.4 Hz, 6.8 Hz, 2H), 0.37 (dt, J= 10.4 Hz, 6.8 Hz, 2H). Measured NMR data are corresponding to the data reported in literature.[12]

Cyclobutyl methanesulfonate (25): $F_3B{\cdot}OEt_2$ (0.06 equiv) was added dropwise at 10 °C to a stirred solution of cyclopropylmethyl methanesulfonate **24** (1 equiv) in anhydrous CH_2Cl_2 (0.5 mL/ mmol). The resulting mixture was warmed to room temperature and stirred for additional 12 h. A cold aq. saturated NH_4Cl solution (0.1 mL/ mmol) was added. The resulting layers were separated and the organic extract was dried over $MgSO_4$ and carefully concentrated under reduced pressure. The product cyclobutyl methanesulfonate **25** was obtained as brown oil with a small amount of impurity **26**, namely but-3-enyl methanesulfonate (10%).

Further purification of the crude product **25**.

An aqueous solution of $KMnO_4$ (2 equiv/impurity, 0.5 mL/ mmol) was added dropwise at 0 °C to a solution of the crude product **25** (1 equiv) in acetone (0.5 mL/ mmol). After stirring for 2 h the reaction mixture was filtered through a bed of Celite®. Subsequently, the Celite® was rinsed with Et_2O (1.5 mL/ mmol) and cold water (0.5 mL/ mmol). The resulting layers were separated and the aqueous layer was extracted twice with Et_2O (2*0.5 mL/ mmol). Finally, the combined organic extracts were dried over $MgSO_4$ and carefully concentrated under reduced pressure. The cyclobutyl methanesulfonate **25** was obtained with a yield of 71% and used without further purification in the next step.

[0.12 mol scale, 71% yield, slightly yellow oil]

^1H NMR (400 MHz, $CDCl_3$); δ (ppm): product: 4.95 (q, J=7.2 Hz, 1H), 2.96 (s, 3H), 2.39 (m, 2H), 2.29 (m, 2H), 1.84 (q, J=10 Hz, 1H), 1.61 (q, J= 10.4 Hz, 1H). Byproduct: 5.78 (m, 1H), 5.15 (dd, J=14, 10.4 Hz, 2H), 4.25 (t, J=9.6 Hz, 2H), 2.97 (s, 3H), 2.49 (dt, J=7.2 Hz, 6.8 Hz, 2H). Measured NMR data are corresponding to the data reported in literature.[12]

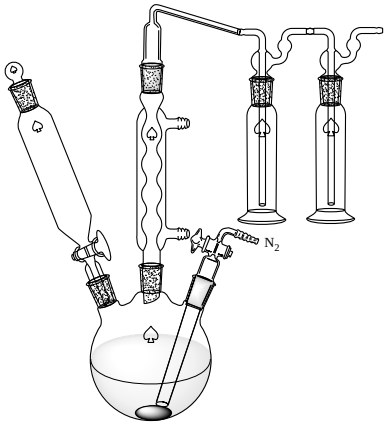

Figure 2.4.1: Cyclobutene synthesis setup.

Cyclobutene (8a): A 250 mL three-necked round bottom flask was equipped with a stirring bar, a dropping funnel, N_2-inlet tube and water-cooled condenser. The outlet of the condenser is attached *via* glass tubes to a trap system (Figure 2.4.1). Two weighed traps which are cooled in an acetone dry ice mixture are attached to the transfer system.

KO*t*Bu (3 equiv) was added to anhydrous DMSO (0.5 mL/ mmol) and heated to 70 °C. A solution of cyclobutyl methanesulfonate **25** (1 equiv) in anhydrous DMSO (0.1 mL/ mmol) was added dropwise over 10 min under a slow stream of N_2. The reaction mixture was stirred and heated for additional 2 h. Cyclobutene **8a** distills off during the reaction and was collected in

the cooled trap. Subsequently, the weight of the filled trap was determined and the obtained product was dissolved in degassed and dry acetone (5 mL). Cyclobutene **8a** was obtained as highly volatile, colorless oil with a yield of up to 60% and was stored in acetone at -70 °C. [0.16 mol scale, 60% yield, colorless oil]

^{1}H NMR (400 MHz, $CDCl_3$); δ (ppm): 6 (s, 2H); 2.55 (s, 4H). Measured NMR data are corresponding to the data reported in leterature.[12]

Tricyclo[4.3.0.0^{2,5}]nonan-7-one (10a): The [2+2] photocycloaddition to obtain cyclobutane derivative **10a** was performed according to the above described general procedure. Cyclobutene **8a** (2 equiv) was added as a cold solution in anhydrous, degassed acetone (5 mL). The title compound **10a** was obtained as colorless oil with a yield of 54%.

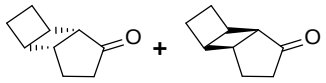

[24 mmol scale, 54% yield, colorless oil]

^{1}H NMR (400 MHz, $CDCl_3$); δ (ppm): 2.99 (t, J= 7 Hz, 1H); 2.77 (d, J= 5 Hz, 1H); 2.64 (m, 1H); 2.57 (m, 4H); 2.27 (dd, J= 20 Hz, J= 11.5 Hz, 1H); 2.18 (m, 2H); 2.06 (m, 1H); 1.95 (m, 1H). ^{13}C NMR (100 MHz, $CDCl_3$); δ (ppm): 221.31 (1C, CO); 53.08 (1C, CH); 42.96 (1C, CH); 41.11 (1C, CH); 37.91 (1C, CH); 36.81 (1C, CH_2); 28.85 (1C, CH_2); 27.08 (1C, CH_2); 26.76 (1C, CH_2). Measured NMR data are corresponding to the data reported in literature.[12]

Tricyclo[5.3.0.0^{2,6}]nonan-8-one (10d): The [2+2] photocycloaddition to obtain cyclobutane derivative **10d** was performed according to the above described general procedure. Cyclopentene **8d** (2 equiv) was added as a cold solution in anhydrous, degassed acetone (5 mL). The title compound **10d** was obtained as colorless oil with a yield of 62%.

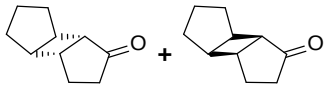

[12.2 mmol scale, 62% yield, colorless oil]

^{1}H-NMR ($CDCl_3$, 400 MHz): δ (ppm) = 2.7 (dq, J= 12.4 Hz, J= 10 Hz, 1H); 2.48 (m, 2H); 2.28 (m, 1H); 2.22 (m, 1H); 2.10 (d, J= 6.4 Hz, 2H); 2.03 (m, 1H); 1.92 (m, 1H); 1.6-1.86 (m, 4H); 1.51 (m, 2H). ^{13}C-NMR ($CDCl_3$, 100 MHz): δ (ppm) = 222.68 (1C; CO); 48.99 (1C, CH); 43.24 (1C, CH); 40.54 (1C, CH); 38.74 (1C, CH); 38.40 (1C, CH_2); 33.27 (1C, CH_2); 33.22 (1C, CH_2); 28.36 (1C, CH_2); 24.78 (1C, CH_2). MS (EI+) (*m/z)*: found 151.112 $[M+H]^+$, calculated 151.112 $[M+H]^+$.

Decahydro-cyclopenta[3,4]cyclobuta[1,2]benzen-1-one (10e):

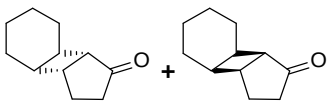

The [2+2] photocycloaddition to obtain cyclobutane derivative **10e** was performed according to the above described general procedure. Cyclopentene **8e** (2 equiv) was added as a cold solution in anhydrous, degassed acetone (5 mL). The title compound **10e** was obtained as colorless oil with a yield of 57%. [12.2 mmol scale, 57% yield, colorless oil]

^{1}H NMR (400 MHz, $CDCl_3$); δ (ppm): mixture of different isomers with broad multiplets from 1.1 to 2.87 ppm. GC/MS: *m/z* = 164.1

Cyclobuta[1,2:3,4]dicyclopentene-1,6-dione (27a) and octahydro-Cyclobuta[1,2:3,4]dicyclopentene-1,4-dione (27b): The [2+2] photocycloaddition to obtain cyclobutane derivative **27a** or **27b** was performed according to the above described general procedure, using cyclopentenone **9** as only substrate. The title compounds **27a** and **27b** were obtained as mixture with a total yield of 62%. The ratio of 1 (**27a**) to 5 (**27b**) was determined *via* NMR studies. Additionally, the separation of both isomers could be performed using two different methods. The first method using flash column chromatography (pentane:ether; 1:1) resulted in the separation of both products **27a** as colorless oil with an isolated yield of 10% and **27b** as colorless crystalline solid with an isolated yield of 51%. The second and faster method however gives only access to the pure isomer **27b**. Thereby, an extraction of isomer **27a,** showing higher solubility in diethyl ether takes place leaving the pure compound **27b** as solid behind. [24 mmol scale, 61% total yield, colorless oil/colorless solid]

27a **27b**

***Endo* (27a):** [10% yield, colorless solid] ^{1}H-NMR ($CDCl_3$, 400 MHz): δ (ppm) = 2.82 (m, 2H); 2.68 (dt, J= 18 Hz, J= 10.4 Hz, 2H); 2.48 (d, J= 5.2 Hz, 2H); 2.35 (dd, J= 17.6 Hz, J= 11.2 Hz, 2H); 2.17 (m, 2H); 2.02 (t, J= 11.6 Hz, 2H). ^{13}C-NMR ($CDCl_3$, 100 MHz): δ (ppm) = 218.37 (2C; CO); 45.00 (2C, CH); 40.19 (2C, CH); 35.68 (2C, CH_2); 27.42 (2C, CH_2). MS (EI+) (*m/z)*: found 165.091 $[M+H]^+$, calculated 165.091 $[M+H]^+$.

***Exo* (27b):** [51% yield, colorless oil] ^{1}H-NMR ($CDCl_3$, 400 MHz): δ (ppm) = 2.82 (m, 2H); 2.68 (dt, J= 18 Hz, J= 10.4 Hz, 2H); 2.59 (d, J= 4.4 Hz, 2H); 2.35 (dd, J= 17.6 Hz, J= 11.2 Hz, 2H); 2.22 (m, 2H); 2.02 (t, J= 11.6 Hz, 2H). ^{13}C-NMR ($CDCl_3$, 100 MHz): δ (ppm) = 219.73 (2C; CO); 49.63 (2C, CH); 37.49 (2C, CH); 36.29 (2C, CH_2); 28.22 (2C, CH_2). MS (EI+) (*m/z)*: found 165.091 $[M+H]^+$, calculated 165.091 $[M+H]^+$.

(E)-1-(2,4-dinitrophenyl)-2-((1*S*,2*R*,5*S*,6*R*)-tricyclo[4.3.0.0^{2,5}]nonan-7-ylidene)hydrazine (29a): Hydrazone **29a** was synthesized using ketone **10a** following the above described procedure. An isolated yield of 75% was obtained after three recrystallization cycles from ethanol.

[0.66 mmol scale, 75% yield, orange solid]

^{1}H-NMR ($CDCl_3$, 400 MHz): δ (ppm) = 10.76 (s, 1H, NH); 9.11 (d, J= 2.8 Hz, 1H); 8.27 (dd, J= 9.6 Hz, J= 2.4 Hz, 1H); 7.89 (d, J= 9.6 Hz, 1H); 3.38 (d, J= 5.6 Hz, 1H); 3.09 (t, J= 7.2 Hz, 1H); 2.81 (m, 1H); 2.71 (dd, J= 8.8 Hz, J= 4.8 Hz, 1H); 2.60 (m, 4H); 2.37 (m, 1H); 2.11 (m, 2H); 1.85 (m, 1H). ^{13}C-NMR ($CDCl_3$, 100 MHz): δ (ppm) = 171.56 (1C; CNNH); 145.48 (1C; CNHN); 137.92 (1C; CNO_2); 130.36 (1C, CH); 129.16 (1C; CNO_2); 124.01 (1C, CH); 116.46 (1C, CH); 45.74 (1C, CH); 45.12 (1C, CH); 40.86 (1C, CH); 37.52 (1C, CH); 32.84 (1C, CH_2); 29.98 (1C, CH_2); 26.52 (1C, CH_2); 26.34 (1C, CH_2). MS (EI+) (*m/z)*: found 339.106 $[M+Na]^+$, calculated 339.107 $[M+Na]^+$.

(E)-1-(2,4-dinitrophenyl)-2-((1*R*,2*S*,6*R*,7*S*)-tricyclo[5.3.0.0^{2,6}]nonan-8-ylidene)hydrazine (29d): Hydrazone **29d** was synthesized using ketone **10d** following the above described procedure. An isolated yield of 72% was obtained after three recrystallization cycles from ethanol.

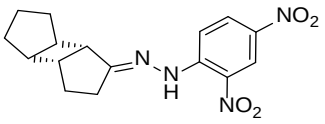

[0.66 mmol scale, 72% yield, orange solid]

^{1}H-NMR ($CDCl_3$, 400 MHz): δ (ppm) = 10.91 (s, 1H, NH); 9.12 (d, J= 2.4 Hz, 1H); 8.27 (dd, J= 9.6 Hz, J= 2.8 Hz, 1H); 7.91 (d, J= 9.6 Hz, 1H); 2.73 (m, 3H); 2.42 (m, 2H); 2.32 (m, 1H); 2.00 (dt, J= 10 Hz, J= 4.4 Hz, 2H); 1.83 (m, 3H); 1.67 (m, 1H); 1.43-1.61 (m, 2H). ^{13}C-NMR ($CDCl_3$, 100 MHz): δ (ppm) = 172.35 (1C; CNNH); 145.60 (1C; CNHN); 137.96 (1C; CNO_2); 130.34 (1C, CH); 129.20 (1C; CNO_2); 124.00 (1C, CH); 116.66 (1C, CH); 47.00 (1C, CH); 42.86 (1C, CH); 42.49 (1C, CH); 39.67 (1C, CH); 33.02 (1C, C_2); 32.81 (1C, CH_2); 30.59 (1C, CH_2); 26.39 (1C, CH_2); 24.71 (1C, CH_2). MS (EI+) (*m/z)*: found 331.139 $[M+H]^+$, calculated 331.140 $[M+H]^+$.

4,15-Diamino[2.2] paracyclophane (14): The reusable spacer **14** was synthesized according to literature procedures given in reference 14 and 20. Measured NMR data are corresponding to the data reported in literature.[14,20] Obtained yields are reported in scheme 2.2.6.

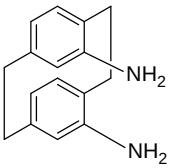

The following steps have been modified from the in reference 19 described procedures:

[2.2] Paracyclophane-4,15-dicarbonyl dichloride (38): A suspension of the bis (acid) **37** (1 equiv) was dissolved in thionyl chloride (30 mL/ mmol and heated at reflux for 24 h. Filtration of the hot solution, subsequent cooling of the filtrate and finally the evaporation of thionyl chloride under vacuum yielded the bis(acid chloride) **38** as brown solid with a yield of 89%. The bis(acid chloride) **38** was used for the further synthesis without additional purification.

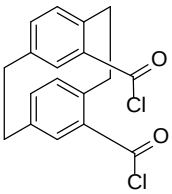

[2.2] Paracyclophane-4,15-dicarbonyl diazide (39): A solution of sodium azide (10 equiv) in water (5 mL/ mmol) was added to a stirred suspension of the bis(acid chloride) **38** (1 equiv) in acetone (6 mL/ mmol). After stirring for 24 h ice water (5 mL/ mmol) was added and the resulting suspension was filtered. The solid was washed with water and dried under vacuum. The product **39** was obtained as a dark yellow solid with a yield of 96% and was used without further purification. NMR dates are in accordance with literature.[20]

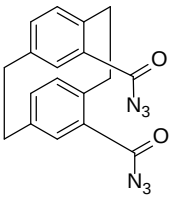

(2E,4E)-5-phenylpenta-2,4-dienoic acid (43): The cinnamaldehyde **41** was purified *via* column chromatography (AlOx; pentane:EtOAc; 14:1) before use. Zinc triflate (2.2 equive) was added to a solution of 2-(diethoxyphosphoryl)acetic acid **42** (1 equiv) in THF (3 mL/ mmol). To the resulting mixture TMEDA (1.1 equiv) and DBU (4 equiv) were added. Subsequently the cinnamaldehyde **41** (1.1 equiv) was added and the reaction mixture was stirred at room temperature for 12 h. An aq. 1M HCL solution (1 mL/ mmol) was added and the resulting layers were separated. The aqueous phase was extracted with CH_2Cl_2 (3x 1 mL/

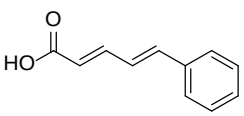

mmol) and all organic layers were combined afterwards. The organic phase was dried over $MgSO_4$ and the solvent was evaporated under reduced pressure. Purification using flash column chromatography (pentane:EtOAc; 7:3) yielded the pure title compound **43** with an isolated yield of 60%. [5.2 mmol scale, 60% yield, colorless solid]
^{1}H-NMR ($CDCl_3$, 400 MHz): δ (ppm) = 7.55 (dd, J= 15.2 Hz, J=9.6 Hz, 1H); 7.50 (m, 2H); 7.35 (m, 3H); 6.94 (m, 2H); 6.00 (d, J= 15.2 Hz, 1H). Measured NMR data are corresponding to the data reported in literature.[22]

(2E,4E)-5-phenylpenta-2,4-dienoyl chloride (44): The carboxylic acid (1 equiv) **43** was dissolved in CH_2Cl_2 (1 mL/ mmol) and thionyl chloride (1.5 equiv) was added. The resulting solution was heated at reflux for 12 h and cooled to room temperature. The precipitate was filtered off and washed with cold CH_2Cl_2. The acid chloride **44** was obtained as a yellowish solid with a yield of 96% and was used without further purification.

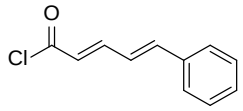

[2.9 mmol scale, 96% yield, colorless oil]
^{1}H-NMR ($CDCl_3$, 400 MHz): δ (ppm) = 7.62 (dd, J= 14.8 Hz, J=11.2 Hz, 1H); 7.52 (m, 2H); 7.39 (m, 3H); 7.10 (d, J= 15.2 Hz, 1H); 6.93 (dd, J=15.6 Hz, J= 11.2 Hz, 1H); 6.20 (d, J= 14.8 Hz, 1H).

[2.2] Paracyclophane-4,15-bis ((2E,4E)-5-phenylpenta-2,4-dienoyl amide) (30): To a suspension of the spacer **14** (1 equiv) in dioxane (20 mL/ mmol) was added a solution of the acid chloride **44** (2 equiv) in dioxane (4 mL/ mmol). The reaction mixture was stirred for 24 h at room temperature before the solvent was removed under reduced pressure. Subsequently, CH_2Cl_2 (30 mL/ mmol) was added to the crude product and the resulting suspension was filtered. The precipitate was washed with CH_2Cl_2 (30 mL/ mmol) and dried under reduced pressure. Subsequently, the solvent of the filtrate was evaporated and the residue was dissolved in a small amount of hot ethanol. Finally after cooling the ethanol solution to room temperature pentane was added and the new formed precipitate was filtered off, washed with CH_2Cl_2 and dried under reduced pressure. The combined fractions gave a total yield of 82% of the compound **30** as a yellowish solid.[14] [2 mmol scale, 82% yield, yellow solid]

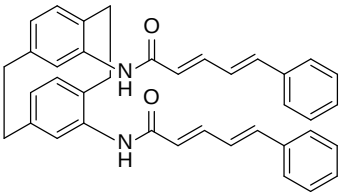

^{1}H-NMR ($CDCl_3$, 400 MHz): δ (ppm) = 7.54 (dd, J= 14.8 Hz, J=10.8 Hz, 2H); 7.3 (d, J= 7.6 Hz, 4H); 7.24 (t, J= 7.2 Hz, 2H); 7.12 (t, J= 7.6 Hz, 4H); 6.88 (d, J= 15.6 Hz, 2H); 6.74 (m, 4H); 6.48 (d, J= 8 Hz, 2H); 6.38 (d, J= 7.6 Hz, 2H); 6.1 (d, J= 14.8 Hz, 2H); 3.34 (m, 2H); 3.05 (m, 4H); 2.86 (m, 2H). MS (EI+) (*m/z*): found 151.112 $[M+H]^+$, calculated 151.112 $[M+H]^+$.

2.5 References

1) G. Ciamician, P. Silber. Chemische Lichtwirkungen. *Chem. Ber.*, **41**, 1928-1935 (1908).
2) G. Büchi, I. M. Goldman. Photochemical Reactions. VII. The Intramolecular Cyclization of Carvone to Carvonecamphor, *J. Am. Chem. Soc.*, **79**, 4741-4748 (1957).
3) N. Hoffmann. Photochemical Reactions as Key Steps in Organic Synthesis. *Chem. Rev.*, **108**, 1052 – 1103 (2008).
4) P. E. Eaton, T. W. Cole. Cubane. *J. Am. Chem. Soc*., **86**, 3157–3158 (1964).
5) P. Lu, T. Bach. Total Synthesis of (+)-Lactiflorin by an Intramolecular [2+2] Photocycloaddition. *Angew. Chem. Int. Ed*., **51**, 1261-1264 (2012).
6) S. C. Coote, T. Bach. Enantioselective Intermolecular [2+2] Photocycloadditions of Isoquinolone Mediated by a Chiral Hydrogen-Bonding Template. *J. Am. Chem. Soc*., **135**, 14948-14951 (2013).
7) M. Racamonde, R. Alibés, M. Figueredo, J. Font, P. de March. Photochemical Cycloaddition of Mono-, 1,1- and 1,2-Disubstituted Olefins to a Chiral 2(*5H*)-Furanone. Diastereoselective Synthesis of (+)-Lineatin. *J. Org. Chem*. **73**, 5944–5952 (2008).
8) A. Rauk. Orbital Interaction Theary of Organic Chemistry. *John Wiley & Sons*, 2nd Ed. 209-212 (2001).
9) A. Jabłoński. Efficiency of Anti-Stokes Fluorescence in Dyes. *Nature*. **131**, 839-840 (1933).
10) J. S. Sinninghe Damsté, M. Strous, W. I. C. Rijpstra, E. C. Hopmans, J. A. J. Geenevasen, A. C. T. van Duin, L. A. van Niftrik, M. S. M. Jetten. Linearly concatenated cyclobutane lipids form a dense bacterial membrane. *Nature*, **419**, 708-712 (2002).
11) V. Mascitti, E. J. Corey. Total Synthesis of (±)-Pentacycloanammoxic Acid *J. Am. Chem. Soc.*, **126**, 15664-15665 (2004**)**.
12) V. Mascitti, E. J. Corey. Enantioselective Synthesis of Pentacycloanammoxic Acid. *J. Am. Chem. Soc.*, **128**, 3118–3119 (2006).
13) a) H. Hopf, H. Greiving, C. Beck, I. Dix, P. G. Jones, J.-P. Desvergne, H. Bouas-Laurent. One-Pot Preparation of [n]Ladderanes by [2π+2π] Photocycloaddition. *Eur. J. Org. Chem*., **2005**, 567-581 (2005). b) Also reported in C. Beck's Ph.D. Dissertation: Synthesis and Photochemistry of [2.2]Paracyclophane Derivatives. Braunschweig, 1999.
14) H. Zitt, I. Dix, H. Hopf, P. G. Jones. 4,15-Diamino[2.2]paracyclophane, a Reusable Template for Topochemical Reaction Control in Solution. *Eur. J. Org. Chem.*, **2002**, 2298-2307 (2002).
15) T. Friščić, L. R. MacGillivray. Reversing the code of a template-directed solid-state synthesis: a bipyridine template that directs a single-crystal-to-single-crystal [2+2] photodimerisation of a dicarboxylic acid. *Chem. Commun*., **2005**, 5748–5750 (2005).
16) L. R. MacGillivray, G. S. Papaefstathiou, T. Friščić, T. D. Hamilton, D.-K. Bučar, Q. Chu, D. B. Varshney, I. G. Georgiev. Supramolecular Control of Reactivity in the Solid State: From Templates to Ladderanes to Metal-Organic Frameworks. Acc. *Chem. Res*., **41**, 280-291 (2008).

17) X. Mei, S. Liu, C. Wolf. Template-Controlled Face-to-Face Stacking of Olefinic and Aromatic Carboxylic Acids in the Solid State. *Org. Lett*., **9**, 2729-2732 (2007).
18) J. Salaün, A. Fadel. Cyclobutene. *Org. Syn.*, **7**, 117 (1990) or *Org. Syn.*, **64**, 50 (1986).
19) J. Grota, I. Domke, I. Stoll, T. Schröder, J. Mattay, M. Schmidtmann, H. Bögge, A. Müller. Synthesis, Fragmentation, and Rearrangement Reactions of Annelated Cyclobutylcarbinols. *Synthesis*, **14**, 2321-2326 (2005).
20) M. Psiorz, R. Schmid. Cyclophane, I. Ein einfacher Zugang zu funktionalisierten [2.2] Paracyclophanen. *Chem. Ber*., **120**, 1825-1828 (1987).
21) T. Curtius. 20. Hydrazide und Azide organischer Säuren I. Abhandlung. *J. Prak. Chem.*, **50**, 275-294 (1894).
22) D. J. Schauer, P. Helquist. Mild Zinc-Promoted Horner-Wadsworth-Emmons Reactions of Diprotic Phosphonate Reagents. *Synthesis*, **2006**, 3654–3660 (2006).
23) M. V. S. N. Maddipatla, M. Pattabiraman, A. Natarajan, K. Srivastav, J. T. Mague, V. Ramamurthy. Regioselective photodimerization of pyridyl-butadienes within cucurbit[8]uril cavities. *Org. Biomol. Chem*., **10**, 9219-9222 (2012).

Chapter 3

Synthesize of Ladderane based fatty acids

It has been found that fatty acids incorporating cyclobutane moieties show exceptional properties which make the surviving of the host organism in harsh and toxic environment possible. An example is the presence of linear fused cyclobutane rings, named a ladderane unit, in natural products, such as *Pentacycloanammoxic* acid. However, the synthesis of these natural products bearing ladderane structures is challenging. Therefore, after having synthesized successfully precursors in Chapter 2, the ketone bearing fused cycloalkanes are employed in this chapter to synthesize new ladderane fatty acids. The new amphiphilic structures exhibiting three cycloalkane rings and a double bond were obtained employing seven synthetic steps in overall yield of up to 15%.

3.1 Introduction

Several studies have indicated the existence of bacteria which are able to oxidize ammonium (NH_4^+) under anaerobic conditions.[1,2] This was demonstrated experimentally for the first time in The Netherlands in 1995 where in a bioreactor ammonium was converted into nitrogen (N_2) gas under anaerobic conditions in presence of nitrite (NO_2^-) (Figure 3.1.1a).[2,3] In 1999, *Strous et al.* identified the for this process responsible **an**aerobic **amm**onium **ox**idizing (anammox) bacteria as a new member of the *planctomycetes*.[4] *Jetten et al.* described in 2001 the oxidation of ammonium *via* anammox bacteria forming toxic intermediates, i.e. hydroxylamine (NH_2OH) and hydrazine (N_2H_4).[3] As shown in Figure 3.1.1b, reduction of nitrite to hydroxylamine takes place followed by the formation of hydrazine through the incorporation of ammonium. Finally, nitrogen gas is generated by oxidation of the previously formed hydrazine. The through the anammox bacteria performed anaerobic process described in Figure 3.1.1 is of great interest for wastewater treatment.[5] This process gives access to a new strategy to remove nitrogen-containing compounds from wastewater combining two conventional applied technologies, i.e. nitrification and denitrification (Figure 3.1.1c).[6] The advantage of the application of anammox bacteria for this purpose is that they perform both steps, nitrification and denitrification. Furthermore, no external electron donor like methanol and no oxygen are required.

a $NH_4^+ + NO_2^- \longrightarrow N_2 + 2\ H_2O$

b $NO_2^- + 5\ H^+ + 4\ e^- \longrightarrow NH_2OH + H_2O$

$NH_2OH + NH_4^+ \longrightarrow N_2H_4 + H_2O + H^+$

$N_2H_4 \longrightarrow N_2 + 4\ H^+ + 4\ e^-$

c

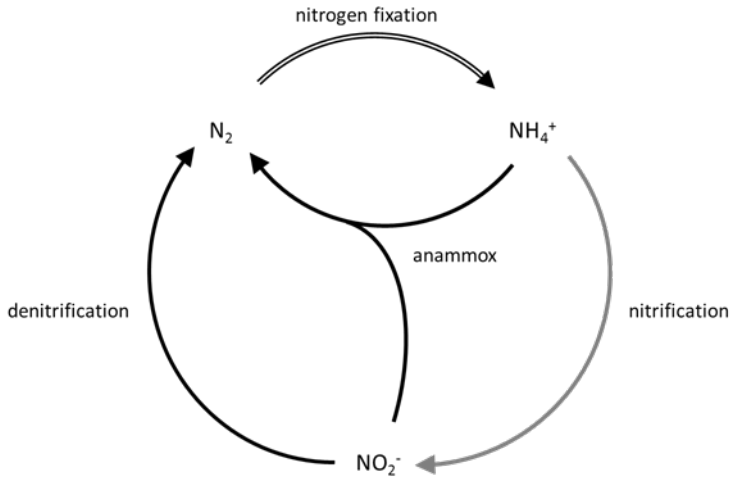

Figure 3.1.1: (a) Overall redox reaction during the anammox process. (b) Stepwise process showing the generation of toxic intermediates hydrazine (N_2H_4) and hydroxylamine (NH_2OH). (c) Nitrogen cycle. Color code: Black arrow represents anaerobic reactions, gray arrow represents aerobic reactions and hollow arrow represents anaerobic and aerobic reactions. Figure adapted from the in reference 6 and 7 reported data.

The above described anammox catabolism is located at the for bacteria unique organelle, the anammoxosome (Figure 3.1.2). This organelle represents the largest compartment of the bacteria occupying around 60% of the cell.[8] As shown in Figure 3.1.2, the surface of the compartment is enlarged by extensive folding of the membrane.[9] In the anammoxosome the energy metabolism takes place which is necessary for the grow of the anammox and therefore, the function of this organelle can be compared to that of eukaryotic mitochondria.[10] The anammoxosome is surrounded by a cytoplasmic compartment, the riboplasm, in which ribosomes and nucleotides are located. Furthermore, the cell wall typical for *Planctomycetes*, consisting of an intracytoplasmic and a cytoplasmic membrane, is also present in anammox bacteria. As shown in Figure 3.1.2, between these two membranes the paryphoplasm, the outermost compartment, is located. The function of this compartment is still unknown and the presence of ribonucleic acids is presumed.[7,11]

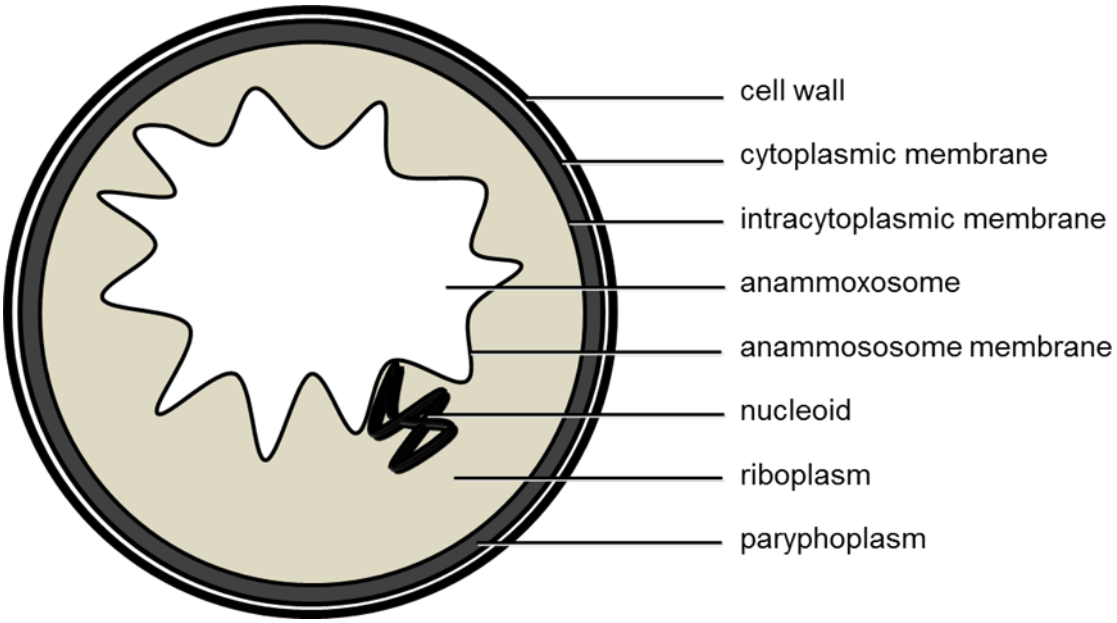

Figure 3.1.2: Schematic drawing of the anammox bacteria cell adapted from reference 7.

The anammoxosome exhibits a membrane known as anammoxosome membrane. Various studies have shown that this membrane incorporates several highly interesting lipids.[12-16] In 2002 *Sinninghe Damsté et al.* reported the discovery of fatty acids carrying three to five linear fused cyclobutane rings (Figure 3.1.3).[12] Due to the three-dimensional structure of this acids they are known as [3]- and [5]-ladderanes. A variety of the most common compositions of the ladderane-containing lipids are shown in Figure 3.1.3. Furthermore, it was observed that in addition to the ester bonds typical for bacteria and eukaryotes also ether bonds are present to connect the aliphatic alcohol to the glycerol backbone.[14] Those connections, which are mainly found in *Archaea*, have been found so far in only a few bacteria, such as *Aquifex* and *Thermotoga*.[17,18] It needs to be noted that both genera are found in locations with high temperatures. Also, *Sinninghe Damsté et al.* demonstrated in 2002 the low permeability of the anammoxosome membrane for small molecules at temperatures between 0 and 92 °C as well as pH values between 4 to 9 via staining experiments.[12] Additionally, molecular modeling of

ladderane-containing membranes resulted in calculated density values of up to 50% higher than for conventional membranes.[6,12] The low permeability, high temperature- and pH tolerance of this unique membrane facilitate the anammox catabolism with its toxic intermediates.

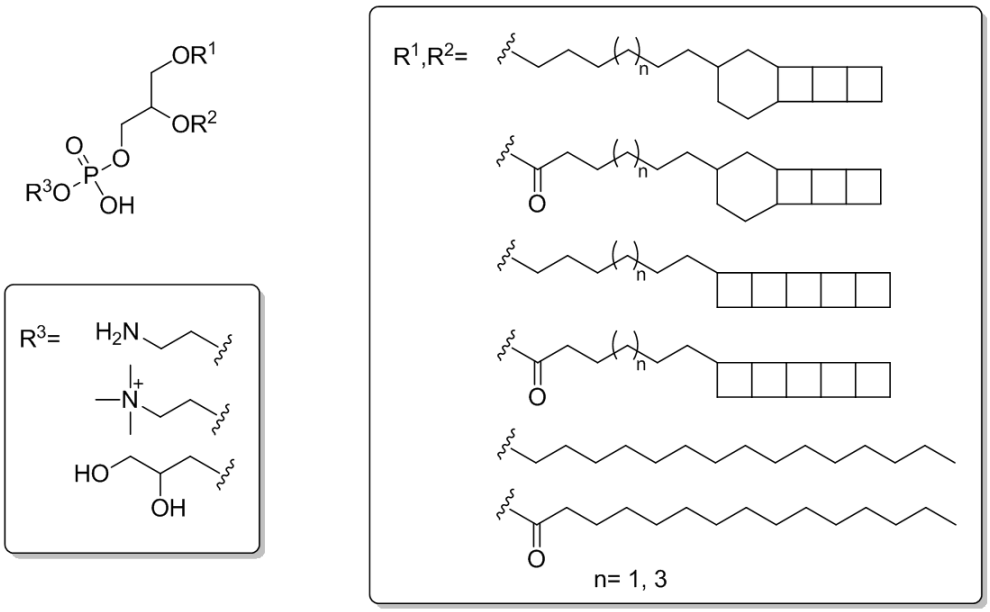

Figure 3.1.3: Variable composition of Ladderane lipids.

The unique structure, the interesting properties and the low availability of ladderane lipids resulted in growing interest in the synthesis of the natural products shown in Figure 3.1.3. The first total synthesis of *pentacycloanammoxic acid* **1** was reported by *Mascitti and Corey* in 2004 (Scheme 3.1.1).[19] The 13-step synthesis contains three photo induced reactions leading to the five linear fused cyclobutane rings of the acid **1**. As shown in Scheme 3.1.1, a [2+2] photocycloaddition between the commercial available cyclopentenone **3** and the in two steps accessible alkene **2** yielded the intermediate **4**. Subsequently, the carbonyl group of **4** was protected and the resulting dimethyl acetal **5** was used for a second photo reaction enabling the formation of two additional cyclobutene rings. To obtain the fifth cyclobutene moiety a ring contraction of the cyclopentenone **6** was performed in three steps. As shown in Scheme 3.1.1, formylation in the α-position followed by a *Regitz* diazo-transfer yielded an α-diazo ketone **7** which was employed in a photo-induced *Wolff* rearrangement resulting in derivative **8** exhibiting five cyclobutane rings. Reduction of methyl ester **8** with DIBAL-H (**di**iso**b**utyl**al**uminium**h**ydride) and subsequent *Swern* oxidation gave access to the aldehyde **9**. Finally, by applying a *Wittig* olefination and reduction of the obtained olefin resulted in the desired natural ladderane lipid **1**. However, do to the low yield (6%) during the photochemical N_2 extrusion only a moderate overall yield of less than 1% for **1** could be reached. Hence, *Mascitti and Corey* published in 2006 a modified pathway and obtained the *Pentacycloanammoxic acid* **1** with an overall yield of 5% employing 18 synthetic steps.[20]

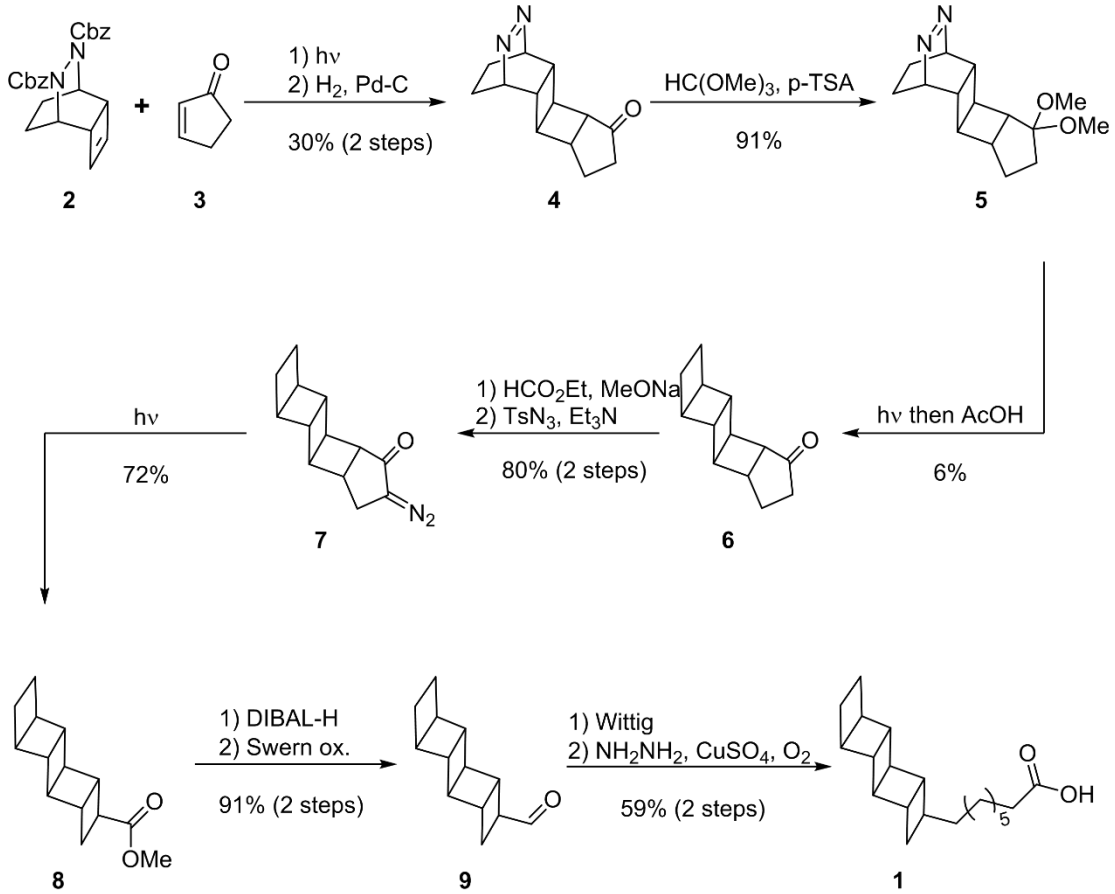

Scheme 3.1.1: Fist total synthesis of *Pentacycloanammoxic acid* **1** by *Mascitti* and Corey in 2004.[19]

3.2 Results and Discussion

In this chapter we describe the syntheses of ladderane molecules **1a** and **1d** (Scheme 3.2.1) based on the in nature discovered [5]- and [3]-ladderane fatty acids. As shown in Scheme 3.2.1, these derivatives are carrying three linear fused cycloalkane rings with a cyclobutane or cyclopentane moiety in terminal position of the hydrophilic tail. Hence, the in Chapter 2 synthesized cyclobutane derivatives **10a** and **10d** (Scheme 3.2.1) are used as starting materials. To obtain fatty acids **1a** and **1d** we followed the synthetic pathway described by *Mascitti* and *Corey* in 2006.[20] In the following past, the total synthesis of **1a** and **1d** carrying each a mono unsaturated C11 chain and three linear fused cycloalkane rings is described.

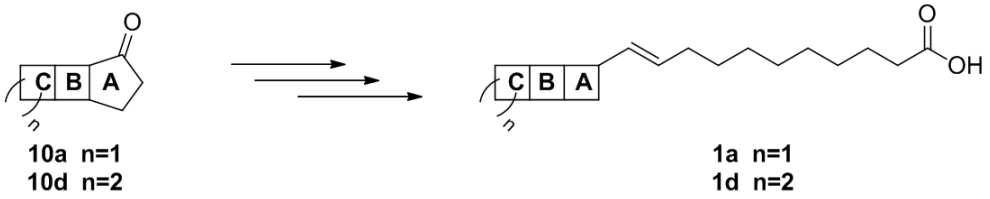

Scheme 3.2.1: Molecular structure of starting materials **10a** and **10d** as well as of the desired ladderane derivatives **1a** (n=1) and **1d** (n=2).

To obtain a trisubstituted cyclobutene moiety (ring A in **1a** and **1d**, Scheme 3.2.1) in the terminal position of fatty acid **1** we chose to perform a *Wolff* rearrangement. As shown in Scheme 3.2.2, to obtain the required α-diazo ketones **12a** and **12d** for the rearrangement reaction, the cyclopentenone moiety (ring A) of **10a** and **10d** needs to be activated in the α-position by a formylation reaction using **e**thyl **f**ormate (EF) resulting in *α*-hydroxymethylene ketones **11a** and **11d**, respectively. The subsequent *Regitz* diazo-transfer reaction gives access to the desired starting materials **12a** and **12d** for the *Wolff* rearrangement (Scheme 3.2.2).

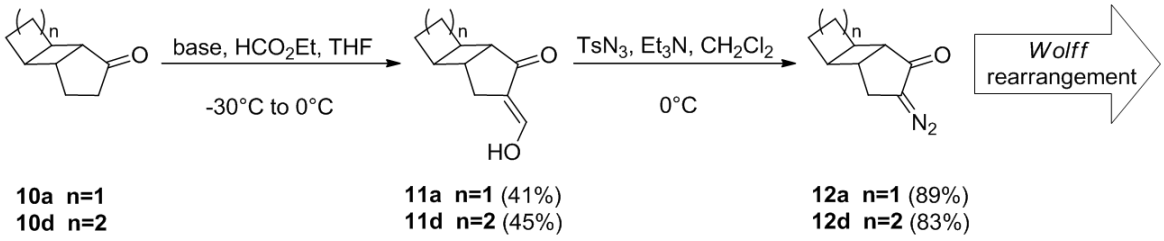

Scheme 3.2.2: Synthesis of α-diazo ketones **12a** and **12d**, precursors for the Wolff rearrangement.

In order to optimize the formylation reaction, different reaction conditions were tested. In this regard, cyclohexanone **13** was used as a model substrate to obtain the corresponding activated ketone **14** (Scheme 3.2.3). The utilization of the commercial available organic bases like Et_3N, *n*-BuLi (*n*-**bu**tyl**li**thium), NaHMDS (sodium **h**exa**m**ethyl**d**i**s**ilazide), KHMDS (potassium **h**exa**m**ethyl**d**i**s**ilazide), NaOMe and freshly prepared LDA (**l**ithium **d**iisopropyl**a**mide) resulted

in isolated yields of up to 75% of **14** (Scheme 3.2.3). However, using same conditions and **e**thyl **f**ormate (EF) for the transformation of ketone **10a** resulted only in moderate yields of **11a** ranging from 25 % to 41% (Table 3.2.1, entries 1 to 4). In order to increase the yield of the formylation reaction we tested the application of freshly synthesized 2,2,2-**t**ri**f**luoro**e**thyl **f**ormate (TFEF) instead of EF. This reagent was already employed successfully by *Zayia* in 1999.[21] However, as shown in Table 3.2.1 (entry 5) the application of TFEF resulted in a comparable yield of **11a** as observed previously employing EF (entry 4). Using ketone **10d** as starting compound and EF as reagent in the presence of LDA gave the corresponding α-hydroxymethylene ketone **11d** in a yield of 45%.

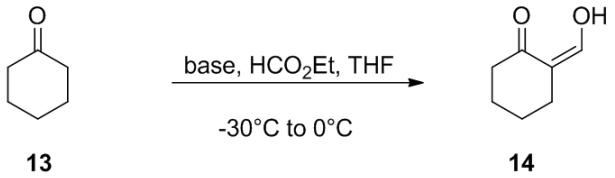

Scheme 3.2.3: Model reaction used to optimize the formylation reaction.

Table 3.2.1: Reaction conditions used for the formylation of ketone **10a**.

Entry	Base	Formate	Temp. (°C)	Time (h)	*Yield (%)
1	NaHMDS	EF	-45 to 0	3	25
2	*n*-BuLi	EF	-45 to 0	3	28
3	LDA	EF	-78 to -45	3	38
4	LDA	EF	-78 to -45	8	41
5	LDA	TFEF	-78 to -45	8	40

All reactions were performed employing the general procedure (see Experimental part, 3.4.2). *Yields are given for α-hydroxymethylene ketone **11a**.

As shown in scheme 3.2.2, the obtained α-hydroxymethylene derivatives **11a** and **11d** were further transformed in a *Regitz* diazo-transfer reaction. The tosylazide necessary for this diazotation was synthesized accordingly to the procedure described by *Ghosh et al.* in 2003.[22] The corresponding α-diazoketones **12a** and **12d** were obtained in isolated yields of 89% and 83%, respectively. Both synthetic steps, i.e. formylation and the diazo-transfer reaction, were performed subsequently avoiding the purification of the intermediates **11a** and **11d** resulting in comparable overall yields of up to 33% and 35% for **12a** and **12d**, respectively.

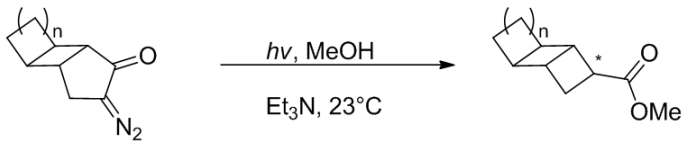

12a n=1
12d n=2

15a n=1 (77%)
15d n=2 (75%)

Scheme 3.2.4: *Wolff* rearrangement of **12a** and **12d**.

After successful synthesis of α-diazoketones **12a** and **12d** a *Wolff* rearrangement was performed to give access to **15a** and **15d** exhibiting a trisubstituted cyclobutene moiety (ring A, Scheme 3.2.4). Methyl esters **15a** and **15d** were obtained reaching yields of 77% and 75%, respectively. It needs to be noted that the rearrangement resulted in two isomers, i.e. the *endo*- and *exo*-isomer (stereo center marked in Scheme 3.2.4). ^{1}H-NMR studies revealed that compounds **15a** and **15d** were obtained in a ratio of 3 to 1 of their corresponding *endo*- and *exo*-isomers. Nevertheless, as shown in Scheme 3.2.5, we utilized methyl esters **15a** and **15d** as isomer mixture for subsequent reactions to obtain aldehydes **17a** and **17d**, respectively. First, **15a** and **15d** were reduced applying DIBAl-H (**D**i**i**so**b**utyl**al**uminium **h**ydride) resulting in alcohols **16a** and **16d**, respectively (Scheme 3.2.5). Employing a *Swern* oxidation of the corresponding alcohol the desired aldehyde **17a** or **17d** was obtained reaching isolated yields of up to 86% and 68%, respectively, over two steps (Scheme 3.2.5).

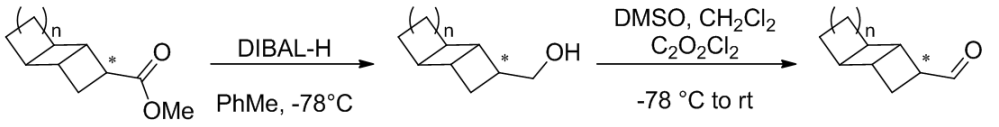

15a n=1
15d n=2

16a n=1 (95%)
16d n=2 (93%)

17a n=1 (90%)
17d n=2 (73%)

Scheme 3.2.5: Synthesis of the aldehyde **17a** and **17d**.

Finally, a isomerization of **17a** and **17d** was performed to give access to the desired *exo*-isomer as main product (Figure 3.2.1a). Hence, isomer mixture of **17a** and **17d** was stirred in triethylamine at room temperature. The isomerization process was monitored by ^{1}H-NMR spectroscopy. As shown in Figure 3.2.1b, employing a reaction time of six days the isomerization resulted in a final *endo*/*exo* ratio of 1 to 6 for compound **17a**. A similar result was obtained for the isomerization of aldehyde **17d** (data not shown).

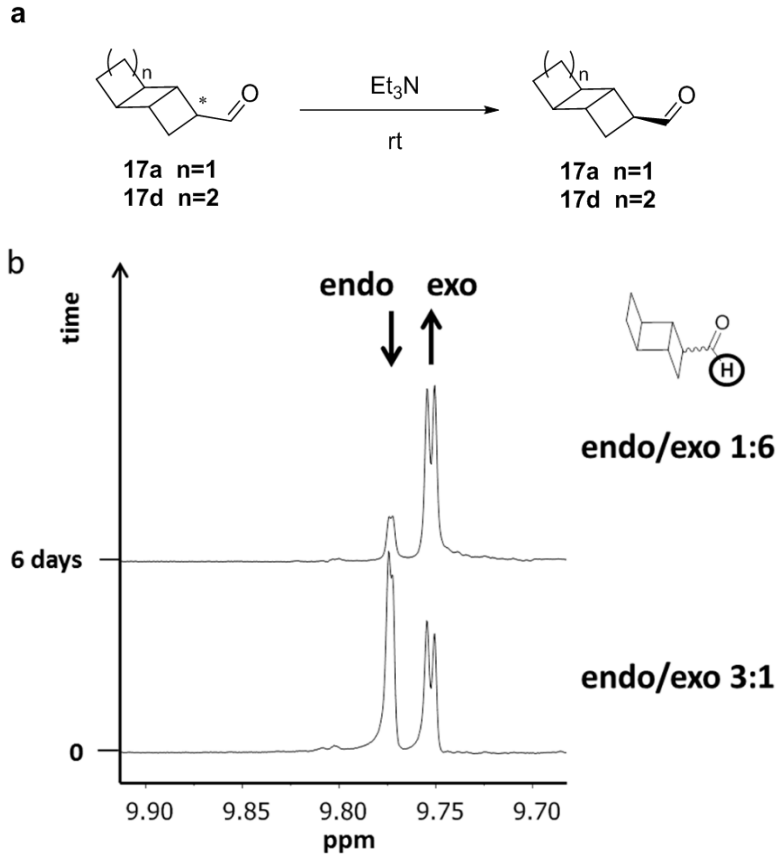

Figure 3.2.1: (a) Thermal isomerization of aldehydes **17a** and **17d**. (b) ^{1}H-NMR spectra of the isomer mixture of **17a** before isomerization (lower spectrum) and after isomerization (upper spectrum).

After having successfully synthesized ladderane aldehydes **17a** and **17d** we performed an elongation at the terminal position to obtain the final ladderane fatty acids **1a** and **1d**. As shown in Scheme 3.2.6c, for this purpose we have chosen to employ the *Wittig* reaction using the aliphatic phosphonium salt **19**. But prior to the final synthetic step, the *Wittig* salt **19** was first synthesized from 10-bromodecanoic acid **18** (Scheme 3.2.6.a). Using solvent free conditions, bromide **18** was transform to salt **19** in melted PPh_3 at 100 °C in quantitative yield. Also, before transforming **17a** and **17b** to their corresponding fatty acids **1a** and **1d**, respectively, we decided to use the obtained salt **19** to perform a *Wittig* reaction employing valeraldehyde **20** as a model compound (Scheme 3.2.6b). In this study, it was found that due to the low solubility of **19** an excess of base was needed and longer deprotonation times were necessary to form the more soluble ylide. Furthermore, in order to optimize the reaction conditions of the Wittig reaction, several bases were used to obtain the olefin **21** (Scheme 3.2.6b, Table 3.2.2, entries 1-5). While *n*-BuLi and LiHMDS gave the desired product **21** in only low yields (Table 3.2.2, entries 1 and 3), using NaHMDS resulted in a moderate yield (Table 3.2.2, entry 2). Nevertheless, best results were achieved employing LDA as base (Table 3.2.2, entries 4 and 5). However, it needs to be emphasized that fresh preparation of LDA is essential to obtain olefin **21** in a high yield reaching 82% (Table 3.2.2, entry 5).

After optimization of the reaction conditions, aldehydes **17a** and **17d** were used in a *Wittig* reaction with salt **19** to provide the corresponding ladderane fatty acids **1a** and **1d**, respectively (Scheme 3.2.6c). As shown in Table 3.2.2 (entry 6 and 7), the amphiphilic compounds **1a** and

1d were obtained in a yield of 62% and 53%, respectively, using LDA as base. The crude product, composed of a *Z*:*E* mixture with a ratio of 1:2 and 1:3 for **1a** and **1d**, respectively, was purified by column chromatography yielding the pure E-isomer. Both products **1a (E)** and **1d (E)** were analyzed using ^{1}H-, ^{13}C-NMR and exact mass (Data shown in experimental section 3.4.2). No further modification of **1a** and **1d** were performed due to shortage of material. However, already at this point the optimized synthetic pathway for fatty acids containing ladderane moieties gives access to several derivatives of the naturally occurring acid. Hence, further studies are of high interest analyzing the direct influence of ring-size and unsaturation on the packing behavior of ladderane fatty acids. Therefore, the synthesis of phospholipids containing these fatty acids would allow aggregation studies using analytical methods like cryo-TEM (**cryo**genic **t**ransmission **e**lectron **m**icroscopy) and DSC (**d**ifferential **s**canning **c**alorimetry).

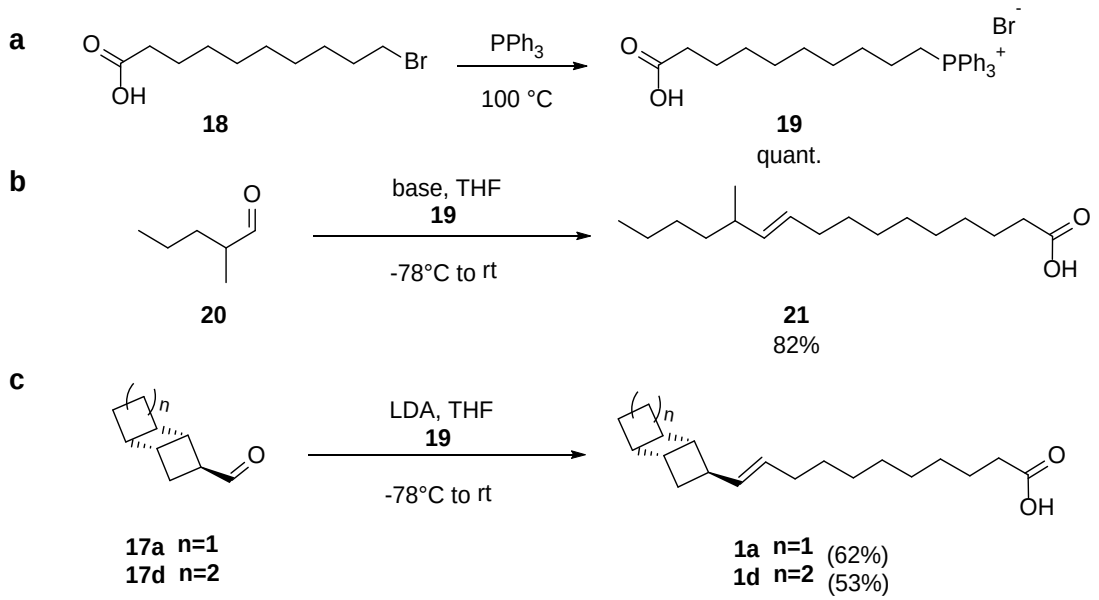

Scheme 3.2.6: (a) Synthesis of the *Wittig* salt **19**. (b) Test reaction with valeraldehyde **20**. (c) Synthesis of the desired ladderane derivatives **1a** and **1d**.

Table 3.2.2: Reaction conditions applied during the *Wittig* reaction using **20**, **17a** and **17d** as starting material.

Entry	Substrate	Product	Base (equiv)	Time (h)	Yield (%)
1	**20**	**21**	BuLi	4	23*
2	**20**	**21**	NaHMDS	2	50
3	**20**	**21**	LiHMDS	2	24
4	**20**	**21**	LDA	2	59
5	**20**	**21**	LDA**	2	82
6	**17a**	**1a**	LDA**	2	62
7	**17d**	**1d**	LDA**	2	53

All reactions were performed employing the general procedure (see experimental part 3.4.2) in THF at temperatures between -78 °C and 0 °C. * Including small amount of unknown side product; reaction was performed using temperatures between -78 °C and room temperature. ** Fresh prepared LDA.

3.3. Conclusion

In this chapter, new ladderane fatty acid derivatives **1a** and **1d** have been successfully synthesized. Amphiphiles **1a** and **1d** were obtained in seven synthetic steps starting from the corresponding ketones **10a** and **10d** (see synthesis in Chapter 2.2) in an overall yield of 15% and 10%, respectively. Essential for the success was the optimization of two key steps, i.e. formylation reaction of the ketones **10a** and **10d** and the *Wittig* reaction to transform the corresponding aldehydes **17a** and **17d** to the desired products **1a** and **1d**, respectively. A further key step in this synthetic path way is the application of an isomerization reaction of the aldehydes **17a** and **17d**. It needs to be emphasized that employing *Wolff* rearrangement yielded both aldehydes as mixture of isomers resulting mainly in an undesired *endo*-product. However, employing subsequently a thermal isomerization under basic conditions both aldehydes **17a** and **17d** were obtained mainly as *exo*-isomer.

Having in mind that ladderane structures allow bacteria to survive in an environment of high temperatures and of a broad range of pH value, the obtained compounds **1a** and **1d** will be of use for future studies allowing access to more stable artificial membranes.

3.4 Experimental Section

3.4.1 Materials and Methods

All chemicals and reagents were purchased from commercial suppliers (*Acros* and *Sigma-Aldrich*) and used without further purification. Dry solvents were taken from an *MBraun* solvent purification system (SPS-800). Thin layer chromatographic (TLC) analysis was performed on Merck silicagel 60/Kieselguhr F254, 0.25 mm TLC plates and visualized by UV and staining with *Seebach's* reagent.[23] Column chromatography was performed using silica gel (P60, 230 – 400 mesh).

^{1}H-NMR-, ^{13}C-NMR-, heteronuclear single-quantum correlation- (HSQC) spectra, Nuclear *Overhauser* effect spectroscopy (NOESY) and correlation spectroscopy (COESY) were recorded on a *Agilent 400* (400 MHz for ^{1}H-NMR, 100.59 MHz for ^{13}C-NMR) using $CDCl_3$ ($CDCl_3$: δ 7.26 for ^{1}H-NMR, δ 77.16 for ^{13}C-NMR). Data are reported as follows: chemical shifts, multiplicity (s= singlet, d= doublet, t= triplet, q= quartet, br= broad, m= multiplet), coupling constants *J* (Hz) and integration.

High resolution mass spectrometry (HRMS) was carried out on a LTQ ORBITRAP XL spectrometer (*Thermo Scientific*) employing **e**lectro**s**pray **i**onization (ESI) in positive ion mode (EI^+) and negative ion mode (EI^-).

3.4.2 Synthesis and Characterization

LDA (Lithium diisopropylamide):

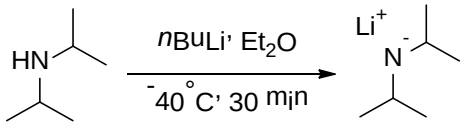

Diisopropylamine (1 equiv) was added slowly to a solution of *n*-BuLi (1.6 M in hexane; 1 equiv.) in Et_2O (1 mL/mmol) at -40 °C. After additional stirring for 30 min at this temperature the LDA solution was used without further purification.

Tosyl azide:

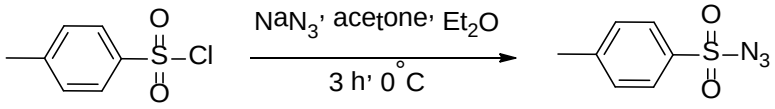

A solution of NaN_3 (1.2 equiv) in water (1.2 mL/ mmol) was added at 0 °C to a solution of tosyl chloride (1 equiv) in acetone (1.2 mL/ mmol). The mixture was stirred for 3 h at this temperature and subsequently diluted with water (4 mL/ mmol). Finally, the organic phase was separated and the aqueous solution extracted twice with Et_2O (2x 2 mL/ mmol), the combined organic extracts were dried over $MgSO_4$ and carefully (<30 °C) concentrated. The tosyl azide was used without further purification in the next step.
[16 mmol scale, full conversion, colorless oil]. ^{1}H-NMR ($CDCl_3$, 400 MHz): δ (ppm) = 7.84 (d, J= 7.2 Hz, 2H); 7.41 (d, J= 8 Hz, 2H); 2.48 (s, 3H). ^{13}C-NMR ($CDCl_3$, 100 MHz): δ (ppm) = 130.41 (2C; CH); 127.68 (2C, CH); 21.91 (1C, CH3). IR (film, cm^{-1}): 2122, 1368, 1164, 1086, 813, 746, 659, 591, 539.

10-(bromotriphenylphosphoranyl)decanoic acid (19): Triphenyl phosphine (1 equiv) was melted and the 10-bromodecanoic acid **18** (1 equiv) was added. The resulting reaction mixture was heated for 16 h at 100 °C. Subsequently, the melt was cooled down to room temperature and washed with pentane. The obtained solid was used without further purification.

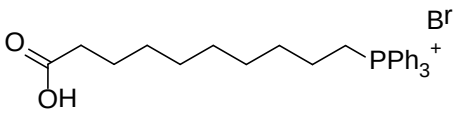

^{1}H-NMR ($CDCl_3$, 400 MHz): δ (ppm) = 7.81 (m, 9H); 7.71 (m, 6H); 3.65 (t, J=11.2 Hz, 2H); 2.36 (t, J=7.2 Hz, 2H); 1.59 (m, 6H); 1.23 (m, 8H). ^{31}P-NMR ($CDCl_3$, 162 MHz): δ (ppm) = 24.37.

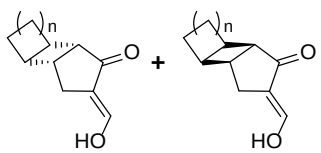

A solution of the ketone **10a** or **10d** (1 equiv) in anhydrous THF (1.5 mL/ mmol) was added over 20 min dropwise to a THF solution of the base (1M in THF, 1.2 equiv) at -45 °C. After warming the reaction mixture slowly (30 min) to -30 °C fresh distilled ethyl formate (3 equiv) was added in one portion. The reaction mixture was allowed to warm up during 2 h to 0 °C to complete the reaction. The mixture was diluted with Et_2O (2 mL/ mmol) and quenched at 0 °C with an aqueous HCl solution (1M, until pH 5-6). The layers were separated and the aqueous layer was extracted three times with Et_2O (3x 2 mL/ mmol), the combined organic extracts were washed with brine (1 mL/ mmol), dried over $MgSO_4$ and concentrated under reduced pressure. The α-hydroxymethylene ketones **11a** or **11d** were used without further purification in the next step.

n=1: 8-(hydroxymethylene)tricyclo[4.3.0.0^{2,5}]nonan-7-one (11a): [0.6 mmol scale, 41% yield, yellowish oil]

n=2: 9-(hydroxymethylene)tricyclo[5.3.0.0^{2,6}]nonan-8-one (11d): [2.7 mmol scale, 45% yield, yellowish oil]

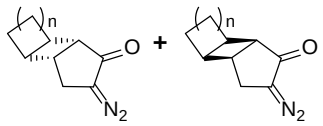

A solution of fresh prepared tosyl azide (1 equiv) in anhydrous CH_2Cl_2 (0.5 mL/ mmol) was added at 0 °C to a solution of the α-hydroxymethylene ketone **11a** or **11d** (1 equiv) in anhydrous CH_2Cl_2 (1.5 mL/ mmol). After adding of Et_3N (2 equiv) the reaction mixture was stirred at this temperature for 30 min, concentrated under reduced pressure and purified by flash chromatography over silica gel (pentane/Et_2O : 8/2).

n=1: 8-diazotricyclo[4.3.0.0^{2,5}]nonan-7-one (12a): [0.3 mmol scale, 89% yield, yellow oil that solidifies upon standing]. ^{1}H NMR (400 MHz, $CDCl_3$); δ (ppm): 3.40 (dd, J= 13.6 Hz, J= 8.8 Hz, 1H); 3.06 (d, J= 6,1 Hz H); 2.93 (m, 1H); 2.89 (d, J= 13.6 Hz, 1H); 2.83 (m, 1H); 2.59 (m, 1H); 2.52 (m, 2H); 2.19 (m, 1H); 2.01 (m, 1H). Measured NMR data are corresponding to those reported in the literature.[20]

n=2: 9-diazotricyclo[5.3.0.0^{2,6}]nonan-8-one (12d): [1.5 mmol scale, 83% yield, yellow oil that solidifies upon standing]. ^{1}H NMR (400 MHz, $CDCl_3$); δ (ppm): 3.27 (m, 1H); 2.90 (d, J= 13.6 Hz, 1 H); 2.74 (m, 1H); 2.52 (m, 1H); 2.44 (m, 1H); 2.23 (m, 1H); 1.84 (m, 1H); 1.68 (m, 3H); 1.51 (m, 2H). ^{13}C NMR (100 MHz, $CDCl_3$); δ (ppm): 203.1 (1C, C=O); 147.11 (1C, C=N); 50.83 (1C, CH_2); 45.74 (1C, CH_2); 42.92 (1C, CH_2); 35.41 (1C, CH_2); 33.16 (1C, CH); 32.85 (1C, CH); 31.37 (1C, CH); 24.98 (1C, CH). IR (film, cm^{-1}): 1939; 2857; 2068; 1655; 1459; 1340; 1317; 1291; 1277; 1246; 1223.

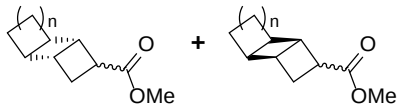

Et_3N (1 equiv) was added to an anhydrous and degassed solution of α-diazo ketone **12a** or **12d** (1 equiv) in MeOH (10 mL/ mmol). The reaction mixture was placed in a photo reactor and irradiated at room temperature for 1 h. After full conversion the mixture was concentrated under reduced pressure and purified by flash chromatography over silica gel (pentane/CH_2Cl_2 : 6/4).

n=1: methyl tricyclo[4.2.0.0^{2,5}]octane-3-carboxylate (15a): [6.2 mmol scale, 77% yield, colorless oil]. ^{1}H NMR (400 MHz, $CDCl_3$); δ (ppm): **major (*endo*):** 3.66 (s, 3H); 3.59 (dt, J= 11.6 Hz, J= 8 Hz, 1 H); 3.04 (m, 1H); 2.76 (m, 1H); 2.90 (m, 1H); 2.65 (m, 1H); 2.40-2.62 (m, 3H); 2.35 (ddd, J= 12.8 Hz, J= 7.6 Hz, J= 3.2 Hz, 1H); 1.87-1.99 (m, 2H). ^{1}H NMR (400 MHz, $CDCl_3$); δ (ppm): **minor (*exo*)**: 3.67 (s, 3H); 3.06 (m, 1 H); 2.89 (m, 1H); 2.80 (m, 1H); 2.76 (m, 2H); 2.40-2.62 (m, 3H); 2.17 (ddd, J= 12.4 Hz, J= 8.7 Hz, J= 1.6 Hz, 1H); 1.87-1.99 (m, 2H). Measured NMR data are corresponding to those reported in the literature.[20]

n=2: methyl tricyclo[4.3.0.0^{2,5}]nonane-3-carboxylate (15d): [5.7 mmol scale, 75% yield, colorless oil]. ^{1}H NMR (400 MHz, $CDCl_3$); δ (ppm): **major (*endo*):** 3.70 (s, 3H); 3.47 (dt, J= 11.2 Hz, J= 8 Hz, 1H); 2.69 (m, 2H); 2.57 (t, J= 6 Hz, 1H); 2.45-2.54 (m, 1H); 2.39-2.45 (m, 1H); 2.10 (dt, J=7.6 Hz, J=3.6 Hz, 1H); 1.74 (m, 1H); 1.45-1.69 (m, 5H). ^{1}H NMR (400 MHz, $CDCl_3$); δ (ppm): **minor (*exo*):** 3.67 (s, 3H); 3.15 (t, J=6.8 Hz, 1 H); 2.39-2.52 (m, 3H); 2.32

(m, 1H); 2.25 (dd, J= 12.4 Hz, J= 8.8 Hz, 1H); 2.31 (m, 1H); 1.74 (m, 1H); 1.45-1.69 (m, 5H).
MS (EI+) (*m/z*): found 181.122 $[M+H]^+$, calculated 181.122 $[M+H]^+$.

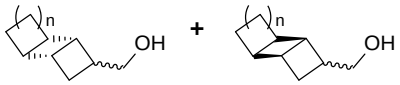

DIBAL-H (5 equiv, 0,5 M in toluene) was added dropwise at -78 °C to a solution of the diastereomeric methyl esters **15a** or **15d** (1 equiv) in toluene (5 mL/ mmol). The reaction mixture was stirred additionally for 30 min at this temperature. Subsequently, an aqueous HCl (1 M) solution was added dropwise to quench the reaction (pH 5) followed by a mixture of pentane/Et_2O (1/1). After warming up to room temperature the mixture was stirred for 30 min. The layers were separated and the organic layer was washed with water (0.5 mL/ mmol) and brine (0.5 mL/ mmol), dried over $MgSO_4$ and concentrated under reduced pressure. The crude alcohol was used without further purification in the next step.

n=1: tricyclo[4.2.0.0^{2,5}]octan-3-ylmethanol (16a): [1.2 mmol scale, 95% yield, colorless oil]

n=2: tricyclo[4.3.0.0^{2,5}]nonan-3-ylmethanol (16d): [1.2 mmol scale, 93% yield, colorless oil]

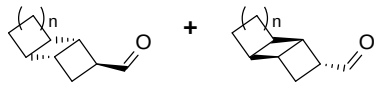

DMSO (6 equiv) was added as solution in CH_2Cl_2 (0.5 mL/ mmol) at -78 °C to a solution of oxalyl chloride (3 equiv) in CH_2Cl_2 (2 mL/ mmol) and the mixture stirred for 30 min at this temperature. To this mixture a solution of the crude alcohol **16a** or **16d** (1 equiv) in CH_2Cl_2 (0.5 mL/ mmol) was added dropwise and the temperature was allowed to increase over 30 min to -60 °C. After Et_3N (9 equiv) was added the reaction mixture was stirred for additional 30 min at -60 °C before being warmed to room temperature. An aqueous HCl (1 M) solution was added followed by CH_2Cl_2 (0.5 mL/ mmol). The layers were separated and the aqueous layer was extracted with CH_2Cl_2 (2x 0.5 mL/ mmol), the combined organic extracts were washed with brine (0.5 mL/ mmol), dried over $MgSO_4$ and concentrated under reduced pressure. The residue was filtered over silica gel (pentane/Et_2O: 8/2). This mixture of *exo* and *endo* aldehyde was dissolved in degassed Et_3N and stirred at room temperature for 6 days. After removing of the triethylamine under reduced pressure the aldehyde was used without further purification in the next step.

n=1: tricyclo[4.2.0.0^{2,5}]octane-3-carbaldehyde (17a): [1 mmol scale, 90% yield, colorless oil]. ^{1}H NMR (400 MHz, $CDCl_3$); δ (ppm): 9.76 (*endo*, d, J= 0.8 Hz, 1H); 9.74 (*exo*, d, J=1.6 Hz, 1H); 3.16 (t, J= 6.8 Hz, 1H); 2.95 (m, 1H); 2.85 (m, 1H); 2.77 (m, 1H); 2.67 (m, 1H); 2.38-2.55 (m, 3H); 2.06 (ddd, J= 12.8 Hz, J= 8.8 Hz, J= 2.4 Hz, 1H); 1.96 (m, 2H).
MS (EI+) (*m/z*): found 137.096 $[M+H]^+$, calculated 137.096 $[M+H]^+$.

n=2: tricyclo[4.3.0.0^{2,5}]nonane-3-carbaldehyde (17d): [1 mmol scale, 73% yield, colorless oil]. ^{1}H NMR (400 MHz, $CDCl_3$); δ (ppm): 9.84 (*endo*, d, J= 0.8 Hz, 1H); 9.72 (*exo*, d, J=1.6 Hz, 1H); 2.89 (t, J= 6 Hz, 1H); 2.79 (m, 1H); 2.65 (dt, J= 22 Hz, J= 4.8 Hz, 1H); 2.49 (q, J=6.8 Hz, 2H); 2.21 (m, 1H); 1.95-2.10 (m, 2H); 1.63-1.79 (m, 2H); 1.45-1.62 (m, 3H).
MS (EI+) (*m/z*): found 151.112 $[M+H]^+$, calculated 151.112 $[M+H]^+$.

A solution of fresh prepared LDA (0.15 M in THF, 4.16 equiv) was added at -78 °C to a suspension of the *Wittig* salt **19** (2 equiv) in THF (5 mL/ mmol). The reaction mixture was warmed over 2 h to room temperature before being cooled again to -78°C. After dropwise adding of the aldehyde (1 equiv) as a solution in THF (1 mL/ mmol) the reaction mixture was stirred for 1 h at this temperature before being warmed over 4 h to room temperature. The resulting reaction mixture was quenched with HCl (1 M, aqueous solution) and diluted with ether (0.5 mL/ mmol). The layers were separated and the aqueous layer was extracted with ether (2*0.5 mL/ mmol), the combined organic extracts were dried over $MgSO_4$ and concentrated under reduced pressure. The crude product was obtained as mixture of E and Z isomers, which were purified and separated by flash chromatography over silica gel (pentane/ ether : 95/5).

n=1: (E)-11-(tricyclo[4.2.0.0^{2,5}]octan-3-yl)undec-10-enoic acid (1a): [0.5 mmol scale, 62% yield, colorless oil]. ^{1}H NMR (400 MHz, $CDCl_3$); δ (ppm): 5.38 (m, 1H); 5.24 (m, 1H); 2.9 (m, 1H); 2.74 (m, 1H); 2.37-2.70 (m, 4H); 2.34 (t, J= 7.6 Hz, 2H); 2.28 (dd, J= 12.8 Hz, J= 4 Hz, 1H); 2.04 (m, 1H); 2.01 (s, 2H); 1.91 (m, 3H); 1.62 (m, 2H); 1.27 (m, 10H).
^{13}C NMR (100 MHz, $CDCl_3$); δ (ppm): 178.95 (1C, CO); 131.52 (1C, C=C); 130.76 (1C, C=C); 53.78 (1C, CH); 42.50 (1C, CH); 40.38 (1C, CH_2); 38.73 (1C, CH); 38.35 (1C, CH); 30.02 (1C, CH_2); 29.56 (1C, CH_2); 29.45 (1C, CH_2); 29.33 (1C, CH_2); 29.18 (1C, CH_2); 28.58 (1C, CH_2); 25.99 (1C, CH_2); 25.54 (1C, CH_2); 24.83 (1C, CH_2); 12.07 (1C, CH).
MS (EI+) (*m/z)*: found 291.232 $[M+H]^+$, calculated 291.232 $[M+H]^+$.

n=2: (E)-11-(tricyclo[4.3.0.0^{2,5}]nonan-3-yl)undec-10-enoic acid (1d): [0.5 mmol scale, 53% yield, colorless oil]. ^{1}H NMR (400 MHz, $CDCl_3$); δ (ppm): 5.43 (dt, J= 10.8 Hz, J= 7.6 Hz, 1H); 5.26 (d, J= 11.2 Hz, 1H); 2.9 (m, 1H); 2.52 (ddd, J= 12.8 Hz, J= 7.2 Hz, J=3.2 Hz, 1H); 2.39 (m, 2H); 2.34 (t, J= 7.6 Hz, 2H); 2.21 (m, 2H); 2.04 (m, 1H); 1.97 (s, 2H); 1.89 (m, 2H); 1.74 (m, 2H); 1.52-1.67 (m, 4H); 1.23-1.35 (m, 10H). ^{13}C NMR (100 MHz, $CDCl_3$); δ (ppm): 178.89 (1C, CO); 130.31 (1C, C=C); 129.84 (1C, C=C); 49.32 (1C, CH); 44.76 (1C, CH); 41.13 (1C, CH_2); 39.79 (1C, CH); 33.72 (1C, CH); 33.13 (1C, CH_2); 32.75 (1C, CH_2); 32.02 (1C, CH_2); 29.08 (1C, CH_2); 28.62 (1C, CH_2); 28.50 (1C, CH_2); 28.32 (1C, CH_2); 28.17 (1C, CH_2); 27.79 (1C, CH_2); 24.71 (1C, CH_2); 11.20 (1C, CH). MS (EI+) (*m/z)*: found 305.247 $[M+H]^+$, calculated 305.248 $[M+H]^+$.

3.5 References

1) E. Broda. Two kinds of lithotrophs missing in nature. *Z. Allg. Mikrobiol.*, **17**, 491-493, (1977).
2) A. A. van de Graaf, A. Mulder, P. de Bruijn, M. S. Jetten, L. A. Robertson, J. G. Kuenen. Anaerobic oxidation of ammonium is a biologically mediated process. *Appl. Environ. Microbiol*., **61**, 1246 -1251 (1995).
3) M. S. M. Jetten, M. Wagner, J. Fuerst, M. van Loosdrecht, J. G. Kuenen, M. Strous. Microbiology and application of the anaerobic ammonium oxidation (‘anammox’) process. *Curr. Opin. Biotechnol*., **12**, 283-288 (2001).
4) M. Strous, J. A. Fuerst, E. H. M. Kramer, S. Logemann, G. Muyzer, K. T. van de Pas-Schoonen, R. Webb, J. G. Kuenen, M. S. M. Jetten. Missing lithotroph identified as new planctomycete. *Nature*, **400**, 446-449 (1999).
5) B. Kartal, J. G. Kuenen, M. C. M. van Loosdrecht. Sewage treatment with anammox. *Science*, **328**, 702-703 (2010).
6) M. C. F. van Teeseling, S. Neumann, L. van Niftrik. The Anammoxosome Organelle Is Crucial for the Energy Metabolism of Anaerobic Ammonium Oxidizing Bacteria. *J. Mol. Microbiol. Biotechnol*., **23**, 104-117 (2013).
7) L. van Niftrik, M. S. M. Jetten. Anaerobic Ammonium-Oxidizing Bacteria: Unique Microorganisms with Exceptional Properties. *Microbiol. Mol. Biol. Rev*., **76**, 585-596 (2012).
8) L. van Niftrik. Cell biology of unique anammox bacteria that contain an energy conserving prokaryotic organelle. *Antonie van Leeuwenhoek*, **104**, 489-497 (2013).
9) L. van Niftrik, W. J. C. Geerts, E. G. van Donselaar, B. M. Humbel, A. Yakushevska, A. J. Verkleij, M. S. M. Jetten, M. Strous. Combined structural and chemical analysis of the anammoxosome: A membrane-bounded intracytoplasmic compartment in anammox bacteria. *J. Struct. Biol*., **161**, 401–410 (2008).
10) L. A. van Niftrik, J. A. Fuerst, J. S. Sinninghe Damsté, J. G. Kuenen, M. S. M. Jetten, M. Strous. The anammoxosome: an intracytoplasmic compartment in anammox bacteria. *FEMS Microbiol. Lett,*. **233**, 7-13 (2004).
11) M. R. Lindsay, R. I. Webb, M. Strous, M. S. M. Jetten, M. K. Butler, R. J. Forde, J. A. Fuerst. Cell compartmentalisation in planctomycetes: novel types of structural organisation for the bacterial cell. *Arch. Microbiol*., **175**, 413-429 (2001).
12) J. S. Sinninghe Damsté, M. Strous, W. I. C. Rijpstra, E. C. Hopmans, J. A. J. Geenevasen, A. C. T. van Duin, L. A. van Niftrik, M. S. M. Jetten. Linearly concatenated cyclobutane lipids form a dense bacterial membrane. *Nature*, **419**, 708-712 (2002).
13) J. E. Rattray, J. van de Vossenberg, E. C. Hopmans, B. Kartal, L. van Niftrik, W. I. C. Rijpstra, M. Strous, M. S. M. Jetten, S. Schouten, J. S. Sinninghe Damsté. Ladderane lipid distribution in four genera of anammox bacteria. *Arch. Microbiol*., **190**, 51-66 (2008).

14) I. Lanekoff, R. Karlsson. Analysis on intact ladderane phospholipids, originating from viable anammox bacteria, using RP-LC-ESI-MS. *Anal. Bioanal. Chem.*, **397**, 3543-3551 (2010).
15) H. A. Boumann, E. C. Hopmans, I. van de Leemput, H. J. M. op den Camp, J. van de Vossenberg, M. Strous, M. S. M. Jetten, J. S. Sinninghe Damsté, S. Schouten. Ladderane phospholipids in anammox bacteria comprise phosphocholine and phosphoethanolamine headgroups. *FEMS Microbiol. Lett.*, **258**, 297-304 (2006).
16) M. N. Kozlov, M. V. Kevbrina, A. G. Dorofeev, E. A. Kazakova, V. A. Grachev, D. Yu. Polyakov, V. G. Aseeva, Yu. A. Nikolaev. Lipid Composition of Activated Sludge in a Pilot Plant for Anaerobic Ammonium Oxidation. *Appl. Biochem. Microbiol.*, **49**, 485-494 (2013).
17) R. Huber, T. Wilharm, D. Huber, A. Trincone, S. Burggraf, H. König, R. Reinhard, I. Rockinger, H. Fricke, K. O. Stetter. *Aquifex pyrophilus* gen. nov. spec. nov., represents a novel group of marine hyperthermophilic hydrogen-oxidizing bacteria. *Syst. Appl. Microbiol.*, **15**, 340-351 (1992).
18) M. De Rosa, A. Gambacorta, R. Huber, V. Lanzotti, B. Nicolaus, K. O. Stetter, A. Trincone. A new 15,16-dimethyl-30-glyceryloxytriacontanoic acid from lipids of Thermotoga maritima. *J. Chem. Soc., Chem. Commun.*, 1300-1301 (1988).
19) V. Mascitti, E. J. Corey. Total Synthesis of (±)-Pentacycloanammoxic Acid. *J. Am. Chem. Soc.*, **126**, 15664-15665 (2004).
20) V. Mascitti, E. J. Corey. Enantioselective Synthesis of Pentacycloanammoxic Acid. *J. Am. Chem. Soc.*, **128**, 3118-3119 (2006).
21) G. H. Zayia. First General Method for Direct Formylation of Kinetically-Generated Ketone Enolates. *Org. Lett.*, **1**, 989-991 (1999).
22) A. K. Ghosh, A. Bischoff, J. Cappiello. Asymmetric Total Synthesis of the Gastroprotective Microbial Agent AI-77-B. *Eur. J. Org. Chem.*, **2003**, 821-832 (2003).
23) D. Seebach, R. Imwinkelried, G. Stucky. Optisch aktive Alkohole aus 1,3-Dioxan-4-onen: eine praktikable Variante der enantioselektiven Synthese unter nucleophiler Substitution an Acetal-Zentren. *Helv. Chim. Acta.*, **70**, 448-464 (1987).

Chapter 4

Total Synthesis of Majusculoic acid, a Natural *Trans*-Cyclopropyl Fatty Acid

Emerging trends in drug discovery are stimulating interest in natural fatty acids as a source of lead compounds. In the last decade their application as potentials drug candidates was demonstrated to fight diseases such as tuberculosis, cancer and fungal infections. In this regard, the natural product majusculoic acid has been proven to be of potential as drug lead, since it owns antifungal activity against *Candida* species. However, the availability of this natural fatty acid is limited due to the fact that it has been so far only isolated from natural sources. To allow extensive biological studies and lead optimization in the drug discovery process, the synthesis of this structurally complex amphiphilic molecule is essential. Here, for the first time we demonstrate two total synthesis pathways giving access to majusculoic acid. In this study a number of key synthetic steps, i.e. asymmetric cyclopropanation, selective reduction of alkenes and double bound isomerization, have been successfully employed. Undoubtedly, the synthesis of majusculoic acid developed in the present study will accelerate the lead optimization of this class of fatty acids resulting in new potential drug candidates.

4.1 Introduction

Marine microorganisms are an important source of a variety of still undiscovered organic compounds exhibiting fascinating molecular structures.[1] Especially, a growing interest for these molecules is reported, since they can be applied as lead compounds for drug development.[2-5] In this regard, during the last decades many molecules were isolated and characterized revealing often intriguing chemical and biological properties.[1,6,7] Furthermore, approaches to use these substances as potential drugs against diseases like malaria,[8] tuberculosis,[9] cancer[10,11] and fungal infection have been published.[12,13]

Among the isolated molecules a broad range of unique, rare and biological active fatty acids is contained. Different studies showed that some of these fatty acids can act as inhibitors during the fatty acid biosynthesis of the bacteria leading to a reduced progeny of parasites. For example, in 1992 *Kumaratilake et al.* observed the antimalarial properties of polyunsaturated fatty acids.[14]

In 2005, *MacMillan et al.* reported the isolation of majusculoic acid **1** (Figure 4.1.1) from a cyanobacterial mat assemblage.[15] As shown in Figure 4.1.1, the molecular structure of fatty acid **1** offers unique structural features. One of these, is the presence of a *trans*-substituted cyclopropyl ring at the C4-position of acid **1**. Other features are the di- and the tri-substituted double bound which are located in C9- and C11-position, respectively. The latter alkene is brominated at the C12-position of the molecule. Using 1D and 2D NMR (**n**uclear **m**agnetic **r**esonance) spectroscopy the configurations of both olefins and of the cyclopropyl ring were analyzed revealing the structure of the natural product **1** (Figure 4.1.1).[15] This study performed by *MacMillan et al.* proved the E- and Z-configuration of the first (C9-C10) and second double bond (C11-C12) as well as the *trans*-configuration of the cyclopropyl ring (Figure 4.1.1). However, the absolute configuration at the C4 and C6 position could not be established so far.

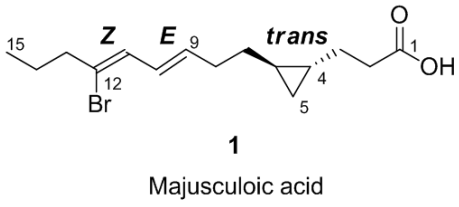

1

Majusculoic acid

Figure 4.1.1: Molecular structure of majusculoic acid **1**.

Furthermore, biological studies of majusculoic acid **1** revealed its antifungal activity against *Candida albicans* ATCC 14503 and *Candida glabrata* with a **m**inimum **i**nhibition **c**oncentration (MIC) of 8 µM and 19.3 µM, respectively.[15] During the last decade a growing interest in such antimycotic agents was observed. This can be traced back to the fast increasing amount of fungal species, infection and resistance against current available drugs resulting in serious problems for debilitated humans e.g. in hospitals and during transplantations.[16] Additionally, in 2012 *Fisher et al.* summarized also the rising fungal threat to animals, plants and the ecosystem leading to a decreased biodiversity through extinction of wild species.[17]

Hence, the investigation of potential antifungal compounds, such as majusculoic acid **1**, and the understanding of the mode of action of these substances are necessary to antagonize the fast growing threat through fungal infections. However, due the low availability of these natural compounds, which have been so far isolated from limited natural resources, an efficient synthesis is required to allow access to a sufficient amount of material for extensive biological, chemical and physiological studies as well as for the synthesis of derivatives in the drug development process.

Therefore, in this Chapter an efficient synthesis for the naturally occurring fatty acid, majusculoic acid **1**, is described to give access to a sufficient amount of the antifungal compound **1** and its derivatives for future studies. Furthermore, the absolute configuration of the natural product was unequivocally established for the first time.

4.2 Results and Discussion

4.2.1 Synthesis of Majusculoic Acid

From a retrosynthetic point of view the molecular structure of majusculoic acid **1** can be divided into two building blocks (Scheme 4.2.1), which can be combined via a coupling reaction in the last steps to the final product **1**. As shown in Scheme 4.2.1, the most suitable cleavage position seems to be the *trans*-disubstituted double bound located in the center of the majusculoic acid **1**. The two resulting units **2** and **3** exhibit synthetically challenging moieties, i.e. a *cis*-alkene substituted with a bromide and a *trans*-substituted cyclopropane unit, respectively.

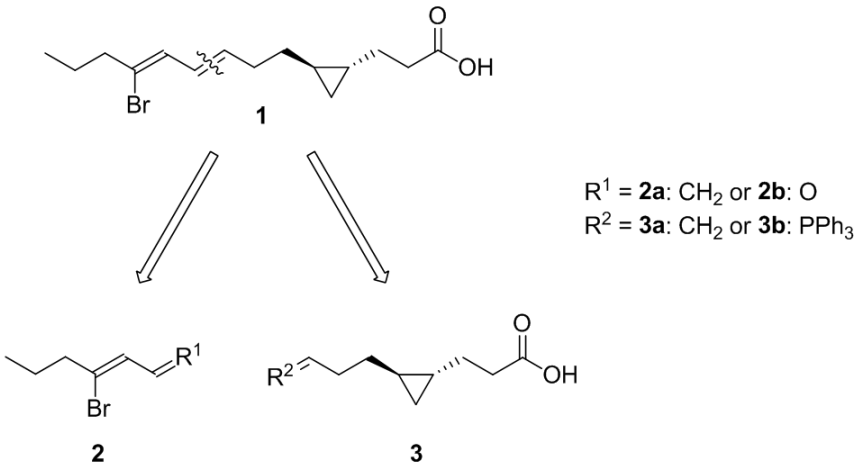

Scheme 4.2.1: Retrosynthetic pathway for majusculoic acid **1** resulting in two key compounds **2** and **3**.

Efficient synthetic strategies considered to allow the combination of both fragments **2** and **3** are a cross metathesis or a *Wittig* reaction. Both pathways result in the formation of a carbon-carbon double bound that is also present in **1**. For the cross metathesis it is required that both building blocks are carrying a terminal alkene. In contrast, during a *Wittig* olefination an aldehyde **2b** and a triphenyl phosphonium bromide salt **3b** are reacting with each other.
As shown in Scheme 4.2.2, the brominated building block **2** exhibiting a terminal alkene, i.e. **2a**, or an aldehyde moiety, i.e. **2b**, can be synthesized in three and four synthetic steps, respectively. Here, it needs to be emphasized that both compounds **2a** and **2b** are sharing the same synthetic pathway. Hence, alkene **2a** can be synthesized from aldehyde **2b** in only one additional synthetic step (Scheme 4.2.2).

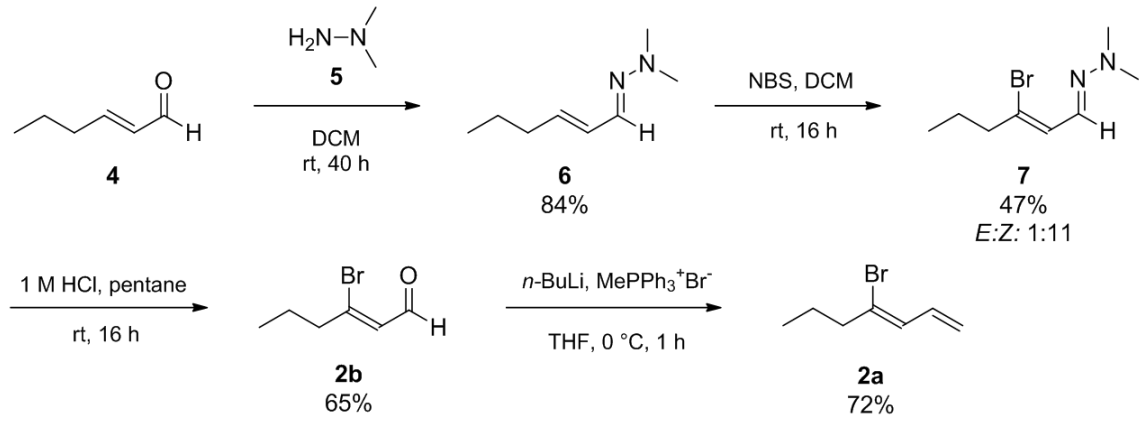

Scheme 4.2.2: Synthesis of the brominated aldehyde **2b** and diene **2a**.

As shown in Scheme 4.2.2, the synthesis of olefin **2a** and aldehyde **2b** starts with the commercial available *trans*-2-hexenal **4**. During the first reaction, the aldehyde moiety of **4** was converted into the corresponding hydrazone **6** with a yield of 84% using 1,1-dimethylhydrazine **5**. Subsequent bromination in β-position using ***N*-bromo**succinimide (NBS) yielded the bromide substituted *cis*-alkene **7**.[18] Finally, hydrolysis of the dimethylhydrazone **7** under acidic conditions yielded the first building block **2b** exhibiting an aldehyde moiety required for the *Wittig* reaction. As emphasized above, an additional step was performed to obtain **2a,** exhibiting a terminal alkene, via a *Wittig* olefination using methyltriphenylphosphonium bromide. Therewith, the building block **2a** that can be used in a cross metathesis was synthesized in only four synthetic steps.

After successful synthesis of the brominated building blocks **2a** and **2b** the second molecular part **3** (Scheme 4.2.1) carrying the *trans*-cyclopropyl moiety had to be approached. The retrosynthetic strategy for the corresponding phosphonium salt **3b** and the olefin **3a** applicable in a *Wittig* reaction and cross metathesis, respectively, is shown in Scheme 4.2.3. Hereby, the olefin **3a** can be synthesized in six synthetic steps, whereas phosphonium salt **3b** is accessible in nine steps. However, employing this synthetic pathway we face two major challenges. The first hurdle is the selective reduction of the double bound which is conjugated to the cyclopropyl- and ester moieties in **8**, while the terminal olefin needs to be retained (Scheme 4.2.3, step **a**). The second challenge is the diastereo- and enantioselective incorporation of a *trans*-disubstituted cyclopropane ring resulting in intermediate **9** (Scheme 4.2.3, step **b**). As shown in Scheme 4.2.3, the precursor for the cyclopropanation, namely E-*S*-ethyl 4-chlorobut-2-enethionate **10**, can be obtained in two synthetic steps starting from the commercially available 3-butenoic acid **11**.

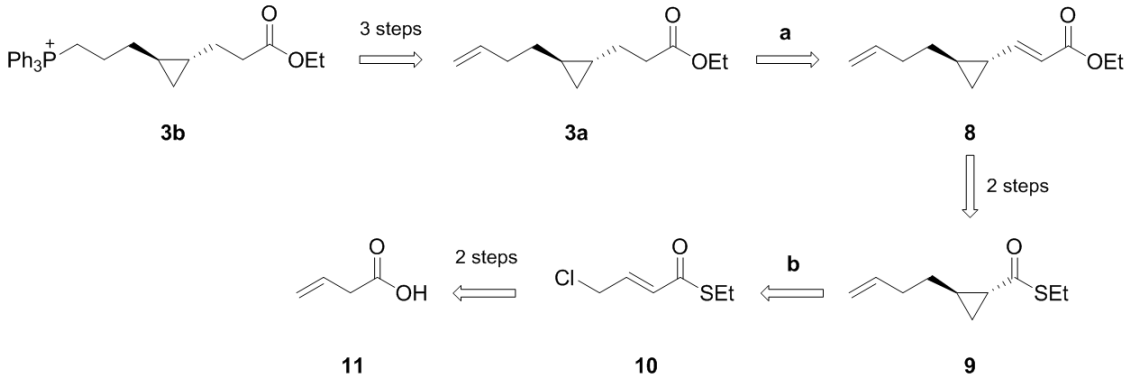

3b **3a** **8** **11** **10** **9**

Scheme 4.2.3: Retrosynthetic pathway for building block **3** applying a nine synthetic step.

The terminal position of 3-butenoic acid **11** was chlorinated using recrystallized ***N*-c**hloro**s**uccinimide (NCS) and **ph**enyl**se**lenyl **ch**loride (PhSeCl) (Scheme 4.2.4).[19] The resulting product, i.e. E-4-chlorobut-2-enoic acid **12**, was used for the subsequent esterification employing ethanethiol (EtSH) yielding the corresponding thioester **10** as main product. However, under the applied reaction condition a side reaction took place resulting also in formation of the disubstituted cyclopropane **13** (Scheme 4.2.4). This side product **13** is formed through a nucleophilic addition of a second ethanethiol in the β-position of thioester **10** followed by an intramolecular nucleophilic substitution at the chlorinated carbon. The resulting mixture of **10** and **13** was successfully separated using Oxone® (potassium peroxymonosulfate) as oxidizing reagent for thioether **13** followed by an extraction yielding the desired α-β unsaturated thioester **10** with an isolated yield of 61%.

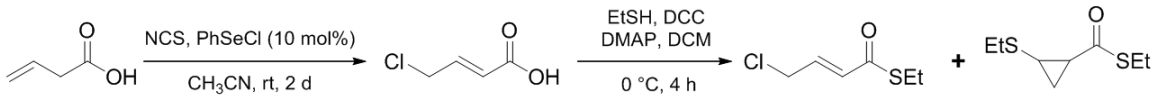

11 **12** 68% **10** 61% **13**

Scheme 4.2.4: Two-step synthesis of E-*S*-ethyl 4-chlorobut-2-enethionate **10**.

To obtain the desired *trans*-cyclopropyl moiety, an asymmetric conjugate addition and a subsequent intramolecular trapping reaction of the enolate **15** as described by *den Hartog* et. al. in 2010 was applied.[20] As shown in Scheme 4.2.5, during the first step of this reaction the freshly synthesized *Grignard* reagent **14** and catalytic amounts of *R*-TolBINAP ((***R***)-(+)-2,2′-Bis(di-p-**tol**ylphosphino)-1,1′-**binap**hthyl) were used to convert **10** to the intermediate **15**. In the second part of the asymmetric cyclopropanation the resulting reaction mixture was warmed slowly to room temperature before it was quenched with ethanol and aq. NH_4Cl resulting in thioester **9** with a cyclopropyl moiety (Scheme 4.2.5). It needs to be emphasized that the resulting compound **9** exist as pure *trans*-diastereomer with an enantiomeric excess of 95%. Furthermore, the amount of *Grignard* reagent (1.1 equiv.) is crucial to reduce side reactions and to enable the isolation of 70% of the compound **9**.

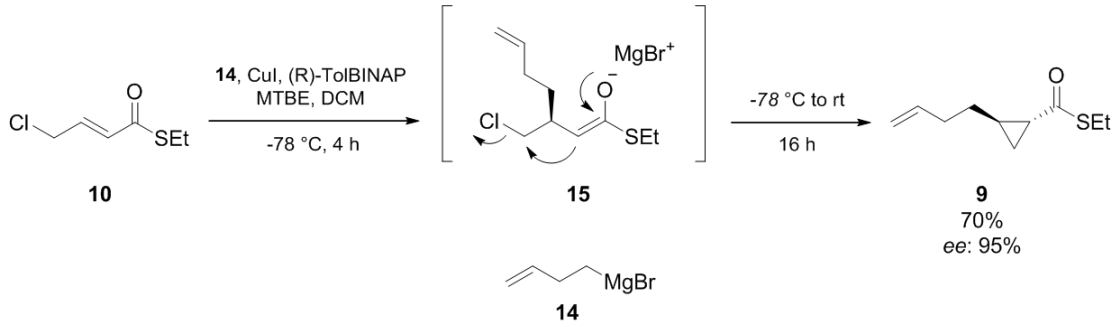

Scheme 4.2.5: Cyclopropanation using an asymmetric conjugate addition of *Grignard* reagent **14** followed by a cyclization leading to the disubstituted *trans* cyclopropane **9**.

After successful incorporation of the *trans*-cyclopropyl moiety, in the next steps an elongation of the chain was performed (Scheme 4.2.6). First, thioester **9** was selectively reduced to an aldehyde **16** using **di**iso**b**utyl**a**luminium **h**ydride (DIBAL-H) reaching an isolated yield of 70%. Then, the freshly synthesized aldehyde **16** was immediately utilized in a ***H**orner-**W**adsworth-**E**mmons* (*HWE*) olefination using the commercially available triethyl phosphonoacetate **17** resulting in α,β-unsaturated ethyl ester **8** (Scheme 4.2.6).

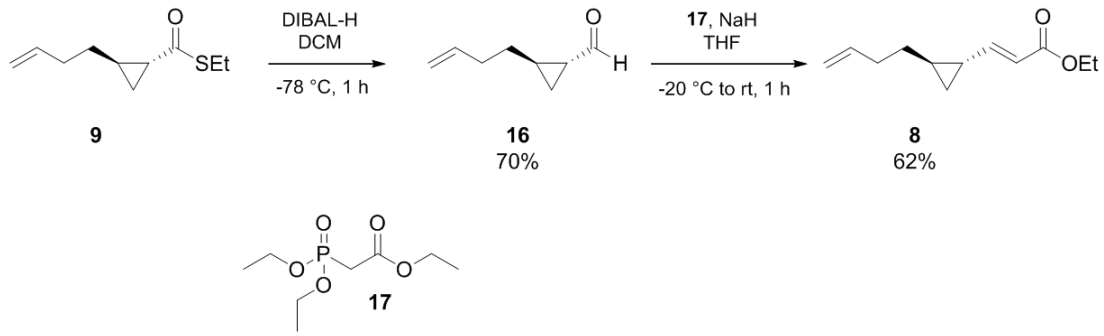

Scheme 4.2.6: Chain elongation using a DIBAL-H reduction followed by a *HWE* olefination resulting in a α,β-unsaturated ethyl ester **8**.

Finally, a selective reduction of the conjugated carbon-carbon double bound of **8** with $NaBH_4$ resulted in the above introduced building block **3a.** However, as shown in Scheme 4.2.7, depending on the reaction condition, a simultaneous reduction of the terminal olefinic group occurred leading also to side products **18** and **19**.

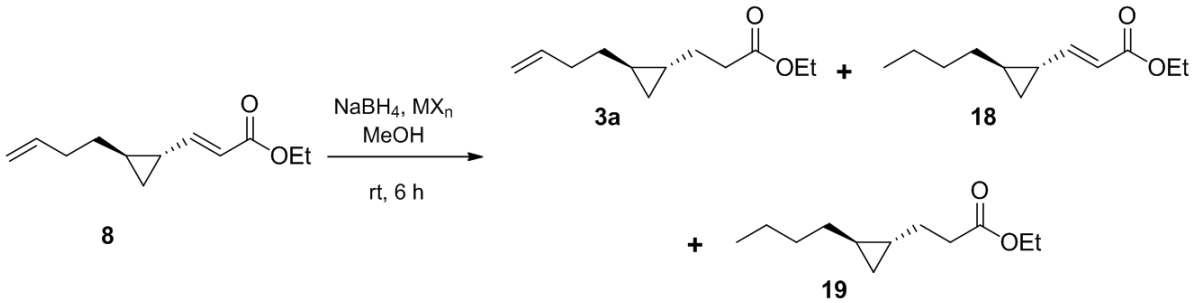

Scheme 4.2.7: Reduction of the carbon-carbon double bound of ethyl ester **8** using $NaBH_4$ and metal halides (MX_n).

In order to optimize the selective reduction of the conjugated olefinic group, a set of reactions was carried out using different metal halides (MX_n), different quantities $NaBH_4$ and employing different temperatures and reaction times. The results are summarized in Table 4.2.1 showing a major influence of the metal halides on the product formation and conversion.
As shown in Table 4.2.1, using 20 mol% CuCl and employing a reaction temperature of 0 °C no conversion of **8** was detected (entry 1), while performing the reduction at room temperature a low conversion could be observed resulting in the desired building block **3a** as the main product (entry 2). Comparable results were observed using 20 mol% of CuI at room temperature (Table 4.2.1, entry 3). In contrast, using $CoCl_2$ lead to a significant acceleration of the reaction through the *in situ* formation of highly reactive cobalt boride species.[21] At room temperature full conversion of the starting material **8** was already observed after 30 minutes (Table 4.2.1, entry 4). However, employing the latter conditions only the fully saturated ester **19** was isolated. Further, at lower temperatures mainly compounds **18** and **19** were obtained as a mixture (Table 4.2.1 entry 5) suggesting that the terminal olefin is more reactive than the one conjugated to the ester moiety. Considering the higher reactivity of the terminal double bound using $CoCl_2$ as metal halide (Table 4.2.1, entries 4 and 5) we decided to utilize Cu(I) halide as catalyst, since a selective reduction was previously observed (Table 4.2.1, entries 1-3). However, in order to increase the conversion of the selective reduction an increased amount of $NaBH_4$ was employed. As shown in Table 4.2.1 (entry 6), the ester **8** was selectively reduced to the desired product **3a** in presence of six equivalents of $NaBH_4$ reaching an isolated yield of 81% (Table 4.2.1, entry 6). The necessity of CuCl for this reaction was demonstrated in entry 7 of Table 4.2.1, where no reaction took place.

Table 4.2.1: Optimization of reaction conditions for a selective double bound reduction.

Entry	MX_n *	$NaBH_4$ (equiv.)	temp. (°C)	Time (h)	conv. (%)	Product
1	CuCl	1.5	0	24	0	-
2	CuCl	1.5	rt	24	5	**3a**
3	CuI	1.5	rt	24	2	**3a**
4	$CoCl_2$	1.5	rt	0.5	100	**19**
5	$CoCl_2$	1	0	0.5	100	**18**
6	CuCl	6**	rt	5	84	**3a**
7	-	6**	rt	5	0	-

*20 mol% were used of the metal halide. **Repetitive addition of one equivalent $NaBH_4$ every 45 minutes.

After a successful synthesis of building block **3a** for the cross metathesis, the same compound was also employed as starting material to obtain the corresponding triphenylphosphonium bromide salt **3b**, which represents a reactant for the *Wittig* reaction (*vide supra*). As shown in Scheme 4.2.8, employing an ozonolysis and reductive workup with $NaBH_4$ alkene **3a** was converted to a primary alcohol **20** reaching a yield of 86%. The alcohol **20** was further reacted in an *Appel*[22] reaction using tetrabromomethane (CBr_4) and triphenylphosphine (PPh_3) resulting in the corresponding bromide **21**, which was directly used for the synthesis of the

above mentioned phosphonium building block **3b** (Scheme 4.2.8). As shown in Scheme 4.2.8, the final step was performed in melted triphenylphosphine resulting in *Wittig* salt **3b** with an isolated yield of 67%.

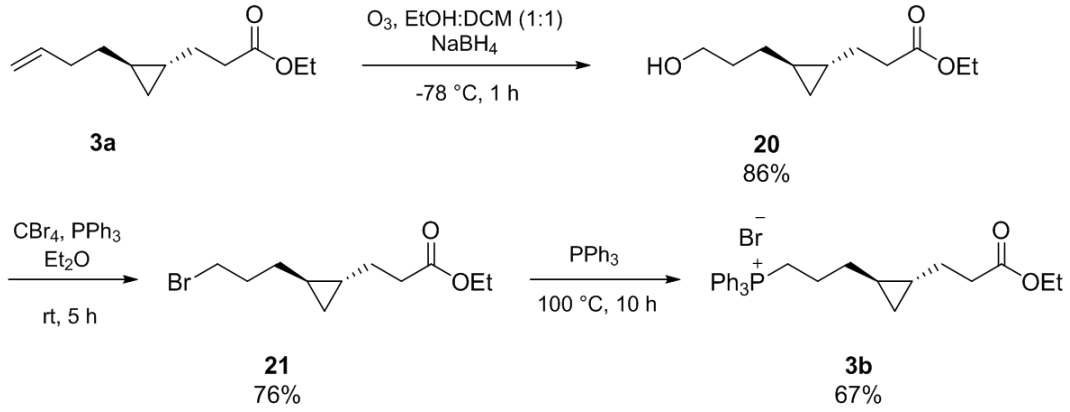

Scheme 4.2.8: Three-step synthesis of *Wittig* salt **3b** from building block **3a**.

With all four building blocks **2a**, **3a**, **2b** and **3b** in hand, the final part of the synthesis of the majusculoic acid ethyl ester **22** was performed. As shown in Scheme 4.2.9, a cross metathesis reaction using compounds **2a** and **3a** can result in the desired ester **22**. Alternatively, employing a *Wittig* reaction of compounds **2b** and **3b** the majusculoic acid derivative **22** can be obtained as well (Scheme 4.2.9).

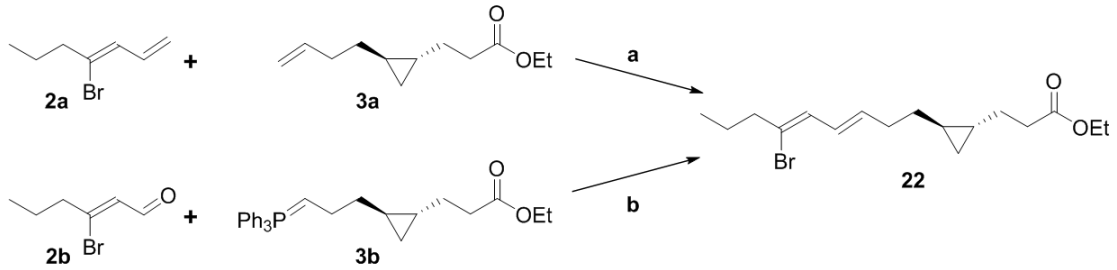

Scheme 4.2.9: Two possible synthetic pathways using **2a**, **3a**, **2b** and **3b** to form the majusculoic acid ethyl ester **22**: (**a**) cross methathesis and (**b**) *Wittig* reaction.

To obtain the final product **22** we evaluated first the cross metathesis. As shown in Scheme 4.2.10, employing this reaction not only the desired products **22**, but also side products **23** and **24** can be expected due to homodimerization of the corresponding building blocks. Also attention deserves the choice of the catalyst, which can influence the ratio of the corresponding E- to Z-isomer ratio of **22**. In this regard, different generations of the ***G**rubbs*- (G), ***H**oveyda **G**rubbs*- (HG) as well as the **M**etathesis- (M) catalysts (Figure 4.1.1) were tested in order to obtain the required E-isomer of **22**. The obtained results utilizing the same reaction conditions for all catalysts are summarized in Table 4.2.2. In presence of G-I exclusively the homodimers **23** and **24** were formed (Table 4.2.2, entry 1). The formation of the same product was observed using the second generation of catalysts G-II, HG-II and MII, as shown in Table 4.2.2 entries 2, 4 and 6, respectively. However, traces of the desired heterodimer **22** could be detected via

NMR-spectroscopy. In contrast, in presence of catalysts HG-I and M-I exclusively heterodimer **22** was obtained. Employing NMR to examine the latter reaction mixtures revealed a slow reaction resulting in low conversions (< 10%) of the building block **2a** and **3a**. Also, change of reaction conditions, such as solvent, reaction time and temperature (RT – 110 °C), or using different concentrations and stoichiometry of reactants/catalyst did not result in increased conversion. Another drawback of the performed cross metathesis is the fact that only a mixture of E- and Z-isomers of **22** was obtained using HG-I and M-I as catalyst, as shown in Table 4.2.2, entries 3 and 5, respectively.

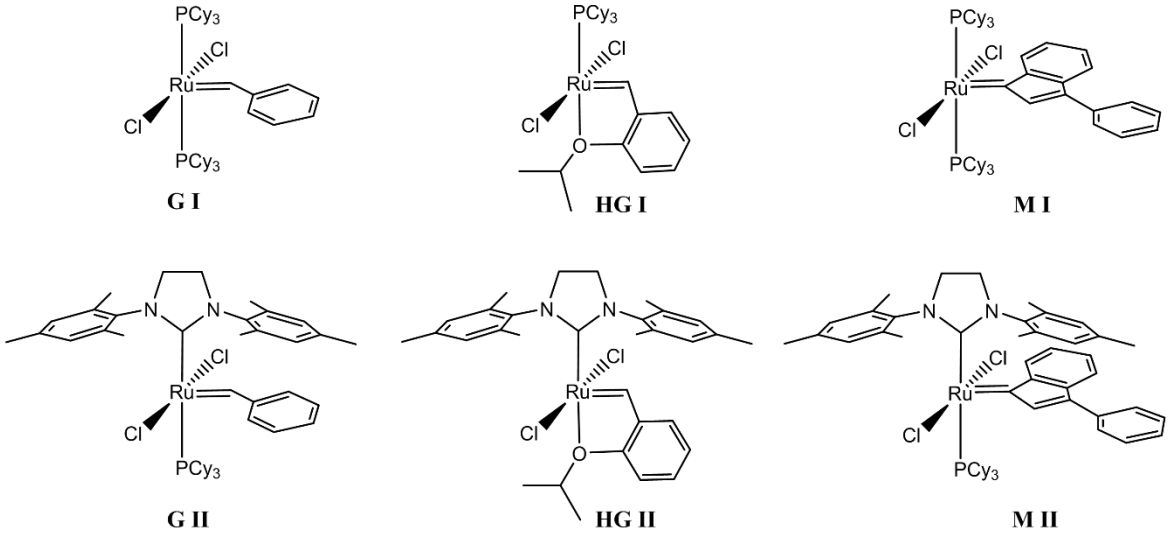

Figure 4.1.1: Chemical structure of all used ruthenium-based metathesis catalysts (*Grubbs*- (G), *Hoveyda Grubbs*- (HG), Metathesis- (M) catalysts).

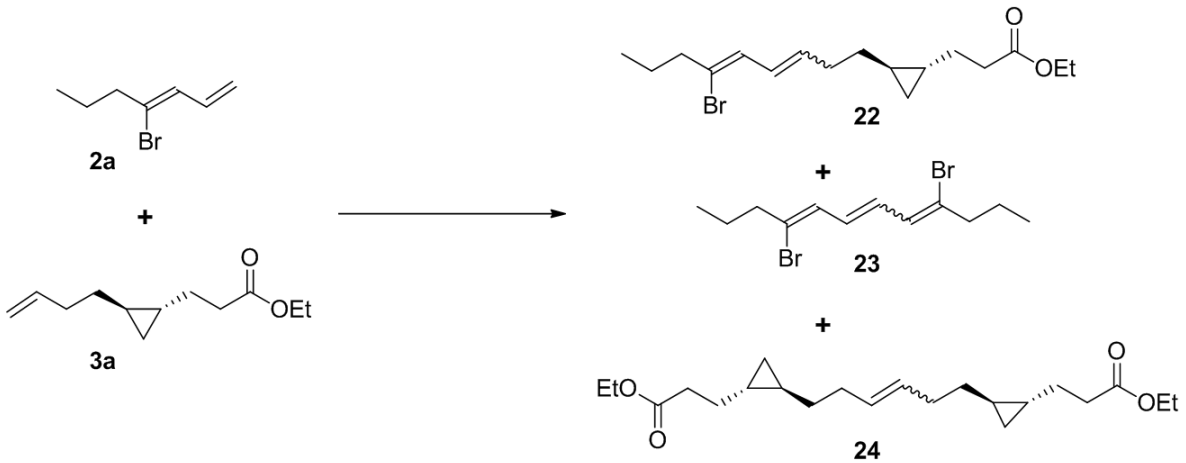

Scheme 4.2.10: Possible product formation during cross metathesis using building block **2a** and **3a**.

Table 4.2.2: Catalyst screening for cross metathesis.

entry	catalyst	homodimer	heterodimer	*E*:*Z* ratio*
1	**GI**	√	-	-
2	**GII**	√	traces	*E*
3	**HGI**	-	√**	2:1
4	**HGII**	√	traces	*E*
5	**MI**	-	√**	2:1
6	**MII**	√	traces	*E*

*Ratio given for heterodimer **22**. **Yield lower than 10%.

Considering the formation of isomer mixtures of **22** and the low yield performing the cross metathesis reaction, a second synthetic strategy was carried out. As shown in Scheme 4.2.11, aldehyde **2b** and triphenylphosphonium bromide salt **3b** were used in a *Wittig* reaction to obtain the desired product **22**. In order to minimize the formation of the undesired Z-isomer and in the same time obtain the E-isomer of **22** in a good yield the *Wittig* reaction was performed in presence of different bases (B). Table 4.2.3 summarizes the outcome of this study using *n*-**bu**tyl **li**thium (*n*-BuLi), **l**ithium **d**iisoprolyl**a**minde (LDA), **Li**thium **h**exa**m**ethyl**d**i**s**ilazide (LiHMDS) and sodium (**Na**) **h**exa**m**ethyl**d**i**s**ilazide (NaHMDS) as a base. Comparing the *Wittig* reaction (Scheme 4.2.11, Table 4.2.3) with the cross metathesis (*vide supra*) the Majusculoic acid ethyl ester **22** could be obtained with higher yields of up to 43%. However, at the same time also this reaction resulted mainly in Z-isomer of **22** independent of the base utilized (Table 4.2.3).

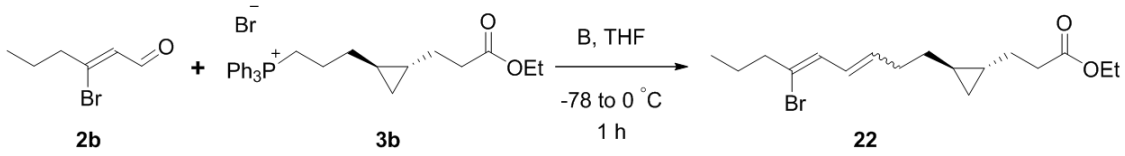

2b **3b** **22**

Scheme 4.2.11: *Wittig* reaction using building block **2b** and **3b**. (B = base)

Table 4.2.3: Base screening for *Wittig* reaction.

Base	Yield (%)	*E*:*Z* ratio
***n*-BuLi**	43	1:3
LDA	19	1:9
LiHMDS	39	1:10
NaHMDS	40	0:1

Due to the unfavorable diastereomeric ratio of E- and Z-isomer (Table 4.2.3) we considered to perform an isomerisation reaction of the disubstituted double bound of **22** employing iodine. Therefore, the isomer mixture obtained from the reaction performed in the presence of *n*-BuLi (Table 4.2.3) was incubated with a small amount of iodine in D-chloroform at 40 °C. The progress of the reaction was followed by NMR-spectroscopy (Figure 4.2.2). The NMR-study

demonstrates a successful isomerization of the Z-isomer to the desired E-isomer of **22**. An equilibrium of the isomerization was reached after a reaction time of 30 minutes and the excess of iodine was eliminated through extraction with aqueous $Na_2S_2O_3$ solution. The isomerization resulted in the **E-22** isomer containing less than 10% of the corresponding **Z-22** isomer (Figure 4.2.2).

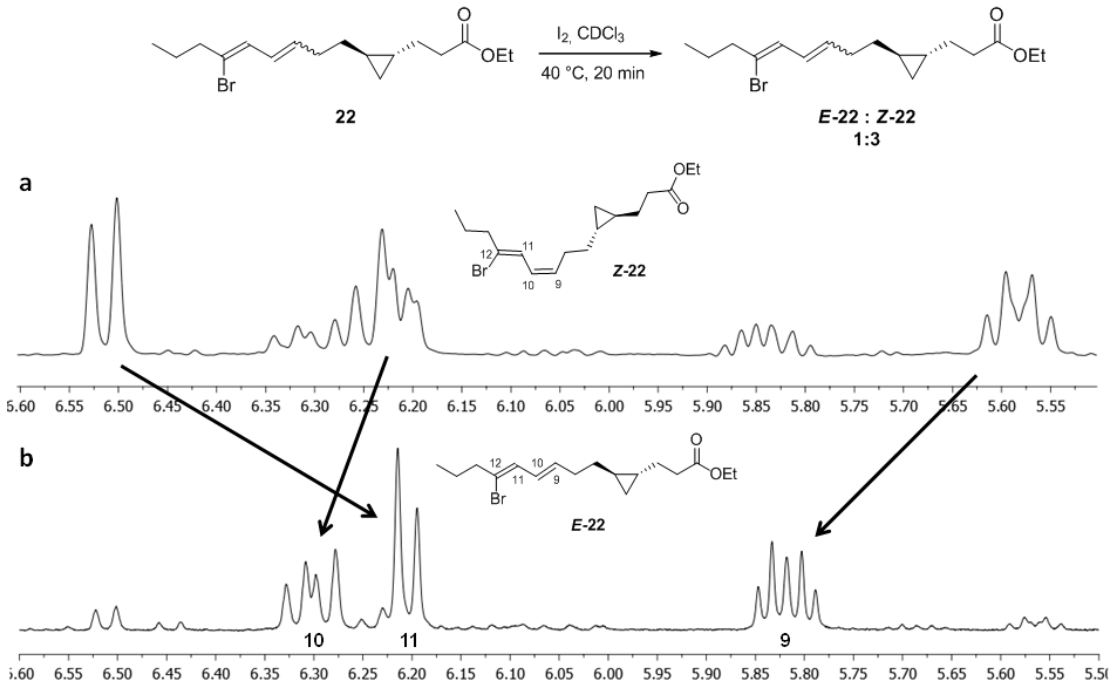

Figure 4.2.2: Isomerisation of the disubstituted double bound of compound **22**. (a) ^{1}H-NMR of the isomer mixture of **22** before isomerisation. (b) ^{1}H-NMR of the isomer mixture of **22** after isomerisation.

Finally, in order to obtain the natural product, namely majusculoic acid **1**, the ethyl ester **E-22** was subsequently hydrolyzed under basic conditions resulting in the corresponding acid **1** with an isolated yield of 75% (Scheme 4.2.12). Majusculoic acid **1** was obtained as colorless solid which was analyzed by NMR-spectroscopy, exact mass (see Chapter 4.5) and determination of the optical rotation ($[\alpha]_D$). The NMR-spectra obtained from the in this work synthesized majusculoic acid **1** carrying a *trans*-(4R,5R)-cyclopropane moiety are in accordance with the in ref. 15 reported data. Furthermore, a value of $[\alpha]_D$ = -16.2 for the optical rotation was determined which is also comparable with the in 2005 by *MacMillan et al.* determined rotation for majusculoic acid isolated from cyanobacteria ($[\alpha]_D$ = -15.8).[15] Based on this data we can conclude that the natural occurring majusculoic acid **1** should have the same absolute configuration (4*R*, 5*R*) as the in our laboratories synthesized acid **1** (Scheme 4.2.12).

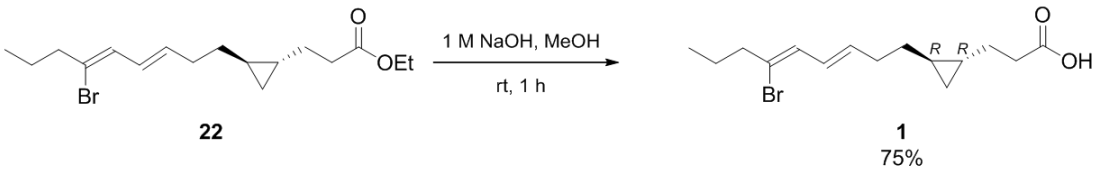

Scheme 4.2.12: Basic hydrolysis of **22** resulting in majusculoic acid **1**.

4.3. Conclusion

In conclusion, the natural product majusculoic acid that is produced in cyanobacteria was successfully synthesized for the first time. In this regard, two total synthetic pathways were identified reaching overall yields of 1.4% over 12 steps (cross metathesis) and 3.7% over 14 steps (*Wittig* reaction) for the natural product. It needs to be emphasized that majusculoic acid bears synthetically challenging molecular units, which require advanced diastereo- and enantioselective chemistry. Examples are the incorporation of a *trans*-cyclopropane moiety and selective introduction of E- and Z- olefinic groups. Those exceptional structural features were successfully incorporated employing first the by *den Hartog* et. al. in our laboratories established asymmetric conjugate addition of Grignard reagent followed by a subsequent intramolecular trapping reaction of the enolate leading to the desired disubstituted *trans*-cyclopropane moiety with high *ee* and known absolute configuration.[20] Furthermore, cross metathesis, Wittig reaction and thermodynamic double bond isomerization were applied resulting in the first synthesizes of majusculoic acid **1**, allowing for the first time the determination of the absolute configuration (4*R*,5*R*) of the *trans*-cyclopropyl unit incorporated in the natural compound.

This natural product is of interest to be investigated more in detail, since it shows antifungal activity against *Candida* species. However, biological test were so far restricted due to the limited availability of the majusculoic acid **1**. Now, having this compound in hand and having evaluated its scalable total synthesis this natural product is accessible for further biological studies to allow understanding of its action and role. Furthermore, the gained knowledge might result in new drug candidates inspired by natural fatty acids in the near future.

4.4 Experimental Section

4.4.1 Materials and Methods

All chemicals and reagents were purchased from commercial suppliers (*Acros* and *Sigma-Aldrich*) and used without further purification. Dry solvents were taken from an *MBraun* solvent purification system (SPS-800). Thin layer chromatographic (TLC) analysis was performed on Merck silicagel 60/Kieselguhr F254, 0.25 mm and visualized by UV and staining with *Seebach's* reagent. Column chromatography was performed using silica gel (P60, 230 – 400 mesh).
^{1}H-NMR-, ^{13}C-NMR-, ^{31}P-NMR-, heteronuclear single-quantum correlation- (HSQC) spectra, Nuclear *Overhauser* effect spectroscopy (NOESY) and correlation spectroscopy (COSY) were recorded on a *Agilent 400* (400 MHz for ^{1}H-NMR, 100.59 MHz for ^{13}C-NMR) using $CDCl_3$ ($CDCl_3$: δ 7.26 for ^{1}H-NMR, δ 77.16 for ^{13}C-NMR). Data are reported as follows: chemical shifts, multiplicity (s= singlet, d= doublet, t= triplet, q= quartet, br= broad, m= multiplet), coupling constants *J* (Hz) and integration.
High resolution mass spectrometry (HRMS) was carried out on a LTQ ORBITRAP XL spectrometer (*Thermo Scientific*) employing **e**lectro**s**pray **i**onization (ESI) in positive ion mode (EI+) and negative ion mode (EI-). Optical rotations were measured on a *Schmidt + Haensch* polarimeter (Polartronic MH8) with a 10 cm cell (concentration *c* given in g/100 mL).
Melting points were measured on a *Büchi* B-545 and recorded in °C. The **e**nantiomeric **e**xcess (*ee*) was determined by chiral GC (HP6890, Chiraldex G-TA 30 m x 0.25 mm x 0.25 μm) using flame ionization detection.
Optical rotations were measured on a *Schmidt + Haensch* polarimeter (Polartronic MH8) with a 10 cm cell (concentration *c* given in g/100 mL).

4.4.2 General Procedures

Copper catalyst
Cu(I) (1 equiv) and *R*-TolBINAP (1.5 equiv) were dissolved in anhydrous *t*BME (800 mL/mmol of Cu(I)) and stirred for 2 h at rt. The obtained mixture was used without further purification.

Grignard reagent 14
Grinded Mg (1.1 equiv) was added to anhydrous ether (4 mL/30 mmol). 1/20 of the amount of bromide (0.05 equiv) was added at once to the solution to start the reaction. The rest of the bromide (0.95 equiv) was dissolved in anhydrous ether (1 mL/3 mmol of substrate) and added slowly to the reaction mixture. The molarity of the resulting Grignard solution was determined by titration before it was used in the next synthetic step.

Titration of *Grignard* reagent 14

1 mL of the *Grignard* solution **14** is added to a solution of one crystal of 1.10 phenanthroline in 5 mL ether. 2-Butanol is added slowly to the resulting red mixture till the color disappears.

4.4.3 Synthesis and Characterization

(E)-2-((E)-Hex-2-en-1-ylidene)-1,1-dimethylhydrazine (6). Aldehyde **4** (1 equiv) was dissolved in anhydrous CH_2Cl_2 (10 mL/ mmol). Dimethylhydrazine (1.05 equiv) was added at rt to the solution and the mixture stirred for 40 h. Subsequently, water (10 mL/ mmol) was added and the resulting mixture was extracted with ether (10 mL/ mmol). All organic layers were combined, dried over $MgSO_4$ and the solvent was removed by rotary evaporation. The hydrazone **6** was obtained as a yellowish oil with a yield of 87% and was used without further purification in the next step of the synthesis. ^{1}H NMR (400 MHz, $CDCl_3$); δ (ppm): 7.0 (d, J= 8.8 Hz, 1H); 6.17 (dd, J= 15.2 Hz, J= 8.8 Hz, 1H); 5.79 (dt, J= 16.6 Hz, J= 6.8 Hz, 1H); 2.81 (s, 6H); 2.12 (q, J= 7.2 Hz, 2H); 1.42 (q, J= 7.2 Hz, 2H); 0.91 (t, J= 7.2 Hz, 3H). ^{13}C NMR (100 MHz, $CDCl_3$); δ (ppm): 137.22 (1C; CH); 135.79 (1C, CH); 129.2 (1C, CH); 43.07 (2C, CH_3); 34.85 (1C, CH_2); 22.39 (1C, CH_2); 13.80 (1C, CH_3). HR-MS (EI+) (*m/z)*: found 141.139 $[M+H]^+$, calculated 141.139 $[M+H]^+$.

(E)-2-((Z)-3-Bromohex-2-en-1-ylidene)-1,1-dimethylhydrazine (7). An solution of NBS (1 equiv) in anhydrous CH_2Cl_2 (15 mL/ mmol) was added dropwise to a solution of the α,β-unsaturated hydrazone **6** (1 equiv) in CH_2Cl_2 (10 mL/ mmol). The resulting mixture was stirred for additional 20 h at rt. Subsequently, water (10 mL/ mmol) was added and the resulting mixture was extracted with CH_2Cl_2 (10 mL/ mmol). All organic layers were combined, dried over $MgSO_4$ and concentrated under reduced pressure. Flash column chromatography (1:6, ether: pentane) gave the pure product **7** as yellow oil with a yield of 45%. The isolated product contains a isomeric mixture of 1:11 (*E*:*Z*).

^{1}H NMR (400 MHz, $CDCl_3$); δ (ppm): **Z-7**: 7.06 (d, J= 8.4 Hz, 1H); 6.42 (d, J= 8.4 Hz, 1H); 2.89 (s, 6H); 2.48 (t, J= 7.2 Hz, 2H); 1.61 (q, J= 7.2 Hz, 2H); 0.88 (t, J= 7.2 Hz, 3H); **E-7**: 6.96 (d, J= 8.4 Hz, 1H); 6.62 (d, J= 8.4 Hz, 1H); 2.86 (s, 6H); 2.55 (t, J= 7.2 Hz, 2H); 1.63 (q, J= 7.2 Hz, 2H); 0.91 (t, J= 7.2 Hz, 3H). ^{13}C NMR (100 MHz, $CDCl_3$); δ (ppm): 133.54 (1C; CH); 128.53 (1C, CBr); 126.62 (1C, CH); 43.71 (1C, CH_2); 43.54 (2C, CH_3); 21.16 (1C, CH2); 12.69 (1C, CH_3). HR-MS (EI+) (*m/z)*: found 219.049 $[M(^{79}Br)+H]^+$, 221.047 $[M(^{81}Br)+H]^+$, calculated 219.049 $[M(^{79}Br)+H]^+$, 221.047 $[M(^{81}Br)+H]^+$.

(*Z*)-3-Bromohex-2-enal (2b). The hydrazone **7** (1 equiv) was added at rt to an aq solution of

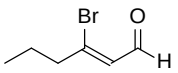

HCl (1 M, 10 mL/ mmol). After 5 min stirring pentane was added (10 mL/ mmol) and the reaction mixture was stirred for additional 16 h. The layers were separated and the aq. layer was extracted with pentane (2*10 mL/ mmol). The combined organic layers were dried over $MgSO_4$ and carefully concentrated under reduced pressure. Flash column chromatography (1:99, ether: pentane) yielded the pure colorless oil **2b** with a yield of 73%. The isolated product contains less than 3% of the E-isomer. ^{1}H NMR (400 MHz, $CDCl_3$); δ (ppm): **Z-2b**: 9.89 (d, J= 6.8 Hz, 1H); 6.28 (d, J= 6.8 Hz, 1H); 2.63 (t, J= 7.2 Hz, 2H); 1.69 (q, J= 7.2 Hz, 2H); 0.93 (t, J= 7.2 Hz, 3H); **E-2b**: 9.81 (d, J= 7.2 Hz, 1H); 6.54 (d, J= 7.2 Hz, 1H); 2.97 (t, J= 7.2 Hz, 2H); 1.73 (q, J= 7.2 Hz, 2H); 0.87 (t, J= 7.2 Hz, 3H). ^{13}C NMR (100 MHz, $CDCl_3$); δ (ppm): 94.44 (1C; CHO); 128.6 (1C, CH); 45.01 (1C, CH_2); 20.91 (1C, CH_2); 12.73 (1C, CH_3). HR-MS (EI+) (*m/z)*: found 176.990 $[M(^{79}Br)+H]^+$, 178.888 $[M(^{81}Br)+H]^+$, calculated 176.991 $[M(^{79}Br)+H]^+$, 178.889 $[M(^{81}Br)+H]^+$.

(*Z*)-4-Bromohepta-1,3-diene (2a). Methyltriphenylphosphonium bromide (1.5 equiv) was

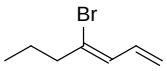

dissolved in anhydrous THF (10 mL /mmol) and cooled to 0 °C. *n*BuLi (1.6M, 1.4 equiv) was added drop wise and the resulting reaction mixture was stirred for 1 h at this temperature. Subsequently, the aldehyde **2b** was added and the solution was stirred for additional 30 min before it was quenched by adding water (10 mL/mmol), followed, by an extraction with ether (3*10 mL/ mmol). The combined organic layers were dried over $MgSO_4$ and carefully concentrated under reduced pressure. Flash column chromatography (1:99, ether: pentane) provided the pure colorless oil **2a** with a yield of 72%. ^{1}H NMR (400 MHz, $CDCl_3$); δ (ppm): 6.59 (dt, J= 16.8 Hz, J= 10.4 Hz, 1H); 6.28 (d, J= 9.6 Hz, 1H); 5.31 (d, J= 16 Hz, 1H); 5.26 (d, J= 10.4 Hz, 1H); 2.45 (t, J= 7.2 Hz, 2H); 1.61 (q, J= 7.2 Hz, 2H); 0.87 (t, J= 7.2 Hz, 3H). ^{13}C NMR (100 MHz, $CDCl_3$); δ (ppm): 134.79 (1C, CH); 130.07 (1C, CBr); 128.39 (1C, CH); 118.99 (1C, CH_2); 43.84 (1C, CH_2); 21.52 (1C, CH_2); 13.08 (1C, CH_3). HR-MS (EI+) (*m/z)*: found 175.010 $[M(^{79}Br)+H]^+$, 177.001 $[M(^{81}Br)+H]^+$, calculated 175.012 $[M(^{79}Br)+H]^+$, 177.010 $[M(^{81}Br)+H]^+$.

(E)-4-chlorobut-2-enoic acid (12). NCS was recrystallized in acetic acid and dried overnight

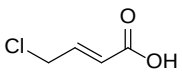

under vacuum before use. The commercial available acid **11** (1 equiv) and PhSeCl (10 mol%) were dissolved in acetonitrile (5 mL/ mmol). Subsequently, a solution of NCS (1.1 equiv) in acetonitrile (2 mL/ mmol) was added slowly at rt over a time period of 24 h. After stirring for an additional 40 h at this temperature the reaction mixture was concentrated. Ether was added until the precipitation of a white solid was completed and the resulting suspension was filtered. The precipitate was washed with ether, before the organic layer was washed with water (2*0,5 mL/ mmol), dried over $MgSO_4$ and concentrated under reduced pressure. Recrystallization in pentane:ether (4:1) leads to the pure white product **12** with an isolated yield of 68%. ^{1}H NMR (400 MHz, $CDCl_3$); δ (ppm): 7.09 (dt, J= 15.6 Hz, J= 6.0 Hz, 1H), 6.12 (dt, J= 15.6 Hz, J= 1.6 Hz, 1H), 4.19 (dd, J= 6 Hz, J= 1.6 Hz, 2H). HR-MS (EI+) (*m/z)*: found 121.006 $[M+H]^+$, calculated 121.005 $[M+H]^+$. Mp= 74-75 °C. Data in accordance with those described in literature, ref 19.

(E)-*S*-Ethyl 4-chlorobut-2-enethioate (10). A solution of DMAP (0.1 equiv) and the acid **12** (1equiv) in anhydrous CH_2Cl_2 (1.5 mL/ mmol) was stirred at rt for 5 min. After cooling the reaction mixture to 0 °C, a solution of ethanethiol (1 equiv) and DCC (1.05 equiv) in anhydrous CH_2Cl_2 (0.5 mL/ mmol of substrate) was added. The resulting reaction mixture was stirred for an additional 4 h in which period the temperature was allowed to rise to rt. Subsequently, the precipitate was filtered over celite and washed with pentane. The organic layer was dried over $MgSO_4$ and concentrated underreduced pressure. Flash column chromatography (1:99, ether:pentane) yielded the product **10** with 5-10% of byproduct **13** (*trans*-*S*-ethyl 2-(ethylthio) cyclopropanecarbothioate).

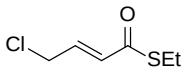

Further purification: The crude mixture of E-*S*-ethyl 4-chlorobut-2-enethioate **10** was dissolved in a mixture of water and acetonitrile (1:4, 3 mL/ mmol). OXONE® (0.1 equiv) was added at 0 °C to the mixture. After stirring at this temperature for 20 min the solution was warmed to rt and stirred for an additional 40 min. The reaction mixture was quenched with brine (10 mL/ mmol) at 0 °C and extracted with ether (3*10 mL/ mmol). All organic layers were combined, dried over $MgSO_4$ and concentrated under reduced pressure. Flash column chromatography (1:99, ether: pentane, R_f= 0.2) yielded the pure product **10** as colorless oil with a yield of 63% over both steps. ^{1}H NMR (400 MHz, $CDCl_3$); δ (ppm): 6.87 (dt, J= 15.2 Hz, J= 6.0 Hz, 1H), 6.34 (d, J= 15.6 Hz, 1H), 4.15 (d, J= 6 Hz, 2H); 2.95 (q, J= 7.6 Hz, 2H); 1.27 (t, J= 7.6 Hz, 3H). ^{13}C NMR (100 MHz, $CDCl_3$); δ (ppm): 190.12 (1C, CO); 137.66 (1C, CH); 130.95 (1C, CH); 42.46 (1C, CH_2); 23.22 (1C, CH_2); 14.40 (1C, CH_3). HR-MS (EI+) (*m/z*): found 165.014 $[M(^{35}Cl)+H]^+$, 167.010 $[M(^{37}Cl)+H]^+$, calculated 165.014 $[M(^{35}Cl)+H]^+$, 167.011 $[M(^{37}Cl)+H]^+$.

(1*R*,2*R*)-*S*-Ethyl 2-(but-3-en-1-yl)cyclopropanecarbothioate (9). The Grignard reagent (1-2 M solution in ether, 1.1 equiv) was added at -78 °C to a solution of the premade copper catalyst (CuI (1 mol%), *R*-TolBINAP (1.5 mol%) in anhydrous *t*BuOMe (8 mL/ mmol)) and the mixture stirred for 10 min. This was followed by a slow addition over 2 h with a syringe pump of a solution of the substrate **10** (1 equiv) in anhydrous CH_2Cl_2 (0.5 mL/ mmol). After additional stirring for 2 h at this temperature the reaction mixture was allowed to warm up slowly to rt overnight. Subsequently, the reaction mixture was quenched with EtOH (0.4 mL/ mmol) and an aq. solution of NH_4Cl (1 M, 2 mL/ mmol). Ether (10 mL/ mmol) and an aq. solution of NH_4Cl (1 M, 10 mL/ mmol) were added. The resulting layers were separated and the aq. layer was extracted with ether (2*10 mL/ mmol of substrate). All organic layers were combined, dried over $MgSO_4$ and carefully concentrated under reduced pressure. Flash column chromatography (1:99, ether:pentane) yielded the pure product **9** as colorless oil with a yield of 75%. ^{1}H NMR (400 MHz, $CDCl_3$); δ (ppm): 5.8 (ddt, J= 17.2 Hz, J= 10.4 Hz, J= 6.8 Hz, 1H), 5.97 (m, 2H), 2.86 (q, J= 7.6 Hz, 2H); 2.13 (dtt, J= 7.2 Hz, J= 6.8 Hz, J= 1.2 Hz, 2H); 1.75 (dt, J= 8 Hz, J= 4 Hz, 1H), 1.51 (m, 1H), 1.4 (dtd, J= 7.6 Hz, J= 3.6 Hz, J= 7.6 Hz, 2H), 1.33 (dt, J=8.8 Hz, J= 4.4 Hz, 1H); 1.22 (t, J= 7.6 Hz, 3H); 0.78 (ddd, J= 8 Hz, J= 6.4 Hz, J= 4 Hz, 1H). ^{13}C NMR (100 MHz, $CDCl_3$); δ (ppm): 199.39 (1C, CO); 138.34 (1C, CH); 115.36 (1C, CH_2); 33.11 (1C, CH_2); 32.47 (1C, CH_2); 30.07 (1C, CH); 24.78 (1C, CH); 23.08 (1C, CH_2); 17.52 (1C, CH_2); 14.64 (1C, CH_3).

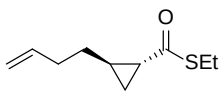

HR-MS (EI+) (*m/z)*: found 185.100 $[M+H]^+$, calculated 185.100 $[M+H]^+$. *Ee*: 95%, column: Chiraldex-G-TA, 70 °C for 50 min, retention times (min): 17.269 (*R*,*R*), 19.419 (*S*,*S*). $[\alpha]_D$ = -106.2 (10 mg/mL in MeOH).

The enantiomeric excess (*ee*) of **9** was determined using the methyl ester of **9**: 10 mg of the acid **9** and 20 mg of K_2CO_3 were dissolved in 0.5 mL MeOH and stirred for 3 h. Subsequently, 0.5 mL of an aq. NH_4Cl solution (1 M) was added and the resulting mixture was extracted with ether (3*0.5 mL). All organic layers were combined, dried over $MgSO_4$ and carefully concentrated under reduced pressure. The methyl ester was filtered over SiO_2 using ether as eluent. After evaporation of the ether the *ee* of the ester was determined in MeOH using a chiral GC.

(1*R*,2*R*)-2-(But-3-en-1-yl)cyclopropanecarbaldehyde (16). DIBAL-H (1.2 equiv, 1 M) was added dropwise to a stirred solution of the thioester **9** (1 equiv) in anhydrous CH_2Cl_2 (0.5 mL/ mmol) at -78°C. After stirring for 3 h at this temperature the reaction mixture was poured into a aq. Rochelle`s salt-solution (saturated, 5 mL/ mmol) and stirred for 1h at rt. The layers were separated and the aq. layer was extracted with $CH_2Cl_2$ (2x 5 mL/ mmol). All organic layers were combined, washed with the aq. Rochelle`s salt-solution (saturated, 2*5 mL/ mmol), dried over $MgSO_4$ and carefully concentrated under reduced pressure. Flash column chromatography (5:95, ether:pentane) yielded the pure product **16** as colorless oil with an isolated yield of 74%. The obtained aldehyde **16** was used immediately in the next synthetic step to avoid decomposition. ^{1}H NMR (400 MHz, $CDCl_3$); δ (ppm): 9 (d, J= 5.6 Hz, 1H); 5.79 (ddt, J= 16.8 Hz, J= 10 Hz, J= 6.8 Hz, 1H), 4.98 (m, 2H), 2.16 (dt, J= 6.8 Hz, J= 6 Hz, 2H); 1.61 (m, 1H); 1.46 (m, 3H), 1.28 (m, 1H), 0.92 (m, 1H). ^{13}C NMR (100 MHz, $CDCl_3$); δ (ppm): 201.68 (1C, CO); 138.12 (1C, CH); 115.57 (1C, CH_2); 33.17 (1C, CH_2); 31.9 (1C, CH_2); 30.35 (1C, CH); 22.02 (1C, CH); 14.64 (1C, CH_2). HR-MS (EI+) (*m/z)*: found 125.096 $[M+H]^+$, calculated 125.096 $[M+H]^+$.

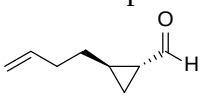

(E)-Ethyl 3-((1*R*,2*R*)-2-(but-3-en-1-yl)cyclopropyl)acrylate (8). Triethyl phosphonoacetate (1.75 equiv) was added dropwise at 0 °C to a stirred solution of NaH (60% dispersion in mineral oil, 1.75 equiv) in anhydrous THF (1 mL/ mmol). The mixture was stirred additionally for 30 min before it was cooled to -20 °C. A solution of the aldehyde (1 equiv) in anhydrous THF (0.1 mL/ mmol) was added dropwise. The resulting mixture was stirred for 20 min at -20 °C, for 30 min at rt and diluted with ether (2 mL/ mmol). Subsequently the solution was washed with NH_4Cl (saturated aq. solution, 2 mL/ mmol), Na_2CO_3 (saturated aq. solution, 2 mL/ mmol) and brine (2 mL/ mmol). The organic layer was dried over $MgSO_4$ and carefully concentrated under reduced pressure. Flash column chromatography (5:95, ether: pentane) yielded the pure product **E-8** as colorless oil with an isolated yield of 61%. ^{1}H NMR (400 MHz, $CDCl_3$); δ (ppm): 6.46 (dd, J= 15.6 Hz, J= 10 Hz, 1H); 5.82 (d, J= 15.6 Hz, 1H), 5.79 (ddt, J= 17.2 Hz, J= 10 Hz, J= 6.4 Hz, 1H); 4.97 (m, 2H); 4.15 (q, J= 7.2 Hz, 2H); 2.13 (dt, J= 7.2 Hz, J= 7.2 Hz, 2H); 1.39 (m, 2H); 1.3 (m, 1H); 1.26 (t, J= 7.2 Hz, 3H); 1.01 (m, 1H); 0.8 (ddd, J= 9.2 Hz, J= 4.8 Hz, J= 4.4 Hz, 1H); 0.76 (m, 1H). ^{13}C NMR (100 MHz, $CDCl_3$); δ (ppm): 167.34 (1C, CO); 153.90 (1C, CH); 138.53 (1C, CH); 117.92 (1C, CH); 115.09 (1C, CH); 59.92 (1C, CH); 33.23

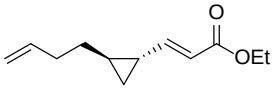

(1C, CH); 32.87 (1C, CH); 22.56 (1C, CH_2); 21.86 (1C, CH_2); 15.7 (1C, CH_3); 14.05 (1C, CH_2). HR-MS (EI+) (*m/z)*: found 195.138 $[M+H]^+$, calculated 195.138 $[M+H]^+$. $[\alpha]_D$ = -84.6 (10 mg/mL in MeOH).

Ethyl 3-((1*R*,2*R*)-2-(but-3-en-1-yl)cyclopropyl)propanoate (3a). Cu(I)Cl (20 mol%) was added to a stirred solution of the unsaturated ester **8** (1 equiv) in MeOH (5 mL/ mmol). $NaBH_4$ (6x 1 equiv) was carefully added in portions of 1 equiv (every 45 min) to the reaction mixture. Subsequently, the reaction was quenched with HCl (2 M aq. solution) until a pH of 4 was reached. The resulting mixture was filtered and diluted with ether (0.5 mL/ mmol). After separation of the layers the organic layer was washed with water, dried over $MgSO_4$ and carefully concentrated under reduced pressure. Flash column chromatography (5:95, ether:pentane) yielded the pure product **3a** as a colorless oil with an isolated yield of 84%. ^{1}H NMR (400 MHz, $CDCl_3$); δ (ppm): 5.81 (ddt, J= 17.2 Hz, J= 10.4 Hz, J= 6.8 Hz, 1H); 4.95 (m, 2H); 4.1 (q, J= 7.2 Hz, 2H); 2.34 (t, J= 7.2 Hz, 2H); 2.08 (q, J= 7.2 Hz, 2H); 1.48 (m, 2H); 1.29 (m, 2H), 1.22 (t, J= 7.2 Hz, 3H); 0.41 (m, 2H); 0.18 (t, J= 6.4 Hz, 2H). ^{13}C NMR (100 MHz, $CDCl_3$); δ (ppm): 174.33 (1C, CO); 139.31 (1C, CH); 114.59 (1C, CH_2); 60.15 (1C, CH_2); 34.34 (1C, CH_2); 33.71 (1C, CH_2); 33.42 (1C, CH_2); 29.46 (1C, CH_2); 18.17 (1C, CH); 18.01 (1C, CH); 13.99 (1C, CH_3); 11.58 (1C, CH_2). HR-MS (EI+) (*m/z)*: found 197.154 $[M+H]^+$, calculated 197.154 $[M+H]^+$. $[\alpha]_D$ = -50.8 (10 mg/ mL in MeOH).

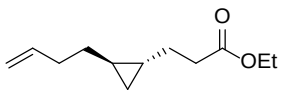

Ethyl 3-((1*R*,2*R*)-2-(3-hydroxypropyl)cyclopropyl)propanoate (20). A dried tree neck flask equipped with a stirring bar and an inlet tube was connected to a gas-washing bottle filled with an aq. KI solution. The ozone generator was connected to the inlet tube.

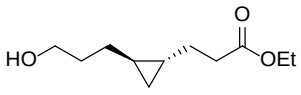

The olefin **3a** (1 equiv) was dissolved under inert atmosphere in a mixture of EtOH and CH_2Cl_2 (1:1, 20 mL/ mmol). After cooling to -78°C a slow stream of O_3 was passing through the solution until a blue color remains. Before quenching the reaction with $NaBH_4$ (1.5 equiv) at -78 °C the solution was flushed with N_2 to remove the excess of O_3. The reaction mixture was stirred for 30 min at rt, an aq. HCl solution (2 M, pH 5) was added and diluted with CH_2Cl_2 (0.5 mL/ mmol). After separation of the phases the aq. layer was extracted with CH_2Cl_2 (1 mL/ mmol). Subsequently, the combined organic layers were washed with water, dried over $MgSO_4$ and carefully concentrated under reduced pressure. Flash column chromatography (1:1, ether:pentane) yielded the pure product **20** as a colorless oil with a yield of 86%. ^{1}H NMR (400 MHz, $CDCl_3$); δ (ppm): 4.13 (q, J= 7.2 Hz, 2H); 3.67 (t, J= 6.8 Hz, 2H), 2.38 (t, J= 7.6 Hz, 2H), 1.66 (qi, J= 7.2 Hz, 2H); 1.54 (qi, J= 7.6 Hz, 2H); 1.31 (m, 2H); 1.39 (m, 2H); 1.26 (t, J= 7.2 Hz, 3H), 0.47 (m, 2H); 0.24 (m, 2H). ^{13}C NMR (100 MHz, $CDCl_3$); δ (ppm): 174.47 (1C, CO); 62.59 (1C, CH_2); 60.25 (1C, CH_2); 34.32 (1C, CH_2); 32.48 (1C, CH_2); 30.08 (1C, CH_2); 29.40 (1C, CH_2); 18.10 (1C, CH); 17.99 (1C, CH); 13.96 (1C, CH_3); 11.56 (1C, CH_2). HR-MS (EI+) (*m/z)*: found 201.149 $[M+H]^+$, calculated 201.149 $[M+H]^+$. $[\alpha]_D$ = -7.2 (10 mg/ mL in MeOH).

Ethyl 3-((1*R*,2*R*)-2-(3-bromopropyl)cyclopropyl)propanoate (21). CBr_4 (2 equiv) was added to a solution of the alcohol **20** (1 equiv) in ether (10 mL/ mmol). The reaction mixture was cooled to 0 °C and PPh_3 (2 equiv) was added in portions. After stirring for 6 h the solution was filtered and washed with ether. The combined organic layers were washed with water, dried over $MgSO_4$ and carefully concentrated under reduced pressure. Flash column chromatography (1:1, ether:pentane) yielded the pure product **20** as a colorless oil with a yield of 76%. ^{1}H NMR (400 MHz, $CDCl_3$); δ (ppm): 4.12 (q, J= 7.2 Hz, 2H); 3.41 (t, J= 6.8 Hz, 2H), 2.35 (t, J= 8 Hz, 2H), 1.91 (qi, J= 7.2 Hz, 2H); 1.52 (q, J= 8 Hz, 2H); 1.32 (qi, J= 6.8 Hz, 2H); 1.24 (t, J= 7.2 Hz, 3H); 0.44 (m, 2H); 0.23 (t, J= 7.2 Hz, 2H). ^{13}C NMR (100 MHz, $CDCl_3$); δ (ppm): 174.25 (1C, CO); 60.28 (1C, CH_2); 34.33 (1C, CH_2); 33.63 (1C, CH_2); 32.73 (1C, CH_2); 32.32 (1C, CH_2); 29.39 (1C, CH_2); 17.97 (1C, CH); 17.63 (1C, CH); 14.06 (1C, CH_3); 11.52 (1C, CH_2). HR-MS (EI+) (*m/z)*: found 263.064 [M(^{79}Br)+H]$^+$, 265.062 [M(^{81}Br)+H]$^+$, calculated 263.064 [M(^{79}Br)+H]$^+$, 265.062 [M(^{81}Br)+H]$^+$. $[\alpha]_D$ = -13.5 (10 mg/ mL in MeOH).

(3-((1*R*,2*R*)-2-(3-Ethoxy-3-oxopropyl)cyclopropyl)propyl)triphenylphosphonium bromide (3b). PPh_3 (1 equiv) and the bromide **21** (1 equiv) were heated for 16 h at 100 °C. The obtained mixture was washed with anhydrous pentane and used after drying without further purification. ^{1}H NMR (400 MHz, $CDCl_3$); δ (ppm): 7.77 (dd, J= 12.8 Hz, J= 8 Hz, 6H); 7.73 (t, J= 7.2 Hz, 3H); 7.64 (m, 6H); 4 (t, J= 6.8 Hz, 2H); 3.72 (m, 2H), 2.21 (q, J= 6.4 Hz, 2H), 1.65 (m, 2H); 1.53 (m, 2H); 1.42 (m, 2H); 1.16 (q, J= 7.2 Hz, 3H); 0.41 (m, 2H); 0.16 (m, 2H). ^{31}P-NMR ($CDCl_3$, 162 MHZ); δ (ppm): 24.61. HR-MS (EI+) (*m/z)*: found 445.229 [M-Br$^-$]$^+$, calculated 445.229 [M-Br$^-$]$^+$.

Ethyl 3-((1*R*,2*R*)-2-((3E,5Z)-6-bromonona-3,5-dien-1-yl)cyclopropyl)propanoate (22).

Strategy 1: Cross metathesis

A solution of the alkene **2a** (1.5 equiv) and the alkene **3a** (1 equiv) in toluene (2 mL/ mmol) was added to a solution of the ruthenium catalyst (5 mol%) and dichlorobenzoquinone (10 mol%) in toluene (16 mL/ mmol). The resulting reaction mixture was heated at reflux for 16 h after it was stirred for 20 min at rt. Subsequently, the reaction was quenched at rt with ethylvinylether and the mixture stirred for an additional 20 min at this temperature. The resulting solution was dried over $MgSO_4$ and carefully concentrated under reduced pressure. Flash column chromatography (1:99, ether:pentane) yielded the pure product **22** as a colorless oil with a yield lower that 10% as a diastereomer mixture (*E*:*Z*, 2:1).

Note: Changes of the substrate ration, solvent, temperature, catalyst loading and of the ruthenium catalyst were not leading to improved yields. Instead the amount of both homodimers **23** and **24** increased resulting in a product mixture of **22**, **23** and **24**, which was challenging to purify.

Strategy 2: *Wittig* reaction

Triphenylphosphonium bromide **3b** (1 equiv) was dissolved in anhydrous THF (10 mL/ mmol) and the solution cooled to -78 °C. *n*BuLi (1.6M, 1.2 equiv) was added dropwise and the resulting reaction mixture was stirred for 1 h at this temperature. Subsequently, the mixture was warmed up slowly to 0 °C, stirred for additionally 30 min and was cooled again to -78 °C. The aldehyde **2b** (1 equiv) was dropwise added and the solution was stirred for additional 1 h at this temperature before it was quenched by adding HCl (1M, 10 mL/ mmol). This was followed, by an extraction with CH_2Cl_2 (3*10 mL/ mmol). The combined organic layers were dried over $MgSO_4$ and carefully concentrated under reduced pressure. Flash column chromatography (1:99, ether: pentane) yielded the pure colorless oil **22** with a yield of 43% as a diastereomer mixture (E:Z, 1:3). Further isomerization of the diastereoisomers was performed. Therefore, a solution of **22** and iodine (1 crystal for 20 mg of **22**) in $CHCl_3$ (2 mL/ mmol) was heated for 30 min at 40 °C. The excess of iodine was destroyed by adding $Na_2S_2O_3$ (sat. solution, 1 mL/ mmol). The resulting solution was extracted with $CHCl_3$ (2 mL/ mmol), dried over $MgSO_4$ and carefully concentrated under reduced pressure yielding in the E-isomer of **22** (less than 10% of the Z-isomer remains). ^{1}H NMR (400 MHz, $CDCl_3$); δ (ppm): 6.29 (q, J= 14.8 Hz, J= 10, 1H); 6.19 (d, J= 10 Hz, H), 5.79 (dt, J= 14.8 Hz, J= 7.2 Hz, 1H), 4.11 (q, J= 7.2 Hz, 2H); 2.44 (t, J= 7.2 Hz, 2H); 2.36 (t, J= 7.2 Hz, 2H); 2.19 (q, J= 7.2 Hz, 2H); 1.59 (m, 3H); 1.53 (m, 2H); 1.37 (qi, J= 6.8 Hz, 1H); 1.25 (t, J= 7.2 Hz, 3H); 0.91 (t, J= 7.6 Hz, 3H); 0.46 (m, 2H); 0.23 (t, J= 6.4 Hz, 2H). ^{13}C NMR (100 MHz, $CDCl_3$); δ (ppm): 173.85 (1C, CO); 136.89 (1C, CH); 128.17 (1C, CH); 127.90 (1C, CH); 127.04 (1C, CBr); 60.32 (1C, CH_2); 43.75 (1C, CH_2); 34.63 (1C, CH_2); 33.87 (1C, CH_2); 33.12 (1C, CH_2); 29.73 (1C, CH_2); 21.60 (1C, CH_2); 18.56 (1C, CH); 18.44 (1C, CH); 14.40 (1C, CH_3); 13.1 (1C, CH_3); 12.03 (1C, CH_2). HR-MS (EI+) (*m/z)*: found 343.127 $[M(^{79}Br)+H]^+$, 345.125 $[M(^{81}Br)+H]^+$, calculated 343.127 $[M(^{79}Br)+H]^+$, 345.125 $[M(^{81}Br)+H]^+$. $[\alpha]_D$ = -6 (10 mg/ mL in MeOH).

3-((1*R*,2*R*)-2-((3E,5Z)-6-Bromonona-3,5-dien-1-yl)cyclopropyl)propanoic acid (majusculoic acid) (1). 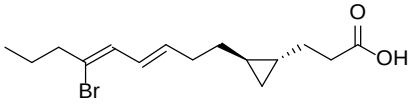

The ethyl ester **22** was dissolved in MeOH and NaOH (1M, 1mL/ mmol) was added. The solution was stirred for 2 h at rt before extraction with ether (3*2 mL/ mmol) took place. The combined organic layer were dried over MgSO4 and carefully concentrated under reduced pressure. The majusculoic acid **1** was isolated as a colorless solid with a yield of 82%. HR-MS (EI+) (*m/z)*: found 315.095 [M(^{79}Br)+H]$^+$, 317.093 [M(^{81}Br)+H]$^+$, calculated 315.095 [M(^{79}Br)+H]$^+$, 317.093 [M(^{81}Br)+H]$^+$. $[\alpha]_D$ = -16.2 (10 mg/ mL in MeOH).

Table 4.5.1: NMR data (ppm,$CDCl_3$) for majusculoic acid **1**.

Carbon	^{1}H NMR (J in Hz)	COSY** H-> H	TOCSY** H-> H	^{13}C NMR	HMBC** C-> H
1	-			179.6	
2	2.42 (t, 7.2)	3	3,4,5,6	29.2	2
3	1.54 (q, 7.2)	2,4*	2,4,5,6	32.87	2,5
4	0.48 (t, 6.8)	3*,5	2,3,5,7,8	18.03	7,9
5	0.24 (qi, 6.4)	4,6	2,3,4,6,7,8	11.66	2,3
6	0.48 (t, 6.8)	5,7*	2,3,5,7,8	18.3	7
7a	1.27 (m)	6*,8	4,5,6,8	33.95	7,8
7b	1.33 (m)	6*,8	4,5,6,8		3,5,8
8	2.19 (q, 7.6)	7,9	4,5,6,7,9, 10,11,13*	33.6	5*,8
9	5.81 (dt, 14.8, 7.6)	8,10	8,10,11	128.47	8,10*
10	6.3 (dd, 14.8, 10)	11,9	8,9,11	128.16	9,16
11	6.21 (d, 10)	10	8,9,10	137.16	13,14
12	-			127.39	11,13,14
13	2.42 (t, 7.2)	14	8*,14,15	43.58	11,14,15
14	1.58 (q, 7.2)	13,15	13,15	21.31	13,15
15	0.89 (t, 7.6)	14	13,14	12.77	13,14

*Weak signals. **Number of the corresponding carbon atom is given.

4.5 References

1) J. W. Blunt, B. R. Copp, W.-P. Hu, M. H. G. Munro, P. T. Northcote, M. R. Prinsep. Marine natural products. *Nat. Prod. Rep.*, **24**, 31–86 (2007).
2) G. M. Cragg, D. J. Newman. Biodiversity: A continuing source of novel drug leads. *Pure Appl. Chem.*, **77**, 7-24 (2005).
3) D. J. Newman, G. M. Cragg. Natural Products as Sources of New Drugs over the 30 Years from 1981 to 2010. *J. Nat. Prod.*, **75**, 311-335 (2012).
4) M. S. Butler. The role of Natural Product Chemistry in Drug Discovery. *J. Nat. Prod.*, **67**, 2141–2153 (2004).
5) Y.-W. Chin, M. J. Balunas, H. B. Chai, A. D. Kinghorn. Drug discovery from natural sources. *AAPS J.*, **8**, E239–E253 (2006).
6) S. Singh, B. N. Kate, U. C. Banerjee. Bioactive Compounds from Cyanobacteria and Microalgae: An Overview. *Crit. Rev. Biotechnol.*, **25**, 73-95 (2005).
7) I. Bhatnagar, S.-K. Kim. Immense Essence of Excellence: Marine Microbial Bioactive Compounds. *Mar. Drugs*, **8**, 2673-2701 (2010).
8) E. Fattorusso, O. Taglialatela-Scafati. Marine Antimalarials. *Mar. Drugs*, **7**, 130-152 (2009).
9) K. A. El Sayed, P. Bartyzel, X. Shen, T. L. Perry, J. K. Zjawiony, M, T. Hamann. Marine Natural Products as Antituberculosis Agents, *Tetrahedron*, **56**, 949-953 (2000).
10) T. L. Simmons, E. Andrianasolo, K. McPhail, P. Flatt, W. H. Gerwick. Marine natural products as anticancer drugs. *Mol. Cancer Ther.*, **4**, 333-342 (2005).
11) M. Costa, J. Costa-Rodrigues, M. H. Fernandes, P. Barros, V. Vasconcelos, R. Martins. Marine Cyanobacteria Compounds with Anticancer Properties: A Review on the Implication of Apoptosis. *Mar. Drugs*, **10**, 2181-2207 (2012).
12) N. M. Carballeira. New advances in fatty acids as antimalarial, antimycobacterial and antifungal agents. *Prog. Lipid Res.*, **47**, 50-61 (2008).
13) A. M. S. Mayer, A. D. Rodríguez, O. Taglialatela-Scafati, N. Fusetani. Marine Pharmacology in 2009–2011: Marine Compounds with Antibacterial, Antidiabetic, Antifungal, Anti-Inflammatory, Antiprotozoal, Antituberculosis, and Antiviral Activities; Affecting the Immune and Nervous Systems, and other Miscellaneous Mechanisms of Action. *Mar. Drugs*, **11**, 2510-2573 (2013).
14) L. M. Kumaratilake, B. S. Robinson, A. Ferrante, A. Poulos. Antimalarial Properties of *n*-3 and *n*-6 Polyunsaturated Fatty Acids: In Vitro Effects on *Plasmodium falciparum* and In Vivo Effects on *P. berghei*. *J. Clin. Invest.*, **89**, 961-967 (1992).
15) J. B. MacMillan, T. F. Molinski. Majusculoic Acid, a Brominated Cyclopropyl Fatty Acid from a Marine Cyanobacterial Mat Assemblage. *J. Nat. Prod.*, 68, 604-606 (2005).
16) A. Chakrabarti. Microbiology of systemic fungal infections. *J. Postgrad. Med.*, **51**, 16-20 (2005).
17) M. C. Fisher, D. A. Henk, C. J. Briggs, J. S. Brownstein, L. C. Madoff, S. L. McCraw, S. J. Gurr. Emerging fungal threats to animal, plant and ecosystem health. *Nature*, 484, 186-194 (2012).

18) J. A. Tunge, S. R. Mellegaard. Selective Selenocatalytic Allylic Chlorination. *Org. Lett.*, 6, 1205-1207 (2004).
19) A. G. Anderson Jr., R. P. Ko. Synthesis and Electrophilic Substitution of 1-Methyl-, 1,2-Dimethyl-, and 1-Methyl-2-phenyl-2*H*-cyclopenta[*d*]pyridazines. *J. Org. Chem*., **49**, 4769-4772 (1984).
20) T. den Hartog, A. Rudolph, B. Maciá, A. J. Minnaard, B. L. Feringa. Copper-Catalyzed Enantioselective Synthesis of *trans*-1-Alkyl-2-substituted Cyclopropanes via Tandem Conjugate Addition−Intramolecular Enolate Trapping. *J. Am. Chem. Soc.*, **132**, 14349-14351 (2010).
21) T. J. Caggiano. Cobalt Boride. *EROS*, 1287-1291 (2001).
22) R. H. Mach, H.F. Kung, P. Jungwiwattanaporn, Y.-Z. Guo. Synthesis and Biodistribution of a New Class of ^{99m}Tc-labeled Fatty Acid Analogs for Myocardial Imaging. *Nucl. Med. Biol*., **18**, 215-226 (1991).

Chapter 5

New Class of Amphiphilic *N*-Phosphoamino Acids Synthesis and Characterization

In this chapter a new and promising class of amphiphilic phosphoamino acids is introduced. These amphiphiles combine a number of attractive features. First, they consist of only natural building blocks, i.e. amino acids, aliphatic alcohols and phosphonates. Second, these compounds can be synthesized in just four steps leading to a broad variety of amphiphilic *N*-phosphoamino acids in a short time. Different techniques, like nuclear magnetic resonance, differential scanning calorimetry and acid base titration were employed to characterize and study the amphiphiles. Finally, transmission electron microscopy was employed showing the ability of *N*-phosphoamino acids to form a variety of aggregates like micelles, vesicles, sheets and ribbons depending on the building blocks used in their respective structures.

5.1 Introduction

Phosphor plays an important role in the chemistry of life and is found in different natural products like **d**eoxyribo**n**ucleic **a**cid (DNA) with a phosphate backbone and coenzymes like **a**denosine **t**riphos**p**hate (ATP).[1,2] Also, it contributes to many processes like peptide and ester synthesis, transesterification, signal transduction and energy transfer.[2] Predominantly, these phosphorus-containing compounds are esters and anhydrides of phosphoric acid.[1,2] Furthermore, phosphoric esters are also present in amphiphilic structures, like phospholipids and contribute to the polarity of the hydrophilic head group.[1] The primary structural role of phospholipids is the formation of lipid bilayers and therefore, these amphiphilic molecules are major components of the cell membrane (see Chapter 1). In this regard it is interesting to mention that in 1999 *Segré et al.* described the theory of a prebiotic lipid world assuming that small molecules with lipid like properties and self-activating catalytic features could have played a crucial role during prebiotic evolution.[3,4] Already, low concentrations of amphiphiles in the water-rich environment on earth would lead to their enrichment due to self-aggregation properties, since the non-covalent interactions enable a fast exchange of compounds and growth of the assemblies.[5] For such assembly a chain length of at least ten carbons and an appropriate balance between charge and hydrophobicity are the minimum required properties as described by *Hargreaves et al.* in 1977.[6] With the above mentioned features and properties in mind it is interesting to study phosphorus-containing lipid like structures, like *N*-phosphoamino acids **1** and their derivatives (Fig. 5.1.1).

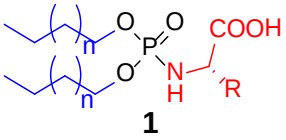

1

Figure 5.1.1: Chemical structure of *N*-phosphoamino acids **1** consisting of three natural occurring building blocks, i.e. amino acids (red), aliphatic alcohol (blue) and phosphoric acid (black).

A further advantage of amphiphilic *N*-phosphoamino acids **1** is that they consist of three natural building blocks (Figure 5.1.1). The hydrophilic head group is an amino acid connected through a central phosphoric acid unit to two aliphatic alcohols representing the hydrophobic tail. Additionally, *Zhao* and coworkers described already around 20 years ago high reactivity of *N*-phosphoamino acids in aqueous media leading to self-activating bioorganic reactions.[7,8] As shown in Scheme 5.1.1, the reactivity is based on the presence of the mixed anhydride **3** that can be formed directly from the acid **1** or *via* an cyclization to anhydride **2** and subsequent elimination of an aliphatic alcohol. In 2009, *Ni et al.* postulated that the resulting **c**yclic **a**cyl**p**hospho**r**amidate (CAPA) **3** can act as a reactive intermediate leading to a variety of different structures (**4**, **5**, **6** and **7**) that exhibit similarity to products originating from *Leuchs* anhydride **8** (Scheme 5.1.1).[9,10] This research indicates a potential role of *N*-phosphoamino acids **1** as chemically active compound for the understanding of prebiotic synthetic pathways to oligopeptides and the phosphorylation as well as de-phosphorylation of amino acids and peptides.[11]

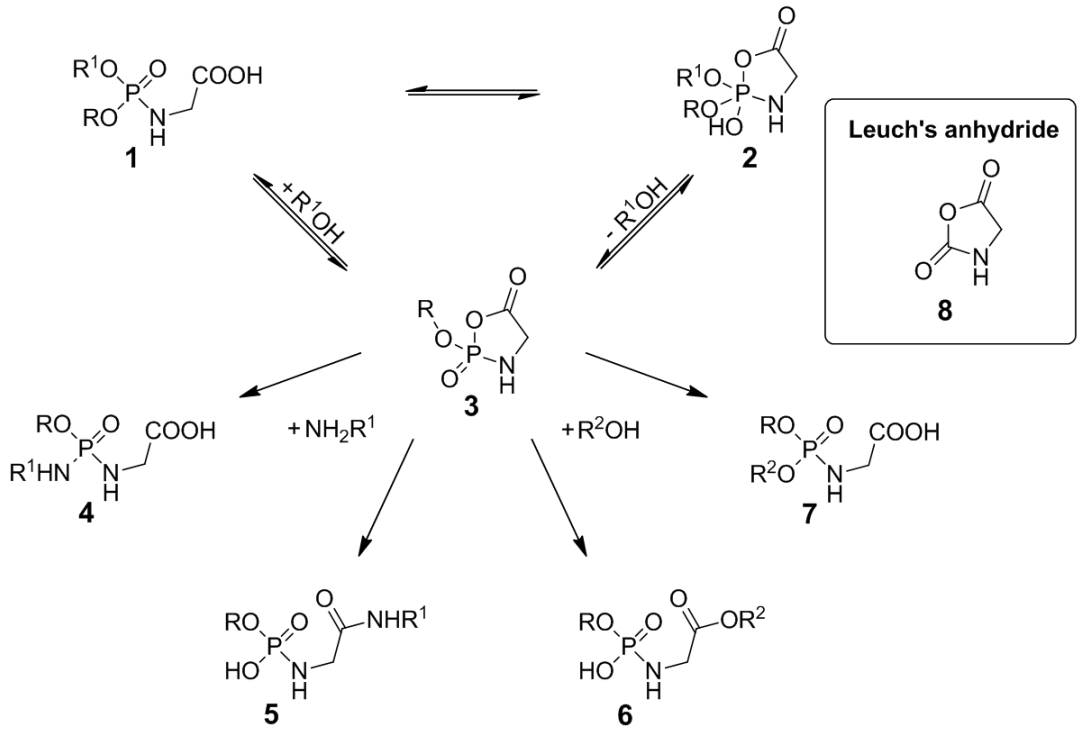

Scheme 5.1.1: Proposed self-activation of *N*-phosphoamino acid **1** forming a mixed anhydride **3** as reactive intermediate and its subsequent transformations.[9]

This simple structure of *N*-phosphoamino acids, with diverse reaction possibilities seems to be a promising model to study the aggregation behavior of lipid like compounds considering that all building blocks are of natural origin. Hence, different methods have been established to give access to *N*-phosphoramides. Already, in 1910 *Neuberg* and *Pollak* demonstrated the use of phosphoryl chloride as phosphorylating agent for amines.[12] However, due to the low stability of these chlorides in aqueous solution only low yields were reported for the obtained *N*-phosphoramides. To overcome this drawback *Fischer* described in 1914 an improved synthesis using anhydrous condition to increase the stability of the phosphoryl chloride.[13] But at the same time they faced solubility issues for the nucleophilic component and the phosphorochloridic acid. Therefore, *Todd* and coworkers published in 1945 two studies with the main focus on phosphorylation using dibenzyl phosphate **9** or dialkyl phosphites **12** as starting materials (Scheme 5.1.2).[14,15] First, phosphate **9** was used as precursor for the dibenzyl phosphorylchloride **10**, i.e. the phosphorylation agent for a variety of amines giving the desired *N*-phosphoamides **11**.[14] Second, to improve yields and allow the application of mild reaction conditions *Todd* and coworkers used an in-situ activation of phosphite **12** with tetrachloromethane resulting in trichloromethyl phosphate **13** for phosphorylation of amines (Scheme 5.1.2).[15]

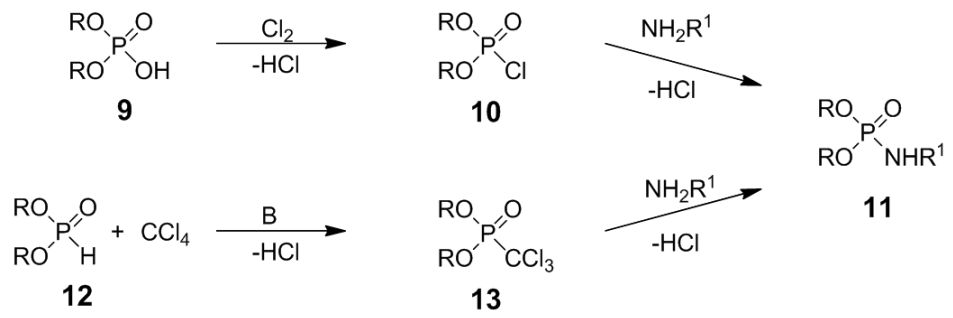

B= C_5H_5N or NMM; R= Bn, alkyl; R^1= H, Bn, Ph, CHMePh, C_6H_{11}

Scheme 5.1.2: Synthesis of *N*-phosphoamides **11** using phosphoryl chloride **10** and trichloromethyl phosphate **13** as phosphorylation agents.

Additional advantages of the latter method were discovered and successfully used by different groups.[16,17] For example, in 1992 *Hulst et al.* applied successfully *Todd*'s method using phosphites **12** in presence of free amino acids and triethylamine as base in aqueous solution. This study demonstrated that free acids are well tolerated and at the same time, the aqueous conditions allow good solubility of the amino compound.[16] However, this method is still limited to phosphites **12** exhibiting short alkyl residues to obtain sufficient yield with high purity of the product **11**. Long alkyl chains are causing an increase of the required reaction temperature, which leads to a variety of side-products at the same time.[17]

In order to develop a general method for novel amino acid derived amphiphiles based on phosphoamides **1**, in this chapter both methods introduced by *Todd* (Scheme 5.1.2) will be evaluated. Moreover, in this study the physical properties of *N*-phosphoamino acids **1** are investigated and the aggregation behavior of these compounds is studied.

5.2 Results and Discussion

5.2.1 Synthesis of *N*-Phosphoamino Acids

As introduced in Chapter 5.1, *N*-phosphoamino acids **1** can be synthesized using two different phosphorylation agents, namely phosphoryl chloride **10** and in-situ activated phosphite **12** (Chapter 5.1, Scheme 5.1.2).[14,15] Since both reagents are showing different properties it was crucial to choose the one with higher stability as well as higher tolerance for functional groups. Therefore the method established by *Todd et al.* using phosphite **12** was first applied in this studies.[15] Phosphites **12** are relatively stable and they show a low reactivity towards unprotected acid moieties during the reaction.
As shown in Scheme 5.2.1, didodecyl phosphite **15** was synthesized in only one synthetic step using three equivalents of the aliphatic alcohol **14** and phosphorus trichloride. When the reaction was performed in anhydrous conditions in the presence of pyridine as base the desired product **15** was obtained with an isolated yield of 86%.

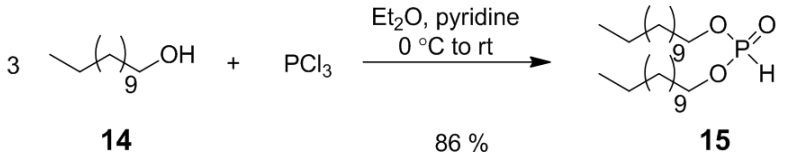

Scheme 5.2.1: Synthesis of didodecyl phosphite **15**.

In the next step, *Todds´*s method[15] using tetrachloromethane was applied to obtain the first *N*-phosphoamino acid **1a** (Scheme 5.2.2). Since no protection of the acid moiety of amino acids was necessary as demonstrated by *Feringa* and coworkers[16] it was to be expected that phosphite **15** could be transformed to *N*-phosphoamino acid **1a** using phenylalanine **16** as nucleophile (Scheme 5.2.2). However, this reaction resulted in very low conversions of the phosphite **15** due to its low reactivity. Hence, more harsh conditions were applied using longer reactions times and higher temperatures up to 40 °C. Unfortunately, these reaction conditions resulted in a mixture of undefined products. Additionally, due to the high polarity of the formed compounds given by the acid moiety no efficient separation could be achieved.

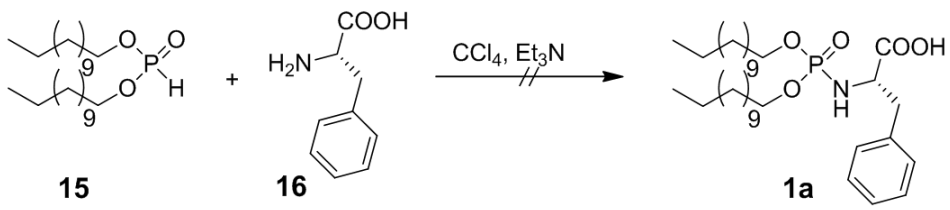

Scheme 5.2.2: Synthesis of (L) 2-((bis(dodecyloxy)phosphoryl)amino)-3-phenylpropanoic acid **1a**.

To increase the conversion of the phosphorylation reaction and avoid creation of side products, we decided to employ the first method introduced by *Todd* in 1945 using the more reactive phosphoryl chlorides **17** (Scheme 5.2.3).[14] As shown in Scheme 5.2.3, phosphorylation reagent **17** was synthesized successfully from dodecyl alcohol **14** using phosphorus oxychloride (Scheme 5.2.3). Due to the high reactivity of **17** no purification was carried out to avoid its decomposition. Hence, product **17** was used immediately in the next synthetic step.

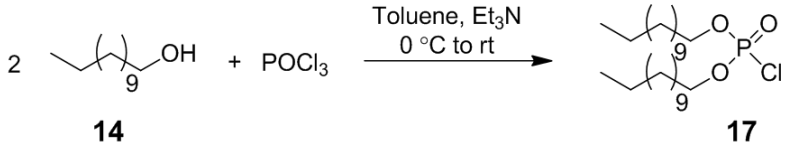

Scheme 5.2.3: Synthesis of didodecyl phosphorochloridate **17**.

Another consequence of the high reactivity of **17** is that this pathway requires the application of methyl protected amino acids **18** (Scheme 5.2.4), since the free carboxylic acid would lead to side reactions. The advantage of using amino acid esters **18** is the formation of uncharged *N*-phosphoamino acid esters **19** facilitating their purification at the same time.
As shown in Table 5.2.1, the transformation of a broad variety of amino acids ester **18** with didodecyl phosphorochloridate **17** in the presence of triethylamine at room temperature and with a reaction time of three hours resulted in the desired *N*-phosphoamino acid esters **19** (Scheme 5.2.4) with isolated yields of up to 83% (Table 5.2.1). It needs to be mentioned that amino acids exhibiting two carboxylic acid moieties, i.e. glutamic acid and aspartic acid, resulted in slightly lower yields (entries 9 and 10, Table 5.2.1). Furthermore, using the amino acid histidine various products were obtained besides **19n**. The reason is the presence of an additional reactive nitrogen in the heterocyclic residue of the amino acid leading to an isolated yield of only 19% of the *N*-phosphoramide **19n** (entries 13, Table 5.2.1).

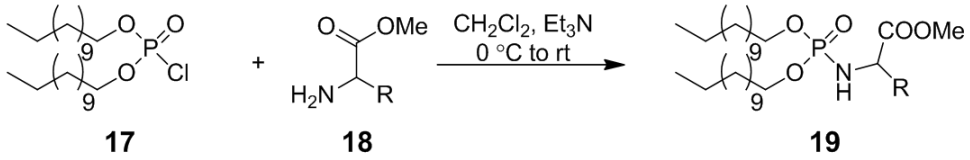

Scheme 5.2.4: Synthesis of *N*-phosphoamino acid derivatives **19**.

Finally, alkaline hydrolysis of methyl esters **19** was performed to obtain the amphiphilic *N*-phosphoamino acids **1** (Scheme 5.2.5). The hydrolyses of the methyl ester **19** in 1 M aqueous sodium hydroxide solution resulted in the formation of the corresponding Na^+-salt which was converted into the *N*-phosphoramide **1** carrying a free acid moiety employing an acid-base extraction reaching isolated yields of up to 89% (Table 5.2.1). The exact mass of amphiphilic compound **1** revealed that after the above mentioned purification no Na^+ or K^+ salt remained and acid **1** showed a high solubility in chloroform. In contrast, *N*-phosphoamino acids **1** possess a poor solubility in water. Depending on the nature of the residue incorporated at the head group of acid **1** a variation of basicity was needed to deprotonate the acid moiety and to induce the formation of aggregates in aqueous solutions.

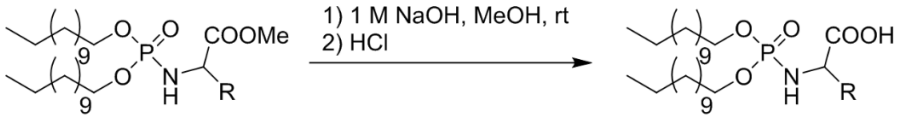

Scheme 5.2.5: Hydrolysis of the methyl ester **19** leading to *N*-phosphoamino acid **1**.

Table 5.2.1: Yields for *N*-phosphoamino ester **19** and acid **1** using different amino acids.

Entry	Amino acid	Methyl ester 19	Yield† (%) (methyl ester 19)	*N*-phospho-amino acid 1	Yield† (%) (acid 1)
1	L-Phe	**19a**	83	**1a**	83
2	L-Gly	**19b**	76	**1b**	89
3	L-β-ala	**19c**	80	**1c**	88
4	L-Ala	**19d**	79	**1d**	85
5	L-Val	**19e**	74	**1e**	84
6	L-Leu	**19f**	72	**1f**	87
7	L-Ile	**19g**	74	**1g**	89
8	L-Pro	**19h**	76	**1h**	89
9	L-Asp^	**19i**	65	**1i**	79
10	L-Glu^	**19j**	62	**1j**	76
11	L-Ph-Gly	**19k**	69	**1k**	82
12	L-Trp	**19m**	72	**1m**	83
13	L-His^^	**19n**	19	**1n**	78
14	L-Cystine^*	**19o**	54	**1o**	75
15	D-Phe	**19p**	76	**1p**	81
16	D-Pro	**19q**	74	**1q**	83
17	D-Trp	**19r**	75	**1r**	80

All reactions were carried out according to the general procedure described in the experimental section 5.4.2.2 using 1 equiv. of didodecyl phosphorochloridate in CH_2Cl_2 (13 mL/ mmol), 6.5 equiv. Et_3N and 1.5 equiv. of a methylated amino acid hydrochloride to obtain the methyl ester **19**. 1 mL/mmol of EtOH and 1 mL/mmol 1M aq. NaOH were used to obtain the free acid **1**. ^ During the hydrolysis of the methyl ester the double amount of base was used. ^^ The double amount of triethylamine was used during the synthesis of the methyl ester **19**. * 2 equiv. of didodecyl phosphorochloridate (26 mL/ mmol CH_2Cl_2), 13 equiv. Et_3N and 1.5 equiv. of a methylated amino acid hydrochloride were used to obtain methyl ester **19o**. † All reported yields are isolated yields.

All synthesized methyl esters **19** and their corresponding acids **1** were obtained as a colorless oil which partly solidified upon standing. This observation can be explained by the fact that all molecules are able to complex water as well as forming dimers and trimers. The aqua-complex formation for methyl esters was demonstrated by DART-MS (**d**irect **a**nalysis in **r**eal **t**ime **m**ass **s**pectroscopy) detecting the molecular mass of different aggregates (Figure 5.2.1). As shown in Figure 5.2.1, methyl ester **19m** is complexing up to two water molecules (A) and can form dimeric (B) and trimeric (C) structures that can also coordinate water molecules. Additionally, the same complex formation behavior was observed for the corresponding acid **1** during the determination of the exact mass.

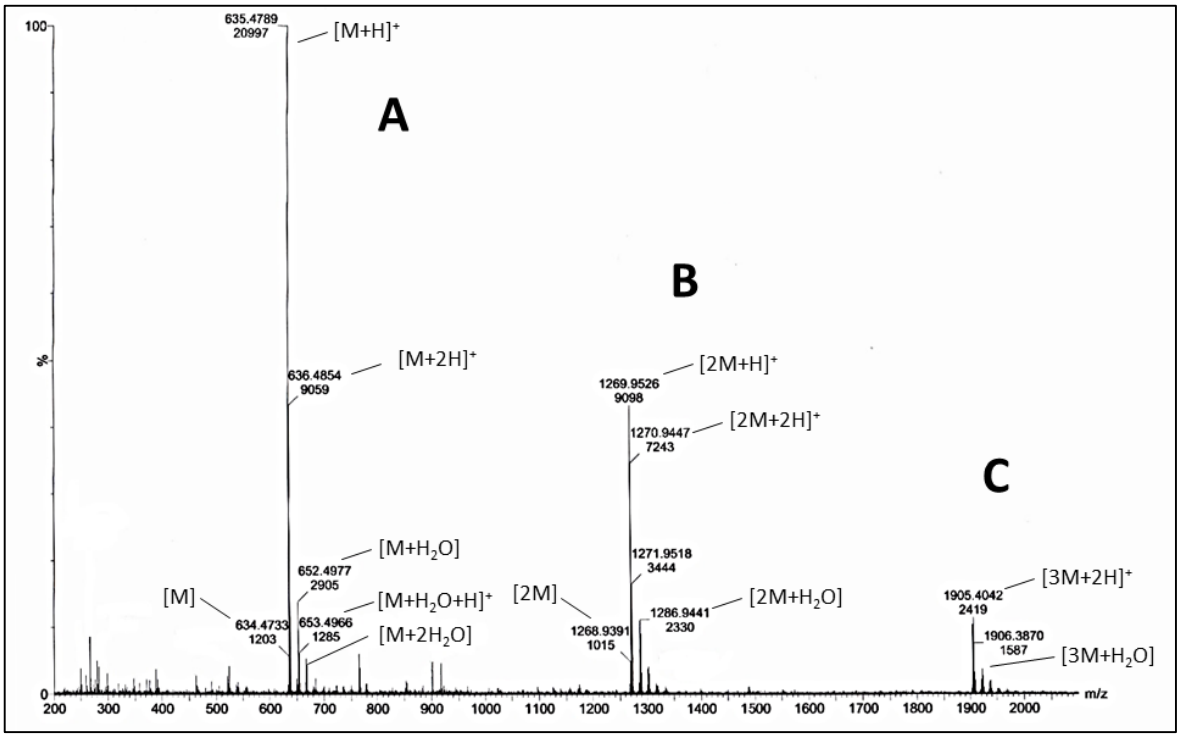

Figure 5.2.1: DART-MS of **19m** showing the formation of different complexes: monomer (A), dimer (B), trimer (C).

5.2.2 Influence of Aggregation on the pK_a-Value of *N*-Phosphoamino Acids Carrying Two Aliphatic C_{12}-Chains

The length of the aliphatic chain as well as the charge of the molecule are important parameters for the aggregation of amphiphiles. Already, in 2003 *Kanicky et al.* demonstrated the influence of the chain length and the effect of amphiphile concentration on the pK_a-value of simple fatty acids.[18] They observed that a chain length of more than six carbons leads to a significant increase of the pK_a-value due to *van der Waals* and hydrophobic interactions between the aliphatic chains.[18,19,20] These interactions give rise to a smaller distance between the acid moieties resulting in trapping of acid protons between two carboxylates as shown in Figure 5.2.2 for *N*-phosphoamino acid **1**.

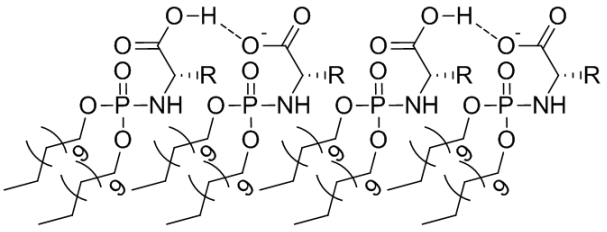

Figure 5.2.2: Stabilization of acid protons between two carboxylates in phosphoamino acid aggregates.

To ensure the amphiphilic character and allow aggregation studies of the synthesized *N*-phosphoamino acids **1**, deprotonation of the carboxylic acid is required. Therefore, in the next step determination of the pK_a-values of amphiphilic acids **1** was performed by acid base titration. In Table 5.2.2 the pK_a-values of the free amino acid and the corresponding *N*-phosphoamino acid **1** are given. As expected the determined pK_a-values of **1** are in average four to five units higher compared to the ones of the corresponding amino acid.

Table 5.2.2: pK_a-Values for amino acids and their corresponding *N*-phosphoamino acids **1**.

Amino acid	pK_a-Value*	Phosphor-amino acid **1**	pK_a**
L-Phe	1.83	**1a**	6.32
L-Gly	2.34	**1b**	6.25
L-β-ala	3.60	**1c**	7.44
L-Ala	2.34	**1d**	6.35
L-Val	2.32	**1e**	6.97
L-Leu	2.36	**1f**	7.43
L-Ile	2.36	**1g**	7.36
L-Pro	1.99	**1h**	7.01
L-Asp	1.88 and 3.65	**1i**	6.83 and 8.76
L-Glu	2.19 and 4.25	**1j**	7.05 and 8.94
L-Ph-Gly	1.94	**1k**	6.57
L-Trp	2.38	**1m**	6.94
L-Cystine	1.50 and 2.05	**1o**	6.07 and 8.19
D-Phe	n.a.	**1p**	6.40
D-Pro	n.a.	**1q**	7.27
D-Trp	n.a.	**1r**	6.35

*Literature values from Lehninger Principles of Biochemistry, Fourth Edition[21a] and CRC Handbook of Chemistry and Physics, 95th Edition.[21b] ** All measurements were performed at room temperature. The titration was carried out by adding 20 mM aq. HCl solution to a turbid solution of **1** in bi-distilled water at pH 10.5 (adjusted using 2M NaOH solution).

5.2.3 Determination of Transition Temperatures using Differential Scanning Calorimetry (DSC)

Differential **s**canning **c**alorimetry (DSC) is a generally applied technique to determine phase transition temperatures of amphiphiles. The transition temperature is defined as the temperature needed to cause a change in the physical state of amphiphilic compounds.
This technique was developed and patented by *Watson* and *O'Neill* in 1962 and is based on the different amount of heat which is required to increase the temperature of the sample cell compared to a reference cell.[22] Depending on the nature of the process i.e. if an exothermic or endothermic process takes place, an increase or decrease of the required heat can be determined. The transition temperature of amphiphiles is strongly dependent of the chain length and unsaturation of the tail as well as charge and head group species.[23] However, a variety of different phase transitions can be observed for amphiphiles. The corresponding transition temperatures are not only determined by the structure of the amphiphile but also the concentration and composition have a major influence.[24,25] This correlation was already demonstrated by *Mitchell et al.* in 1983 using polyoxyethylene surfactants.[24] Another example demonstrating this relation was published in 2003 by *Danino et al.* observing a temperature- and concentration-dependent micelle to vesicle transition for anionic surfactants.[25]
Phospholipids exhibiting C_{12}-chains show often a phase transition caused by melting of the chains at temperatures of around 0 °C. Assuming that *N*-phosphoamino acids **1** are behaving similar to other phospholipids we expect with a chain length of 12 carbons present in their structures a transition temperature in the same range. It needs to be noted that only temperatures higher than the freezing point of water could be measured, since all measurements are performed in basic aqueous solution at a pH of 8.5.
It turned out that all *N*-phosphoamino acids **1** carrying only one acid moiety revealed no phase transition at temperatures higher than 0 °C.
In contrast, for amphiphiles **1i** and **1j**, exhibiting two carboxylate residues, a transition temperature higher than the freezing point was observed. The observed behavior of these two *N*-phosphoamino acids **1i** and **1j** can be explained by the presence of additional hydrogen bonds due to the second acid moiety at the head group (Figure 5.2.3).

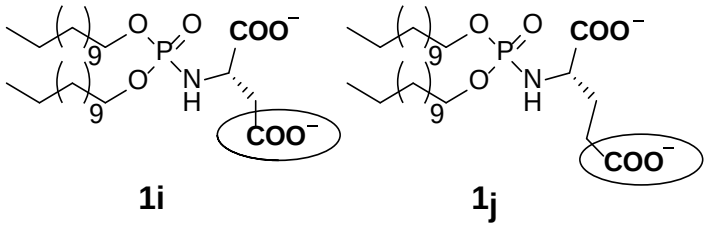

Figure 5.2.3: Molecular structure of amphiphiles **1i** and **1j**.

However as shown for **1i** in Figure 5.2.4, subsequent repetition of the DSC resulted in an increase of the observed temperature from 25 °C to 43 °C and from 23 °C to 42 °C for **1i** and **1j**, respectively. After three cycles a stabilization of the temperature at 43 °C and 42 °C for **1i** and **1j**, respectively, was obtained.

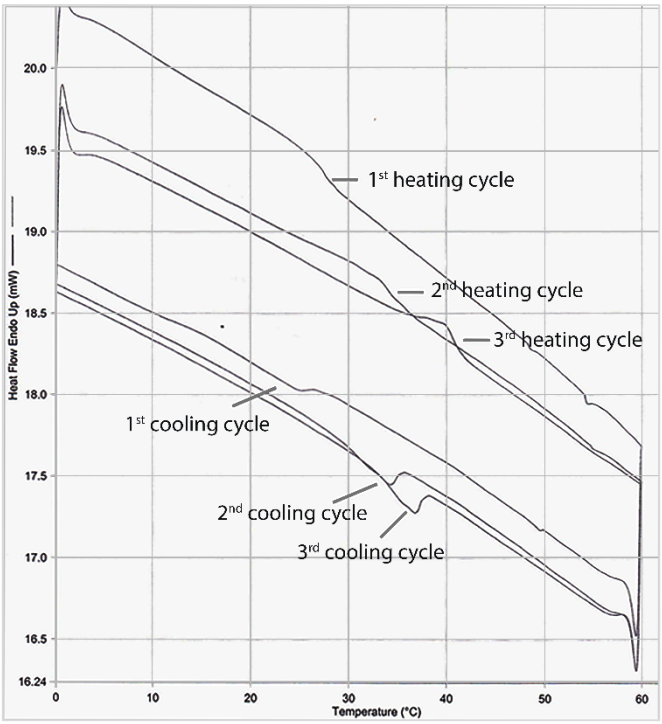

Figure 5.2.4: DSC spectra of **1i** in TRIS-buffer at pH 8.5. Three heating and cooling cycles were performed observing an increase of T_m from 25 to 40 °C.

Furthermore, during an additional experiment simulating the heating process for **1i** and **1j** the formation of insoluble material was observed. It turned out that the formed precipitate was insoluble and remains during the following cooling process.

Considering the pK_a-value of the carboxylic acid at the amino acid residue which is 8.7 for **1i** we can assume at the applied pH of 8.5 a mixture of two different charged species $\mathbf{1i^{-1}}$ and $\mathbf{1i^{-2}}$. Hence, the determined phase transition temperature during the first heating cycle represented a mixture of both different charged amphiphiles. Furthermore, during each heating cycle the formation of precipitate was observed which indicates that a composition change in the solution occurs. Subsequently, after two heating cycles an equilibrium between the mono- and di-anionic species is reached resulting in a final composition. Further studies are necessary to completely understand this process.

Similar observations have been obtained for **1j** which exhibit a pK_a-value of 8.9. Furthermore, the existence of a phase transition temperature for **1i** and **1j** were confirmed by cryo-TEM studies shown in Chapter 5.3.4.

5.3.4 Aggregation Behavior of *N*-Phosphoamino Acids

Cryogenic **T**ransmission **E**lectron **M**icroscopy (Cryo-TEM) is one of the most powerful tools to study supramolecular aggregates in aqueous media. This direct imaging technique with an resolution of 1 to 2 nm provides assemblage specific information and is also applied for time- and temperature-dependent studies.[26]
To preserve the three-dimensional aggregates, which are often sensitive to changes in concentration, hydration, pH and temperature, samples are physical fixed by rapid freezing. Therefore a drop of the aqueous sample is added on a holey carbon film (Figure 5.2.5) supported by a copper grid followed by blotting to remove the excess solution. Finally ultra- fast cooling using liquid ethane results in a vitrified film with a thickness of less than 300 nm in which the aggregates are trapped in their natural environment.[27]

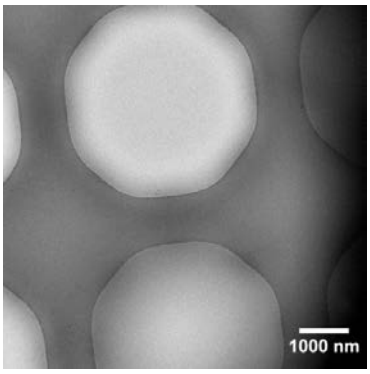

Figure 5.2.5: Cryo-TEM image of holey carbon film.

Due to the amphiphilic character of the synthesized *N*-phosphoamino acids **1** and their potential to form aggregates in aqueous conditions cryo-TEM was used to identify the aggregation behavior formed by these amphiphiles (Table 5.2.3). Considering the determined pK_a-values for *N*-phosphoamino acids **1** (Chapter 5.2.2, Table 5.2.2) cryo-TEM imaging was performed in 20 mM aqueous **tris**(hydroxymethyl)-aminomethane (TRIS) buffered solution with a pH of 8.5. Employing slightly basic conditions ensured deprotonation of the carboxylic acid functionality of the amino acid moiety and at the same time introducing a negative charge at the head group giving it its hydrophilic character needed for the molecule to be amphiphilic.
Table 5.2.3 shows the nature of the aggregates formed by *N*-phosphoamino acids **1** including vesicle, sheets and ribbons. As introduced in Chapter 1 simplified methods have been created already more than 38 years ago to predict packing parameter (PP) of amphiphilic compounds.[20,28] In 1976 *Israelachvili* concluded that the PP, which is mainly dependent of the tail length (l_0) and effective head group area (a_0), can be used to predict the final shape of the amphiphile and the subsequent resulting aggregates.[28] In this regard, a_0 and l_0 are not just dependent of the physical size of the molecules as intramolecular interactions between the amphiphiles play also an important role.[29] *Van der Waals* interactions, hydrophobic effects and charge repulsion or attraction can lead to a significant change of the final area occupied by the amphiphile which complicate the prediction of packing parameters.[18,19,28,29] Furthermore,

several additional conditions, like temperature, salt concentration, counter ions, additives and dilution, have a strong influence on the aggregate formation.[29]

Taking into account that all amphiphiles **1** exhibit the same hydrophobic tail and were treated the same way during the cryo-TEM sample preparation, we can assume that the difference of the observed aggregates between **1a** till **1r** is mainly dependent on the amino acid acting as head group and carrying the negative charge. As introduced by *Israelachvili*[28] a_0 is strongly influenced by its charge. Therefore it has to be taken in account that due to the different pK_a-values for **1a** till **1r** we also expect small differences in the degree of deprotonation influencing the final charge. Furthermore, studies have shown that residues at the α-position of amino acids, which are located close to the charge, could influence the resulting aggregates.[30,31] Although, bulky residues can on one hand result in an increased a_0 but on the other hand a large but flat residue can cause a decrease of charge repulsion through shielding effects and finally lead to an decrease of the effective area a_0. Also, interactions between the residues, like π-π-interaction, H-bonds, additional charges and hydrophobic interactions can lead to a change of a_0.[30,31]

Table 5.2.3: Aggregation determined using cryo-TEM.

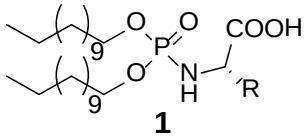

1

	Amino acid	Aggregates*
1a	L-Phe	Vesicle
1b	L-Gly	Vesicle
1c	L-β-ala	Vesicle
1d	L-Ala	Sheets/ vesicle
1e	L-Val	Vesicle
1f	L-Leu	Vesicle
1g	L-Ile	Vesicle
1h	L-Pro	Vesicle
1i	L-Asp**	Thread-like micelles
1i	L-Asp†	Vesicle
1j	L-Glu**	Thread-like micelles/ discs
1j	L-Glu†	Vesicle
1k	L-Ph-Gly	Sheet/ vesicle
1m	L-Trp	Vesicle
1o	L-Cystine	Twisted and coiled ribbons
1p	D-Phe	Vesicle
1q	D-Pro	Vesicle
1r	D-Trp	Vesicle

All samples were prepared using thin layer technique followed by hydration with 20 mM buffer solution followed by three freeze dry cycles. *Aggregates observed from an aqueous solution at pH 8.5 and room temperature. The pH was adjusted using 20 mM TRIS buffer and concentrated HCl solution. ** Aggregates were prepared at 4 °C. † Aggregates were prepared at 70 °C.

In this regard, it is noticeable that in most cases these amphiphiles form lamellar phases, e.g. vesicles and sheets (Table 5.2.3). As an example, in Figure 5.2.6 vesicles are shown that are formed by **1h** (a), **1g** (b) and **1m** (c) carrying L-proline, L-isoleucine and L-tryptophan as head group, respectively. According to *Israelachvili*[28] we can conclude that the amphiphiles **1** forming vesicles have a truncated cone shape (Figure 5.2.6d).

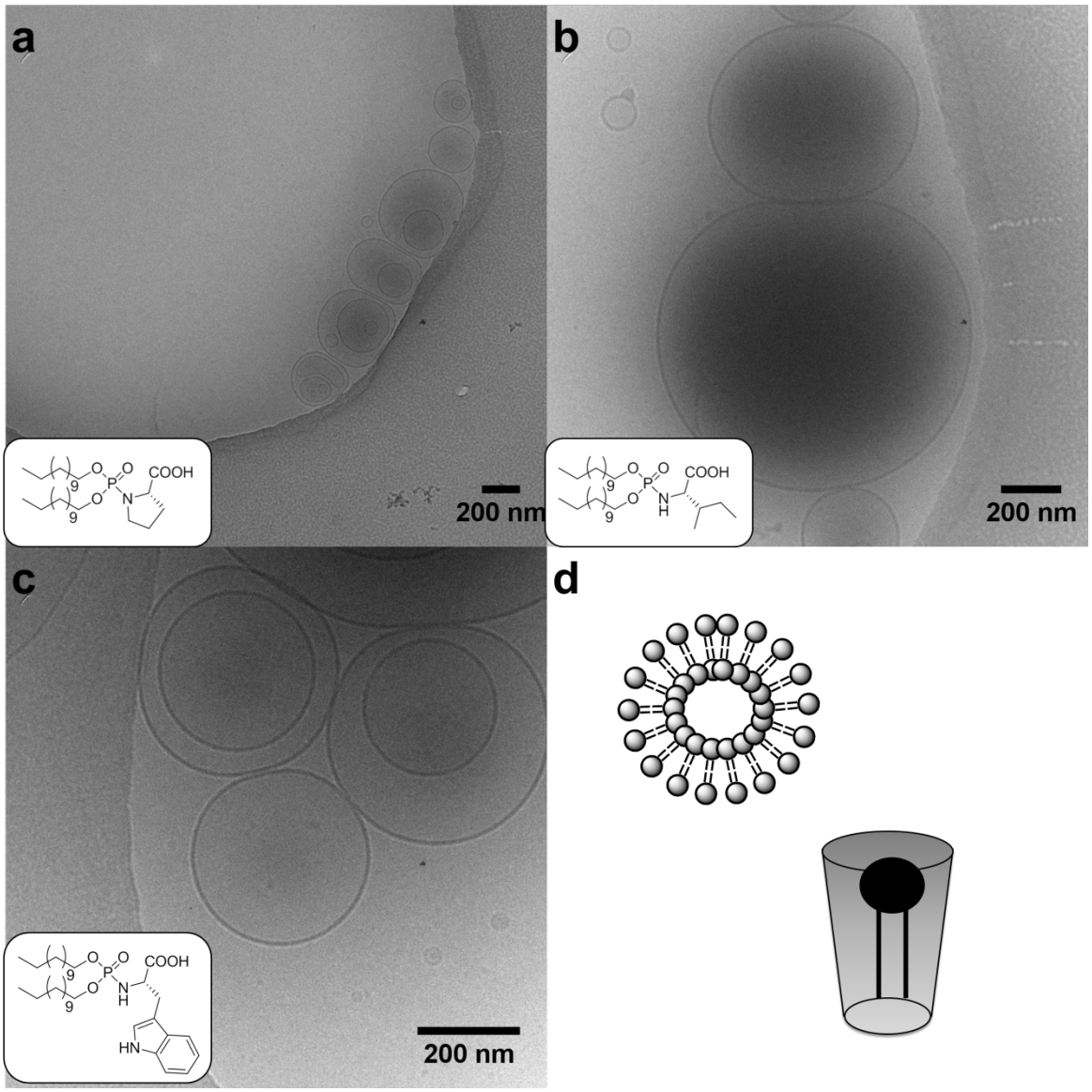

Figure 5.2.6: Cryo-TEM images of **1h** (a), **1g** (b) and **1m** (c) showing vesicle. (d) Schematic representation of a vesicle and the truncated cone structure.

However, other aggregates, such as sheets and thread-like micelles and ribbons, were observed for some *N*-phosphoamino acids **1** (Table 5.2.3). As shown in Figure 5.2.7, *N*-phosphoamino acids **1d** and **1k** exhibiting L-alanine and L-phenylglycine as head group, respectively, form not only vesicles but also lamellar sheets.

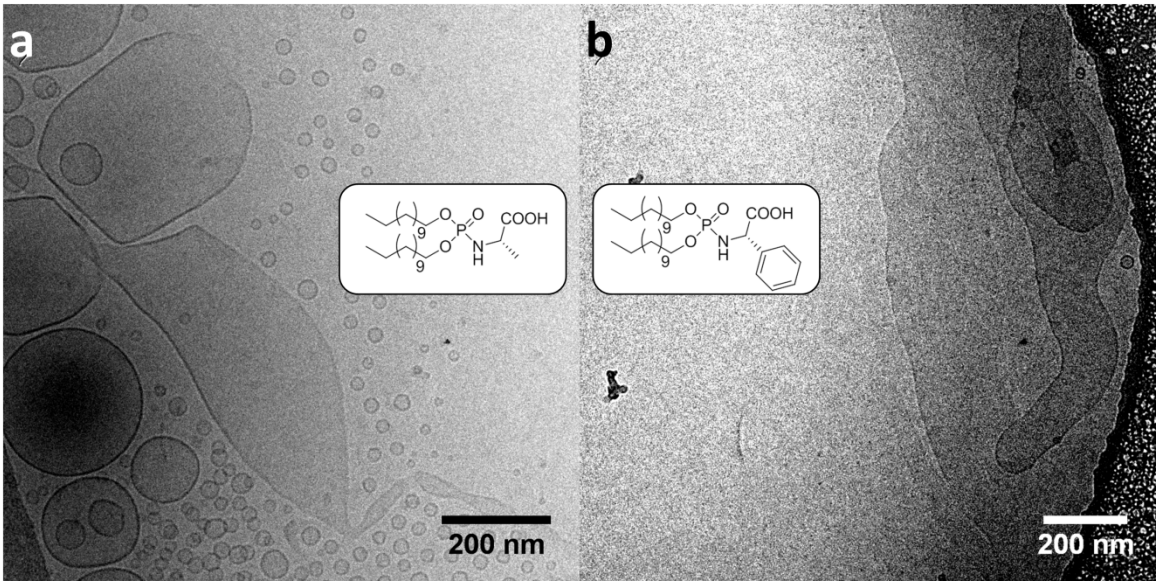

Figure 5.2.7: (a) Cryo-TEM image of **1d** showing vesicles as well as sheets. (b) Cryo-TEM image of **1k** showing mainly sheets.

So far, *N*-phosphoamino acids **1** were discussed carrying a single carboxylic acid moiety with one negative charge. In contrast, *N*-phosphoamino acids **1i** and **1j** exhibiting amino acids aspartic acid and glutamic acid as head groups, respectively, allow up to two negative charged units per amphiphile. At this point it needs to be mentioned that in contrast to other *N*-phosphoamino acid **1** amphiphiles **1i** and **1j** exhibit a phase transition temperature above the freezing point of water (see Chapter 5.2.3). Therefore, cryo-TEM images were recorded at 4 °C and 70 °C (Figure 5.2.8).

As discussed in Chapter 5.2.3 different influences have to be considered to assure that the observed aggregates at higher temperatures reflect the final equilibrium assembly with a stable transition temperature. Therefore, every sample was heated for two hours at 70 °C before taking cryo-TEM images. All temperature-dependent samples were prepared using a Vitrobot, allowing the rapid freezing of samples with variable temperatures.

As shown in Table 5.2.3 and Figure 5.2.8a, at 4 °C **1i** and **1j** form threat-like micelles and discs (not shown) which transform at higher temperature (70 °C) into vesicles. These images confirm the above described observation obtained during the DSC measurements. The higher number of negatively charged carboxylic moieties causes stronger charge repulsion and results according to *Israelachvili*[28] in a cone shaped amphiphile at lower temperatures. Furthermore, this shape would lead to the observed aggregates, namely threat-like micelles and discs (see Chapter 1, Figure 1.2.3, p. 11). An increase of the temperature however leads to more flexibility of the tail resulting in a change of the amphiphile shape giving the observed vesicles (Figure 5.2.8b and c).

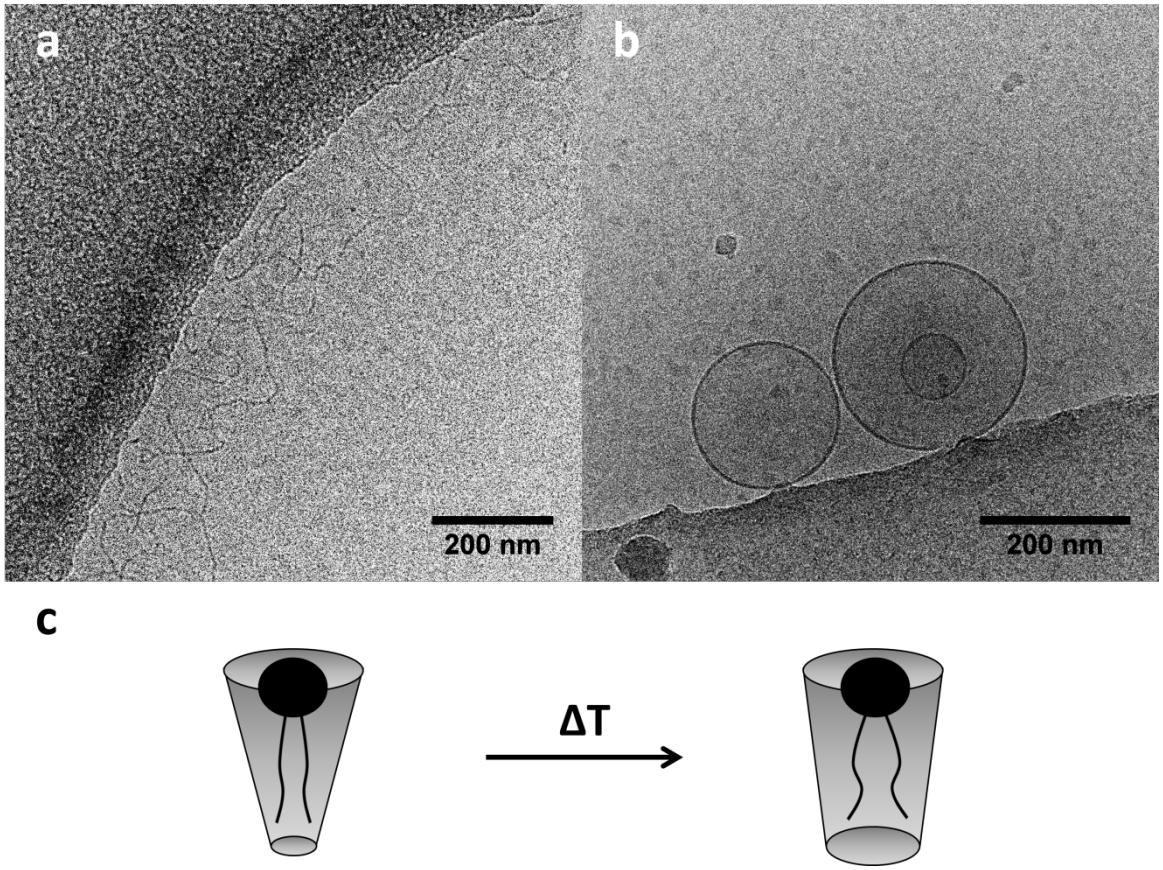

Figure 5.2.8: (a) Cryo-TEM image of **1i** at 4 °C showing thread-like micelles. (b) Cryo-TEM image of **1i** at 70 °C showing vesicles. (c) Schematic representation of a cone structure and a truncated cone structure.

As shown in Table 5.2.3, also ribbons were formed as aggregates by *N*-phosphoamino acid **1o** carrying a cystine as head group. As shown in Figure 5.2.9, this dimeric so called gemini[32] amphiphile **1o** consist of two similar *N*-phosphoamino acids which are connected via a disulfide bound. The resulting molecule includes two stereogenic centers, two negative charges and four hydrophobic tails.

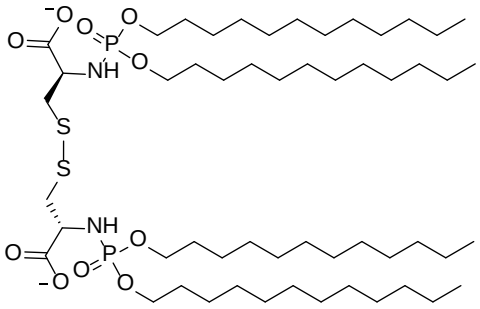

Figure 5.2.9: Molecular structure of *N*-phosphoamino acids **1o**.

As shown in Figure 5.2.10, amphiphile **1o** results in twisted and coiled structures. The driving force to form this aggregates is unfortunately still poorly understood. However, we assume that the chirality as well as hydrogen bonds play an important role.

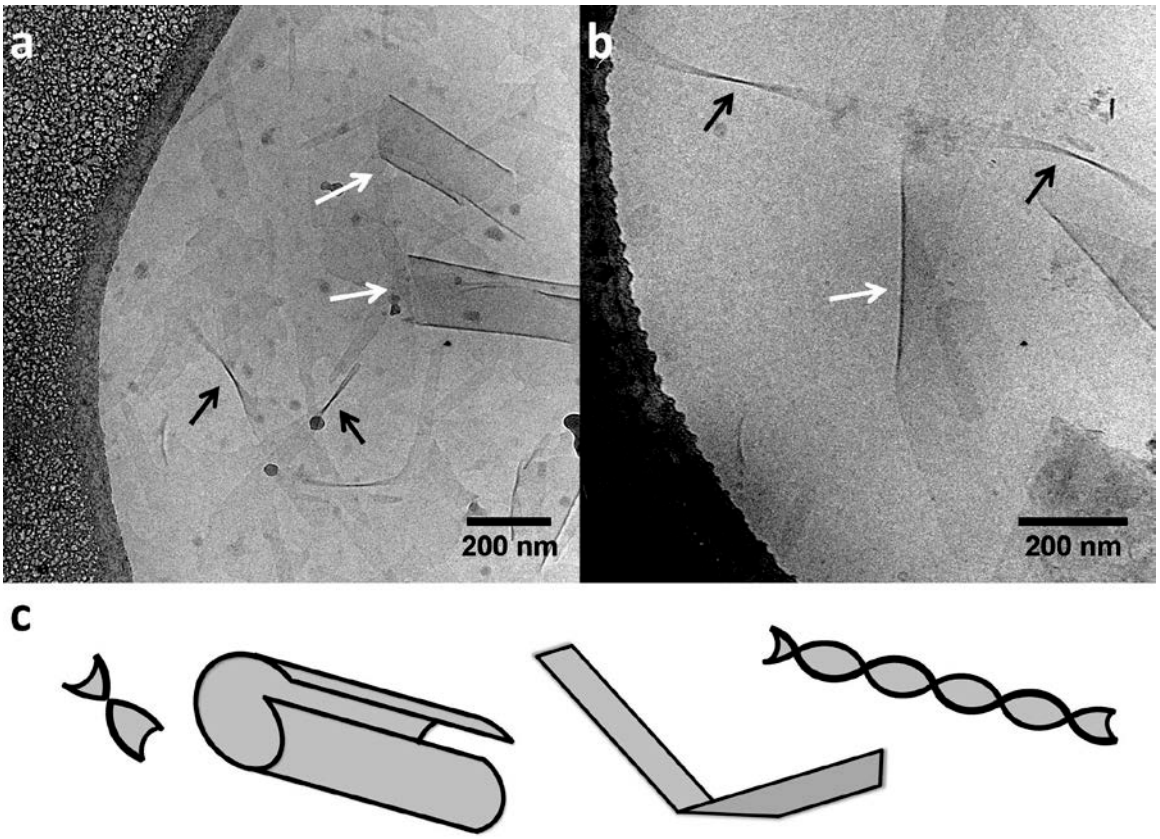

Figure 5.2.10: (a) Cryo-TEM image of **1o** showing twisted (black arrow) and coiled (white arrow) sheets. (b) Cryo-TEM image of **1o** showing twisted (black arrow) and folded (white arrow) ribbons. (c) Illustration of twisted and coiled sheets as well as folded and twisted ribbons (from left to right).

Finally, it needs to be pointed out that also open vesicles for *N*-phosphoamino acids **1b** and **1c** were recorded. These observations will be discussed in detail in Chapter 6.

5.3. Conclusion

In this chapter, we introduced a new class of amphiphiles, namely *N*-phosphoamino acids **1** consisting only of natural building blocks, i.e. amino acids, aliphatic alcohols and phosphonates. Furthermore, an efficient and fast synthesis was elaborated resulting in 18 new amphiphilic phosphoamidates in just three synthetic steps and isolated overall yields of up to 70%.

The characterization of *N*-phosphoamino acids **1** have been performed using nuclear resonance spectroscopy, DART-MS and exact mass determination. Additional, differential scanning calorimetry and the determination of pK_a-values were carried out to gain useful information for further studies, like the aggregation behavior of these compounds. Moreover, cryo-TEM was employed to study the aggregation of these amphiphilic compounds at a pH of 8.5. It was found that *N*-phosphoamino acids **1** can form a broad variety of assembles, such as micelles, vesicles, sheets and ribbons. In this regard, it was demonstrated that the nature of the aggregate is not only dependent of the head group charge. Rather it was demonstrated that the residue at the α-position of the amino acid can slightly interfere with the expected amphiphile shape leading to a variety of aggregates. Furthermore a micelle to vesicle transition depending on the composition and temperature was observed for **1i** and **1j**.

5.4 Experimental Section

5.4.1 Materials and Methods

All chemicals and reagents were purchased from commercial suppliers (*Acros* and *Sigma-Aldrich*) and used without further purification. Dry solvents were taken from an *MBraun* solvent purification system (SPS-800). Thin layer chromatographic (TLC) analysis was performed on Merck silicagel 60/Kieselguhr F254, 0.25 mm TLC plates and spots were visualized by UV and staining with *Seebach's* reagent. Column chromatography was performed using silica gel (P60, 230 – 400 mesh).

^{1}H-NMR-, ^{13}C-NMR-, ^{31}P-NMR-, heteronuclear single-quantum correlation- (HSQC) spectra, Nuclear *Overhauser* effect spectroscopy (NOESY) and correlation spectroscopy (COESY) were recorded on a *Agilent 400* (400 MHz for ^{1}H-NMR, 100.59 MHz for ^{13}C-NMR) using $CDCl_3$ ($CDCl_3$: δ 7.26 for ^{1}H-NMR, δ 77.16 for ^{13}C-NMR). Data are reported as follows: chemical shifts, multiplicity (s= singlet, d= doublet, t= triplet, q= quartet, qi= quintet, br= broad, m= multiplet) coupling constants *J* (Hz) and integration.

High resolution mass spectrometry (HRMS) was carried out on a LTQ ORBITRAP XL spectrometer (*Thermo Scientific*) employing **e**lectro**s**pray **i**onization (ESI) in positive ion mode (EI+) and negative ion mode (EI-).

Optical rotations were measured on a *Schmidt + Haensch* polarimeter (Polartronic MH8) with a 10 cm cell (concentration *c* given in g/100 mL).

Melting points were measured on a *Büchi* B-545 and recorded in °C.

A pH-meter (Hanna Instruments pH 209) equipped with a glass combination electrode was used for pH adjustments of the reaction buffers.

Cryo TEM images were taken on an FEI Tecnai T20 transmission electron microscope and on a Philips CM12 cryo transmission electron microscope operating at 200 and 120 kev, respectively. Images were recorded on a slowscan CCD camera under low-dose conditions.

Transition temperatures were measured on a DSC7 *Perkin Elmer* spectrometer with a heating rate of 5 °C/min.

5.4.2 General Procedures

Cryo-TEM

Sample preparation: After dissolving a *N*-phosphoamino acid in chloroform the solvent was carefully evaporated under a slow stream of nitrogen and continuing rotation. The resulting thin film was stored for 30 min under high vacuum to assure the complete removal of organic solvents. Subsequently, an aqueous buffered solution was added to a final concentration of 3 mg/ mL. The resulting sample was vortexed to obtain a homogenous suspension. Finally three freeze-thaw cycles were performed to enable aggregate formation. The resulting turbid solution was used for cryo-TEM measurements.
Buffer preparation:
pH 8.5 (20 mM TRIS buffer): 1.21 g of tris(hydroxymethyl)aminomethane was dissolved in 500 mL water and the pH was adjusted by adding 1M aqueous HCl solution. Next water was added to obtain a total volume of 500 mL.

pK_a-Determination

After dissolving *N*-phosphoamino acid **1** in chloroform the solvent was carefully evaporated under a slow stream of nitrogen and continuous rotation. The resulting thin film was stored for 30 min under high vacuum to assure the complete removal of organic solvents. Afterwards a slightly basic aqueous solution (10 mM NaOH) was added leading to a final concentration of 3 mg/ mL. The resulting sample was vortexed to obtain a homogenous suspension and the pH was adjusted to approximately 10.5 to ensure full deprotonation using a 1 M aqueous NaOH solution. Finally three freeze-thaw cycles were performed to enable aggregate formation. The resulting turbid solution was used to determine the pKa-value. The titration experiments were performed using a 20 mM HCl solution till a pH of lower than 1.5 was obtained. Measured pK_a-values are given in Table 5.2.2.

DSC

To assure solubility, all samples were measured in TRIS buffer pH 8.5 and prepared according to the above-described method (cryo-TEM). The samples were used immediately after preparation and three to six heating and cooling cycles were performed. With a heating rate of 5 °C per min the measurement was carried out with a starting temperature of 1 °C and a maximum temperature of 60 °C. 25 μL of the sample solution with a concentration of 10 mg/ mL was used.

Synthesize of (bis(dodecyloxy)phosphoryl)amino derivate using didodecyl phosphonate

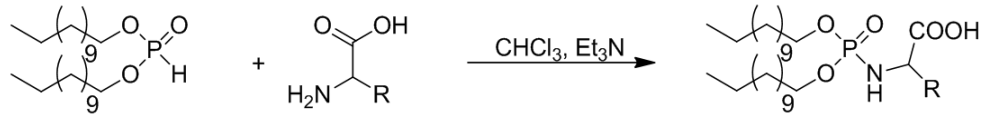

A solution of an amino acid (1 equiv) and triethylamine (1 equiv) in EtOH (3 mL/ mmol) was cooled to 0 °C. Didodecyl phosphonate (1.2 equiv) was carefully added as a solution in $CHCl_3$ (6 equiv) and the temperature was kept below 5 °C. Subsequently, the resulting solution was stirred for 2 h at room temperature and quenched with aqueous HCl (1M, 25 mL/ mmol). Finally the mixture was extracted three times with $CHCl_3$ and the combined organic phases dried with $MgSO_4$. Rotary evaporating of the solvent led to the crude product which was not further purified.

Synthesise of methyl ((bis(dodecyloxy)phosphoryl)amino) derivate using didodecyl phosphorochloridate

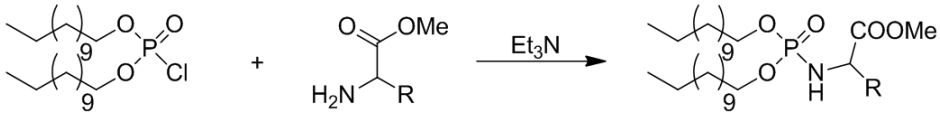

A solution of didodecyl phosphorochloridate (1 equiv) in dry CH_2Cl_2 (13 mL/ mmol) was cooled to 0 °C and 1.5 equiv of a methylated amino acid hydrochloride was added in one portion. After addition of 6.5 equiv of triethylamine the reaction mixture was stirred for 5 h at room temperature. Subsequently the mixture was quenched with water and the organic phase was extracted three times with brine. Drying of the organic solution with $MgSO_4$ and rotary evaporating of the solvent led to the crude product which was further purified by column chromatography (SiO_2, Et_2O/CH_2Cl_2 8:2).

Hydrolysis of methyl ((bis(dodecyloxy)phosphoryl)amino) derivate to a free acid

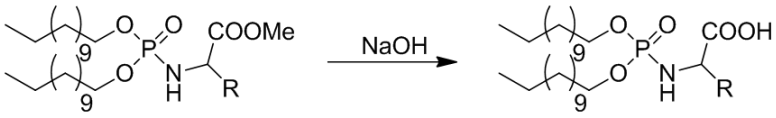

A 1M aqueous solution of NaOH (1 mL/ mmol) was added to a solution of a methyl ester (1 equiv) in EtOH (1 mL/ mmol) and the mixture stirred for 2h at room temperature. Water (10 mL/ mmol) was added and the resulting solution acidified by using a 3M aqueous solution of HCl. The acidic solution with pH 1 was extracted three times with CH_2Cl_2 and the combined organic layers were dried with $MgSO_4$. Rotary evaporation of the solvent led to the product. No further purification was necessary. All compounds showed single ^{31}P-NMR signals corresponding to pure products.

5.4.3 Synthesis and Characterization

Didodecyl phosphonate (15). To an ice cooled solution of lauryl alcohol (3 equiv) and pyridine (2 equiv) in dry Et_2O (0.5 mL/ mmol) was slowly added PCl_3 (1 equiv) over 1h. After the complete addition the reaction mixture was slowly warmed up to room temperature and stirred overnight. To remove pyridine hydrochloride from the reaction mixture the solution was filtered under suction and washed with Et_2O. The combined filtrates were dried ($MgSO_4$) and the solvent was removed by rotary evaporation. The crude colourless oil was further purified by column chromatography (SiO_2, Pentane/EtOAc 8:2) give **15** in an isolated yield of 86%. ^{1}H-NMR ($CDCl_3$, 400 MHz): δ (ppm) = 4.18 (t, J= 9.2 Hz, 4H); 1.73 (m, 4H); 1.26 (br, 36H); 0.88 (t, J= 7.0 Hz, 6H). ^{31}P-NMR ($CDCl_3$, 162 MHz): 1.03.

Didodecyl phosphorochloridate (17). To an ice cooled solution of lauryl alcohol (2.1 equiv) and Et_3N (4 equiv) in dry toluene (6 mL/ mmol) was slowly added a solution of phosphorus oxychloride (1 equiv) in toluene (1 mL/ mmol). After the reaction mixture was slowly warmed to room temperature it was stirred overnight. The resulting suspension was filtered under suction through Celite® and rinsed with toluene. The combined filtrates were dried ($MgSO_4$) and the solvent was removed by rotary evaporation. The colourless oil (solidifies in cold environment) was used without further purification (full conversion). [2.55 mmol scale] ^{1}H-NMR ($CDCl_3$, 400 MHz): δ (ppm) = 4.18 (t, J= 9.6 Hz, 4H); 1.73 (m, 4H); 1.39 (m, 4H); 1.26 (br, 32H); 0.88 (t, J= 6.5 Hz, 6H). ^{13}C-NMR ($CDCl_3$, 100 MHz): δ (ppm) = 69.88 (d, J= 7.3 Hz, 2C, CH_2); 32.04 (2C, CH_2); 29.94 (d, J= 7.8 Hz, 2C, CH_2); 29.75 (4C, CH_2); 29.67 (2C, CH_2); 29.58 (2C, CH_2); 29.47 (2C, CH_2), 29.16 (2C, CH_2); 25.45 (2C, CH_2); 22.81 (2C, CH_2), 14.12 (2C, CH_3). ^{31}P-NMR ($CDCl_3$, 162 MHz): δ (ppm) = 4.8.

Methyl 2-((bis(dodecyloxy)phosphoryl)amino)acetate (19b). The title compound was prepared according to the general procedure described above (5.4.2.2) using (L)-glycine methyl ester hydrochloride. **19b** was obtained as colourless solid with an isolated yield of 76 %. [0.55 mmol scale] Mp: 25.9-28 °C.[33] ^{1}H-NMR ($CDCl_3$, 400 MHz): δ (ppm) = 3.8 (m, 4H); 3.67 (s, 3H); 3.36 (q, J= 9.2 Hz, 1H, NH); 3.32 (s, 2H); 1.56 (m, 4H); 1.24 (br, 36H); 0.87 (t, J= 6.2 Hz, 6H). ^{13}C-NMR ($CDCl_3$, 100 MHz): δ (ppm) = 172.91 (1C; CO); 68.3 (2C, CH_2); 52.57 (1C, CH_3); 34.11 (1C, CH_2); 32.07 (2C, CH_2); 30.43 (d, J= 7.6, 2C, CH_2); 29.80 (2C, CH_2); 29.78 (2C, CH_2); 29.74 (2C, CH_2); 29.68 (2C, CH_2); 29.50 (2C, CH_2); 29.26 (2C,CH_2); 25.75 (2C, CH_2); 22.79 (2C, CH_2), 14.13 (2C, CH_3). ^{31}P-NMR ($CDCl_3$, 162 MHz): δ (ppm) = 7.92. HR-MS (EI+) (*m/z*): found 506.397 $[M+H]^+$, calculated 506.397 $[M+H]^+$.

(L)-Methyl 2-((bis(dodecyloxy)phosphoryl)amino)propanoate (19d). The title compound was prepared according to the general procedure described above (5.4.2.2) using (L)-alanine methyl ester hydrochloride. **19d** was obtained as colourless and sticky solid with an isolated yield of 79 %. [0.55 mmol scale] ^{1}H-NMR ($CDCl_3$, 400 MHz): δ (ppm) = 3.95 (q, J= 6.8 Hz, 1H); 3.93 (m, 4H); 3.72 (s, 3H); 3.23 (t, J= 9.6 Hz, 1H, NH); 1.63 (m, 4H); 1.36 (d, J= 7.2 Hz, 3H); 1.23 (br, 36H); 0.85 (t, J= 6.4 Hz, 6H). ^{13}C-NMR ($CDCl_3$, 100 MHz): δ (ppm) = 174.97 (d, J= 7.2 Hz, 1C; CO); 66.68 (d, J= 6.5 Hz, 1C, CH_2); 66.62 (d, J= 6.5 Hz, 1C, CH_2); 52.32 (1C, CH_3); 49.92 (d, J= 1.4 Hz, 1C, CH); 31.80 (2C, CH_2); 30.22 (d, J= 7.1 Hz, 1C, CH_2); 30.19 (d, J= 7.1 Hz, 1C, CH_2); 29.52 (2C, CH_2); 29.50 (2C, CH_2); 29.45 (2C, CH_2); 29.41 (2C, CH_2); 29.22 (2C, CH_2); 29.07 (2C, CH_2); 25.40 (d, J= 1.3 Hz, 2C,CH_2); 22.52 (2C, CH_2); 20.98 (d, J= 4.8 Hz, 1C, CH_3), 13.89 (2C, CH_3). ^{31}P-NMR ($CDCl_3$, 162 MHz): δ (ppm) = 8.09. HR-MS (EI+) (*m/z)*: found 520.412 $[M+H]^+$, calculated 520.413 $[M+H]^+$.

Methyl 3-((bis(dodecyloxy)phosphoryl)amino)propanoate (19c). The title compound was prepared according to the general procedure described above (5.4.2.2) using β-alanine methyl ester hydrochloride **19c** was obtained as colourless solid with an isolated yield of 80 %. [0.55 mmol scale] Mp: 28.5-30.4 °C.[33] ^{1}H-NMR ($CDCl_3$, 400 MHz): δ (ppm) = 3.95 (t, J= 6.8 Hz, 4H); 3.67 (s, 3H); 3.16 (m, 2H); 3.1 (m, 1H, NH); 2.51 (t, J= 6 Hz, 2H); 1.63 (qi, J= 7.6 Hz, 4H); 1.23 (br, 36H); 0.85 (t, J= 6.8 Hz, 6H). ^{13}C-NMR ($CDCl_3$, 100 MHz): δ (ppm) = 173.08 (1C; CO); 66.91 (2C, CH_2); 52.18 (1C, CH_3); 37.48 (1C, CH_2); 36.31 (d, J= 4.5 Hz, 1C, CH_2); 32.37 (2C, CH_2); 30.83 (d, J= 6.9 Hz, 2C, CH_2); 30.11 (2C, CH_2); 30.09 (2C, CH_2); 30.04 (2C, CH_2); 30 (2C, CH_2); 29.80 (2C, CH_2), 29.66 (2C,CH_2); 26.04 (2C, CH_2); 23.14 (2C, CH_2), 14.56 (2C, CH_3). ^{31}P-NMR ($CDCl_3$, 162 MHz): δ (ppm) = 9.97. HR-MS (EI+) (*m/z)*: found 520.413 $[M+H]^+$, calculated 520.413 $[M+H]^+$.

(L)-Methyl 2-((bis(dodecyloxy)phosphoryl)amino)-3-methylbutanoate (19e). The title compound was prepared according to the general procedure described above (5.4.2.2) using (L)-valine methyl ester hydrochloride. **19e** was obtained as colourless solid with an isolated yield of 74 %. [0.55 mmol scale] Mp: 44.6-45.8 °C.[33] ^{1}H-NMR ($CDCl_3$, 400 MHz): δ (ppm) = 3.97 (m, 4H); 3.73 (s, 3H); 3.65 (m, 1H); 3.10 (t, J= 10.4 Hz, 1H, NH); 2.03 (m, 1H); 1.63 (m, 4H); 1.26 (br, 36H); 0.97 (d, J= 6.8 Hz, 3H); 0.9 (d, J= 6.8 Hz, 3H); 0.88 (t, J= 6.8 Hz, 6H). ^{13}C-NMR ($CDCl_3$, 100 MHz): δ (ppm) = 173.68 (d, J= 3.4 Hz, 1C; CO); 66.69 (d, J= 5.4 Hz, 2C, CH_2); 59.86 (1C, CH); 52.05 (1C, CH_3); 32.31 (d, J= 6.4 Hz, 1C, CH); 32.04 (2C, CH_2); 30.43 (d, J= 7.1 Hz, 2C, CH_2); 29.78 (2C, CH_2); 29.76 (2C, CH_2); 29.70 (2C, CH_2); 29.66 (2C, CH_2); 29.33 (2C, CH_2); 29.32 (2C, CH_2), 25.67 (d, J= 2.8 Hz, 2C,CH_2); 22.81 (2C, CH_2); 19.08 (1C, CH_3); 17.59 (1C, CH_3); 14.23 (2C, CH_3). ^{31}P-NMR ($CDCl_3$, 162 MHz): δ (ppm) = 7.89. HR-MS (EI+) (*m/z)*: found 548.443 $[M+H]^+$, calculated 558.444 $[M+H]^+$.

(L)-Methyl 2-((bis(dodecyloxy)phosphoryl)amino)-4-methylpentanoate (19f). The title compound was prepared according to the general procedure described above (5.4.2.2) using (L)-leucine methyl ester hydrochloride. **19f** was obtained as colourless solid with an isolated yield of 72 %. [0.55 mmol scale] Mp: 48.1-50.0 °C.[33] ^{1}H-NMR ($CDCl_3$, 400 MHz): δ (ppm) = 3.97 (m, 4H); 3.73 (s, 3H); 3.65 (m, 1H); 3.10 (t, J= 10.4 Hz, 1H, NH); 2.03 (m, 1H); 1.63 (m, 4H); 1.5 (m, 2H); 1.26 (br, 36H); 0.97 (d, J= 6.8 Hz, 3H); 0.9 (d, J= 6.8 Hz, 3H); 0.88 (t, J= 6.8 Hz, 6H). ^{13}C-NMR ($CDCl_3$, 100 MHz): δ (ppm) = 170.17 (1C; CO); 66.63 (d, J= 5.4 Hz, 2C, CH_2); 59.1 (1C, CH); 51.92 (1C, CH_3); 39.28 (1C, CH_2); 36.51 (d, J= 6.5 Hz, 1C, CH); 31.94 (2C, CH_2); 30.39 (d, J= 6.8 Hz, 2C, CH_2); 29.79 (2C, CH_2); 29.76 (2C, CH_2); 29.68 (2C, CH_2); 29.59 (2C, CH_2); 29.29 (2C, CH_2); 29.22 (2C, CH_2), 25.63 (2C, CH_2); 22.63 (2C, CH_2); 16.92 (1C, CH_3); 15.3 (1C, CH_3); 14.17 (2C, CH_3). ^{31}P-NMR ($CDCl_3$, 162 MHz): δ (ppm) = 7.22. HR-MS (EI+) (*m/z*): found 562.459 $[M+H]^+$, calculated 562.460 $[M+H]^+$.

(L)-Methyl 2-((bis(dodecyloxy)phosphoryl)amino)-3-methylpentanoate (19g). The title compound was prepared according to the general procedure described above (5.4.2.2) using (L)-isoleucine methyl ester hydrochloride. **19g** was obtained as colourless solid with an isolated yield of 74 %. [0.55 mmol scale] Mp: 46.7-47.5 °C.[33] ^{1}H-NMR ($CDCl_3$, 400 MHz): δ (ppm) = 3.94 (m, 4H); 3.71 (s, 3H); 3.67 (m, 1H); 3.14 (t, J= 10 Hz, 1H, NH); 1.73 (m, 1H); 1.61 (m, 4H); 1.45 (m, 2H), 1.24 (br, 36H); 0.88 (m, 12H). ^{13}C-NMR ($CDCl_3$, 100 MHz): δ (ppm) = 173.31 (d, J= 3.8 Hz, 1C; CO); 66.37 (d, J= 5.7 Hz, 2C, CH_2); 58.61 (1C, CH); 51.69 (1C, CH_3); 39.01 (d, J= 5.9 Hz, 1C, CH); 31.73 (2C, CH_2); 30.16 (d, J= 7.1 Hz, 1C, CH_2); 30.14 (d, J= 7.1 Hz, 1C, CH_2); 29.47 (2C, CH_2); 29.45 (2C, CH_2); 29.39 (2C, CH_2); 29.36 (2C, CH_2); 29.16 (2C, CH_2); 29.02 (2C, CH_2), 25.37 (d, J= 2.9 Hz, 2C,CH_2); 24.58 (1C, CH_2); 22.5 (2C, CH_2); 15.12 (1C, CH_3); 13.92 (2C, CH_3); 11.31 (1C, CH_3). ^{31}P-NMR ($CDCl_3$, 162 MHz): δ (ppm) = 6.58. HR-MS (EI+) (*m/z*): found 562.460 $[M+H]^+$, calculated 562.460 $[M+H]^+$.

Methyl 1-(bis(dodecyloxy)phosphoryl)pyrrolidine-2-carboxylate (19h) or (19q).

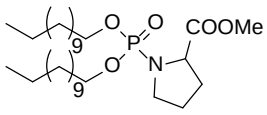

The title compound was prepared according to the general procedure described above (5.4.2.2) using (L) or (D)-proline methyl ester hydrochloride. **19h** or **19q** was obtained as colourless oil. [0.55 mmol scale] ^{1}H-NMR ($CDCl_3$, 400 MHz): δ (ppm) = 4.02 (m, 4H); 3.92 (m, 1H); 3.7 (s, 3H); 3.28 (t, J= 6.8 Hz, 2H); 1.93 (m, 4H); 1.64 (qi, J= 6.8 Hz, 4H); 1.25 (br, 36H); 0.87 (t, J= 6.8 Hz, 6H). ^{13}C-NMR ($CDCl_3$, 100 MHz): δ (ppm) = 173.28 (d, J= 7.0 Hz, 1C; CO); 66.29 (d, J= 6.5 Hz, 2C, CH_2); 59.41 (1C, CH); 52.13 (1C, CH_3); 46.71 (d, J= 6.2 Hz, 1C, CH_2); 31.99 (2C, CH_2); 31.1 (d, J= 6.4 Hz, 1C, CH_2); 30.24 (d, J= 7.0 Hz, 1C, CH_2); 30.2 (d, J= 7.1 Hz, 1C, CH_2); 29.53 (2C, CH_2); 29.50 (2C, CH_2); 29.47 (2C, CH_2); 29.43 (2C, CH_2); 29.24 (2C, CH_2); 29.1 (2C, CH_2), 25.57 (1C,CH_2); 25.37 (2C, CH_2); 22.1 (2C, CH_2); 14.03 (2C, CH_3). ^{31}P-NMR ($CDCl_3$, 162 MHz): δ (ppm) = 6.23. HR-MS (EI+) (*m/z*): found 546.428 $[M+H]^+$, calculated 546.428 $[M+H]^+$.

(L): Yield of 76 %. **(D):** Yield of 75 %.

(L)-Methyl 2-((bis(dodecyloxy)phosphoryl)amino)-2-phenylacetate (19k). The title compound was prepared according to the general procedure described above (5.4.2.2) using (L)-phenylglycine methyl ester hydrochloride. **19k** was obtained as colourless oil which slowly crystallises with an isolated yield of 69 %. [0.55 mmol scale] Mp: 31.2-32.9 °C.[33] ^{1}H-NMR ($CDCl_3$, 400 MHz): δ (ppm) = 7.35 (m, 5H); 4.9 (t, J= 8.4 Hz, 1H); 3.9 (m, 4H); 3.71 (s, 3H); 3.68 (t, J= 8.2 Hz, 1H, NH); 1.6 (m, 4H); 1.26 (br, 36H); 0.88 (t, J= 6.8 Hz, 6H). ^{13}C-NMR ($CDCl_3$, 100 MHz): δ (ppm) = 172.77 (d, J= 5.2 Hz, 1C; CO); 138.72 (1C, C); 129.13 (2C, CH); 128.7 (1C, CH); 127.30 (2C, CH); 66.63 (d, J= 7.2 Hz, 2C, CH_2); 57.95 (d, J= 2.3 Hz, 1C, CH); 52.80 (1C, CH_3); 31.81 (2C, CH_2); 30.14 (d, J= 7.2 Hz, 1C, CH_2); 30.01 (d, J= 7.3 Hz, 1C, CH_2); 29.54 (d, J= 1.3 Hz, 2C, CH_2); 29.52 (2C, CH_2); 29.47 (d, J= 2.2 Hz, 2C, CH_2); 29.37 (d, J= 4.5 Hz, 2C, CH_2); 29.23 (2C, CH_2); 29.02 (d, J= 4.4 Hz, 2C, CH_2); 25.27 (d, J= 8.8 Hz, 2C,CH_2); 22.53 (2C, CH_2); 13.91 (2C, CH_3). ^{31}P-NMR ($CDCl_3$, 162 MHz): δ (ppm) = 6.37. HR-MS (EI+) (*m/z)*: found 582.428 $[M+H]^+$, calculated 582.428 $[M+H]^+$.

Methyl 2-((bis(dodecyloxy)phosphoryl)amino)-3-phenylpropanoat (19a) or (19p). The title compound was prepared according to the general procedure described above (5.4.2.2) using (L) or (D)-phenylalanine methyl ester hydrochloride. **19a** or **19p** was obtained as colourless oil which in case of **19p** slowly crystallises. [0.55 mmol scale] ^{1}H-NMR ($CDCl_3$, 400 MHz): δ (ppm) = 7.38 (m, 3H); 7.25 (d, J= 8 Hz, 2H); 4.17 (m, 1H); 3.95 (m, 3H); 3.79 (s, 3H); 3.76 (m, 1H); 3.14 (m, 1H, NH); 3.06 (m, 2H); 1.66 (qi, J= 6.4 Hz, 4H); 1.35 (br, 36H); 0.97 (t, J= 6.8 Hz, 6H). ^{13}C-NMR ($CDCl_3$, 100 MHz): δ (ppm) = 173.16 (d, J= 4.9 Hz, 1C; CO); 136.15 (1C, C); 129.61 (2C, CH); 128.59 (2C, CH); 127.13 (1C, CH); 66.63 (d, J= 5.7 Hz, 2C, CH_2); 55.74 (1C, CH); 52.22 (1C, CH_3); 40.75 (d, J= 5.9 Hz, 1C, CH_2); 32.03 (2C, CH_2); 30.40 (d, J= 7.2 Hz, 2C, CH_2); 29.77 (2C, CH_2); 29.75 (2C, CH_2); 29.70 (2C, CH_2); 29.66 (2C, CH_2); 29.46 (2C, CH_2); 29.32 (2C, CH_2); 25.62 (2C,CH_2); 22.80 (2C, CH_2); 14.22 (2C, CH_3). ^{31}P-NMR ($CDCl_3$, 162 MHz): δ (ppm) = 6.89. HR-MS (EI+) (*m/z)*: found 596.444 $[M+H]^+$, calculated 596.444 $[M+H]^+$.
(L): Yield of 83 %. Oil. **(D):** Yield of 76 %. Mp: 50.2-52.1 °C.[33]

Methyl 2-((bis(dodecyloxy)phosphoryl)amino)-3-(1*H*-indol-3-yl)propanoate (19m) or (19r). The title compound was prepared according to the general procedure described above (5.4.2.2) using (L) or (D)-tryptophan methyl ester hydrochloride. **19m** or **19r** was obtained as colourless oil which slowly crystallises. [0.55 mmol scale] ^{1}H-NMR ($CDCl_3$, 400 MHz): δ (ppm) = 8.57 (br, 1H); 7.55 (d, J= 8 Hz, 1H); 7.35 (d, J= 8 Hz, 1H); 7.16 (t, J= 8 Hz, 1H); 7.09 (t, J= 8 Hz, 1H); 7.08 (d, J= 2.4 Hz, 1H); 4.18 (m, 1H); 3.9 (m, 4H); 3.63 (s, 3H); 3.25 (t, J= 10.4 Hz, 1H, NH); 3.21 (d, J= 6 Hz, 2H); 1.60 (t, J= 6.8 Hz, 2H); 1.45 (t, J= 6 Hz, 2H); 1.25 (br, 36H); 0.86 (t, J= 6.8 Hz, 6H). ^{13}C-NMR ($CDCl_3$, 100 MHz): δ (ppm) = 173.69 (d, J= 5.2 Hz, 1C; CO); 136.38 (1C, C); 127.61 (1C, C); 123.46 (1C, CH); 122.19 (1C, CH); 119.64 (1C, CH); 118.69 (1C, CH); 111.45 (1C, CH); 109.81 (1C, C); 66.77 (d, J= 5.4 Hz, 2C, CH_2); 54.97 (1C, CH); 52.33 (1C, CH_3); 32.1 (2C, CH_2); 30.54 (d, J= 6.9 Hz, 1C,

CH2); 30.5 (1C, CH_2); 30.4 (d, J= 7.5 Hz, 1C, CH_2); 29.84 (2C, CH_2); 29.82 (2C, CH_2); 29.77 (2C, CH_2); 29.72 (2C, CH_2); 29.53 (2C, CH_2); 29.39 (2C, CH_2); 25.68 (2C, CH_2); 22.68 (2C, CH_2); 14.29 (2C, CH_3). ^{31}P-NMR ($CDCl_3$, 162 MHz): δ (ppm) = 7.12. HR-MS (EI+) (*m/z)*: found 635.455 $[M+H]^+$, calculated 635.455 $[M+H]^+$.
(L): Yield of 72 %. Mp: 44.9-46.7 °C.[33] **(D):** Yield of 74 %. Mp: 47.2-48.5 °C.[33]

(L)-Methyl 2-((bis(dodecyloxy)phosphoryl)amino)-3-(1*H*-imidazol-4-yl)propanoate (19n). The title compound was prepared according to the general procedure described above (5.4.2.2) using (L)-histidine methyl ester dihydrochloride. **19n** was obtained as colourless oil which slowly crystallises with an isolated yield of 19 % (still impure after column chromatography (SiO_2, Et_2O/CH_2Cl_2 8:2)). [0.55 mmol scale] ^{1}H-NMR ($CDCl_3$, 400 MHz): δ (ppm) = 7.76 (s, 1H); 6.93 (s, 1H); 4.13 (m, 1H); 3.97 (m, 4H); 3.71 (t, J= 10.4 Hz, 1H, NH); 3.69 (s, 3H); 3.02 (qd, J= 21.6 Hz, J= 5.2 Hz, 2H); 1.64 (m, 4H); 1.25 (br, 36H); 0.88 (t, J= 6.8 Hz, 6H). ^{31}P-NMR ($CDCl_3$, 162 MHz): δ (ppm) = 7.03. HR-MS (EI+) (*m/z)*: found 586.434 $[M+H]^+$, calculated 586.434 $[M+H]^+$.

(L)-Dimethyl 3,3'-disulfanediylbis(2-((bis(dodecyloxy)phosphoryl)amino)propanoate) (19o). The title compound was prepared according to the general procedure described above (5.4.2.2) using (L)-cystine dimethyl ester dihydrochloride and the double amount of CH_2Cl_2 and Et_3N. **19o** was obtained as colourless oil which slowly crystallises with an isolated yield of 65 %. [0.55 mmol scale] ^{1}H-NMR ($CDCl_3$, 400 MHz): δ (ppm) = 4.16 (m, 2H); 3.97 (m, 8H); 3.74 (s, 6H); 3.5 (t, J= 10 Hz, 2H, NH); 3.02 (qd, J= 43.6 Hz, J= 5.2 Hz, 4H); 1.62 (q, J= 7.2 Hz, 8H); 1.23 (br, 72H); 0.85 (t, J= 6.8 Hz, 12H). ^{13}C-NMR ($CDCl_3$, 100 MHz): δ (ppm) = 173.5 (d, J= 6.3 Hz, 2C; CO); 67.02 (d, J= 4.2 Hz, 2C, CH_2); 66.96 (d, J= 4.2 Hz, 2C, CH_2); 53.58 (2C, CH_3); 52.67 (2C, CH); 43.38 (d, J= 5 Hz, 2C, CH_2); 31.86 (4C, CH_2); 30.3 (d, J= 7.1 Hz, 2C, CH_2); 30.26 (d, J= 7.1 Hz, 2C, CH_2); 29.6 (4C, CH_2); 29.58 (4C, CH_2); 29.54 (4C, CH_2); 29.49 (4C, CH_2); 29.29 (4C, CH_2); 29.16 (4C, CH_2); 25.46 (4C,CH_2); 22.58 (4C, CH_2); 13.96 (4C, CH_3). ^{31}P-NMR ($CDCl_3$, 162 MHz): δ (ppm) = 6.71. HR-MS (EI+) (*m/z)*: found 1101.748 $[M+H]^+$, calculated 1101.748 $[M+H]^+$.

(L)-Dimethyl 2-((bis(dodecyloxy)phosphoryl)amino)succinate (19i). The title compound was prepared according to the general procedure described above (5.4.2.2) using (L)-aspartic acid dimethyl ester hydrochloride and the double amount of Et_3N. **19i** was obtained as colourless oil which slowly crystallises with an isolated yield of 65 %. [0.55 mmol scale] ^{1}H-NMR ($CDCl_3$, 400 MHz): δ (ppm) = 4.12 (m, 1H); 3.96 (t, J= 6.8 Hz, 4H); 3.73 (s, 3H); 3.66 (s, 3H); 3.61 (t, J= 10.4 Hz, 1H, NH); 2.85 (qd, J= 38.4 Hz, J= 5.2 Hz, 2H); 1.61 (q, J= 7.2 Hz, 4H); 1.23 (br, 36H); 0.84 (t, J= 6.8 Hz, 6H). ^{13}C-NMR ($CDCl_3$, 100 MHz): δ (ppm) = 172.71 (d, J= 7.2 Hz, 1C; CO); 171.64 (1C; CO); 66.85 (d, J= 5.7 Hz, 1C, CH_2); 66.72 (d, J= 5.6 Hz, 1C,

CH_2); 52.67 (1C, CH_3); 51.9 (1C, CH_3); 50.94 (1C, CH); 38.45 (d, J= 3.8 Hz, 1C, CH_2); 31.78 (2C, CH_2); 30.21 (d, J= 3.8 Hz, 1C, CH_2); 30.14 (d, J= 3.9 Hz, 1C, CH_2); 29.51 (2C, CH_2); 29.48 (2C, CH_2); 29.44 (2C, CH_2); 29.39 (2C, CH_2); 29.2 (2C, CH_2); 29.06 (2C, CH_2); 25.37 (d, J= 1.3 Hz, 2C,CH_2); 22.5 (2C, CH_2); 13.87 (2C, CH_3). ^{31}P-NMR ($CDCl_3$, 162 MHz): δ (ppm) = 6.98. HR-MS (EI+) (*m/z)*: found 578.418 $[M+H]^+$, calculated 578.418 $[M+H]^+$.

(L)-Dimethyl 2-((bis(dodecyloxy)phosphoryl)amino)pentanedioate (19j). The title compound was prepared according to the general procedure described above (5.4.2.2) using

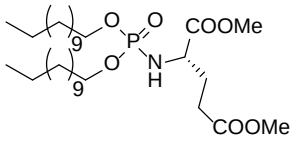

(L)-glutamic acid dimethyl ester hydrochloride and the double amount of Et_3N. **19j** was obtained as colourless oil which slowly crystallises with an isolated yield of 62 %. [0.55 mmol scale] ^{1}H-NMR ($CDCl_3$, 400 MHz): δ (ppm) = 3.9 (m, 1H); 3.92 (t, J= 7.2 Hz, 4H); 3.72 (s, 3H); 3.64 (s, 3H); 3.59 (t, J= 10.4 Hz, 1H, NH); 2.31 (m, 2H); 2.09 (m, 2H); 1.58 (q, J= 7.2 Hz, 4H); 1.21 (br, 36H); 0.84 (t, J= 7.2 Hz, 6H). ^{13}C-NMR ($CDCl_3$, 100 MHz): δ (ppm) = 172.82 (d, J= 7.2 Hz, 1C; CO); 171.24 (1C; CO); 66.83 (d, J= 5.6 Hz, 1C, CH_2); 66.68 (d, J= 5.6 Hz, 1C, CH_2); 52.66 (1C, CH_3); 51.85 (1C, CH_3); 51.73 (1C, CH); 31.76 (2C, CH_2); 30.18 (d, J= 3.9, 1C, CH_2); 30.12 (d, J= 3.9 Hz, 1C, CH_2); 29.49 (2C, CH_2); 29.46 (2C, CH_2); 29.42 (2C, CH_2); 29.38 (2C, CH_2); 29.2 (2C, CH_2); 29.04 (2C, CH_2); 28.97 (2C, CH_2); 25.41 (2C,CH_2); 22.49 (2C, CH_2); 13.7 (2C, CH_3). ^{31}P-NMR ($CDCl_3$, 162 MHz): δ (ppm) = 6.96. HR-MS (EI+) (*m/z)*: found 592.434 $[M+H]^+$, calculated 592.434 $[M+H]^+$.

2-((Bis(dodecyloxy)phosphoryl)amino)acetic acid (1b). The title compound was prepared according to the general procedure described above (5.4.2.3) using **19b**. **1b** was obtained as

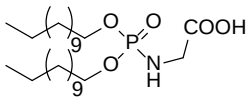

colourless gel with an isolated yield of 89 %. [0.1 mmol scale] ^{1}H-NMR ($CDCl_3$, 400 MHz): δ (ppm) = 5.4 (br, 1H, OH); 3.95 (m, 4H); 3.74 (m, 1H, NH); 3.63 (d, J= 4 Hz, 2H); 1.64 (m, 4H); 1.26 (br, 36H); 0.89 (m, 6H). ^{13}C-NMR ($CDCl_3$, 100 MHz): δ (ppm) = 172.84 (1C; CO); 66.81 (d, J= 5.7 Hz, 2C, CH_2); 42.46 (1C, CH_2); 32.07 (2C, CH_2); 30.32 (d, J= 6.8 Hz, 2C, CH_2); 29.80 (2C, CH_2); 29.79 (2C, CH_2); 29.72 (2C, CH_2); 29.66 (2C, CH_2); 29.50 (2C, CH_2); 29.32 (2C,CH_2); 25.67 (2C, CH_2); 22.84 (2C, CH_2), 14.26 (2C, CH_3). ^{31}P-NMR ($CDCl_3$, 162 MHz): δ (ppm) = 8.34. HR-MS (EI+) (*m/z)*: found 492.381 $[M+H]^+$, calculated 492.381 $[M+H]^+$.

(L)-2-((Bis(dodecyloxy)phosphoryl)amino)propanoic acid (1d). The title compound was

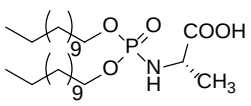

prepared according to the general procedure described above (5.4.2.3) using **19d**. **1d** was obtained as colourless solid with an isolated yield of 85 %. [0.1 mmol scale] ^{1}H-NMR ($CDCl_3$, 400 MHz): δ (ppm) = 4.8 (br, 1H, OH); 3.97 (m, 4H); 3.85 (m, 1H); 3.63 (t, J= 6.8 Hz, 1H, NH); 1.63 (m, 4H); 1.43 (d, J= 7.2 Hz, 3H); 1.25 (br, 36H); 0.87 (t, J= 6.8 Hz, 6H). ^{13}C-NMR ($CDCl_3$, 100 MHz): δ (ppm) = 176.15 (d, J= 7.2 Hz, 1C; CO); 66.68 (2C, CH_2); 49.42 (1C, CH); 31.68 (2C, CH_2); 30.01 (1C, CH_2); 29.94 (1C, CH_2); 29.40 (2C, CH_2); 29.38 (2C, CH_2); 29.35 (d, J= 2.1 Hz, 2C, CH_2); 29.27 (2C, CH_2); 29.11 (d, J= 1.5 Hz, 2C, CH_2); 28.92 (d, J= 2.2 Hz, 2C, CH_2); 25.28 (d, J= 2.3 Hz, 2C, CH_2); 22.40 (2C, CH_2); 20.35 (d, J= 4.6 Hz, 1C, CH_3), 13.78 (2C, CH_3). ^{31}P-NMR

($CDCl_3$, 162 MHz): δ (ppm) = 8.08. HR-MS (EI+) (*m/z)*: found 506.395 $[M+H]^+$, calculated 506.397 $[M+H]^+$.

3-((Bis(dodecyloxy)phosphoryl)amino)propanoic acid (1c). The title compound was prepared according to the general procedure described above (5.4.2.3) using **19c**. **1c** was obtained as colourless solid with an isolated yield of 88 %. [0.1 mmol scale] ^{1}H-NMR ($CDCl_3$, 400 MHz): δ (ppm) = = 4.73 (br, 1H, OH); 3.97 (t, J= 6.4 Hz, 4H); 3.63 (t, J= 6.8 Hz, 1H, NH); 3.09 (m, 2H); 2.84 (t, J= 5.6 Hz, 2H); 1.65 (qi, J= 7.2 Hz, 4H); 1.24 (br, 36H); 0.86 (t, J= 6.8 Hz, 6H). ^{13}C-NMR ($CDCl_3$, 100 MHz): δ (ppm) = 175.13 (1C; CO); 67.02 (2C, CH_2); 42.76 (1C, CH_2); 33.59 (1C, CH_2); 32.08 (2C, CH_2); 30.47 (d, J= 7 Hz, 2C, CH_2); 29.81 (2C, CH_2); 29.78 (2C, CH_2); 29.74 (2C, CH_2); 29.68 (2C, CH_2); 29.50 (2C, CH_2), 29.34 (2C,CH_2); 25.71 (2C, CH_2); 22.81 (2C, CH_2), 14.26 (2C, CH_3). ^{31}P-NMR ($CDCl_3$, 162 MHz): δ (ppm) = 10.14. MS (EI+) (*m/z)*: found 506.397 $[M+H]^+$, calculated 506.397 $[M+H]^+$.

(L)-2-((Bis(dodecyloxy)phosphoryl)amino)-3-methylbutanoic acid (1e). The title compound was prepared according to the general procedure described above (5.4.2.3) using **19e**. **1e** was obtained as colourless solid with an isolated yield of 84 %. [0.1 mmol scale] ^{1}H-NMR ($CDCl_3$, 400 MHz): δ (ppm) = 4.75 (br, 1H, OH); 3.95 (m, 4H); 3.65 (m, 1H); 3.63 (t, J= 6.4 Hz, 1H, NH); 2.1 (m, 1H); 1.65 (m, 4H); 1.27 (br, 36H); 0.99 (d, J= 6.8 Hz, 3H); 0.93 (d, J= 6.8 Hz, 3H); 0.86 (t, J= 6.8 Hz, 6H). ^{13}C-NMR ($CDCl_3$, 100 MHz): δ (ppm) = 174.81 (1C; CO); 66.73 (d, J= 5.3 Hz, 2C, CH_2); 61.35 (1C, CH); 32.26 (d, J= 6.4 Hz, 1C, CH); 32.04 (2C, CH_2); 30.42 (d, J= 7 Hz, 2C, CH_2); 29.8 (2C, CH_2); 29.77 (2C, CH_2); 29.70 (2C, CH_2); 29.68 (2C, CH_2); 29.34 (2C, CH_2); 29.33 (2C, CH_2), 25.66 (2C,CH_2); 22.72 (2C, CH_2); 19.06 (1C, CH_3); 17.54 (1C, CH_3); 14.12 (2C, CH_3). ^{31}P-NMR ($CDCl_3$, 162 MHz): δ (ppm) = 8.62. HR-MS (EI+) (*m/z)*: found 534.428 $[M+H]^+$, calculated 534.428 $[M+H]^+$.

(L)-2-((Bis(dodecyloxy)phosphoryl)amino)-4-methylpentanoic acid (1f).

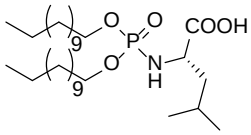

The title compound was prepared according to the general procedure described above (5.4.2.3) using **19f**. **1f** was obtained as colourless gel with an isolated yield of 87 %. [0.1 mmol scale] ^{1}H-NMR ($CDCl_3$, 400 MHz): δ (ppm) = 5.41 (br, 1H, OH); 4.0 (m, 4H); 3.76 (m, 1H); 3.64 (t, J= 6.4 Hz, 1H, NH); 1.8 (m, 1H); 1.61 (m, 4H); 1.53 (m, 2H); 1.3 (br, 36H); 0.88 (m, 12H). ^{13}C-NMR ($CDCl_3$, 100 MHz): δ (ppm) = 171.54 (1C; CO); 66.65 (d, J= 5.6 Hz, 2C, CH_2); 59.24 (1C, CH); 39.19 (1C, CH_2); 36.55 (d, J= 6.3 Hz, 1C, CH); 31.96 (2C, CH_2); 30.42 (d, J= 6.8 Hz, 2C, CH_2); 29.81 (2C, CH_2); 29.77 (2C, CH_2); 29.71 (2C, CH_2); 29.60 (2C, CH_2); 29.29 (2C, CH_2); 29.25 (2C, CH_2), 25.64 (2C,CH2); 22.65 (2C, CH_2); 17.06 (1C, CH_3); 15.64 (1C, CH_3); 14.14 (2C, CH_3). ^{31}P-NMR ($CDCl_3$, 162 MHz): δ (ppm) = 8.09. HR-MS (EI+) (*m/z)*: found 548.443 $[M+H]^+$, calculated 548.444 $[M+H]^+$.

(L)-2-((Bis(dodecyloxy)phosphoryl)amino)-3-methylpentanoic acid (1g).

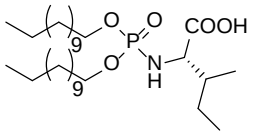

The title compound was prepared according to the general procedure described above (5.4.2.3) using **19g**. **1g** was obtained as colourless oil with an isolated yield of 89 %. [0.1 mmol scale] ^{1}H-NMR ($CDCl_3$, 400 MHz): δ (ppm) = 4.81 (br, 1H, OH); 3.88 (m, 4H); 3.64 (t, J= 6.4 Hz, 1H, NH); 3.52 (m, 1H); 1.82 (m, 1H); 1.6 (m, 4H); 1.52 (m, 2H), 1.26 (br, 36H); 0.88 (m, 12H). ^{13}C-NMR ($CDCl_3$, 100 MHz): δ (ppm) = 173.32 (d, J= 3.5 Hz, 1C; CO); 66.4 (d, J= 5.6 Hz, 2C, CH_2); 59.41 (1C, CH); 39.16 (d, J= 6.1 Hz, 1C, CH); 31.75 (2C, CH_2); 30.16 (d, J= 7 Hz, 2C, CH_2); 29.49 (2C, CH_2); 29.46 (2C, CH_2); 29.41 (2C, CH_2); 29.39 (2C, CH_2); 29.17 (2C, CH_2); 29.05 (2C, CH_2), 25.39 (2C, CH_2); 24.6 (1C, CH_2); 22.4 (2C, CH_2); 15.34 (1C, CH_3); 13.94 (2C, CH_3); 11.42 (1C, CH_3). ^{31}P-NMR ($CDCl_3$, 162 MHz): δ (ppm) = 7.62. HR-MS (EI+) (*m/z)*: found 548.444 $[M+H]^+$, calculated 548.444 $[M+H]^+$.

1-(Bis(dodecyloxy)phosphoryl)pyrrolidine-2-carboxylic acid (1h) or (1q). The title

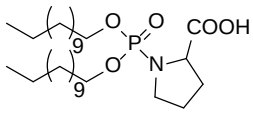

compound was prepared according to the general procedure described above (5.4.2.3) using **19h** or **19q**. **1h** or **1q** was obtained as colourless oil. [0.1 mmol scale] ^{1}H-NMR ($CDCl_3$, 400 MHz): δ (ppm) = 4.67 (br, 1H, OH); 4.02 (m, 1H); 3.87 (m, 4H); 3.26 (t, J= 6.4 Hz, 2H); 2.14 (m, 4H); 1.62 (m, 4H); 1.21 (br, 36H); 0.88 (t, J= 7.2 Hz, 6H). ^{13}C-NMR ($CDCl_3$, 100 MHz): δ (ppm) = 173.68 (d, J= 6.9 Hz, 1C; CO); 66.34 (d, J= 6.6 Hz, 2C, CH_2); 59.23 (1C, CH); 46.69 (d, J= 6.2 Hz, 1C, CH_2); 32.01 (2C, CH_2); 31.97 (d, J= 6.3 Hz, 1C, CH_2); 30.24 (d, J= 6.9 Hz, 2C, CH_2); 29.54 (2C, CH_2); 29.52 (2C, CH_2); 29.49 (2C, CH_2); 29.44 (2C, CH_2); 29.27 (2C, CH_2); 29.12 (2C, CH_2), 25.57 (1C, CH_2); 25.4 (2C, CH_2); 22.11 (2C, CH_2); 14.04 (2C, CH_3). ^{31}P-NMR ($CDCl_3$, 162 MHz): δ (ppm) = 7.49. HR-MS (EI+) (*m/z)*: found 532.412 $[M+H]^+$, calculated 532.413 $[M+H]^+$.
(L): Yield of 89 %. **(D):** Yield of 80 %.

(L)-2-((Bis(dodecyloxy)phosphoryl)amino)-2-phenylacetic acid (1k). The title compound

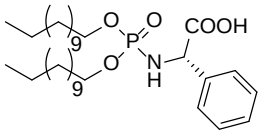

was prepared according to the general procedure described above (5.4.2.3) using **19k**. **1k** was obtained as colourless gel with an isolated yield of 82 %. [0.1 mmol scale] ^{1}H-NMR ($CDCl_3$, 400 MHz): δ (ppm) = 7.41 (m, 5H); 4.92 (t, J= 7.8 Hz, 1H); 4.89 (br, 1H, OH); 3.89 (m, 4H); 3.84 (t, J= 7.8 Hz, 1H, NH); 1.62 (m, 4H); 1.26 (br, 36H); 0.87 (t, J= 6.8 Hz, 6H). ^{13}C-NMR ($CDCl_3$, 100 MHz): δ (ppm) = 173.89 (d, J= 4.9 Hz, 1C; CO); 138.68 (1C, C); 129.1 (2C, CH); 128.15 (1C, CH); 127.01 (2C, CH); 66.64 (d, J= 7.1 Hz, 2C, CH_2); 57.87 (d, J= 2.2 Hz, 1C, CH); 31.8 (2C, CH_2); 30.12 (2C, CH_2); 29.53 (2C, CH_2); 29.51 (2C, CH_2); 29.46 (2C, CH_2); 29.39 (2C, CH_2); 29.23 (2C, CH_2); 29.03 (2C, CH_2); 25.21 (d, J= 8.7 Hz, 2C, CH_2); 22.5 (2C, CH_2); 13.72 (2C, CH_3). ^{31}P-NMR ($CDCl_3$, 162 MHz): δ (ppm) = 7.28. HR-MS (EI+) (*m/z)*: found 568.412 $[M+H]^+$, calculated 568.412 $[M+H]^+$.

2-((Bis(dodecyloxy)phosphoryl)amino)-3-phenylpropanoic acid (1a) or (1p).

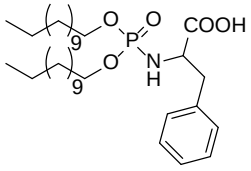

The title compound was prepared according to the general procedure described above (5.4.2.3) using **19a** or **19p**. **1a** or **1p** was obtained as colourless oil which slowly crystallises. [0.1 mmol scale] ^{1}H-NMR ($CDCl_3$, 400 MHz): δ (ppm) = 7.25 (m, 5H); 4.07 (m, 1H, OH); 3.84 (m, 1H, NH); 3.79 (m, 2H); 3.32 (m, 2H); 3.45 (m, 1H); 3.12 (m, 1H); 2.94 (dd, J= 16 Hz, J= 8 Hz, 1H); 1.53 (q, J= 7.2 Hz, 4H); 1.25 (br, 36H); 0.87 (t, J= 7.2 Hz, 6H). ^{13}C-NMR ($CDCl_3$, 100 MHz): δ (ppm) = 174.24 (d, J= 4.7 Hz, 1C; CO); 136.25 (1C, C); 129.63 (2C, CH); 128.61 (2C, CH); 127.16 (1C, CH); 66.59 (2C, CH_2); 55.73 (1C, CH); 40.63 (d, J= 5.6 Hz, 1C, CH_2); 32.0 (2C, CH_2); 30.42 (d, J= 7.1 Hz, 2C, CH_2); 29.75 (2C, CH_2); 29.74 (2C, CH_2); 29.69 (2C, CH_2); 29.66 (2C, CH_2); 29.45 (2C, CH_2); 29.31 (2C, CH_2); 25.62 (2C,CH_2); 22.82 (2C, CH_2); 14.33 (2C, CH_3). ^{31}P-NMR ($CDCl_3$, 162 MHz): δ (ppm) = 7.63. HR-MS (EI+) (*m/z)*: found 582.428 $[M+H]^+$, calculated 582.428 $[M+H]^+$. **(L):** Yield of 83 %. **(D):** Yield of 81 %.

2-((Bis(dodecyloxy)phosphoryl)amino)-3-(1*H*-indol-3-yl)propanoic acid (1m) or (1r).

The title compound was prepared according to the general procedure described above (5.4.2.3)

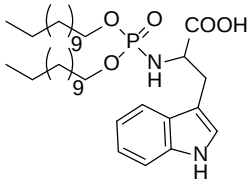

using **19m** or **19r**. **1m** or **1r** was obtained as colourless oil which slowly crystallises. [0.1 mmol scale] ^{1}H-NMR ($CDCl_3$, 400 MHz): δ (ppm) = 8.22 (br, 1H, NH); 7.61 (d, J= 7.2 Hz, 1H); 7.32 (d, J= 7.2 Hz, 1H); 7.15 (t, J= 7.2 Hz, 1H); 7.08 (t, J= 8 Hz, 1H); 7.07 (s, 1H); 3.98 (m, 4H); 3.84 (m, 1H); 3.71 (q, J= 7.2 Hz, 1H, NH); 3.23 (m, 2H); 1.64 (m, 2H); 1.56 (t, J= 7.2 Hz, 2H); 1.25 (br, 36H); 0.87 (t, J= 6.8 Hz, 6H). ^{13}C-NMR ($CDCl_3$, 100 MHz): δ (ppm) = 172.95 (d, J= 4.7 Hz, 1C; CO); 135.65 (1C, C); 128.34 (2C, CH); 128.31 (2C, CH); 126.99 (1C, CH); 63.11 (2C, CH_2); 58.44 (1C, CH); 32.87 (1C, CH_2); 32.04 (2C, CH_2); 30.56 (d, J= 7 Hz, 2C, CH_2); 29.79 (2C, CH_2); 29.76 (2C, CH_2); 29.74 (2C, CH_2); 29.73 (2C, CH_2); 29.57 (2C, CH_2); 29.47 (2C, CH_2); 25.87 (2C,CH_2); 22.81 (2C, CH_2); 14.23 (2C, CH_3). ^{31}P-NMR ($CDCl_3$, 162 MHz): δ (ppm) = 7.83. HR-MS (EI+) (*m/z)*: found 621.439 $[M+H]^+$, calculated 621.439 $[M+H]^+$.

(L): Yield of 83 %. **(D):** Yield of 83 %.

(L)-2-((Bis(dodecyloxy)phosphoryl)amino)-3-(1*H*-imidazol-4-yl)propanoic acid (1n). The

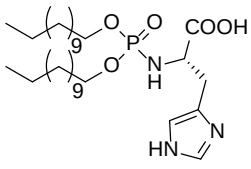

title compound was prepared according to the general procedure described above (5.4.2.3) using **19n**. **1n** was obtained as greyish oil which slowly crystallises with an isolated yield of 78 % (highly impure).[34] [0.1 mmol scale] ^{1}H-NMR ($CDCl_3$, 400 MHz): δ (ppm) = 13.82 (br, 1H, NH); 8.73 (s, 1H); 7.23 (s, 1H); 5.36 (br, 1H, NH); 4.11 (m, 1H); 3.96 (m, 4H); 3.63 (t, J= 8.4 Hz, 1H, NH); 3.22 (m, 2H); 1.62 (m, 4H); 1.24 (br, 36H); 0.86 (t, J= 6.6 Hz, 6H). ^{31}P-NMR ($CDCl_3$, 162 MHz): δ (ppm) = 7.05.

(L)-3,3'-Disulfanediylbis(2-((bis(dodecyloxy)phosphoryl)amino)propanoic acid) (1o). The title compound was prepared according to the general procedure described above (5.4.2.3) using **19o**. **1o** was obtained as yellowish oil which slowly crystallises with an isolated yield of 75 %.

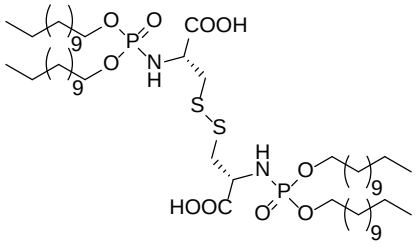

[0.1 mmol scale] ^{1}H-NMR ($CDCl_3$, 400 MHz): δ (ppm) = 4.45 (br, 2H, OH); 4.11 (q, J= 6.4 Hz, 2H); 3.96 (m, 8H); 3.71 (q, J= 6.8 Hz, 2H, NH); 3.18 (m, 2H); 2.81 (m, 2H); 1.64 (m, 8H); 1.25 (br, 72H); 0.87 (t, J= 6 Hz, 12H). ^{13}C-NMR ($CDCl_3$, 100 MHz): δ (ppm) = 174.25 (d, J= 7 Hz, 2C; CO); 66.84 (2C, CH_2); 66.73 (2C, CH_2); 54.62 (2C, CH); 43.42 (2C, CH_2); 31.87 (4C, CH_2); 30.4 (2C, CH_2); 30.27 (2C, CH_2); 29.6 (4C, CH_2); 29.58 (4C, CH_2); 29.54 (4C, CH_2); 29.49 (4C, CH_2); 29.29 (4C, CH_2); 29.17 (4C, CH_2); 25.48 (4C,CH_2); 22.59 (4C, CH_2); 13.93 (4C, CH_3). ^{31}P-NMR ($CDCl_3$, 162 MHz): δ (ppm) = 5.4. HR-MS (EI+) (*m/z)*: found 1073.715 $[M+H]^+$, calculated 1073.715 $[M+H]^+$.

(L)-2-((Bis(dodecyloxy)phosphoryl)amino)succinic acid (1i). The title compound was prepared according to the general procedure described above (5.4.2.3) using **19i**. **1i** was obtained as colourless oil which slowly crystallises with an isolated yield of 79 %.

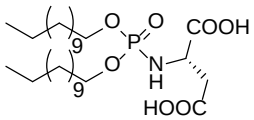

[0.1 mmol scale] ^{1}H-NMR ($CDCl_3$, 400 MHz): δ (ppm) = 4.98 (br, 2H, OH); 4.0 (m, 3H); 3.91 (m, 2H); 3.63 (t, J= 6.4 Hz, 1H, NH); 3.07 (d, J= 16.8 Hz, 1H); 2.76 (d, J= 16.8 Hz, 1H); 1.64 (m, 4H); 1.26 (br, 36H); 0.88 (t, J= 6.6 Hz, 6H). ^{13}C-NMR ($CDCl_3$, 100 MHz): δ (ppm) = 175.12 (d, J= 9.1 Hz, 1C; CO); 174.59 (1C; CO); 67.34 (d, J= 5.5 Hz, 2C, CH_2); 67.23 (d, J= 5.6 Hz, 2C, CH_2); 53.56 (1C, CH); 38.38 (1C, CH_2); 32.08 (2C, CH_2); 30.44 (d, J= 3.4 Hz, 1C, CH_2); 30.37 (d, J= 3.6 Hz, 1C, CH_2); 29.82 (2C, CH_2); 29.78 (2C, CH_2); 29.7 (2C, CH_2); 29.59 (d, J= 6.9 Hz, 2C, CH_2); 29.5 (d, J= 2.6 Hz, 2C, CH_2); 29.37 (d, J= 4 Hz, 2C, CH_2); 25.72 (d, J= 4.1 Hz, 2C,CH_2); 22.84 (2C, CH_2); 14.26 (2C, CH_3). ^{31}P-NMR ($CDCl_3$, 162 MHz): δ (ppm) = 7.8. HR-MS (EI+) (*m/z)*: found 550.387 $[M+H]^+$, calculated 550.387 $[M+H]^+$.

(L)-2-((Bis(dodecyloxy)phosphoryl)amino)pentanedioic acid (1j). The title compound was prepared according to the general procedure described above (5.4.2.3) using **19j**. **1j** was obtained as colourless oil which slowly crystallises with an isolated yield of 76 %.

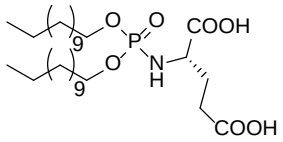

[0.1 mmol scale] ^{1}H-NMR ($CDCl_3$, 400 MHz): δ (ppm) = 6.79 (br, 2H,OH); 3.97 (m, 4H); 3.85 (m, 1H); 3.62 (t, J= 6.4 Hz, 1H, NH); 2.46 (t, J= 6.4 Hz, 2H); 2.1 (m, 1H); 2.01 (m, 1H); 1.63 (m, 4H); 1.24 (br, 36H); 0.85 (t, J= 6.8 Hz, 6H). ^{13}C-NMR ($CDCl_3$, 100 MHz): δ (ppm) = 182.68 (d, J= 7.1 Hz, 1C; CO); 176.54 (1C; CO); 66.93 (d, J= 8 Hz, 1C, CH_2); 66.82 (d, J= 7.3 Hz, 1C, CH_2); 54.45 (1C, CH); 31.49 (2C, CH_2); 29.83 (d, J= 8 Hz, 1C, CH_2); 29.8 (d, J= 7 Hz, 1C, CH_2); 29.24 (2C, CH_2); 29.23 (2C, CH); 29.21 (2C, CH_2); 29.18 (2C, CH_2); 29.11 (2C, CH_2); 28.92 (2C, CH_2); 28.78 (2C, CH_2); 24.92 (2C, CH_2); 22.2 (2C, CH_2); 13.57 (2C, CH_3). ^{31}P-NMR ($CDCl_3$, 162 MHz): δ (ppm) = 7.6. HR-MS (EI+) (*m/z)*: found 564.402 $[M+H]^+$, calculated 564.402 $[M+H]^+$.

5.5 References

1) F. H. Westheimer. Why nature chose phosphates. *Science*, **235**, 1173-1178 (1987).
2) W. W. Cleland, A. C. Hengge. Enzymatic Mechanisms of Phosphate and Sulfate Transfer. *Chem. Rev*., **106**, 3252-3278 (2006).
3) D. Segré, D. Ben-Eli, D. W. Deamer, D. Lancet. The lipid world. *Orig. Life Evol. Biosphere*, **31**, 119-145 (2001).
4) J. R. Cronin, S. Pizzarello, D. P. Cruikshank. Organic Matter in Carbonaceous Chondrites, Planetary Satellites, Asteroids and Comets, In: J. F. Kerridge, M. S. Matthews. Meteorites and the Early Solar System. Tucson AZ, University of Arizona Press, 819-857 (1988).
5) R. Stribling, S. L. Miller. Energy Yields for Hydrogen Cyanide and Formaldehyde: The HCN and Amino Acid Concentration in the Primitive Ocean. *Orig. Life Evol. Biosphere*, **17**, 261-273 (1987).
6) W. R. Hargreaves, S. J. Mulvihill, D. W. Deamer. Synthesis of Phospholipids and Membranes in Prebiotic Conditions. *Nature*, **266**, 78-80 (1977).
7) Y.-M. Li, Y.-F. Zhao. The bioorganic chemical reactions of *N*-phosphoamino acids without side chain functional group participated by phosphoryl group. *Phosphorus, Sulfur, and Silicon*, **78**, 15-21 (1993).
8) Y. Zhao, Y. Ju, Y. Li, Q. Wang, Y. Yin, B. Ton. Self-activation of *N*-phosphoamino acids and *N*-phosphodipeptides in oligopeptide formation. *Int. J. Pep. Prot. Res.*, **45**, 514-518 (1995).
9) F. Ni., X. Gao, Z.-X. Zhao, C. Huang, Y.-F. Zhao. On the electrophilicity of cyclic acylphosphor-amidates (CAPAs) postulated as intermediates. *Eur. J. Org. Chem.* **2009**, 3026-3035 (2009).
10) H. Leuchs. Über die Glycin-carbonsäure. *Ber. Dtsch. Chem. Ges.*, **39**, 857-861 (1906).
11) H.-Y. Wang, Y.-M. Li, Y. Xiao, Y.-F. Zhao, L.-X. Wu. FT-IR studies on Langmuir-Blodgett films of novel phosphorus amphiphiles: Spontaneous polycondensation at the air/water interface. *J. Chem. Res.* **2005**, 385-387 (2005).
12) C. Neuberg, H. Pollak. Über Kohlenhydrat-phosphorsäureester. II. Über Saccharoseschwefel-säure und die Phosphorylierung von Eiweiß. *Ber. Dtsch. Chem. Ges.*, **43**, 2060-2068 (1910).
13) E. Fischer. Über Phosphorsäureester des Methyl-glucosids und Theophyllin-glucosids. *Ber. Dtsch. Chem. Ges.*, **47**, 3193-3205 (1914).
14) F. R. Atherton, H. T. Openshaw, A. R. Todd. Studies on phosphorylation. Part I. Dibenzyl chloro-phosphonate as a phosphorylating agent. *J. Chem. Soc.*, 382-385 (1945).
15) F. R. Atherton, H. T. Openshaw, A. R. Todd. Studies on phosphorylation. Part II. The reaction of dialkyl phosphites with polyhalogen compounds in presence of bases. A new method for the phosphorylation of amines. *J. Chem. Soc.*, 660-663 (1945).

16) R. Hulst, N. K. de Vries, B. L. Feringa. The ^{31}P-NMR Spectroscopic Determination of the Enantiomeric Excess of Unprotected Amino Acids. *Angew. Chem. Int. Ed.*, **31**, 1092-1093 (1992).
17) C.-H. Deng, Y.-M. Li, N. Xu, Y.-F- Zhao. Synthesis of *N*-phosphoamino acids with long dialkoxy chains. *J. Chem. Research (S)*, **10**, 589-589 (1999).
18) J. R. Kanicky, D. O. Shah. Effect of Premicellar Aggregation on the pKa of Fatty Acid Soap Solutions. *Langmuir*, **19**, 2034-2038 (2003).
19) S. H. Donaldson Jr., C. Ted Lee Jr., B. F. Chmelka, J. N. Israelachvili. General hydrophobic interaction potential for surfactant/lipid bilayers from direct force measurements between light-modulated bilayers. *PNAS*, **108**, 15699-15704 (2011).
20) C. Tanford. The Hydrophobic Effect. Wiley-Interscience: New York, (1973).
21) a) D. L. Nelson, M. M. Cox. Lehninger Principles of Biochemistry, Fourth Edition. New York, W. H. Freeman (2004). b) W. M. Haynes. CRC Handbook of Chemistry and Physics, 95th Edition. Boca Raton, Florida, CRC Press (2014).
22) E. S. Watson, M. J. O'Neill, J. Justin, N. Brenner. A differential scanning calorimeter for quantitative differential thermal analysis. *Anal. Chem.*, **36**, 1233-1238 (1964).
23) D. R. Silvius. Lipid-Protein Interaction. New York, John Wiley & Sons, Inc. (1982).
24) D. J. Mitchell, G. J. T. Tiddy, L. Waring, T. Bostock, M. P. McDonald. Phase Behaviour of Polyoxyethylene Surfactants with Water. *J. Chem. Soc., Faraday Trans. 1*, **79**, 975-1000 (1983).
25) D. Danino, D. Weihs, R. Zana, G. Orädd, G. Lindblom, M. Abe, Y. Talmon. Microstructures in the aqueous solutions of a hybrid anionic fluorocarbon/hydrocarbon surfactant. *J. Col. Int. Sci*., **259**, 382-390 (2003).
26) D. Danino. Cyro-TEM of soft molecular assemblies. *Curr. Opin. Coll. Interf. Sci.* **17**, 316-329 (2012).
27) H. Cui, T. K. Hodgdon, E. W. Kaler, L. Abezgauz, D. Danino, M. Lubovsky, Y. Talmon, D. J. Pochan. Elucidating the assembled structure of amphiles in solution via cryogenic transmission electron microscopy. *Soft Matter*, **3**, 945-955 (2007).
28) J. N. Israelachvili, D. J. Mitchell, B. W. Ninham. Theory of self-assembly of hydrocarbon amphiphiles into micelles and bilayers. *J. Chem. Soc., Faraday Trans. 2*, **72**, 1525-1568 (1976).
29) R. Nagarajan. Molecular Packing Parameter and Surfactant Self-Assembly: The Neglected Role of the Surfactant Tail. *Langmuir*, **18**, 31-38 (2002).
30) S. Haldar, S. K. Maji. Role of non-covalent interactions in the molecular organization of *N*-*n*-hexadecanoyl amino acid amphiphiles with hydrophobic C-side chains in Tris buffer (pH 9.3). *Colloids and Surfaces A: Physicochem. Eng. Aspects*, **420**, 10-21 (2013).
31) A. Mohanty, J. Dey. Effect of the Headgroup Structure on the Aggregation Behavior and Stability of Self-Assemblies of Sodium *N*-[4-Dodecyloxy]-L-Aminoacidates in Water. *Langmuir*, **23**, 1033-1040 (2007).
32) A. J. Kirby, P. Camilleri, J. B. F. N. Engberts, M. C. Feiters, R. J. M. Nolte, O. Söderman, M. Bergsma, P. C. Bell, M. L. Fielden, C. L. García Rodríguez, P. Guédat, A. Kremer, C. McGregor, C. Perrin, G. Ronsin, M. C. P. van Eijk. Gemini Surfactants:

New Synthetic Vectors for Gene Transfection. *Angew. Cem. Int. Ed*., **42**, 1448-1457 (2003).

33) No exact melting point could be determined. Repetitive determination resulted in the in this chapter reported broad melting temperature range. This behavior could be explained through the presence of (the in chapter 5.2.1 (Figure 5.2.1) with mass spectrometry demonstrated) dimeric, trimeric and aqueous complexes. Drying under high vacuum overnight did not decrease the temperature range.

34) **1n** was according to the ^{31}P-NMR obtained as a mixture of different compounds which could be not separated *via* column chromatography. Furthermore, the decomposition of the crude product was observed during further purification attempts.

Chapter 6

N-Phosphoamino Acids as Potential Drug Delivery System

After introducing a new class of amphiphiles, namely *N*-phosphoamino acids, and studying the aggregation behavior, we demonstrate in this chapter their potential application as drug delivery system. Towards this goal an investigation of release mechanisms and cytotoxicity was performed. In the latter study the MTT (3-[4,5-dimethylthiazol-2-yl]-2,5 diphenyl tetrazolium bromide) assay was used demonstrating high biocompatibility of representative *N*-phosphoamino acids. Moreover, open vesicles were observed for *N*-phosphoamino acids carrying no residue in the α-position. This degradation of the aggregates, caused by self-activation of the *N*-phosphoamino acids, might be used in further studies towards a time-dependent substrate release mechanism.

6.1 Introduction

Liposomes are artificial vesicles which were reported for the first time by *Bangham et al.* in 1965.[1] They introduced liposomes as a model for cell membranes for biophysical studies. Moreover, in the 1970s liposomes were employed as artificial transport systems for the first time. As shown in Figure 6.1.1, liposomes can act as hosts for hydrophobic, hydrophilic and amphiphilic guest molecules.[2]

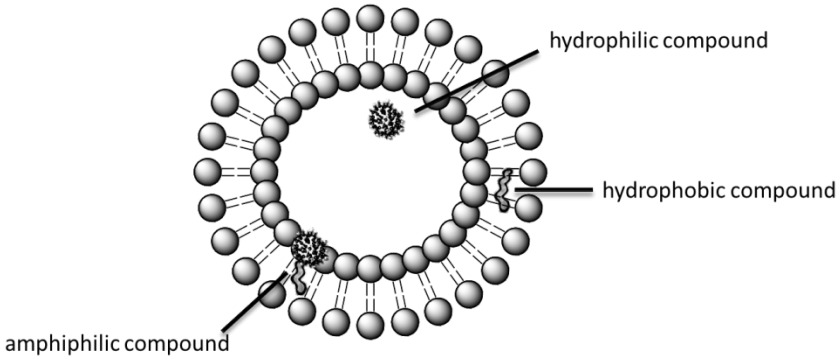

Figure 6.1.1: Schematic representation of a liposome carrying hydrophilic, hydrophobic and amphiphilic compounds.

The first generation of the host-guest systems shown in Figure 6.1.1 was based on naturally occurring phospholipids that show high biocompatibility.[3,4] However, these carrier systems did not allow a controlled release of the transported compound, since they were detected rapidly by the immune system resulting in immediate release of the guest molecules (Figure 6.1.2).
Nowadays, liposomes are common drug carrier systems. However, depending on the indication of the transported drug an immediate or delayed release is necessary. As shown in Figure 6.1.2, both strategies result in high plasma drug concentrations, preferably lower than the **m**inimal **t**oxic **c**oncentration (MTC), and short life times. However, to allow a treatment over time constant plasma drug concentrations above the **m**inimal **e**ffective **c**oncentration (MEC) and below MTC are essential. This can be obtained by a continuous or controlled release mechanism (Figure 6.1.2).
In order to influence the life time of liposomes and control the drug release several studies were performed over the last half century.[6-12] It was found that the clearance of drug delivery systems is caused by the **m**ononuclear **p**hagocyte **s**ystem (MPS) of the immune system, which is triggered by surface charge, saturation, size and composition of the liposome.[6-8] To understand the influence of these parameters different studies were performed demonstrating that the circulation time is strongly dependent on the size of the liposomes. In this regard, a decrease of the life time of the carrier was observed with increasing size of the liposome. In contrast, small carriers were able to pass the endothelium leaving the blood stream or were taken up in shorter time by hepatocytes (liver cells).[6,7] Based on these results an optimal size of about 100 nm in diameter was determined, allowing longer circulation time and delayed release of the drug (Figure 6.1.2).[9,10]

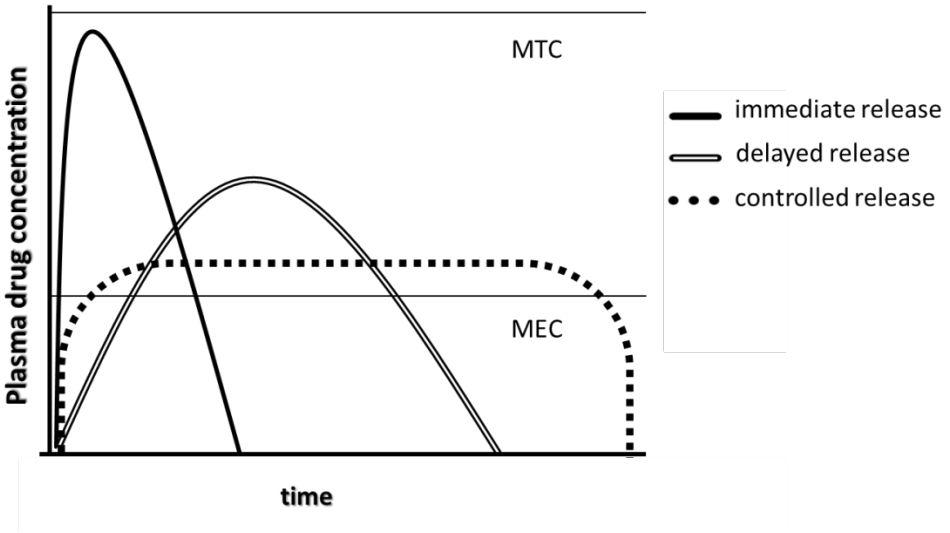

Figure 6.1.2: Schematic representation of drug release dosage over time. **M**inimal **t**oxic **c**oncentration (MTC), **m**inimal **e**ffective **c**oncentration (MEC). Figure based on in reference 5 reported drug release profiles.

Another important parameter influencing the circulation times of transport systems are the composition of liposomes and their surface charge.[11-15] It was shown that negatively charged liposomes are detected by the MPS more rapidly than positive charged liposomes.[11-13] However, in further studies longer circulation times were also observed for negatively charged transport systems.[14,15] This was achieved by changing the molecular structure of the lipid and shielding of negative charges on the liposome. For example, the latter strategy was achieved by coating the negatively charged liposome surface with hydrophilic polymer structures, such as **p**oly(**e**thylene **g**lycol) (PEG) or palmitoylglucuronide.[16,17]

In 1991 *Papahadjopoulos et al.* demonstrated the prolongation of the circulation time and the decreased uptake of PEGylated liposomes (stealth liposomes).[18] During the following year *Lasic et al.* encapsulated successfully the cancer drug doxorubicin applying stealth liposomes.[19] This research lead to the first by the FDA approved PEGylated liposome as drug delivery system for doxorubicin in 1995 (DOXIL in US and Caelyx in Europe).

In order to use the *N*-phosphoamino acids **1** introduced in chapter 5 as drug delivery systems several aspects have to be explored. Therefore in this chapter experimental results are reported demonstrating the high biocompatibility of the amphiphiles and introducing possible drug release mechanisms. However, considering the negative charge of these compounds and the above mentioned literature,[11-15] it is also of high interest to investigate the mixing behavior as well as possible modifications of the liposome surface. Approaches, demonstrating simple modification methods of *N*-phosphoamino acids **1** are explored in Chapter 7 giving excess to more stable negatively charged dipeptides as head group on one hand and showing simple modification methods on the other hand.

6.2 Results and Discussion

6.2.1 Biocompatibility of *N*-Phosphoamino Acids

One of the most important requirements for drug delivery systems is the biocompatibility of the amphiphile. Therefore, not only the surfactant itself but also its metabolic products need to be considered. In this regard, *N*-phosphoamino acid **1** seems to be promising class of amphiphiles, since they consist only of naturally occurring building blocks and their degradation results in amino acids **2**, phosphates **3** and alcohols **4** (Scheme 6.2.1).

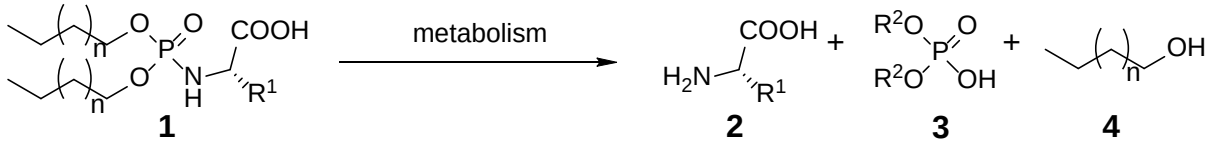

Scheme 6.2.1: Metabolic degradation of *N*-phosphoamino acids **1**.

To study the biocompatibility of *N*-phosphoamino acids **1** we employed the MTT (3-(4,5-di**m**ethyl**t**hiazol-2-yl)-2,5-diphenyl**t**etrazolium bromide) assay. In 1953, MTT **5** was used for the first time by *Black* and *Speer* for chemosensitivity tests (Scheme 6.2.2).[20] Thirty years later *Mosmann* reported the application of MTT **5** in a colorimetric assays to study cellular growth and survival in presence of different compounds reflecting their cytotoxicity.[21] During the following decades a number of reports have been published confirming the correlation of the results obtained by MTT assays with clinical studies.[21-23]
As shown in Scheme 6.2.2, this toxicity test is based on an enzymatic modification of MTT **5** in living cells. Hereby, a reduction of the yellow MTT **5** by a reductase takes place resulting in the water insoluble and blue formazan **6** (Scheme 6.2.2). Further, the amount of formazan **6** formed by the reductase is proportional to the number of metabolically active cells and can be determined through UV/Vis-spectroscopy (absorbance at 570 nm).

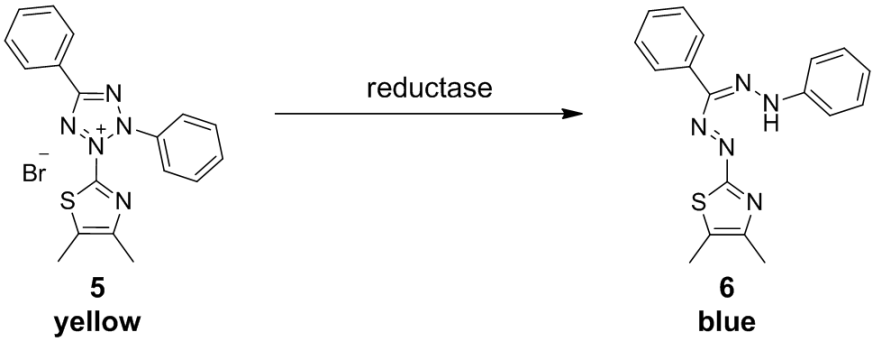

Scheme 6.2.2: Enzymatic reduction of MTT **5** resulting in formazan **6**.

To investigate the cytotoxicity of *N*-phosphoamino acids **1**, *HeLa* (*Henrietta Lacks*) cells were employed. For this study, amphiphiles **1d**, **1i** and **1m** were chosen carrying alanine, aspartic

acid and tryptophan as amino acid head group, respectively. *HeLa* cells were incubated together with each *N*-phosphoamino acid **1** for 16 hours at 37 °C. Subsequently, MTT **5** was added and the resulting solution was incubated for an additional four hours. Finally, to determine the cell viability the formed amount of water insoluble formazan **6** was dissolved in DMSO and the absorbance was measured at 570 nm. In Figure 6.2.1, the results of the MTT assay is shown using of *N*-phosphoamino acid **1d** with a concentration ranging from 0.25 µM to 400 µM. Like expected a high cell viability ranking from 94% to 100% was observed in the presence of compound **1d**. The graph (Figure 6.2.1) shows high biocompatibility for amphiphile **1d** up to a concentration of 100 µM. Corresponding results were obtained for *N*-phosphoamino acids **1i** and **1m** showing a cell viability of more than 80% at concentrations of up to 100 µM. (Figure 6.2.2).

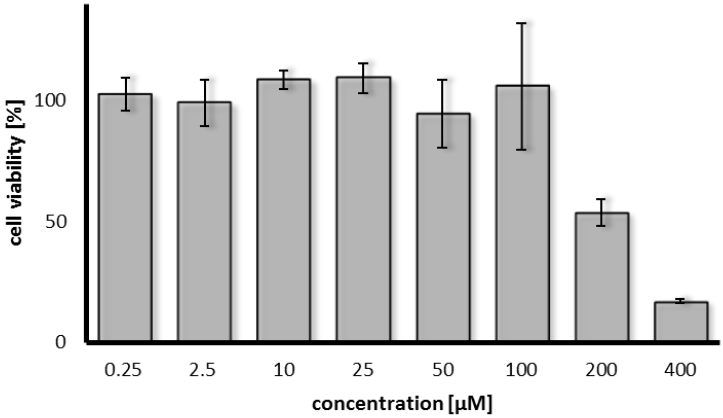

Figure 6.2.1: MTT assay using *N*-phosphoamino acid **1d**. Cell viability is given for **1d** at concentrations between 0.25 µM and 400 µM. Each experiment was performed three times.

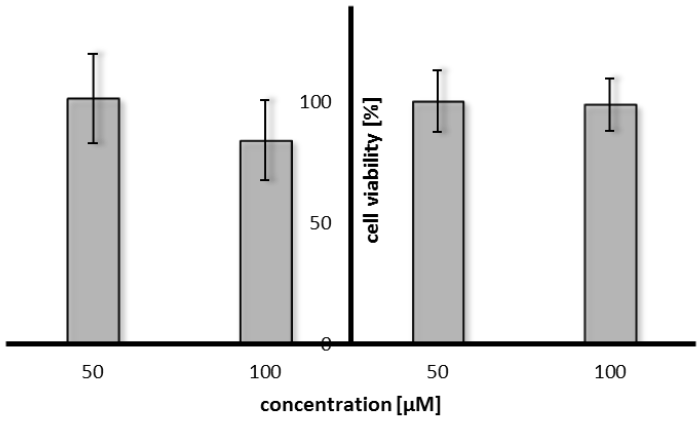

Figure 6.2.2: MTT assay using *N*-phosphoamino acid **1i** (left) and **1m** (right). Cell viability is given for both compounds, **1i** and **1m**, at concentrations of 50 µM and 100 µM. Each experiment was performed three times.

6.2.2 Potential Drug Release Mechanism

After high biocompatibility of *N*-phosphoamino acids **1** was successfully demonstrated the potential release mechanisms for aggregates formed by these amphiphiles was investigated. First, pH-dependent aggregation of **1** was investigated by cryo-TEM. Dependent of the pH value a different protonation state of the acid moiety of the head group of **1** can be expected resulting in changes of the aggregation behavior or even clearance of the aggregate. Therefore, it is necessary to understand the aggregation behavior of *N*-phosphoamino acids **1** at pH-values close to the physiological pH of blood, i.e. 7.4.[24] Considering additionally the pK_a-values of the amphiphiles **1** which are located between 6.1 and 8.9 for the carboxylic acid group (Chapter 5.2.2), aggregation studies were performed at pH 1, 6.5, 8.5 and 11 (Table 6.2.1). Whereas one can expect full protonation and loss of the amphiphilic character under slightly acidic condition (<7), full deprotonation is given in basic conditions (pH 11). For these aggregation studies we employed *N*-phosphoamino acids **1a**, **1i** and **1m** exhibiting L-phenylalanine, L-aspartic acid and L-tryptophan as amino acid head group, respectively, as representatives.
As shown in Table 6.2.1, no aggregation was observed for any of those amphiphiles **1** under very acidic conditions, i.e. pH 1. This is based on the full protonation of the acidic moiety resulting in the loss of the amphiphilic character of the amphiphile. In contrast, aggregates were observed for all *N*-phosphoamino acids, i.e. **1a**, **1i** and **1m**, at higher pH (Table 6.2.1). As shown in Figure 6.2.3a and Table 6.2.1, amphiphile **1a** forms between pH 6.5 and 11 the same aggregates, namely vesicles. However, **1m** form additionally sheets at pH 6.5, while at higher pH exclusively vesicles were observed (Figure 6.2.3b). This can be traced back to the fact that **1m** has a slightly higher pK_a value compared to **1a** giving rise to a lower number of charges per amphiphile. Consequently, the head group of **1m** owns a smaller effective head group area (a_0) and therefore, has almost a cylindrical shape resulting also in sheets at pH 6.5.

Table 6.2.1: Aggregation observed for *N*-phosphoamino acids **1** employing cryo-TEM.

amphiphile	Amino acid	pK_a	pH 1	pH 6.5	pH 8.5	pH 11
1a	L-Phe	6.66	-	vesicle	vesicle	vesicle
1m	L-Trp	6.94	-	vesicle, sheets	vesicle	vesicle
1i	L-Asp	6.83 and 8.76	-	vesicle	wormlike micelles	bicelles

All samples were prepared using the thin layer technique followed by hydration with 20 mM buffer solution and three freeze thaw cycles. Aggregates observed from an aqueous buffered solution at room temperature.

The largest changes in aggregation, depending on the pH value, were observed for *N*-phosphoamino acid **1i** carrying two carboxylic acid moieties at the head group. As shown in Table 6.2.1 and Figure 6.2.3c, unlike **1a** and **1m** amphiphile **1i** forms at pH 8.5 and 11 micelle-based aggregates. The reason is the presence of a number of charges higher than one per

molecule **1i** resulting in a bigger a_0 than for **1a** and **1m** and a cone shaped amphiphile. In contrast, at a pH of 6.5 vesicles for **1i** were observed (Table 6.2.1 and Figure 6.2.3d). Under slightly acidic conditions one carboxylic acid group (pK_a 8.8) is fully protonated, while the other (pK_a 6.8) is only partly deprotonated. This protonation state results in almost the same number of charges per molecules as for **1a** and **1m**. Hence, at this pH all three amphiphiles have a truncated cone shape resulting in vesicles (Table 6.2.1).

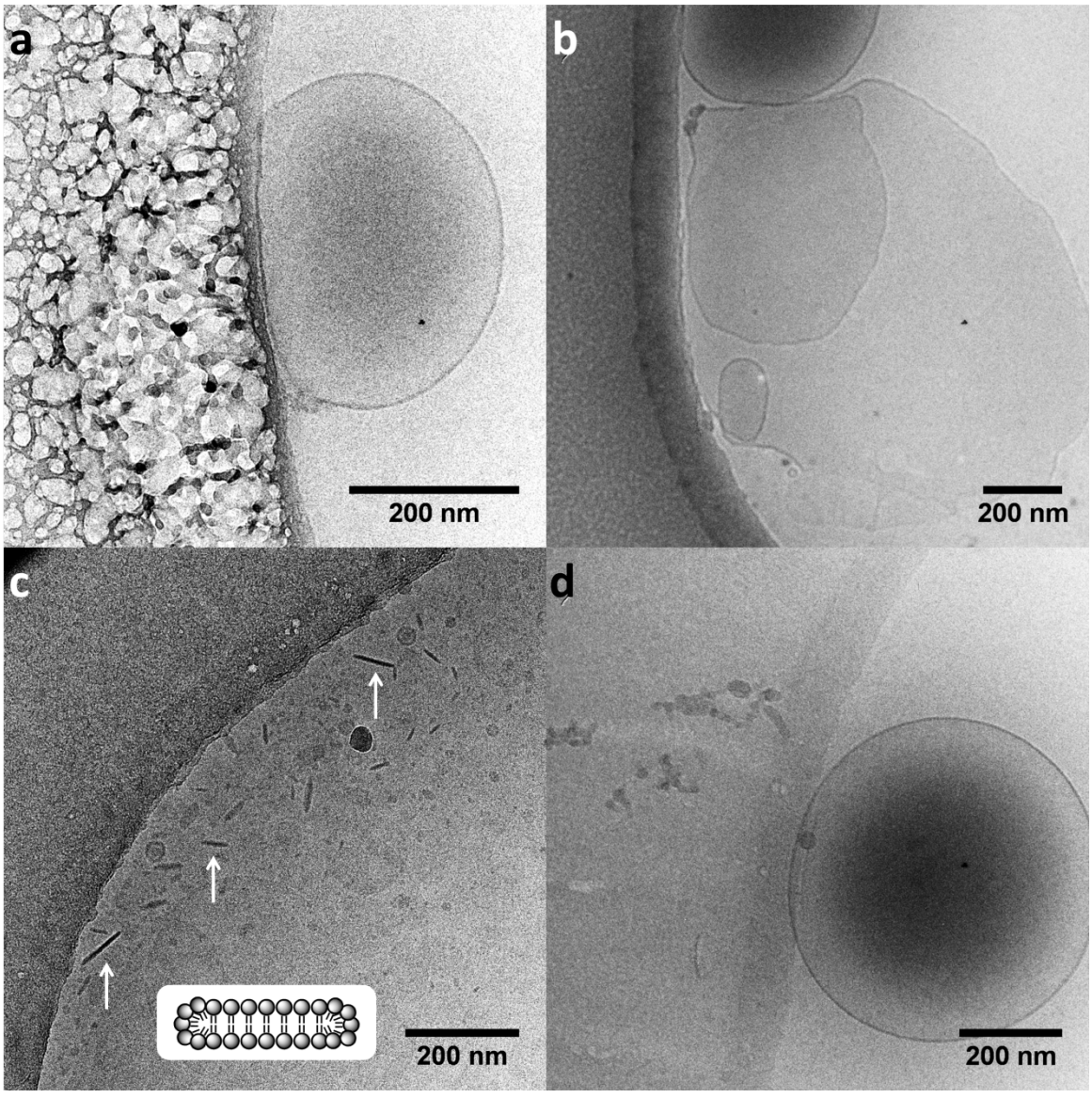

Figure 6.2.3: (a) Cryo-TEM image of **1a** at pH 6.5. (b) Cryo-TEM image of **1m** at pH 6.5. (c) Cryo-TEM image of **1i** at pH 11 (white arrow indicate bicelles) and schematic representation of a bicelle. (d) Cryo-TEM image of **1i** at pH 6.5.

The pH-dependent aggregation and the fact that at pH 1 no aggregation for *N*-phosphoamino acids **1** can be observed and offers the possibility for fast drug release under acidic conditions, i.e. endocytosis. During endocytosis the pH value drops from 6.5 to pH 4.5[25] which would cause full protonation of the amphiphiles **1** head group resulting in clearance of the liposome and drug release.

A second potential release mechanism is based on the formation of open vesicles of *N*-phosphoamino acids **1**. As shown in Figure 6.2.4a-c, for amphiphiles **1b**, **1c** and **1d** carrying glycine, beta-alanine and alanine as head group, respectively, open vesicles were observed.

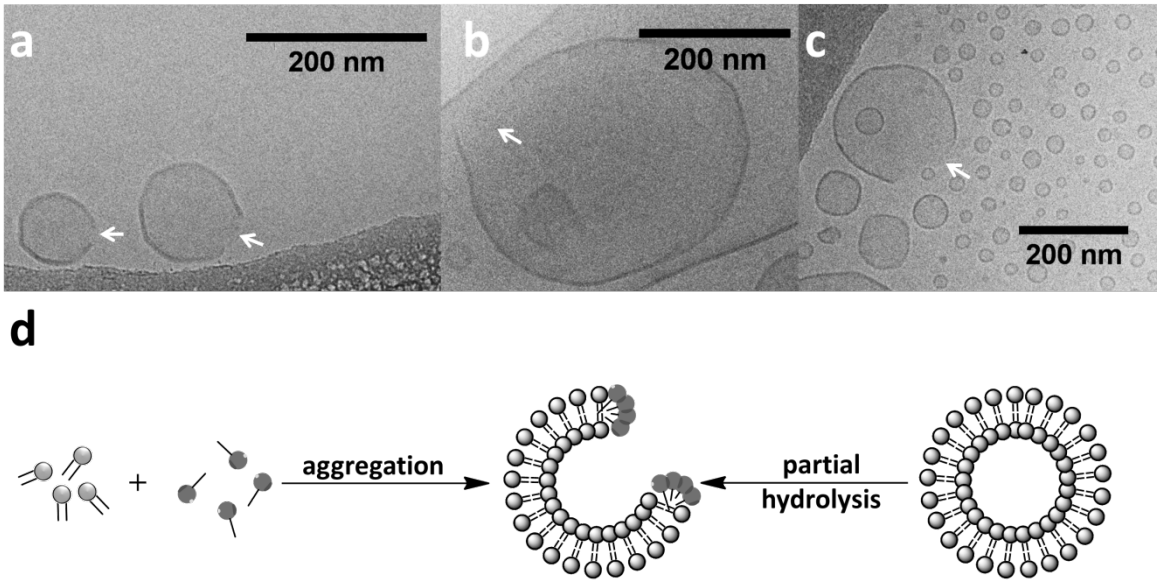

Figure 6.2.4: Cryo-TEM image of **1b** (a), **1c** (b) and **1d** (c) showing open vesicles. (d) Schematic representation of the aggregation of single and double tailed amphiphiles leading to open vesicles (left) and the formation of open vesicle which proceeds through partial hydrolysis of double tailed amphiphiles caused by self-activation (right). White arrow indicates opening.

As reported by *Stuart et al.*,[26] open vesicles can be obtained via mixing single-tailed and double-tailed amphiphiles (Figure 6.2.4d, left). Hereby, the double-tailed surfactant owning a truncated cone shape forms the lipid bilayer, while the amphiphile exhibiting only one hydrophobic tail and a cone shaped structure causes an end-capping of the bilayer, as shown in Figure 6.2.4d (left). Considering the packing parameters for **1b**, **1c** and **1d** (Chapter 5.2) it is expected that those amphiphiles have a truncated cone shape and form only closed vesicles. However, *N*-phosphoamino acids exhibiting a small residue at the amino acid head group can degrade to single-tailed amphiphiles, what could result in opening of vesicles as observed for **1b**, **1c** and **1d** (Figure 6.2.4a-c). As described by *Ni et al.* in 2009,[27] hydrophobic tails can be cleaved stepwise from *N*-phosphoamino acids **1** by a self-activated hydrolysis. As shown in Scheme 6.2.3, the first aliphatic alcohol **7** is cleaved via cyclization of **1** resulting in a mixed anhydride **8**. Then, by subsequent hydrolysis of **8** the single-tailed *N*-phosphoamino acid **9** is obtained owing a cone shaped structure giving rise to end-capped bilayers (Figure 6.2.4a-c). Repetition of both steps results in cleavage of the second tail giving an additional alcohol **7** and the

phosphoamide **11** via cyclic intermediate **10** as products (Scheme 6.2.3). While the first cleavage of **7** will lead to open vesicles the subsequent formation of **10** would lead to clearance of the liposome.

Both cleavage steps shown in Scheme 6.2.3 would result in a drug release from liposomes formed by **1b**, **1c** and **1d**.

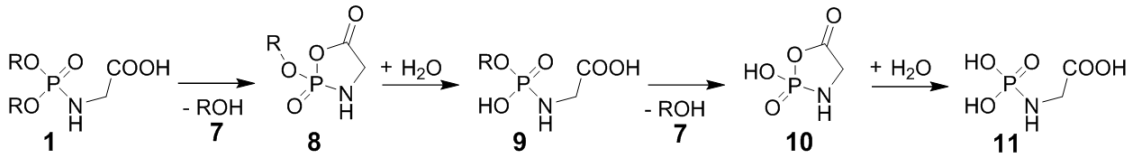

Scheme 6.2.3: Self-activated cleavage of hydrophobic tails from *N*-phosphoamino acids **1** resulting in the formation of lauryl alcohol **7** (ROH=$C_{12}H_{25}OH$).

The formation of lauryl alcohol **7** from *N*-phosphoamino acid **1d** was proven by NMR-spectroscopy (Figure 6.2.5). Hereby, the liposomes formed by **1d** were stored at room temperature in an aqueous buffered solution (pH 8.5) for two weeks and the formed alcohol **7** was extracted from the aqueous solution after acidification. The comparison of the NMR (Figure 6.2.5a and b) spectra of **1d** and the extracted compound confirms the cleavage of **7** under the applied conditions for aggregation. As shown in Figure 6.2.5 (2), no *N*-phosphoamino acid **1d** is present in the extracted mixture suggesting the formation of phosphoamide **10** (Scheme 6.2.3). The formation of lauryl alcohol was confirmed against independent sample of this compound and by comparison with literature data.

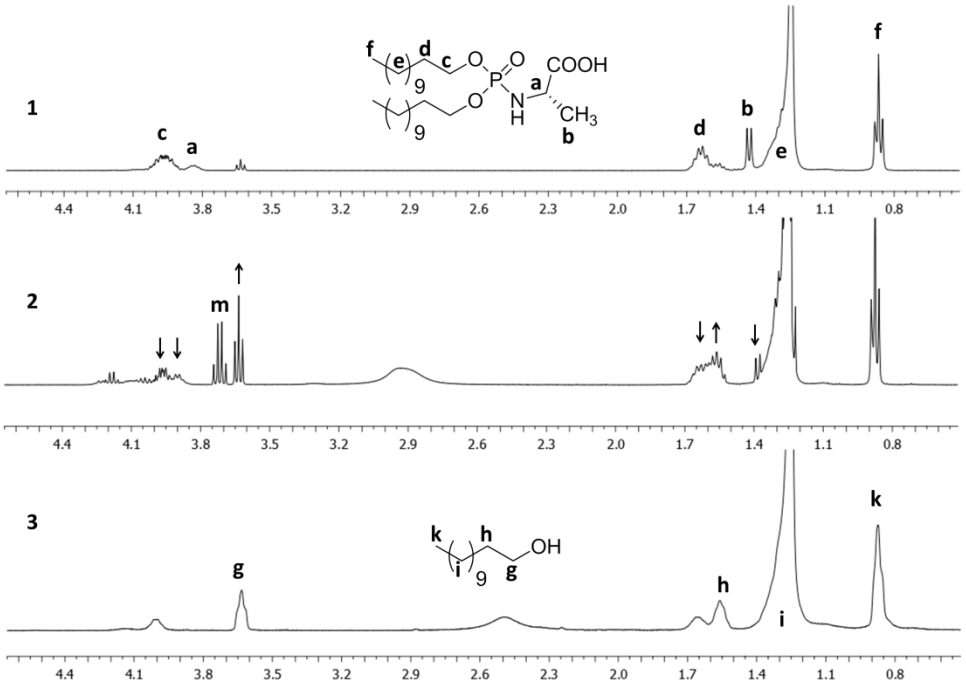

Figure 6.2.5: (1) ^{1}H-NMR of **1d**. (2) ^{1}H-NMR of **1d** after storing for 3 days under basic aqueous condition showing a mixture of **1d** and lauryl alcohol **7**. Solvent impurity: Ethanol: **m** represents the CH_2 group at 3.72 ppm. (3) ^{1}H-NMR of **1d** after storing for 2 weeks under basic aqueous condition showing mainly lauryl alcohol **7**.

In contrast to amphiphile **1b**, **1c** and **1d** no open vesicles were observed during cryo-TEM measurements for freshly preparation sample of *N*-Phosphoamino acids **1a**, and **1e - r** carrying a larger residue at the α-position. However, ^{1}H-NMR as well as ^{13}C-NMR studies show clearly the degradation of these compounds after longer storing under inert atmosphere (N_2) and low temperatures (4 °C) (Figure 6.2.6). Again lauryl alcohol **7** was observed as the main product pointing to a similar hydrolysis mechanism. This suggests a slower hydrolysis based on self-activation resulting in more stability of the observed aggregates. Hence, further studies need to be performed to understand the time- and temperature-dependent self-activation of *N*-phosphoamino acids **1**. This investigation could reveal impressive ways to tune release rates by choosing the right amino acid head group.

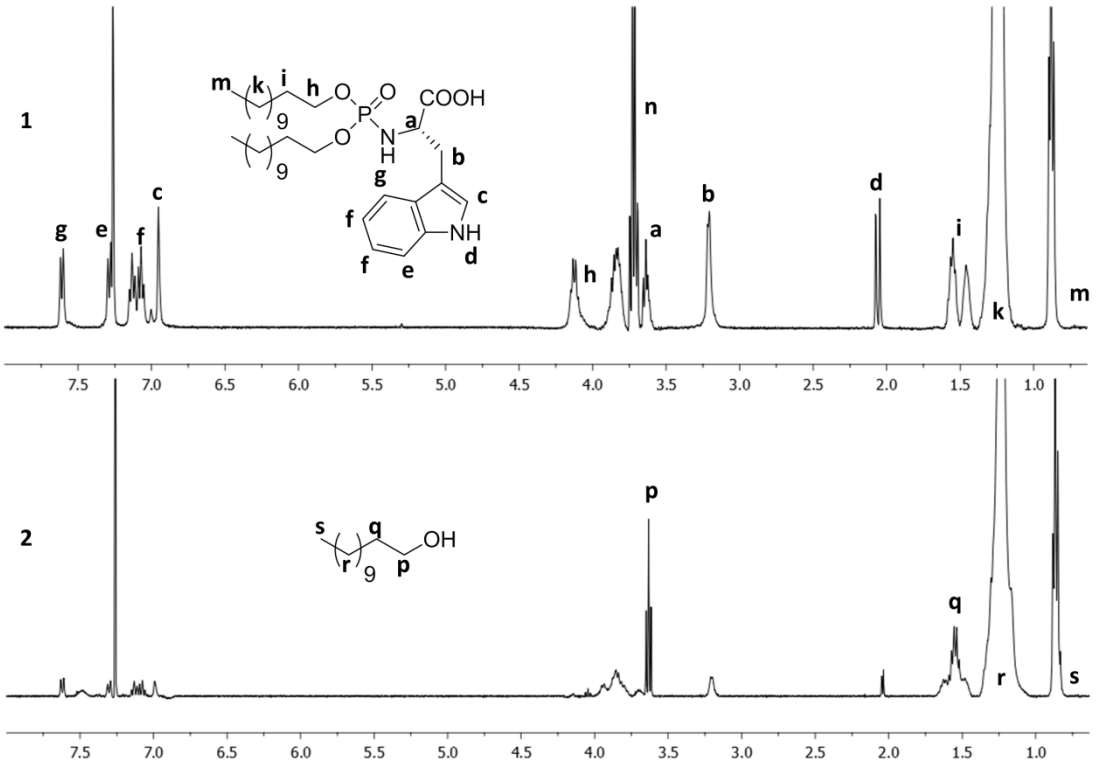

Figure 6.2.6: (1) ^{1}H-NMR of **1m**. (2) ^{1}H-NMR of **1m** after storing for approximately three month under inert atmosphere (N_2) and 4 °C. Solvent impurity: Ethanol: **n** represents the CH_2 group at 3.72 ppm.

6.3. Conclusion

In this chapter, the potential applicability of *N*-phosphoamino acids **1** as drug delivery systems was investigated. First, it was demonstrated that these newly introduced amphiphiles show high biocompatibility. Employing MTT (3-(4,5-di**m**ethyl**t**hiazol-2-yl)-2,5-diphenyl**t**etrazolium bromide) assays high *HeLa* cell viability was shown in the presence of three *N*-phosphoamino acids carrying aliphatic, aromatic and negatively charged residues at the amino acid head group. It needs to be emphasized that all tested amphiphiles own high biocompatibility using concentrations up to 100 μM allowing full cell viability. The low toxicity is based on the fact that *N*-phosphoamino acids **1** exhibiting only natural occurring building blocks, i.e. amino acid, phosphate and aliphatic alcohols.
Second, we demonstrated different potential release mechanisms for *N*-phosphoamino acids **1**. The first strategy is based on the protonation of the negatively charged head group of surfactant **1** resulting in the loss of the amphiphilic character and the clearance of the liposome under acidic conditions. This behavior suggests a fast drug release during endocytosis. A more interesting release mechanism was observed for *N*-phosphoamino acid **1** carrying small amino acids, i.e. glycine, alanine and beta-alanine, as head group. Employing cryo-TEM and NMR studies it was shown that these *N*-phosphoamino acids **1** degrade leading to open vesicles. This degradation is based on a self-activated cleavage of the amphiphilic tail resulting in mono-tailed *N*-phosphoamino acids allowing opening of the liposome.
Considering the facile synthesis, the high biocompatibility and the potential release mechanism, we can conclude that *N*-phosphoamino acids **1** could be promising candidates for future drug delivery systems.

6.4 Experimental Section

6.4.1 Materials and Methods

All chemicals and reagents were purchased from commercial suppliers (*Acros* and *Sigma-Aldrich*) and used without further purification. All buffers were prepared using double distillated water.
^{1}H- and ^{31}P-NMR- spectroscopy were recorded on an *Agilent 400* using $CDCl_3$.
A pH-meter (Hanna Instruments pH 209) equipped with a glass combination electrode was used for pH adjustments of the reaction buffers.
Cryo TEM images were taken on an FEI Tecnai T20 transmission electron microscope and on a Philips CM12 cryo transmission electron microscope operating at 200 and 120 kev, respectively. Images were recorded on a slowscan CCD camera under low-dose conditions.
Synthesis and characterization of all amphiphiles used here are given in chapter 5.

Cryo-TEM

Sample preparation: After dissolving *N*-phosphoamino acid in chloroform the solvent was carefully evaporated under a slow stream of nitrogen and continuing rotation. The resulting thin film was stored for 30 min under high vacuum to assure the complete removal of organic solvents. Next an aqueous buffered solution was added to a final concentration of 3 mg/mL. The resulting sample was vortexed to obtain a homogenous suspension. Finally three freeze-thaw cycles were performed to enable aggregate formation. The resulting turbid solution was used for cryo-TEM measurements.

Sample preparation:
pH 1 was adjusted by using a 1 M aqueous HCl solution to a 4 mg/ mL solution of the *N*-phosphoamino acid in water. The resulting solution was diluted with water to a final concentration of 3 mg/ mL.

Buffer preparation:
pH 6.5 (20 mM Phosphate buffer): 0.76 mL of a 1 M aqueous K_2HPO_4 solution was added to 1.24 mL of a 1 M aqueous KH_2PO_4 solution. The pH and concentration of the resulting solution was adjusted by adding a 1M aq. KOH solution and dilution to a total volume of 100 mL.
pH 8.5 (20 mM TRIS buffer): 1.21 g of tris(hydroxymethyl)aminomethane was dissolved in 500 mL water and the pH was adjusted by adding 1M aqueous HCl solution. Afterwards water was added to obtain a total volume of 500 mL.
pH 11 was adjusted by using a 1 M aqueous NaOH solution to a 4 mg/mL solution of *N*-phosphoamino acid in 10 mM aqueous NaOH (20 mM NaOH for **1i**). The resulting solution was diluted with water to a final concentration of 3 mg/ mL.

6.4.2 Cytotoxicity assay

Cytotoxicity assay: MTT assay[21]

DMEM: Commercial available Dulbecco's Modified Eagle's Medium (DMEM) was supplemented with 10% fetal calf serum, penicillin (100 units/ mL), streptomycin (100 µg/ mL) and L-glutamine (2mM).
Sample preparation: The sample was prepared according to the procedure for cryo-TEM to ensure the aggregate formation. Instead of a buffered aqueous solution DMEM was used for the stock solution. All concentrations were obtained diluting a fresh prepared 3 mM stock solution with DMEM.
Cell line: HeLa cells were grown in DMEM and cultured at 37 °C, 5% CO_2 and 95% relative humidity.
MTT assay: HeLa cells were dispensed in a sterile 96-well plate at a cell density of 10,000 cells/ well and were incubated for 8 hat 37 °C, 5% CO_2 and 95% relative humidity. Afterwards, the *N*-phosphoamino acid solution was added to the cells at various concentrations and was incubated for 16 h. Then MTT was added to a final concentration of 0.5 mg/ mL in each well and the resulting solution was incubated for additional 4 h. Finally, all medium was removed and 100 µL of DMSO was added to dissolve the created formazane. The absorbance of the DMSO solution was measured at 570 nm using a microplate reader (SynergyMX, BioTek). Cell survival was expressed as a relative viability of cells compared to control cultures that were incubated with medium only.

Table 6.4.1: MTT assay

	Amino acid	**0,25 mM***	**2.5 mM***	**10 mM***	**25 mM***	**50 mM***	**100 mM***	**200 mM***	**400 mM***
1a	L-Phe	99.10 (10.23)	96.27 (4.09)	-	107.59 (9.49)	-	-	-	-
1d	L-Ala	102.70 (6.79)	99.03 (9.56)	108.62 (3.86)	109.27 (6.21)	94.51 (13.10)	105.82 (26.24)	53.58 (5.42)	16.91 (0.85)
1i	L-Asp	110.17 (5.10)	109.46 (11.74)	-	102.06 (15.37)	101.59 (18.48)	84.28 (16.67)	-	-
1m	L-Trp	-	-	-	-	100.48 (12.68)	99.00 (10.68)	-	-

Cell survival given in % compared to control samples that were incubated only with DMEM. All given data are the averages of three separate experiments. Standard deviation is given in brackets. * Final concentration during the 16 h of incubation.

6.5 References

1) A. D. Bangham, M. M. Standish, J. C. Watkins. Diffusion of univalent ions across the lamellae of swollen phospholipids. *J. Mol. Biol.*, **13**, 238-252 (1965).
2) D. Papahadjopoulos. Liposomes and Their Uses in Biology and Medicine. *Ann. N.Y. Acad. Sci.*, **308**, 1 (1978).
3) G. Gregoriadis. Liposomes in therapeutic and preventive medicine: The development of the drug-carrier concept. *Ann. N.Y. Acad. Sci.*, **308**, 343-370 (1978).
4) C. Kirby, J. Clarke, G. Gregoriadis. Cholesterol content of small unilamellar liposomes controls phospholipid loss to high density lipoproteins in the presence of serum. *FEBS Lett.*, **111**, 324-328 (1980).
5) Y. Perrie, T. Rades. Pharmaceutics: Drug Delivery and Targeting. 2nd ed., *Pharmaceutical Press* (2012).
6) D. C. Drummond, O. Meyer, K Hong, D. B. Kirpotin, D. Papahadjopoulos. Optimizing Liposomes for Delivery of Chemotherapeutic Agents to Solid Tumors. *Pharmacol. Rev.*, **51**, 691-744 (1999).
7) D. V. Devine, K. Wong, K. Serrano, A. Chonn, P. R. Cullis. Liposome-complement interactions in rat serum: Implications for liposome survival studies. *Biochim. Biophys. Acta.-Biochem.*, **1191**, 43-51 (1994).
8) D. D. Lasic, D. Papahadjopoulos. Liposomes revisited. *Science*, **267**, 1275-1276 (1995).
9) K. Uchiyama, A. Nagayasu, Y. Yamagiwa, T. Nishida, H. Harashima, H. Kiwada. Effect of the size and fluidity of liposomes on their accumulation in tumors: A presumption of their interaction with tumors. *Int. J. Pharm.*, **121**, 195-203 (1995).
10) A. Gabizon, U. Papahadjopoulos. Liposome formulation with prolonged circulation time in blood and enhanced uptake by tumors. *Proc. Natl. Acad. Sci.*, **85**, 6949-6953 (1988).
11) G. Gregoriadis, D. E. Neerunjun. Control of the Rate of Hepatic Uptake and Catabolism of Liposome-Entrapped Proteins Injected into Rats. Possible Therapeutic Applications. *Eur. J. Biochem.*, **47**, 179-185 (1974).
12) M. J. Hsu, R. L. Juliano. Interactions of liposomes with the reticuloendothelial system. II: Nonspecific and receptor-mediated uptake of liposomes by mouse peritoneal macrophages. *Biochim. Biophys. Acta*., **720**, 411-419 (1982).
13) J. H. Senior. Fate and behaviour of liposomes in vivo: A review of controlling factors. CRC *Crit. Rev. Ther. Drug Carrier Syst.*, **3**, 123-193 (1987).
14) R. L. Souhami, H. M. Patel, B. E. Ryman. The effect of reticuloendothelial blockade on the blood clearance and tissue distribution of liposomes. *Biochim. Biophys. Acta.*, **674**, 354-371 (1981).
15) A. Gabizon, D. Papahadjopoulos. The role of surface charge and hydrophilic groups on liposome clearance in vivo. *Biochim Biophys Acta*., **1103**, 94-100 (1992).
16) T. M. Allen, C. Hansen, F. Martin, C. Redemann, A. Yau-Young. Liposomes containing synthetic lipid derivatives of poly(ethyleneglycol) show prolonged circulation half-lives in vivo. *Biochim. Biophys. Acta*., **1066**, 29-36 (1991).

17) T. S. Levchenko, R. Rammohan, A. N. Lukyanov, K. R. Whiteman, V. P. Torchilin. Liposome clearance in mice: The effect of a separate and combined presence of surface charge and polymer coating. *Int. J. Pharm.*, **240**, 95-102 (2002).
18) D. Papahadjopoulos, T. M. Allen, A. Gabizon, E. Mayhew, K. Matthay, S. K. Huang, K. D. Lee, M. C. Woodle, D. D. Lasic, C. Redemann. Sterically stabilized liposomes: improvements in pharmacokinetics and antitumor therapeutic efficacy. *PNAS*, **88**, 11460-11464 (1991).
19) D. D. Lasic, P. M. Frederik, M. C. A. Stuart, Y. Barenholz, T. J. McIntosh. Gelation of liposome interior. A novel method for drug encapsulation. *FEBS Lett*., **312**, 255-258 (1992).
20) M. M. Black, F. D. Speer. Effects of cancer chemotherapeutic agents on dehydrogenase activity of human cancer tissue in vitro. *Am. J. Clin. Pathol*., **23**, 218-227 (1953).
21) T. Mosmann. Rapid colorimetric assay for cellular growth and survival: Application to proliferation and cytotoxicity assays. *J. Immunol. Meth*., **65**, 55-63 (1983).
22) J. M. Sargent, A. W. Elgie, C. J. Williamson, C. G. Taylor. The use of the MTT assay to study drug resistance in acute myeloid leukaemia–an update. *Adv. Blood Dis.*, **3**, 33-41 (1997).
23) C. G. Taylor, J. M. Sargent, A. W. Elgie, C. J. Williamson, G. M. Lewandowicz, O. Chappatte, J. G. Hill. Chemosensitivity testing predicts survival in ovarian cancer. *Eur. J. Gynaecol Oncol.*, **22**, 278-282 (2001).
24) P. Denton, C. Rostron. Pharmaceutics: The Science of Medicine Design. *Oxford University Press. Oxford*, United Kingdom (2013).
25) A. Sorkin, M. von Zastrow. Signal transduction and endocytosis: close encounters of many kinds. *Nature Rev. Mol. Cell Biol.*, **3**, 600-614 (2002).
26) M. C. A. Stuart, E. J. Boekema. Two distinct mechanisms of vesicle-to-micelle and micelle-to-vesicle transition are mediated by the packing parameter of phospholipid-detergent systems. *Biochim. Biophys. Acta.*, **1768**, 2681-2689 (2007).
27) F. Ni, X. Gao, Z.-X. Zhao, C. Huang, Y.-F. Zhao. On the electrophilicity of cyclic acylphosphor-amidates (CAPAs) postulated as intermediates. *Eur. J. Org. Chem.* **2009** 3026-3035 (2009).

Chapter 7

Influencing the Physical, Biological and Chemical Properties of *N*-Phosphoamino Acids by Facile Modifications

In several studies it has been shown that through incorporation of different moieties at the liposome surface the circulation life times, clearance, targeting and decomposition of liposomes can be influenced. Therefore, after introduction of a new class of amphiphiles, namely *N*-phosphoamino acids, in this Chapter two facile modifications of these compounds are established giving access to new amphiphile derivatives. One modification of these compounds results in surfactants carrying a dipeptide residue as head group, while the other modification leads to azobenzene-containing *N*-phosphoamides. These responsive *N*-phosphoamide derivatives are employed for thermal and photo-induced *cis*-*trans* isomerization studies. This data demonstrate clearly the ability of azobenzene exhibiting amphiphiles to act as molecular switches. Furthermore, in this chapter the good biocompatibility of these new amphiphiles is shown and the aggregation behavior of all derivatives is studied.

7.1 Introduction

In previous studies it was demonstrated that modifications at the head group of amphiphiles can be applied as a tool to influence the properties of these compounds used as drug delivery systems.[1-3] On the one hand, modifications were employed to obtain liposomes with increased solubility and longer circulation life time.[1,2] In this regards, PEGylation is the most common and widely used covalent surface modification which results in higher stability and slower clearance of liposomes.[1,2] On the other hand, derivatization of amphiphiles can also be applied to incorporate a drug release mechanism and to obtain controlled targeting of the liposomes.[1-3] For the latter purpose, as shown in the study of *Voinea et al.*, ligands, such as antibodies, were covalently attached via a peptide bound to the amphiphile.[3]

In order to give access to a broad variety of derivatives of *N*-phosphoamino acids **1**, introduced in chapter 5, we show here two facile synthetic pathways leading to *N*-phosphoamino amides **2** and **4**, carrying a dipeptide and azobenzene moiety at the head group, respectively (Scheme 7.1.1). As shown in Scheme 7.1.1, amphiphile derivatives **2** can be synthesized in only two synthetic steps via modification of the free acid moiety of *N*-phosphoamino acids **1** which were introduced in Chapter 5. In contrast, the synthesis of *N*-phosphoamide **4** requires the application of *N*-didodecyl phosphoryl chloride **3** as starting material.

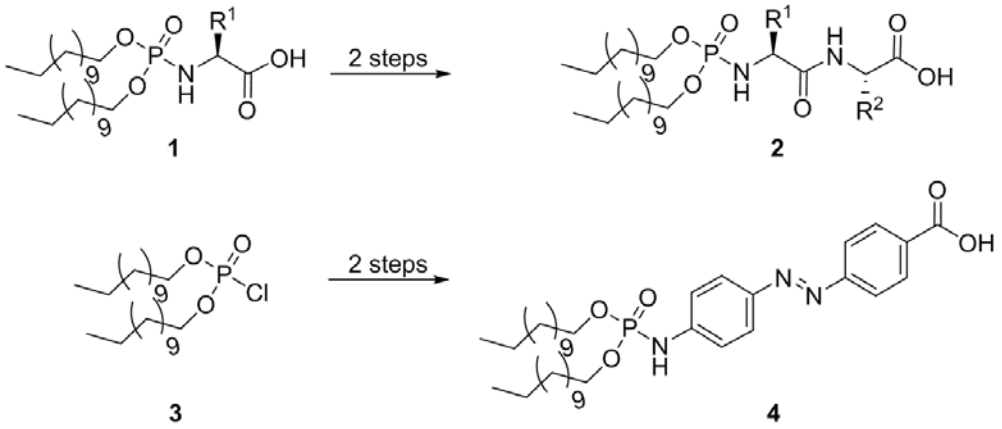

Scheme 7.1.1: Modification of *N*-phosphoamino acid **1** and *N*-didodecyl phosphoryl chloride **3**. R^1 and R^2 are representing amino acid side chains.

7.1.1 Dipeptides as Head Group of Amphiphiles

Since *N*-phosphoamino acids **1** exhibit an amino acid at the head group the introduction of a dipeptide moiety can be obtained via a common peptide coupling reaction using **h**ydr**o**xy**b**enzo**t**riazole (HOBt), *N*,*N*'-**d**icy**c**lohexyl**c**arbodiimide (DCC) and an amino acid ester **8** as reagents (Scheme 7.1.2). As shown in Scheme 7.1.2, the activation of the carboxyl moiety of **1** is carried out in two steps leading first to an activation through DCC resulting in the derivative **5**, followed by a reaction with HOBt leading to the activated ester **6**. During the latter step a by-product 1,3-dicyclohexylurea **7** is formed. Subsequent addition of an amine **8** to the activated ester **6** results in the product **9** carrying a methyprotected dipeptide group (Scheme 7.1.2). This pathway allows a fast synthesis of a broad variety of amphiphilic compounds **2** carrying a dipeptide as head group employing a subsequent hydrolytic step (Scheme 7.1.2).

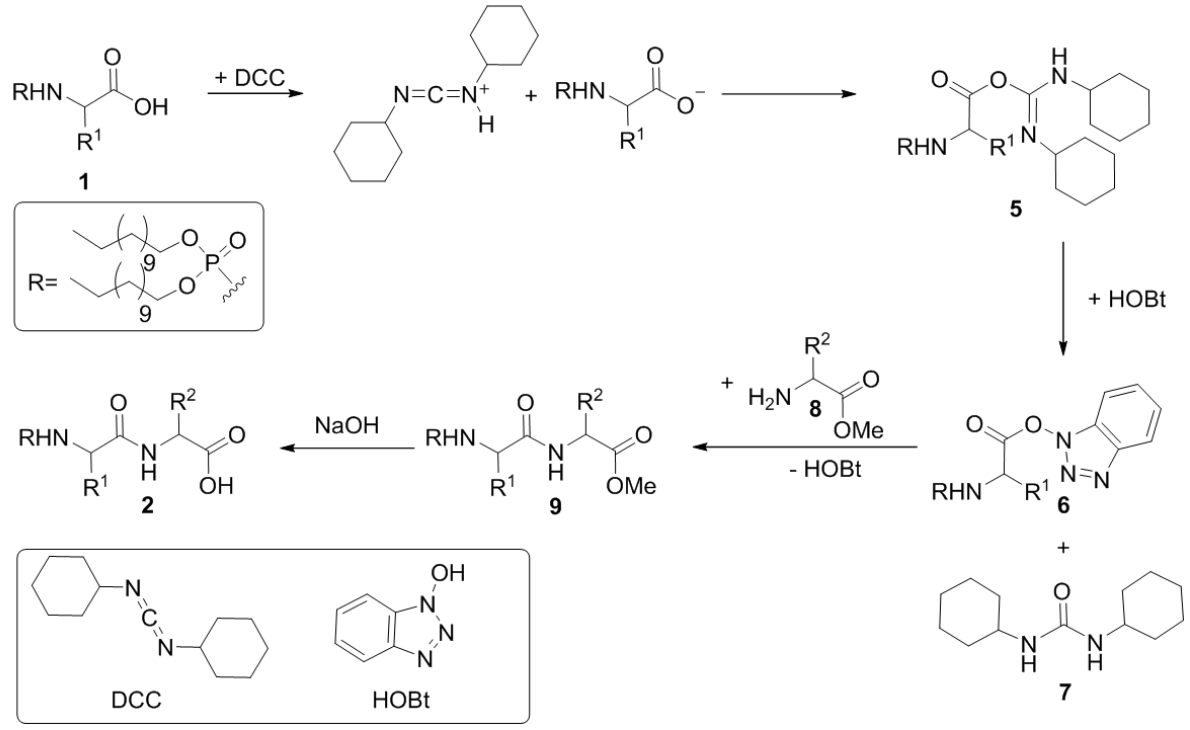

Scheme 7.1.2: Steps in the coupling reactions using HOBt and DCC. R^1 and R^2 are representing amino acid side chains.

The introduction of a dipeptide moiety is very attractive, since several dipeptides are biological active and own, depending on the amino acid residues, a variety of interesting properties. In the last century, different naturally occurring histidine-containing dipeptides were discovered. In Figure 7.1.1 representatives for biologically active dipeptides are shown, i.e. carnosine **10** (1900), anserine **11** (1929) and ophidine **12** (1939).[4,5,6] These highly water soluble molecules occur usually in high concentration in muscles (~20 mmol/ kg dry muscle in humans for carnosine) and consist of β-alanine- and L-histidine-derivatives.[7] Moreover, this class of dipeptides show anti-oxidative properties, due to the fact that these molecule can act as a

scavenger for reactive oxygen species.[8,9] Furthermore, carnosine can function as an intercellular proton buffer-[7] and a pH-dependent inhibitor for phosphorylase in muscles.[10] Additionally, due to the presence of the histidine moiety these dipeptides exhibit a chelating effect towards bivalent metal ions (Fe^{2+}, Cu^{2+}, Ni^{2+} and Pb^{2+}) and anti-cross linking properties for proteins.[11-13]

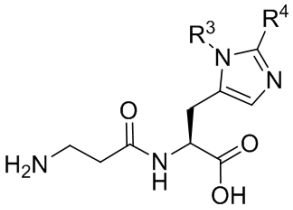

10 R^3= H, R^4=H
11 R^3= CH_3, R^4=H
12 R^3= H, R^4=CH_3

Figure 7.1.1: Molecular structure of carnosine **10**, anserine **11** and ophidine **12**.

7.1.2 Azobenzene Derivatives as Head Group of Amphiphiles

Many biological processes are triggered by light, in which light energy is transformed into chemical energy.[14,15] Examples are visual receptors and photosynthesis. A requirement for such an energy transfer is the presence of light sensitive molecules that transform light energy into chemical or kinetic energy. Azobenzenes, for instance, are known as molecular switches that can undergo photo-induced *cis-trans* isomerization resulting in change of size, polarity and shape of the molecule.[16] As shown in Scheme 7.1.3, the thermodynamically more stable planar E-isomer **13** of azobenzene is thereby converted to the twisted Z-isomer **14** using UV-light. In addition a change in the dipole moment takes place during the isomerization. Whereas the E-isomer **13** has no dipole, a dipole moment of 3.0 D is present for the Z-isomer **14**.[17] As shown in Scheme 7.1.3 the double bond isomerization is reversible employing light and/or heating.

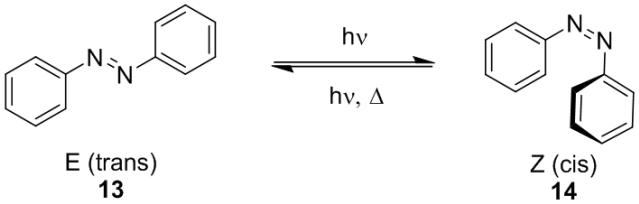

Scheme 7.1.3: Reversible *cis-trans*-isomerization of the planar E-azobenzene **13** to the twisted Z-azobenzene **14**.

Azobenzenes have been studied for decades and were applied successfully as dyeing agent (e.g. *Bismarck* brown, aniline yellow), photoswitchable catalysts[18,19] and liquid crystals[20]. Furthermore, azobenzenes can be incorporated in biomolecules.[21] Thereby, the *cis-trans*-isomerization can be used as an on-off-switch in enzymes[22] and ion-channels[23] triggered by

light. Also several photo-controlled lipids were synthesized and studied to influence the permeability of membranes.[24,25] This light induced change of the surfactant shape and associated destabilization of bilayers can be applied in drug delivery systems using light as external trigger for controlled drug release.[26]

7.2 Results and Discussion

7.2.1 Synthesis of *N*-phosphoamides.

7.2.1.1 Synthesis of *N*-Phosphoamides Exhibiting a Dipeptide Head Group

To synthesize amphiphiles carrying a dipeptide as head group we were using the amphiphiles **1c** and **1h** which were introduced in chapter 5 (Chapter 5, Table 5.2.1), exhibiting β-alanine and proline as head group, respectively. β-Alanine as spacer will allow high flexibility whereas the rigid proline will lead to an less flexible head group. We chose the methyl ester **8a** and **8b** of amino acids histidine and tryptophan, respectively, to be coupled to the head group of **1c** and **1h**. As shown in Scheme 7.2.1, we applied successfully the in Chapter 7.1.1 described peptide coupling using amino acid methyl esters **8** and *N*-phosphoamino acids **1** to obtain methyl protected *N*-phosphoamides **9** carrying a dipeptide as head group. The reaction was performed under anhydrous conditions in presence of catalytic amounts of DMAP. As shown in Table 7.2.1, *N*-phosphoamides **9** were obtained with isolated yields of up to 63%.
However, an additional hydrolysis of methyl ester **9** is required to introduce the amphiphilic character resulting in *N*-phosphoamides **2** (Scheme 7.2.1). By using an 1 M aqueous solution of NaOH and ethanol the free acids **2** were obtained reaching yields of up to 89% (Table 7.2.1). It has to be emphasized that the incorporation of histidine as head group of amphiphiles **1** was not successful when connected directly to the phosphate moiety (see Chapter 5). However, employing the strategy described in this chapter allows the introduction of a terminal histidine residue resulting in surfactants **2a** and **2c**.

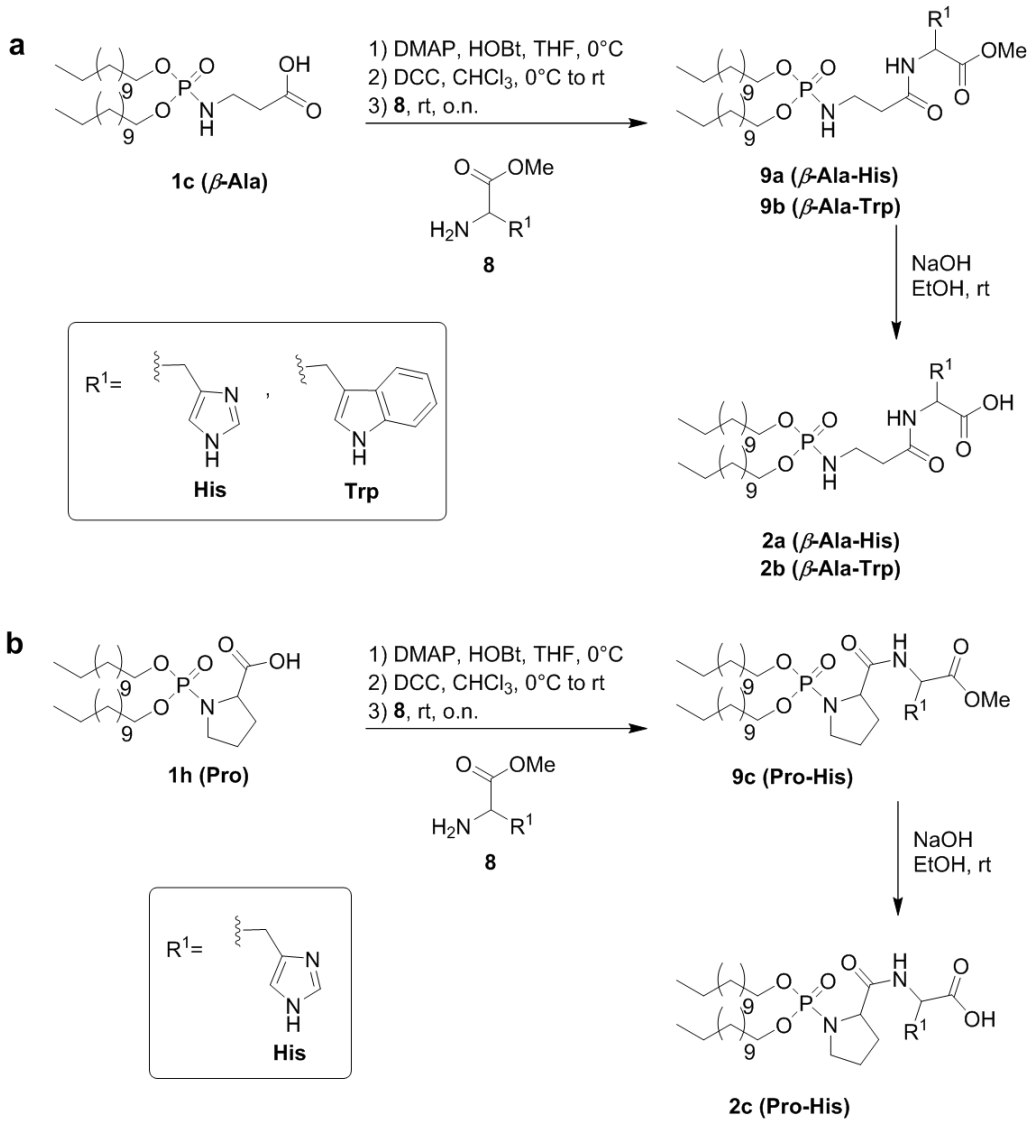

Scheme 7.2.1: Coupling reaction between **1** and **8** leading to the *N*-phosphodipeptide **9**, and subsequent hydrolysis of the methyl ester **9** resulting in amphiphile **2**. (a) β-Alanine derivative **1c** is reacted with histidine (His) and tryptophan (Trp) forming the corresponding amphiphile **2a** (β-Ala-His) and **2b** (β-Ala-Trp), respectively. (b) Proline (Pro) derivative **1h** reacts with histidine (His) results in amphiphile **2c** (Pro-His).

Table 7.2.1: Isolated yields obtained for methyl ester **9** and the corresponding acid **2**.

Entry	Amino acid	*N*-phospho-amino acid 1	Methyl ester 9	Yield† (%) (methyl ester 10)	Acid 2	Yield† (%) (acid 2)
1	L-his	**1c** (β-ala)	**9a** (carnosine (β-ala-his))	51	**2a**	69
2	L-trp	**1c** (β-ala)	**9b** (β-ala-trp)	63	**2b**	70
3	L-his	**1h** (L-pro)	**9c** (pro-his)	63	**2c**	83

All reactions were carried out according to the general procedure described in the experimental section 7.4.2.1 using 1.5 equiv. *N*-phosphoamino acid **1**, a catalytic amount of DMAP and 2.2 equiv. of HOBt in THF (4 mL/ mmol), 2.2 equiv. DCC in $CHCl_3$ (4 mL/ mmol) and 1 equiv. of a methylated amino acid hydrochloride to obtain the methyl ester **9**. 1 mL/ mmol of EtOH and 1 mL/ mmol 2M aq. NaOH were used to obtain the free acid **2**. † All reported yields are given as isolated yields.

The successful and fast variation of *N*-phosphoamino acid **1** gave rise to a variety of new compounds **9a-c** and **2a-c** (Table 7.2.1). These representative modifications demonstrate their high potential in optimization of this drug delivery system, which can be achieved via introduction of different residues located in the head group of the amphiphile. It has to be emphasized that the use of an additional amino acid like histidine or tryptophan will still lead to amphiphiles exhibiting only naturally occurring building blocks. Moreover, the presence of a second amino acid residue at the head group might prevent or slow down the through self-activation caused degradation of *N*-phosphoamides (see Chapter 6.2.2). Hence, due to sterical hindrance and due to increased distance between the acid moiety and the phosphate the formation of the in Chapter 5 (p. 97) described mixed anhydride is not favored any more. This results in higher stability of the formed liposomes. Also additional information on the liposome surface is enabled by this modification, since histidine is known to form chelates with bivalent metal ions, such as Fe^{2+} and Cu^{2+}.

7.2.1.2 Synthesis of *N*-Phosphoamides Exhibiting an Azobenzene Head Group

A different approach was based on the use of azo-benzene switches as part of the head group allowing potential light induced aggregation changes of amphiphiles. To realize this idea the same reaction conditions as described in Chapter 5.2 were employed for the synthesis of *N*-phosphoamide **4** carrying a azo-benzene moiety instead of an amino acid. As shown in Scheme 7.2.2, *p*-amino azobenene derivative **15** and *N*-didodecyl phosphoryl chloride **3** were employed for the synthesis of **4** in two synthetic steps. However, due to low reactivity of the aniline **15** the presence of catalytic amounts of DMAP, an excess (six equiv.) of the phosphorylchloride **3** and a reaction time of six days were necessary. As shown in Scheme 7.2.2, *N*-phosphoamide **16** was successfully synthesized reaching an isolated yield of 61%

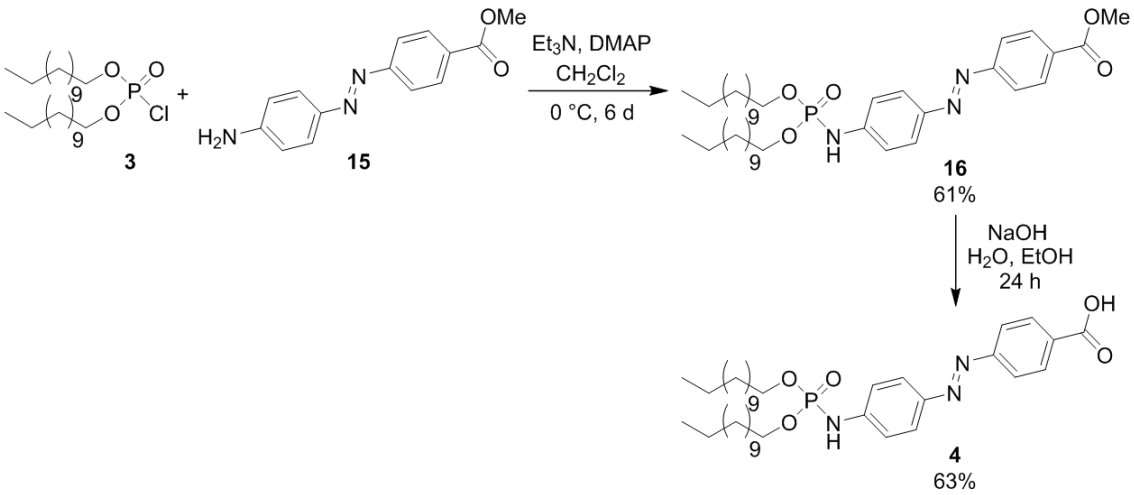

Scheme 7.2.2: Synthesis of amphiphile **4** using phosphorylchloride **3** and azo-benzene **15** leading to the *N*-phosphoamide **16**, followed by hydrolysis of the methyl ester **16**.

After the successful synthesis of **16** the subsequent hydrolysis allowed the introduction of a negative charge at the azobenzene head group resulting in the final amphiphile **4** (Scheme 7.2.2). Employing an aqueous 1M NaOH solution for the hydrolysis followed by acid-base extraction resulted in the free acid of *N*-phosphoamide **4**. An isolated yield of 63% was obtained after a reaction time of 24 hours (Scheme 7.2.2). However, due to the low solubility of the *N*-phosphoamide **4** in aqueous solution we decided to increase the hydrophilic moiety employing the in Chapter 7.1 described coupling reaction. Hence, aspartic acid di-methyl ester **17** was used to obtain derivative **18** with an isolated yield of 73% (Scheme 7.2.3). Finally, the subsequent hydrolysis of **18** gave access to amphiphile **19** exhibiting free acid moieties reaching a yield of 68%. The carried out modification did not result in the desired increase of solubility which hindered at this point aggregation and biocompatibility studies for this compounds.

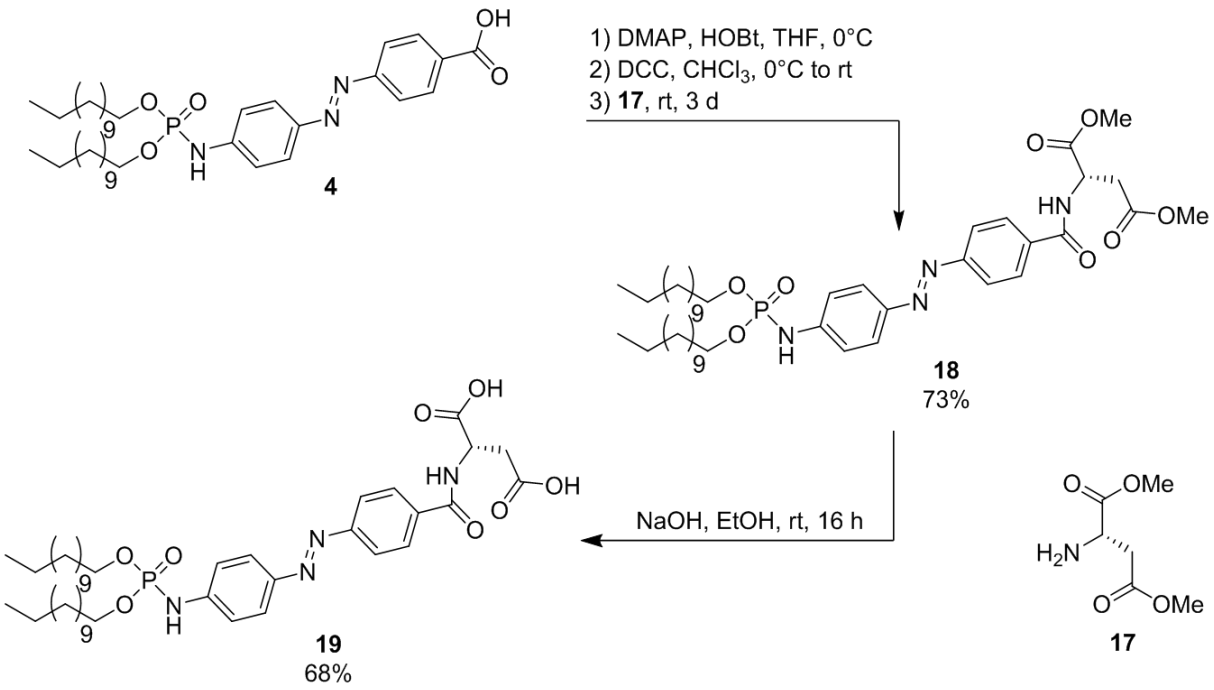

Scheme 7.2.3: Couplings reaction between **4** and **17** leading to the *N*-phosphodipeptide **18**, followed by hydrolysis of the methyl ester **18** yielding the amphiphile **19**.

7.2.2 Biocompatibility of *N*-Phosphoamides

One of the most important requirements for a drug delivery systems is the biocompatibility of the amphiphile. To study the biocompatibility of synthesized *N*-phosphodipeptides **2a-c** MTT (3-(4,5-di**m**ethyl**t**hiazol-2-yl)-2,5-diphenyl**t**etrazolium bromide) assays were employed (Figure 7.2.1), which were already described in detail in Chapter 6.2. Due to the composition of the amphiphiles **2a-c** carrying a dipeptide we expect comparable biocompatibility as for the in Chapter 6.2 tested compounds **1d**, **1i** and **1m** (Chapter 6.2.1). As shown in Figure 7.2.1, all compounds carrying a dipeptide (**2a-c**) show a lower biocompatibility compared to *N*-phosphoamino acids **1** carrying one amino acid as head group (Chapter 6.2.1). Amphiphiles **2b** and **2c** carrying dipeptide β-ala-trp and pro-his, respectively, show at a 50 µM concentration still 100% cell viability. In contrast, *N*-phosphodipeptide **2a** exhibiting the naturally occurring dipeptide carnosine has at the same concentration a cell viability of only 71% (Figure 7.2.1). Conclusively, the modification of the head group is influencing considerably the toxicity of *N*-phosphoamides. However, it needs to be emphasized that all synthesized amphiphiles **2a-c** exhibit still a relatively high biocompatibility with IC_{50} values between 25 µM and 100 µM.

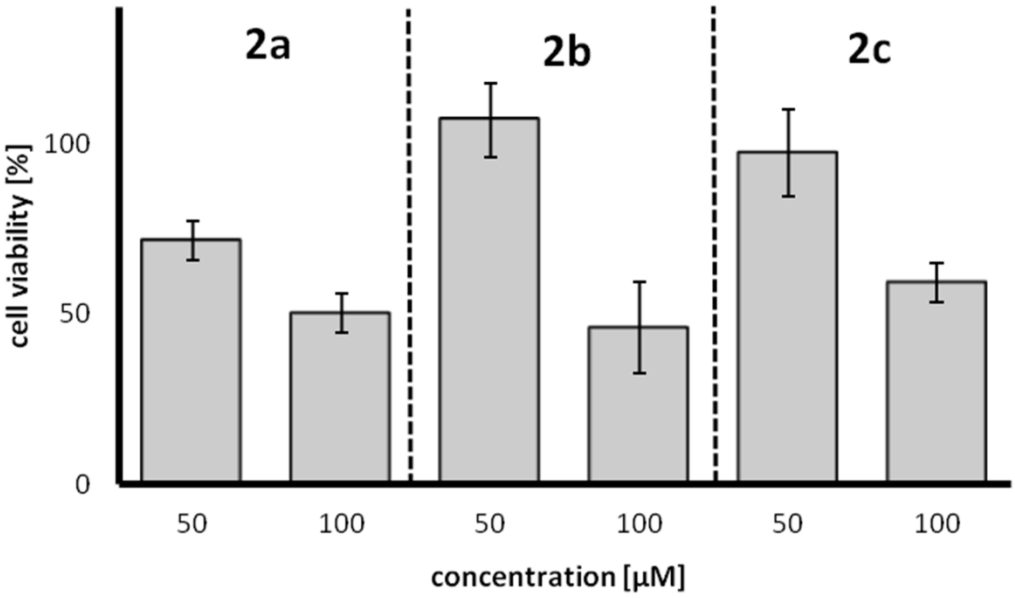

Figure 7.2.1: MTT assay using *N*-phosphoamids **2a**, **2b**, **2c**. Cell viability is given for all amphiphiles at concentrations of 50 µM, 100 µM. Each experiment was performed three times.

7.2.3 Study of the Aggregation Behavior of *N*-Phosphoamides Using Cryogenic Transmission Electron Microscopy (cryo-TEM)

After we had successfully demonstrated the good biocompatibility of *N*-phosphoamides **2a-c** we investigated also the aggregation behavior of these compounds. Therefore, all amphiphiles were dissolved in a buffered solution with a pH of 8.5 and measured using **cryo**genic **t**ransmission **e**lectron **m**icroscopy (cryo-TEM). All measurements were performed at room temperature since, using **d**ifferential **s**canning **c**alorimetry (DSC), a transition temperature higher than 0 °C could not be detected for amphiphiles **2a-c**. As shown in Table 7.2.2, all amphiphiles carrying a dipeptide as head group, i.e. **2a-c**, form aggregates, such as vesicles, tubes or twisted ribbons (Table 7.2.2). However, for compound **19** exhibiting an azobenzene moiety no assemblages were observed employing cryo-TEM. As shown in Table 7.2.2 the pH for compound **19** was increased to 12 again without successful aggregate observation. This behavior can be explained by the low solubility of amphiphiles **19** in aqueous solution.

Table 7.2.2: Aggregation of amphiphiles **2a-c** and **19** determined using cryo-TEM.

	Head group	**Aggregates***
2a	L-β-ala-L-his (carnosine)	vesicle, twisted ribbons, open and end-capped tubes
2a†	L-β-ala-L-his (carnosine)	open and end-capped tubes
2b	L-β-ala-L-trp	vesicle
2c	L-pro-L-his	vesicle
19**	azobenzene-L-asp	-

All samples were prepared using thin layer technique followed by hydration with 20 mM buffer solution and three freeze dry cycles. *Aggregates observed from an aqueous solution at pH 8.5 and room temperature. The pH value was adjusted using 20 mM TRIS buffer and concentrated HCl solution. ** Due to low solubility samples were prepared in aqueous solution with a pH up to 12. † Amphiphiles were measured at room temperature after the sample was heated for 2 h at 70 °C.

As shown in Figure 7.2.2, for amphiphile **2b** and **2c** carrying dipeptide L-β-ala-L-trp and L-pro-L-his, respectively, exclusively vesicle were observed. Considering the packing parameter described by *Israelachvili*[26] and the observed aggregates (Fig. 7.2.2) we can assume that the occupied average space by one molecule is equal to a truncated cone. Furthermore, based on these observations we can conclude that an additional amino acid at the head group of the amphiphiles can be tolerated without influencing the aggregation behavior significantly. As described in Chapter 5, *N*-phosphoamino acids **1c** and **1h** exhibiting a single amino acid at the head group, i.e. L-β-ala and L-pro, respectively, show similar aggregation behavior as surfactants **2b** and **2c**.

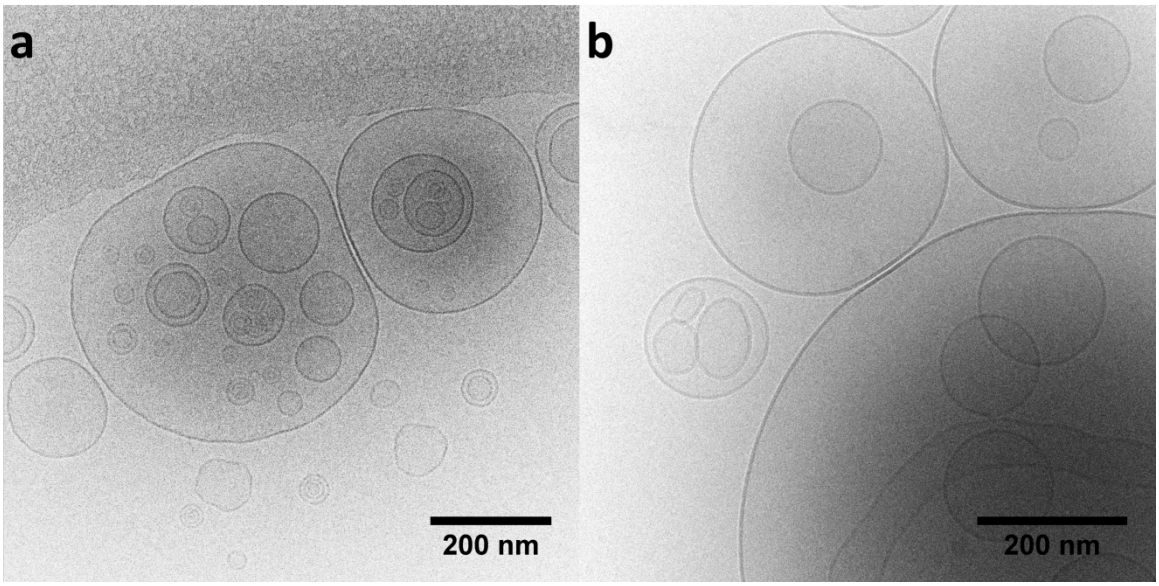

Figure 7.2.2: Cryo-TEM images of **2b** (a) and **2c** (b) showing vesicles. All samples were prepared in 20 mM aq. TRIS buffer (pH 8.5) at rt with a final amphiphile concentration of 3 mg/ mL.

In contrast to compounds **2b** and **2c**, for amphiphile **2a** carrying L-β-ala-L-his (carnosine) at the head group a broad variety of aggregates was detected using cryo-TEM. As shown in Figure 7.2.3a and 7.2.3b, *N*-phosphoamide **2a** forms also vesicles (white dashed arrows) as observed for **2b** and **2c**. However, employing freshly prepared samples for cryo-TEM studies several different assemblages could be observed for **2a** (Figure 7.2.3), i.e. end-capped tubes (white arrows), long tubes (black dashed arrows) and twisted ribbons (black arrows).
Repetitions of these studies show that this system seems to be strongly sensitive to external influences. The ratio of the above described aggregates, especially for vesicles, varied significantly for nearly identically samples. Therefore, it was of great interest to study the aggregation behavior of compound **2a** dependent of time and temperature. Hence, the same sample that was used for the cryo-TEM images in Figure 7.2.3 was analyzed using cryo-TEM once again after being stored for approx. 6 h at room temperature. As shown in Figure 7.2.4, no vesicles for **2a** were observed after storage, instead, an increased amount of long tubes (black arrow) and end-capped tubes (white arrow) were detected (Figure 7.2.4a). Also, tubes connected *via* vesicles (Figure 7.2.4b, white dashed arrow) and twisted ribbons (Figure 7.2.4a, black arrow) were formed by *N*-phosphoamide **2a**.

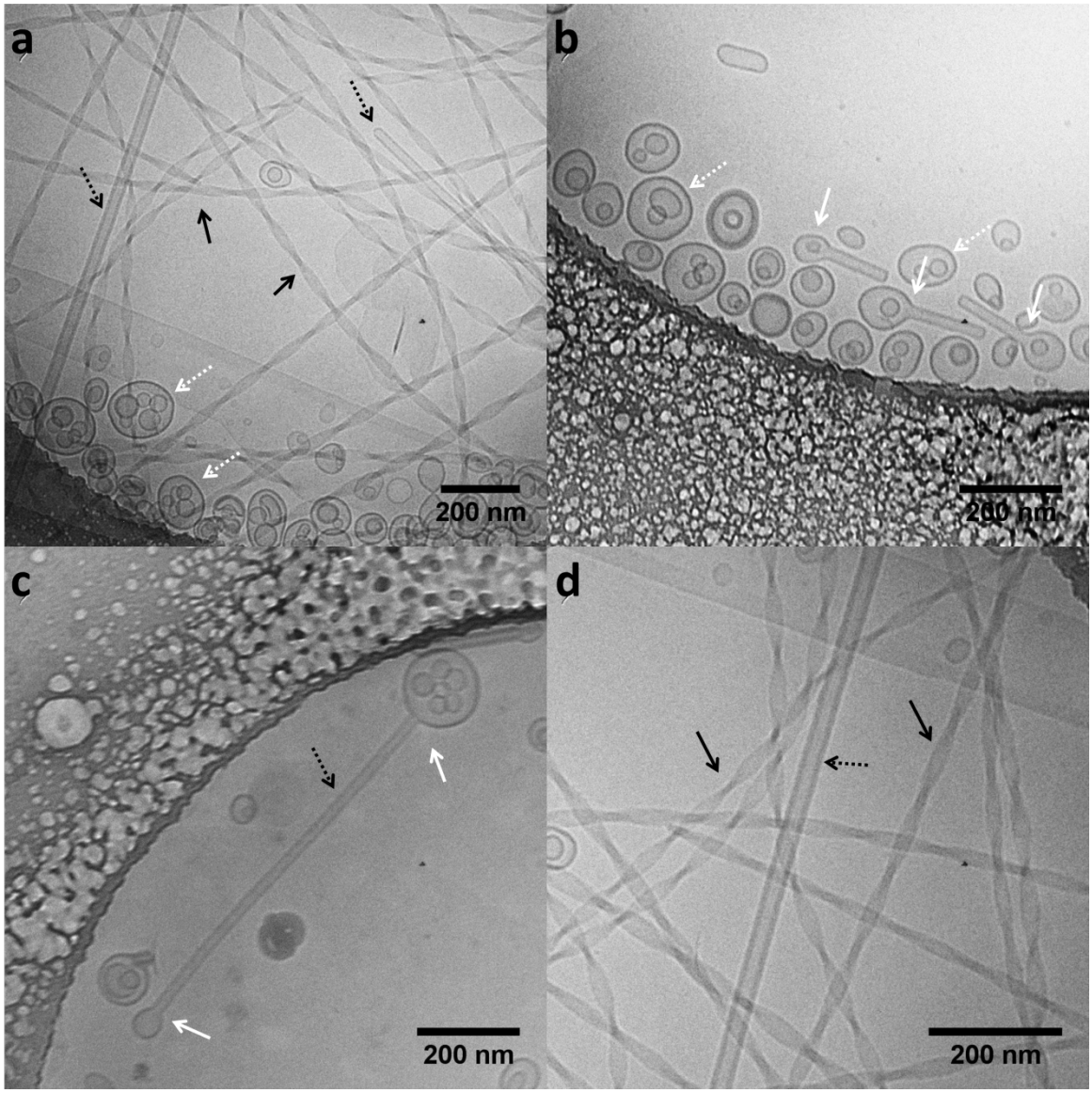

Figure 7.2.3: Cryo-TEM images of a fresh prepared sample of **2a** at room temperature showing vesicles (white dashed arrow), tubes (black dashed arrow) and end-capped tubes (white arrow) as well as twisted ribbons (black arrow). All samples were prepared in 20 mM aq. TRIS buffer (pH 8.5) at rt with a final amphiphile concentration of 3 mg/ mL.

In addition to the time-dependent studies, we performed the aggregation studies of **2a** after being heated for two hours at 70 °C (Figure 7.2.4c and d). Again long tubes and tubes with incorporated vesicles were observed for compound **2a**. However, the amount of end-capped tubes was decreased and no twisted ribbons were present in the sample.

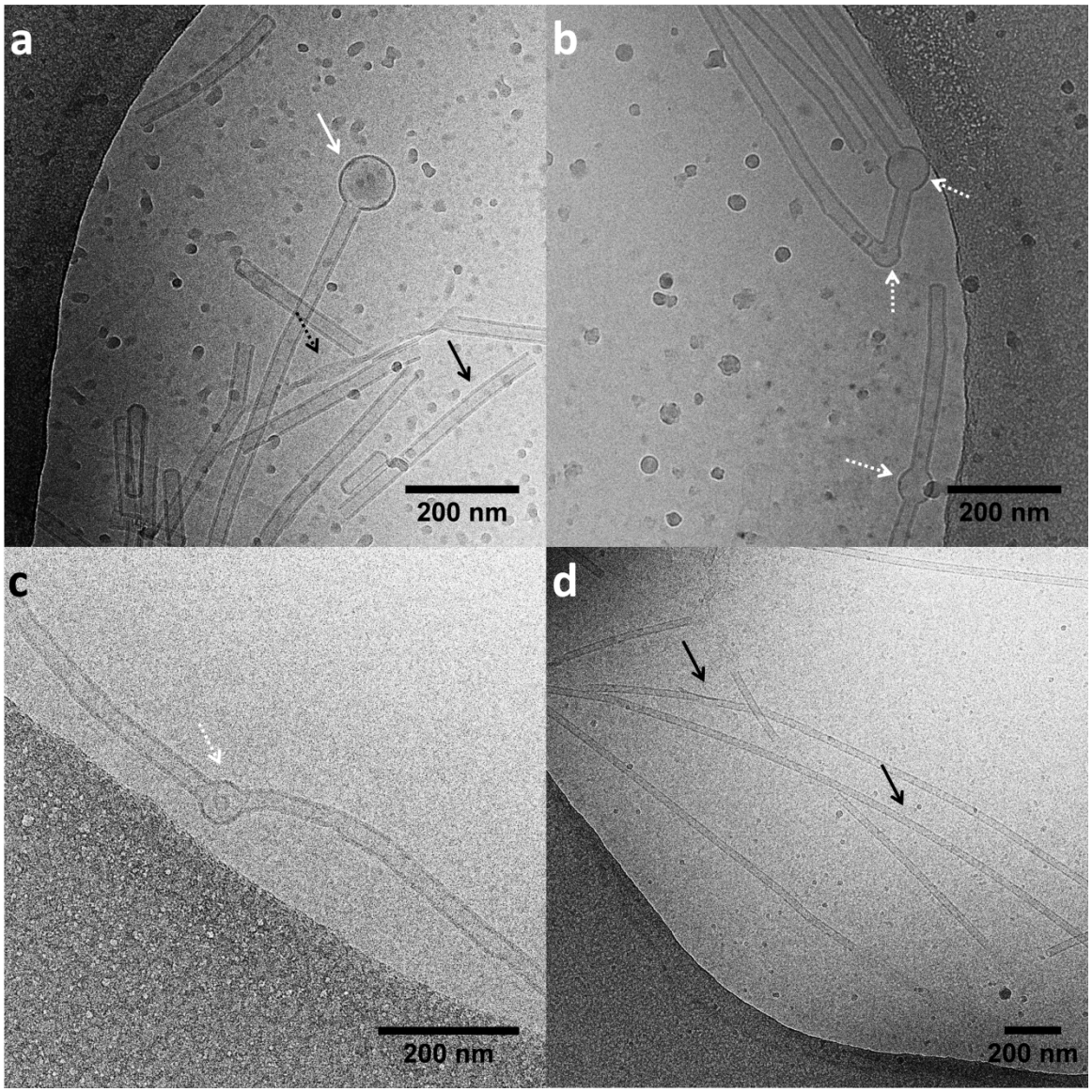

Figure 7.2.4: Cryo-TEM images of a sample of **2a** which was stored for approx. 6 h at room temperature before it was measured at room temperature showing (end-capped) tubes (a, b) and twisted ribbons (a). Cryo-TEM images of a sample of **2a** which was heated for 2 h at 70 °C before it was measured at room temperature showing tubes (c, d). Black arrow indicates tubes, white arrow indicates end-capping, white dashed arrow indicates tubes connected *via* vesicles and black dashed arrow indicates twisted ribbons. All samples were prepared in 20 mM aq. TRIS buffer (pH 8.5) at rt with a final amphiphile concentration of 3 mg/ mL.

The results presented in Figure 7.2.4 demonstrate clearly a time- and temperature-dependent aggregation behavior for the amphiphile **2a**. While at an early stage of aggregation vesicles are mainly formed by **2a** (Figure 7.2.5a), these aggregates could not be observed after storage at room temperature or incubation at higher temperature (Figure 7.2.5c). Based on this study, we assume that reorganization of aggregates takes place resulting in the formation of tubes dependent on time and/or temperature (Figure 7.2.5.d).

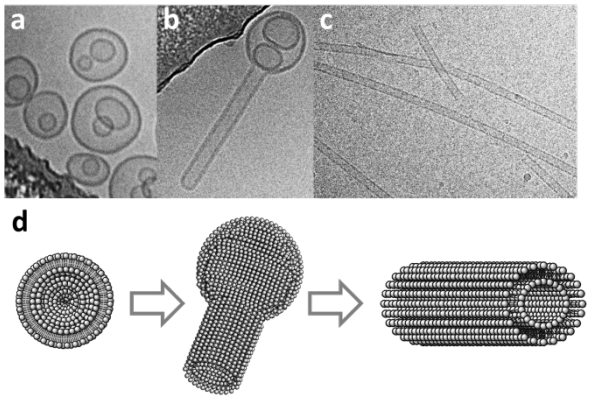

Figure 7.2.5: Cryo-TEM images of a sample of **2a** showing vesicle (a), end-capped tubes (b) and tubes (c). Schematic representation of aggregation change for amphiphile **2a** dependent on time and temperature (d).

Finally, it needs to be emphasized that *N*-phosphoamides **2a** and **2b** exhibiting a dipeptide moiety do not form open vesicles as observed for the corresponding *N*-phosphoamino acid **1c** carrying a single amino acids, i.e. β-alanine (Chapter 6, Figure 6.2.4). This observation supports the in Chapter 6.2.2 discussed self-activation mechanism of *N*-phosphoamino acids **1c** by the carboxylic acid functionality of the amino acids attached to the phosphate group. Hence, it can be concluded that the presence of an additional amino acids as given in **2a-c** prevents the self-activation and formation of open vesicles.

7.2.4 Switching Behavior of Azobenzene-Containing *N*-Phosphoamides

Ultra**v**iolet-**vis**ible (UV/Vis) spectroscopy was employed to study the light induced *cis-trans*-isomerization of the synthesized *N*-phosphoamide methyl esters **16** and **18** as well as the corresponding acid **4** and **19** carrying a azobenzene switch (Figure 7.2.6).

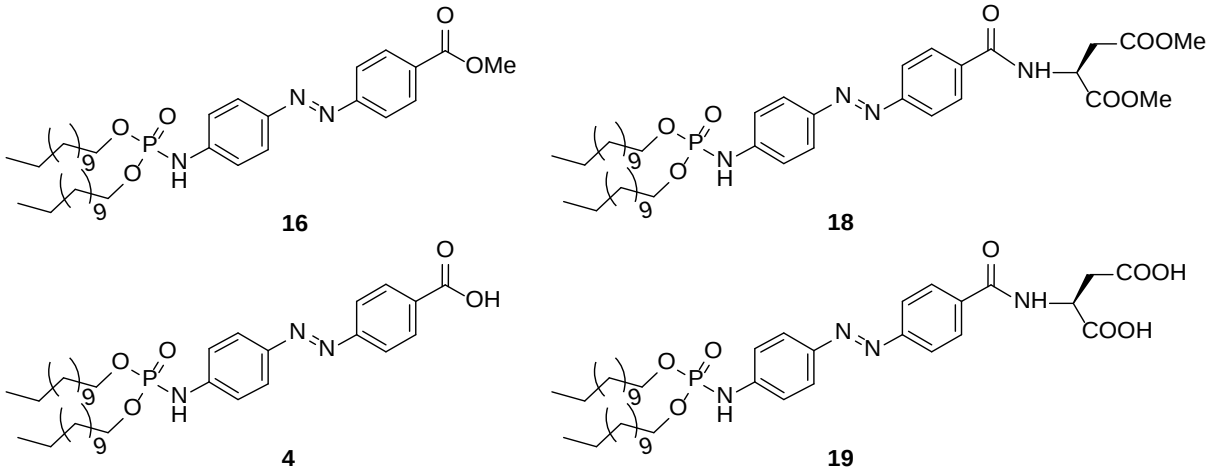

Figure 7.2.6: Molecular structure of *N*-phosphoamide methyl esters **16** and **18** and the corresponding acid **4** and **19**.

In general, two absorption bands are characteristic for azobenzene switches dependent on their configuration.[17,21] As shown in Figure 7.2.7 the bands at approx. 440 nm (n-π*) and 280 nm (π-π*) are distinct for *cis*-azobenzene, while the band at approx. 320 nm corresponds to the *trans*-isomer (π-π*). The wavelength of the adsorption maxima can be influenced by the polarity of the solvent, the molecular structure and the ratio of both isomers in the mixture. Therefore, the surrounding medium (solvents and additives) as well as the molecular structure (residues and ionization) can lead to a shift of the described bands.

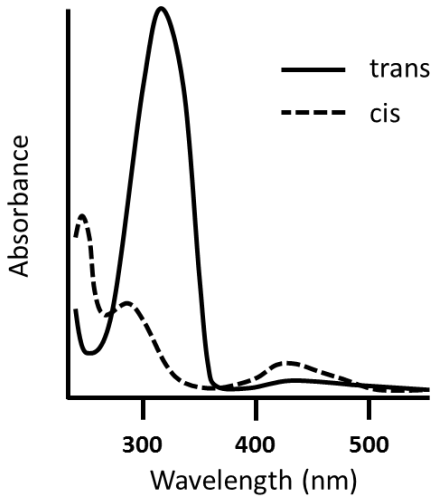

Figure 7.2.7: Adsorption spectra of *cis*- and *trans*-azobenzene in ethanol.[21]

Cis-trans isomerization can be induced by irradiation resulting in *cis-trans* switching or *trans-cis* switching depending on the wavelength used (Figure 7.2.8). However, it needs to be emphasized that photo-induced isomerization results always in a mixture of *trans*- and *cis*-isomers, known as the **p**hoto-**s**tationary **s**tate (PSS). Thereby, the ratio between *cis*- and *trans*-isomer in the PSS is specific for each azobenzene derivative. However, thermal induced isomerization of the *cis*-isomer can result in 100% *trans*-isomer.

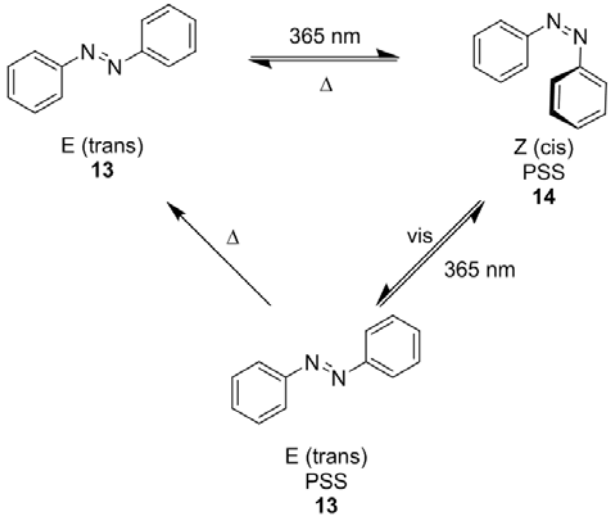

Figure 7.2.8: Photochemical - and thermal-induced *cis-trans* isomerization.

In Figure 7.2.9, representative UV-spectra are shown for amphiphile **19** as non-irradiated *trans*-isomer (100%) as well as in *cis*- and *trans*-isomer in the corresponding photo stationary state.

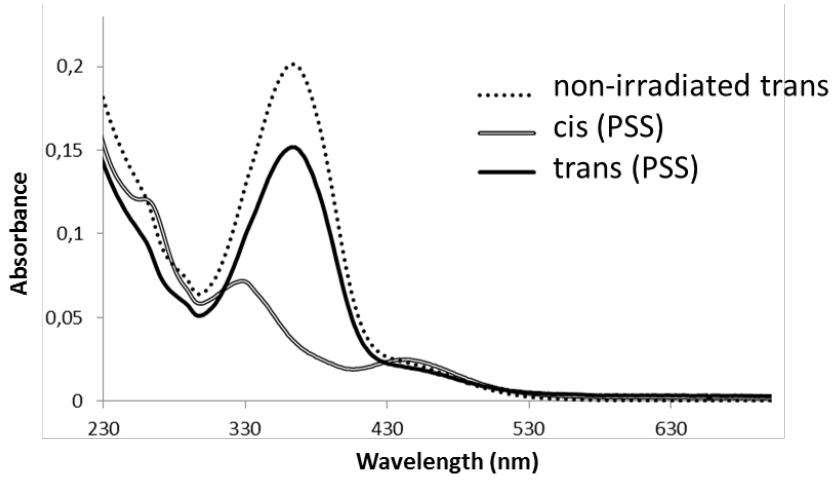

Figure 7.2.9: Adsorption spectra of **19** before and after irradiation with UV (365 nm) and visible light.

The UV/Vis spectra of *N*-phosphoamides **16**, **4**, **18** and **19** were taken in methanol at room temperature using a concentration of 10 µM. As shown in Table 7.2.3 the absorption maximum for the π-π* band of the *trans*-isomer is between 363 nm and 367 nm.

Table 7.2.3: Absorption maxima for the *trans*- and *cis*-isomers in **p**hoto-**s**tationary **s**tate (PSS).

	π-π* ***trans*** **(nm)**	**π-π*** ***cis*** **(nm)**	**n-π*** ***cis*** **(nm)**	**irradiation time (sec)**
18	365	314	458	30
19	363	313	458	30
16	367	337	440	40
4	363	327	442	40

All spectra were taken at room temperature and in methanol. The sample concentration was 10 µM. Irradiation was performed using UV-light with a wavelength of 365 nm.

Based on the average value of the π-π* band of the *trans*-isomers of compounds **16**, **4**, **18** and **19**, we chose UV-light with a wavelength of 365 nm for isomerization studies and the determination of the half life time of the switches. To determine the half life time of all synthesized azobenzene switches of **16**, **4**, **18** and **19**, all samples were irradiated for 2 min with UV-light (365 nm) resulting in *cis*-PSS. Then, the subsequent thermal induced isomerization from *cis*-isomer (PSS) to the thermodynamically favored *trans*-isomer was studied by time-dependent UV-Vis spectroscopy. Representatively, the time-dependent absorbance at 365 nm (π-π*) of amphiphile **19** is given over two and half hours in Figure 7.2.10 demonstrating a half-life time of 21.5 min.

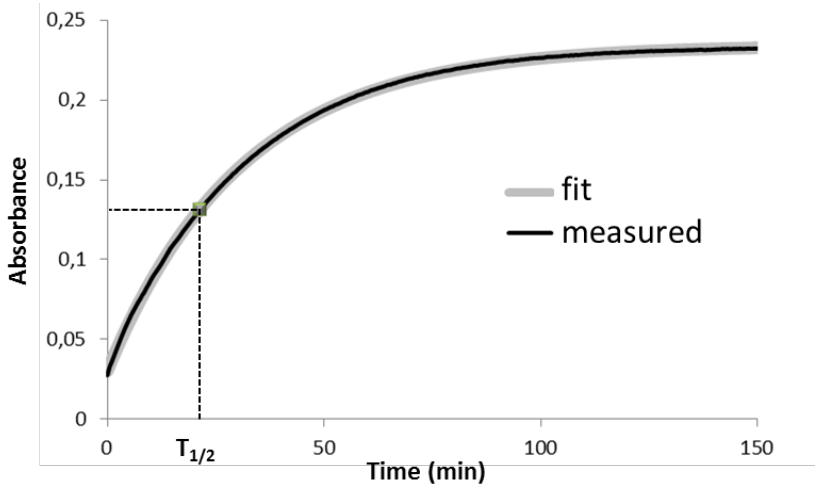

Figure 7.2.10: Adsorption of AA-OH at 365 nm. Recorded at 20 °C over 2.5 hours. Measurements were taken every 30 seconds.

Also, in Table 7.2.4 the half-life times are shown for all switches, i.e. methyl esters **16** and **18** as well as the corresponding free carboxylic acids **4** and **19**, ranging between 21.5 and 88 min (Table 7.2.4).

Table 7.2.4: Half-life time for switches **16**, **4**, **18** and **19.**

	$T_{1/2}$ (min)	R^2
18	78	0.9996
19	21.5	0.9999
16†	45	0,9998
4*	88	0.9998

The half-life time ($t_{1/2}$) was determined at room temperature in methanol with a concentration of 10 µM. The measurement was performed under the exclusion of light and the absorption was recorded every 30 seconds over 2.5, 3(†) or 8(*) h. R^2 is the coefficient of determination.

Additionally to the temperature-dependent studies, we performed light induced *cis-trans* isomerization. Thereby, the samples were irradiated alternately eight times with UV-light (365 nm, π-π*) for isomerization from *trans*-PSS to *cis*-PSS and visible light for isomerization from *cis*-PSS to *trans*-PSS. An example for this light induced isomerization experiment is shown for amphiphile **19** in Figure 7.2.11. This experiment shows clearly that compound **19** can switch reversible by irradiation without decomposing employing eight irradiation cycles, since no decrease in absorption was detected.

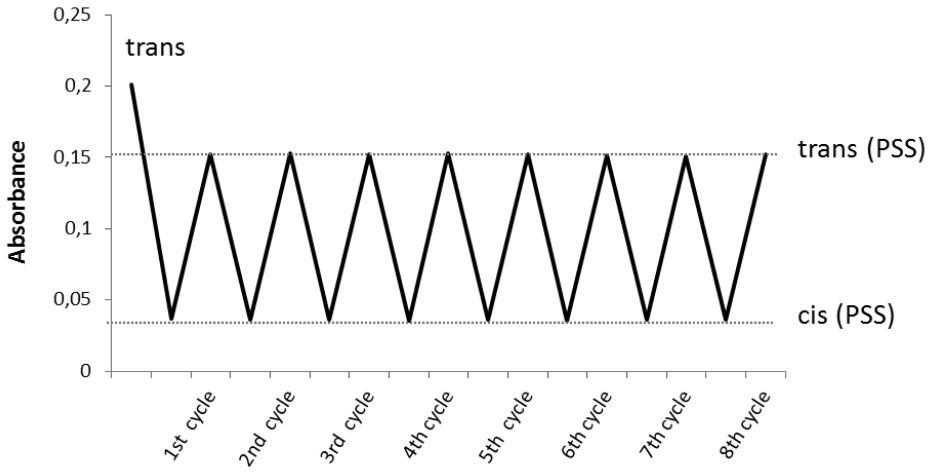

Figure 7.2.11: Absorption at 363 nm of a 10 µM solution of **19** in methanol. Eight isomerization cycles showing no degradation of the sample. Both isomerization's are light induced.

The above described experiment for **19** was performed also for compounds **16**, **4** and **18** demonstrating the ability for photo-induced reversible *cis-trans* isomerization. Summarized, in table 7.2.5, the absorptions of all compounds are given for the corresponding non-irradiated *trans*-isomers as well as in their *trans*- and *cis*-photo stationary state. Hereby, compounds **16**, **4** and **18** behave similar to amphiphile **19** showing the ability for reversible switching without giving any indication for their decomposition (see experimental part Figure 7.4.1).

Table 7.2.5: Absorption for azobenzene switches **4**, **16**, **18** and **19** before and after irradiation.

	Absorbance *trans*†	**Irradiation time 365 nm (sec)**	**Absorbance *cis*-PSS††**	**Irradiation time vis (sec)**	**Absorbance *trans*-PSS††**
18	0.235	30	0.0316 ($2.1*10^{-4}$)	30	0.155 ($3.9*10^{-5}$)
19	0.202	30	0.0344 ($1.7*10^{-4}$)	30	0.152 ($2.7*10^{-4}$)
16*	0.208	40	0.0232 ($3.4*10^{-4}$)	20	0.169 ($6.9*10^{-4}$)
4**	0.441	40	0.0647 ($7.9*10^{-5}$)	20	0.326 ($8.3*10^{-4}$)

The absorption was measured at 365 nm if not otherwise stated. *Absorption was measured at 367 nm. **Absorption was measured of a 20 µM solution in methanol at 363 nm. †Measured adsorption before irradiation. ††All given data are the average of eight irradiation cycles. Standard deviation is given in clamps.

7.3 Conclusion

In conclusion, we successfully employed the newly introduced amphiphilic *N*-phosphoamino acids for further modification to demonstrate their facile modulation for their potential optimization as drug delivery systems. First, we established two synthetic strategies giving access to a broad variety of derivatives in only two synthetic steps using *N*-phosphoamino acids or their precursor, i.e. *N*-didodecyl phosphoryl chloride, as starting materials. On the one hand, using the latter hydrophobic compound two amphiphiles and their corresponding methyl esters were obtained exhibiting an azobenzene moiety at the head group. On the other hand, employing *N*-phosphoamino acids as starting material three amphiphiles and their corresponding methyl esters were successfully synthesized with a dipeptidylic head group. In toxicity studies it was demonstrated that all obtained *N*-phosphoamide derivatives exhibit very good biocompability with IC_{50} up to 100 μM.
Furthermore, using cryo-TEM we revealed that *N*-phosphoamides with a dipeptide head group can form a broad variety of aggregates, i.e. vesicles, twisted ribbons, open and end-capped tubes. In contrast to the *N*-phosphoamino acids exhibiting one amino acid at the head group (Chapter 6), neither decomposing nor formation of open vesicles were observed for amphiphiles with a dipeptidylic head group. Hence, we can conclude that a simple modification at the free acid group of *N*-phosphoamino acids leads to higher stability of liposomes formed by these amphiphiles.
Finally, in this chapter the *N*-phosphoamides exhibiting an azobenze moiety were tested for their ability to act as molecular switches. We demonstrated that all synthesized azobenzene derivatives can still undergo a thermal and photo-induced reversible *cis-trans* isomerization in methanol and in this regard the half-life time of their *cis*-isomers was determined. Moreover, it was shown that several photo-induced isomerization cycles can be performed without decomposition of the synthesized molecular switches. However, no studies considering the aggregation and switching behavior of *N*-phosphoamide **19** could be performed. Further chemical modifications are necessary to increase the hydrophobicity of these compounds resulting in higher solubility.

7.4 Experimental Section

7.4.1 Materials and Methods

All chemicals and reagents were purchased from commercial suppliers (*Acros* and *Sigma-Aldrich*) and used without further purification. Dry solvents were taken from an *MBraun* solvent purification system (SPS-800). Thin layer chromatographic (TLC) analysis was performed on Merck silicagel 60/Kieselguhr F254, 0.25 mm TLC plates and visualized by UV and staining with *Seebach's* reagent. Column chromatography was performed using silica gel (P60, 230 – 400 mesh).
^{1}H-NMR-, ^{13}C-NMR-, ^{31}P-NMR-, **a**ttached **p**roton **t**est- (APT), **h**eteronuclear **s**ingle-**q**uantum **c**orrelation- (HSQC) spectra, **N**uclear ***O****verhauser* **e**ffect **s**pectroscop**y** (NOESY) and **co**rrelation **s**pectroscop**y** (COSY) were recorded on a *Agilent 400* (400 MHz for ^{1}H-NMR, 100.59 MHz for ^{13}C-NMR) using $CDCl_3$ ($CDCl_3$: δ 7.26 for ^{1}H-NMR, δ 77.16 for ^{13}C-NMR). Data are reported as follows: chemical shifts, multiplicity (s= singlet, d= doublet, t= triplet, q= quartet, br= broad, m= multiplet). Coupling constants *J* (Hz) and integration.
High resolution mass spectrometry (HRMS) was carried out on a LTQ ORBITRAP XL spectrometer (*Thermo Scientific*) employing **e**lectro**s**pray **i**onization (ESI) in positive ion mode (EI+) and negative ion mode (EI-).
Cryo TEM images were taken on an FEI Tecnai T20 transmission electron microscope and on an Philips CM12 cryo transmission electron microscope operating at 200 and 120 kev, respectively. Images were recorded on a slowscan CCD camera under low-dose conditions.
Transition temperatures were measured on a DSC7 *Perkin Elmer* spectrometer with a heating rate of 5 °C/min.
UV/Vis spectra were taken with a *Agilent* 8453 UV-Vis spectrophotometer in UVasol® solvent (*Merck*).

Cryo-TEM

Sample preparation: After dissolving *N*-phosphoamino acid in chloroform the solvent was carefully evaporated under a slow stream of nitrogen and continuous rotation. The resulting thin film was stored for 30 min under high vacuum to assure the complete removal of organic solvents. Afterwards a aqueous buffered solution was added to an final concentration of 3 mg/ mL. The resulting sample was vortexed to obtain a homogenous suspension. Finally three freeze-thaw cycles were performed to enable aggregate formation. The resulting turbid solution was used for cryo-TEM measurements.
Buffer preparation:
pH 8.5 (20 mM TRIS buffer): 1.21 g of tris(hydroxymethyl)aminomethane was dissolved in 500 mL water and the pH was adjusted by adding 1M aqueous HCl solution. Next water was added to obtain a total volume of 500 mL.

7.4.2 Cytotoxic Assay

Cytotoxic assay: MTT assay

DMEM: Commercial available Dulbecco's Modified Eagle's Medium (DMEM) was supplemented with 10% fetal calf serum, penicillin (100 units/ mL), streptomycin (100 µg/ mL) and L-glutamine (2mM).
Sample preparation: The sample was prepared according to the procedure for cryo-TEM to ensure the aggregate formation. Instead of a buffered aqueous solution DMEM was used for the stock solution. All concentrations were obtained diluting a fresh prepared 3 mM stock solution with DMEM.
Cell line: HeLa cells were grown in DMEM and cultured at 37 °C, 5% CO_2 and 95% relative humidity.
MTT assay: HeLa cells were dispensed in a sterile 96-well plate at a cell density of 10000 cells/well and were incubated for 8 h at 37 °C, 5% CO_2 and 95% relative humidity. Afterwards, the *N*-phosphoamino acid solution was added to the cells at various concentrations and was incubated for 16 h. Then MTT was added to a final concentration of 0.5 mg/ mL in each well and the resulting solution was incubated for additional 4 h. Finally, all medium was removed and 100 µL of DMSO was added to dissolve the created formazane. The absorbance of the DMSO solution was measured at 570 nm using a microplate reader (SynergyMX, BioTek). Cell survival was expressed as a relative viability of cells compared to control cultures that were incubated with medium only.

Table 7.3.1: MTT assay

	25 mM*	**50 mM***	**100 mM***
2a		71.44 (5.8)	50.25 (5.62)
2b		106.71 (10.96)	45.99 (13.33)
2c		97.22 (12.63)	59.17 (5.58)

Cell survival given in % compared to control samples that were incubated only with DMEM. All given data are the average of three separate experiments. Standard deviation is given between brackets. *Final concentration during the 16 h of incubation.

7.4.3 UV/Vis Spectroscopy

Amphiphiles **4**, **16**, **18** and **19** were dissolves in methanol (UVasol®) resulting in a 10 µM (20 µM for compound **4**) solutions. Eight reversible *cis-trans* isomerization cycles were performed using UV- (365 nm) and visible light (Figure 7.4.1). Absorbance was measured at 365 nm (**18**, **19**), 367 nm (**16**) and 363 nm (**4**).

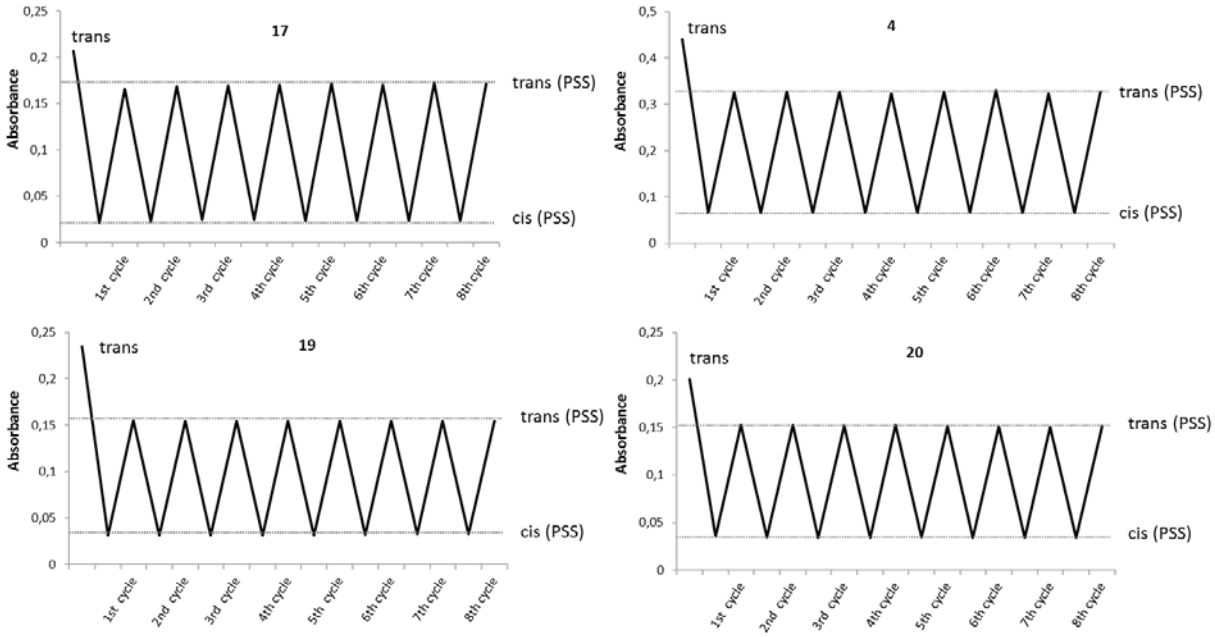

Figure 7.4.1: Absorption the azobenzene switches **4**, **16**, **18** and **19** in methanol. Eight isomerization cycles showing no degradation of the sample. Both isomerizations are light induced.

7.4.4 General Procedures

Hydroxybenzotriazole (HOBt) based peptide coupling

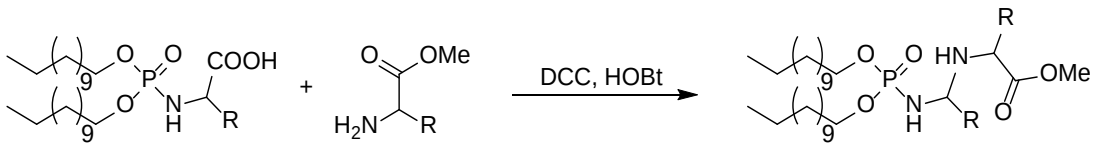

A catalytic amount of 4-Dimethylaminopyridine (DMAP) was added to an icecooled suspension of a carboxylic acid (1.5 equiv) and HOBt (2.2 equiv) in dry THF (4 mL/ mmol). Followed by a solution of *N,N'*-Dicyclohexylcarbodiimide (DCC, 2.2 equiv) in $CHCl_3$ (4 mL/ mmol). The reaction mixture was stirred for 30 min at room temperature before a methylated amino acid hydrochloride (1 equiv) solution in $CHCl_3$ (5.7 mL/ mmol) was added in one portion. Subsequently K_2CO_3 (1 equiv) was added and the mixture was allowed to stir

for additional 16 h at room temperature. After completion of the reaction the resulting solution was diluted with $CHCl_3$ and three times washed with aq. HCL (1 M), $NaHCO_3$ (0.5 M) and brine respectively. Drying of the organic phase with $MgSO_4$ and rotary evaporation of the solvent led to the crude product which was further purified by column chromatography ($CHCl_3$/MeOH 9:1).

Hydrolysis of the methyl ester

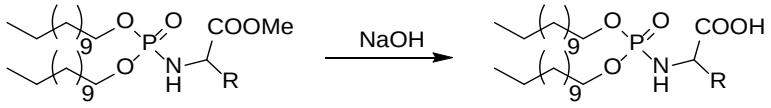

A 1 M aqueous solution of NaOH (1 mL/ mmol) was added to a solution of a methyl ester (1 equiv) in EtOH (1 mL/ mmol) and stirred 2 h at room temperature. Water (10 mL/ mmol) was added and the resulting solution acidified by using a 3 M aqueous solution of HCl. The acidic solution with pH 1 was extracted three times with CH_2Cl_2 and the combined organic extracts were dried with $MgSO_4$. Rotary evaporation of the solvent led to the product. No further purification was necessary.

7.4.5 Synthesis and Characterization

(L)-methyl 2-(3-((bis(dodecyloxy)phosphoryl)amino)propanamido)-3-(1*H*-imidazol-5-yl) propanoate (9a). 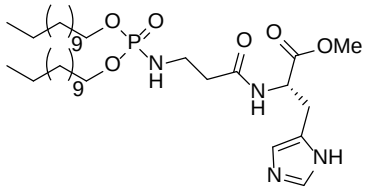
The title compound was prepared according to the general procedure described above (5.4.2.1) using **1c** and (L)-histidine methyl ester dihydrochloride. **9a** was obtained as colourless solid with an isolated yield of 51%. ^{1}H-NMR ($CDCl_3$, 400 MHz): δ (ppm) = 7.5 (s, 1H); 7.33 (d, J= 7.6 Hz, 1H); 6.75 (s, 1H); 4.79 (dt, J= 7.2 Hz, J= 5.2 Hz, 1H); 4.28 (br, 1H); 3.92 (t, J= 6.8 Hz, 4H); 3.68 (s, 3H); 3.18 (m, 2H); 3.09 (t, J= 7.6 Hz, 2H); 2.4 (t, J= 5.2 Hz, 2H); 1.63 (t, J=7.2 Hz, 4H); 1.23 (br, 36H); 0.86 (t, J= 6.8 Hz, 6H). ^{13}C-NMR ($CDCl_3$, 100 MHz): δ (ppm) = 172.54 (1C, CO); 172.08 (1C,CO); 135.86 (1C, CH); 134.16 (1C, C); 116.4 (1C, CH); 66.68 (2C, CH_2); 52.88 (1C, CH); 52.4 (1C, CH_3); 38.15 (1C, CH_2); 38.03 (1C, CH_2); 31.81 (2C, CH_2); 30.27 (d, J= 7, 2C, CH_2); 29.45 (2C, CH_2); 29.52 (2C, CH_2); 29.49 (2C, CH_2); 29.44 (2C, CH_2), 29.33 (2C, CH_2); 29.12 (2C, CH_2); 28.77 (1C, CH_2); 25.47 (2C, CH_2); 22.53 (2C, CH_2), 13.91 (2C, CH_3). ^{31}P-NMR ($CDCl_3$, 162 MHz): δ(ppm) = 9.21. MS (EI+) (*m/z*): found 657.472 $[M+H]^+$, calculated 657.472 $[M+H]^+$.

(L)-ethyl 2-(3-((bis(dodecyloxy)phosphoryl)amino)propanamido)-3-(1*H*-indol-3-yl) propanoate (9b). 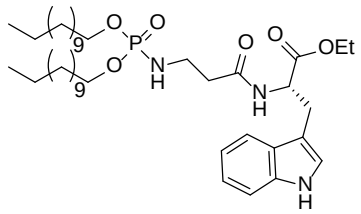 The title compound was prepared according to the general procedure described above (5.4.2.1) using **1c** and (L)-tryptophan ethyl ester hydrochloride. **9b** was obtained as light pink solid with an isolated yield of 63%. ^{1}H-NMR ($CDCl_3$, 400 MHz): δ(ppm) = 8.53 (s, 1H); 7.53 (d, J=7.6 Hz, 1H); 7.35 (d, J= 8 Hz, 1H); 7.18 (t, J= 7.6 Hz, 1H); 7.10 (t, J= 7.2 Hz, 1H); 7.02 (s, 1H); 6.12 (d, J= 7.6 Hz, 1H); 4.91 (q, J= 8 Hz, 1H); 4.16 (m, 2H); 3.92 (m, 4H); 3.29 (m, 2H); 3.22 (m, 1H); 3.13 (m, 2H); 2.31 (t, J= 5.6 Hz, 2H); 1.61 (t, J= 6.8 Hz, 4H); 1.25 (br, 39H); 0.88 (t, J= 6.8 Hz, 6H). ^{13}C-NMR ($CDCl_3$, 100 MHz): δ (ppm) = 172.23 (1C, CO); 171.21 (1C,CO); 136.28 (1C, C); 127.75 (1C, C); 123.1 (1C,CH); 122.3 (1C, CH); 119.71 (1C, CH); 118.52 (1C, CH); 111.52 (1C, CH); 110 (1C, C); 66.70 (d, J= 4.6 Hz, 1C, CH_2); 66,48 (d, J= 4.6 Hz, 1C, CH_2); 61.74 (1C, CH_2); 53.03 (1C, CH); 37.86 (d, J= 5.6 Hz, 1C, CH_2); 37.79 (1C, CH_2); 32.06 (2C, CH_2); 30.54 (d, J= 6.9 Hz, 1C, CH_2); 30.47 (d, J= 7 Hz, 1C, CH_2); 29.8 (2C, CH_2); 29.78 (2C, CH_2); 29.74 (2C, CH_2); 29.7 (2C, CH_2), 29.49 (2C, CH_2); 29.37 (2C, CH_2); 27.76 (1C, CH_2); 25.72 (2C, CH_2); 22.83 (2C, CH_2), 14.25 (3C, CH_3). ^{31}P-NMR ($CDCl_3$, 162 MHz): δ(ppm) = 9.11. MS (EI+) (*m/z)*: found 720.50695 $[M+H]^+$, calculated 720.50750 $[M+H]^+$.

(L)-methyl 2-((L)-1-(bis(dodecyloxy)phosphoryl)pyrrolidine-2-carboxamido)-3-(1*H*-imidazol-5-yl)propanoate (9c). 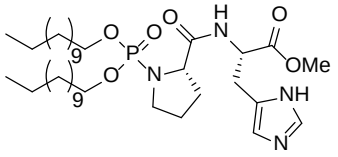 The title compound was prepared according to the general procedure described above (5.4.2.1) using **1h** and (L)-histidine methyl ester dihydrochloride. **9c** was obtained as colourless solid with an isolated yield of 63%. ^{1}H-NMR ($CDCl_3$, 400 MHz): δ (ppm) = 7.43 (s, 1H); 7.33 (s, 1H); 6.65 (s, 1H); 4.71 (m, 1H); 4.28 (br, 1H); 4.06 (m, 1H); 3.93 (m, 4H); 3.62 (s, 3H); 3.16 (m, 2H); 3.09 (m, 2H); 2 (m, 2H); 1.9 (m, 1H); 1.76 (m, 1H); 1.56 (m, 4H); 1.17 (br, 36H); 0.78 (t, J= 7.2, 6H). ^{13}C-NMR ($CDCl_3$, 100 MHz): δ (ppm) = 173.72 (1C, CO); 171.52 (1C, CO); 135.96 (1C, CH); 128.67 (1C, C); 122.29 (1C, CH); 66.68 (d, J= 5.8 Hz, 1C, CH_2); 66.56 (d, J= 5.6 Hz, 1C, CH_2); 61.68 (d, J= 4.7 Hz, 1C, CH); 52.81 (1C, CH); 52.2 (1C, CH_3); 47.22 (d, J= 3.3 Hz, 1C, CH_2); 31.63 (2C, CH_2); 30.95 (d, J= 8.4 Hz, 1C, CH_2); 30.05 (d, J= 6.5 Hz, 1C, CH_2); 29.99 (d, J= 6.8, 1C, CH_2); 29.35 (4C, CH_2); 29.28 (2C, CH_2); 29.25 (2C, CH_2); 29.05 (2C, CH_2), 28.91 (2C, CH_2); 27.7 (1C, CH_2); 25.44 (d, J= 4.6 Hz, 1C, CH_2); 25.32 (1C, CH_2); 25.24 (1C, CH_2); 22.35 (2C, CH_2), 13.72 (2C, CH_3). ^{31}P-NMR ($CDCl_3$, 162 MHz): δ (ppm) = 6.3. MS (EI+) (*m/z)*: found 683.485 $[M+H]^+$, calculated 683.487 $[M+H]^+$.

(L)-2-(3-((bis(dodecyloxy)phosphoryl)amino)propanamido)-3-(1*H*-imidazol-5-yl) propanoic acid (2a). 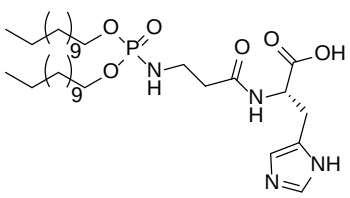 The title compound was prepared according to the general procedure described above (5.4.2.2) using **9a**. **2a** was obtained as colourless solid with an isolated yield of 69%. ^{1}H-NMR ($CDCl_3$, 400 MHz): δ (ppm) = 14.2 (s, 1H); 13.86 (s, 1H); 8.6 (s, 1H); 8.22 (s, 1H); 7.27 (s, 1H); 4.9 (m, 1H); 4.3 (br, 1H); 3.96 (t, J= 6.4 Hz, 4H); 3.27 (m, 2H); 3.17 (m, 2H); 2.61 (m, 1H); 2.49 (m, 1H); 1.64

(q, J= 6 Hz, 4H); 1.23 (br, 36H); 0.86 (t, J= 6.8 Hz, 6H). ^{13}C-NMR ($CDCl_3$, 100 MHz): δ (ppm) = 173.81 (1C, CO); 171.84 (1C,CO); 133.73 (1C, CH); 127.96 (1C, C); 110.72 (1C, CH); 67.26 (2C, CH_2); 52.18 (1C, CH); 38.02 (1C, CH_2); 37.38 (1C, CH_2); 31.83 (2C, CH_2); 30.22 (d, J= 6.2 Hz, 2C, CH_2); 29.6 (2C, CH_2); 29.56 (4C, CH_2); 29.50 (2C, CH_2); 29.27 (2C, CH_2), 29.19 (2C, CH_2); 26.73 (1C, CH_2); 25.50 (2C, CH_2); 22.54 (2C, CH_2), 13.92 (2C, CH_3). ^{31}P-NMR ($CDCl_3$, 162 MHz): δ (ppm) = 8.72. MS (EI+) (*m/z*): found 643.456 $[M+H]^+$, calculated 643.456 $[M+H]^+$.

(L)-2-(3-((bis(dodecyloxy)phosphoryl)amino)propanamido)-3-(1*H*-indol-3-yl)propanoic acid (2b). 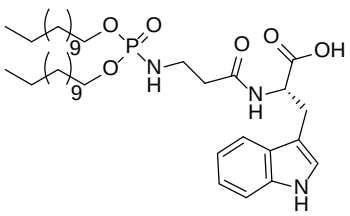
The title compound was prepared according to the general procedure described above (5.4.2.2) using **9b**. **2b** was obtained as pink solid with an isolated yield of 70%. ^{1}H-NMR ($CDCl_3$, 400 MHz): δ (ppm) = 8.43 (br, 1H); 7.56 (d, J=7.2 Hz, 1H); 7.21 (d, J= 8 Hz, 1H); 7.09 (t, J= 8.4 Hz, 2H); 6.94 (s, 1H); 4.86 (s, 1H); 3.86 (m, 4H); 3.29 (m, 2H); 3.07 (m, 1H); 2.98 (m, 1H); 2.22 (m, 2H); 1.55 (m, 4H); 1.24 (br, 36H); 0.87 (t, J= 6.4 Hz, 6H). ^{13}C-NMR ($CDCl_3$, 100 MHz): δ (ppm) = 174.85 (1C, CO); 172.68 (1C,CO); 136.37 (1C, C); 128.36 (1C, C); 123.95 (1C, CH); 122.2 (1C, CH); 119.75 (1C, CH); 118.87 (1C, CH); 111.75 (1C, CH); 109.79 (1C, C); 67.15 (d, J= 5.7 Hz, 2C, CH_2); 53.40 (1C, CH); 37.70 (1C, CH_2); 37.57 (1C, CH_2); 31.82 (2C, CH_2); 30.15 (d, J= 7 Hz, 2C, CH_2); 29.57 (2C, CH_2); 29.54 (2C, CH_2); 29.52 (2C, CH_2); 29.46 (2C, CH_2), 29.25 (2C, CH_2); 29.12 (2C, CH_2); 26.63 (1C, CH_2); 25.42 (2C, CH_2); 22.54 (2C, CH_2), 13.92 (2C, CH_3). ^{31}P-NMR ($CDCl_3$, 162 MHz): δ (ppm) = 8.63. MS (EI+) (*m/z*): found 692.475 $[M+H]^+$, calculated 692.476 $[M+H]^+$.

(L)-2-((L)-1-(bis(dodecyloxy)phosphoryl)pyrrolidine-2-carboxamido)-3-(1*H*-imidazol-5-yl)propanoic acid (2c). 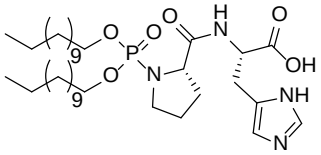
The title compound was prepared according to the general procedure described above (5.4.2.2) using **9c**. **2c** was obtained as colourless solid with an isolated yield of 89%. ^{1}H-NMR ($CDCl_3$, 400 MHz): δ (ppm) = 14.24 (s, 1H); 13.78 (s, 1H); 8.77 (s, 1H); 7.92 (d, J= 6 Hz, 1H); 7.14 (s, 1H); 4.9 (m, 1H); 4.33 (m, 1H); 4.12 (q, J= 6.4 Hz, 4H); 4.02 (q, J= 6.4 Hz, 2H); 3.26 (m, 3H); 3.17 (m, 1H); 2.05 (m, 2H); 1.91 (m, 1H); 1.83 (m, 1H); 1.66 (q, J= 7.2 Hz, 4H); 1.24 (br, 36H); 0.87 (t, J= 6.8 Hz, 6H). ^{13}C-NMR ($CDCl_3$, 100 MHz): δ (ppm) = 174.92 (1C, CO); 172.16 (1C, CO); 134.36 (1C, CH); 128.81 (1C, C); 117.14 (1C, CH); 67.11 (d, J= 5.3 Hz, 1C, CH_2); 67 (d, J= 4.6 Hz, 1C, CH_2); 61.41 (d, J= 8.1 Hz, 1C, CH); 52.6 (1C, CH); 47.26 (1C, CH_2); 31.82 (2C, CH_2); 30.18 (d, J= 7.1 Hz, 1C, CH_2); 30.15 (d, J= 7.5 Hz, 1C, CH_2); 30.07 (d, J= 7.2 Hz, 1C, CH_2); 29.55 (4C, CH_2); 29.49 (2C, CH_2); 29.44 (2C, CH_2); 29.24 (2C, CH_2), 29.14 (2C, CH_2); 26.69 (1C, CH_2); 26.23 (d, J= 8.9 Hz, 1C, CH_2); 25.56 (2C, CH_2); 22.54 (2C, CH_2), 13.92 (2C, CH_3). ^{31}P-NMR ($CDCl_3$, 162 MHz): δ (ppm) = 4.12. MS (EI+) (*m/z*): found 669.470 $[M+H]^+$, calculated 669.471 $[M+H]^+$.

Didodecyl phosphorochloridate (3). To an ice cooled solution of Lauryl alcohol (2.1 equiv) and Et_3N (4 equiv) in dry toluene (6 mL/mmol) was slowly a solution of phosphorus oxychloride (1 equiv) in toluene (1 mL/ mmol) added. After the reaction mixture was slowly warmed up to room temperature it was stirred overnight. The resulting suspension was filtered under suction through Celite® and rinsed with toluene. The combined filtrates were dried ($MgSO_4$) and the solvent was rotary evaporated. The received product was used without further purification (full conversion). ^{1}H-NMR ($CDCl_3$, 400 MHz): δ (ppm) = 4.18 (t, J= 9.6 Hz, 4H); 1.73 (m, 4H); 1.39 (m, 4H); 1.26 (br, 32H); 0.88 (t, J= 6.5 Hz, 6H). ^{13}C-NMR ($CDCl_3$, 100 MHz): δ (ppm) = 69.88 (d, J= 7.3 Hz, 2C, CH_2); 32.04 (2C, CH_2); 29.94 (d, J= 7.8 Hz, 2C, CH_2); 29.75 (4C, CH_2); 29.67 (2C, CH_2); 29.58 (2C, CH_2); 29.47 (2C, CH_2), 29.16 (2C,CH_2); 25.45 (2C, CH_2); 22.81 (2C, CH_2), 14.12 (2C,CH_3). ^{31}P-NMR ($CDCl_3$, 162 MHz): δ (ppm) = 4.8.

(E)-methyl 4-((4-((bis(dodecyloxy)phosphoryl)amino)phenyl)diazenyl)benzoate (16). A solution of didodecyl phosphorochloridate **3** (1 equiv) in dry CH_2Cl_2 (13 mL/ mmol) was cooled to 0 °C and 1.5 equiv of (E)-methyl 4-((4-aminophenyl)diazenyl) benzoate **15** was added in one portion. After addition of 6.5 equiv of triethylamine and a catalytic amount of DMAP the reaction was stirred over night at room temperature. Followed by subsequent addition of 1 equiv didodecyl phosphorochloridate every 24 h over a 5 day period. The mixture was quenched with water and the organic phase was three times extracted by using brine. Drying with $MgSO_4$ and rotary evaporating of the solvent led to the crude product which was further purified by column chromatography (Et_2O/CH_2Cl_2 8:2). **16** was obtained as orange solid with a isolated yield of 61%. ^{1}H-NMR ($CDCl_3$, 400 MHz): δ (ppm) = 8.18 (d, J= 8.4 Hz, 2H); 7.9 (d, J= 8.4 Hz, 2H); 7.88 (d, J= 8.8 Hz, 2H); 7.38 (d, J= 9.2 Hz, NH, 1H); 7.15 (d, J= 8.8 Hz, 2H); 4.12 (m, 2H); 4.05 (m, 2H); 3.94 (s, 3H); 1.69 (qi, J= 7.2 Hz, 4H); 1.19 (br, 36H); 0.84 (t, J= 7.2 Hz, 6H). ^{13}C-NMR ($CDCl_3$, 100 MHz): δ (ppm) = 167.23 (1C, CO); 155.92 (1C, C); 147.87 (1C, C); 144.33 (1C, C); 131.61 (1C, C); 130.99 (2C, CH); 125.27 (2C, CH); 122.74 (2C, CH); 117.82 (1C, CH); 117.75 (1C, CH); 67.18 (1C, CH_2); 67.13 (1C, CH_2); 52.27 (1C, CH_3); 31.80 (2C, CH_2); 30.12 (1C, CH_2); 30.05 (1C, CH_2); 29.55 (2C, CH_2); 29.53 (2C, CH_2); 29.46 (2C, CH_2); 29.41 (2C, CH_2); 29.23 (2C, CH_2), 28.99 (2C,CH_2); 25.41 (2C, CH_2); 22.52 (2C, CH_2), 13.9 (2C,CH_3). ^{31}P-NMR ($CDCl_3$, 162 MHz): δ (ppm) = 1.53. MS (EI+) (*m/z*): found 672.450 $[M+H]^+$, calculated 672.451 $[M+H]^+$.

(E)-4-((4-((bis(dodecyloxy)phosphoryl)amino)phenyl)diazenyl)benzoic acid (4). The title compound was prepared according to the general procedure described above (5.4.2.2) using **16**. **4** was obtained as orange solid with an isolated yield of 63%. ^{1}H-NMR ($CDCl_3$, 400 MHz): δ (ppm) = 8.28 (d, J=7.6 Hz, 2H); 7.96 (d, J= 7.2 Hz, 2H); 7.94 (d, J= 7.2 Hz, 2H); 7.34 (d, J= 7.6 Hz, NH, 1H); 7.17 (d, J= 8.4 Hz, 2H); 4.16 (m, 2H); 4.07 (m, 2H); 1.69 (qi, J= 6.8 Hz, 4H); 1.21 (br, 36H); 0.85 (t, J= 6 Hz, 6H). ^{13}C-NMR ($CDCl_3$, 100 MHz): δ (ppm) = 170.56

(1C, CO); 156.27 (1C, C); 148.05 (1C, C); 143.95 (1C, C); 131.61 (2C, CH); 131.36 (1C, C); 125.38 (2C, CH); 122.84 (2C, CH); 117.93 (1C, CH); 117.85 (1C, CH); 67.5 (1C, CH_2); 67.45 (1C, CH_2); 31.82 (2C, CH_2); 30.08 (1C, CH_2); 30.01 (1C, CH_2); 29.55 (2C, CH_2); 29.54 (2C, CH_2); 29.47 (2C, CH_2); 29.41 (2C, CH_2); 29.25 (2C, CH_2), 28.98 (2C,CH_2); 25.38 (2C, CH_2); 22.55 (2C, CH_2), 13.93 (2C,CH_3). ^{31}P-NMR ($CDCl_3$, 162 MHz): δ (ppm) = 1.78. MS (EI+) (*m/z)*: found 658.432 $[M+H]^+$, calculated 658.434 $[M+H]^+$.

(L,E)-dimethyl 2-(4-((4-((bis(dodecyloxy)phosphoryl)amino)phenyl)diazenyl)benzamido) succinate (18). The title compound was prepared according to the general procedure described above (5.4.2.1) using **4** and (L)-aspartic acid dimethyl ester hydrochloride. **18** was obtained as orange solid with an isolated yield of 72%. ^{1}H-NMR ($CDCl_3$, 400 MHz): δ (ppm) = 7.93 (d, J= 2.8 Hz, 4H); 7.89 (d, J= 8.8 Hz, 2H); 7.31 (d, J= 7.2 Hz, NH, 1H); 7.11 (d, J= 8.8 Hz, 2H); 5.08 (dt, J=7.6 Hz, J= 4.4 Hz, 1H); 4.1 (m, 4H); 3.81 (s, 3H); 3.72 (s, 3H); 3.47 (br, NH, 1H); 3.08 (m, 2H); 1.67 (qi, J= 8 Hz, 4H); 1.2 (br, 36H); 0.85 (t, J= 6.8 Hz, 6H). ^{13}C-NMR ($CDCl_3$, 100 MHz): δ (ppm) = 172.43 (1C, CO); 171.86 (1C, CO); 166.89 (1C, CO); 155.28 (1C, C); 147.97 (1C, C); 143.63 (1C, C); 135.14 (1C, C); 128.57 (2C, CH); 125.28 (2C, CH); 123.1 (2C, CH); 117.79 (1C, CH); 117.72 (1C, CH); 67.29 (2C, CH_2); 53.01 (1C, CH_3); 52.15 (1C, CH_3); 48.98 (1C, CH); 33.88 (1C, CH_2); 31.81 (2C, CH_2); 30.13 (1C, CH_2); 30.06 (1C, CH_2); 29.53 (2C, CH_2); 29.51 (2C, CH_2); 29.45 (2C, CH_2); 29.4 (2C, CH_2); 29.23 (2C, CH_2), 28.98 (2C, CH_2); 25.39 (2C, CH_2); 22.54 (2C, CH_2), 13.92 (2C,CH_3). ^{31}P-NMR ($CDCl_3$, 162 MHz): δ (ppm) = 1.32. MS (EI+) (*m/z)*: found 801.490 $[M+H]^+$, calculated 801.494 $[M+H]^+$.

(L,E)-2-(4-((4-((bis(dodecyloxy)phosphoryl)amino)phenyl)diazenyl)benzamido)succinic acid (19). The title compound was prepared according to the general procedure described above (5.4.2.2) using **18**. **19** was obtained as orange solid with an isolated yield of 68%. ^{1}H-NMR ($CDCl_3$, 400 MHz): δ (ppm) = 7.92 (d, J= 7.6 Hz, 2H); 7.88 (d, J= 7.6 Hz, 2H); 7.82 (d, J= 8 Hz, 2H); 7.76 (d, J= 7.6 Hz, NH, 1H); 6.99 (d, J= 7.6 Hz, 2H); 5.27 (br, OH, 2H); 5.1 (m, 1H); 4.02 (m, 4H); 3.39 (br, NH, 1H); 3.13 (m, 2H); 1.56 (m, 4H); 1.15 (br, 36H); 0.79 (m, 6H). ^{13}C-NMR ($CDCl_3$, 100 MHz): δ (ppm) = 176.55 (1C, CO); 175.43 (1C, CO); 167.56 (1C, CO); 155.19 (1C, C); 147.93 (1C, C); 143.62 (1C, C); 135.26 (1C, C); 128.55 (2C, CH); 125.41 (2C, CH); 123.26 (2C, CH); 117.67 (1C, CH); 117.6 (1C, CH); 67.66 (2C, CH_2); 48.88 (1C, CH); 32.65 (1C, CH_2); 31.8 (2C, CH_2); 29.96 (1C, CH_2); 29.89 (1C, CH_2); 29.54 (1C, CH_2); 29.51 (2C, CH_2); 29.48 (1C, CH_2); 29.45 (1C, CH_2); 29.42 (1C, CH_2), 29.39 (1C, CH_2); 29.36 (1C, CH_2); 29.23 (1C, CH_2); 29.21 (1C, CH_2); 28.96 (1C,CH_2); 28.92 (1C, CH_2); 25.34 (1C, CH_2); 25.3 (1C, CH_2); 22.52 (2C, CH_2), 13.91 (2C,CH_3). ^{31}P-NMR ($CDCl_3$, 162 MHz): δ (ppm) = 1.52. MS (EI+) (*m/z)*: found 773.459 $[M+H]^+$, calculated 773.461 $[M+H]^+$.

7.5 References

1) T. S. Levchenko, R. Rammohan, A. N. Lukyanov, K. R. Whiteman, V. P. Torchilin. Liposome clearance in mice: The effect of a separate and combined presence of surface charge and polymer coating. *Int. J. Pharm.*, **240**, 95–102 (2002).
2) L. Nobs, F. Buchegger, R. Gurny, E. Allémann. Current methods for attaching targeting ligands to liposomes and nanoparticles. *J. Pharm. Sci.*, **93** , 1980-1992 (2004).
3) M. Voinea, I. Manduteanu, E. Dragomir, M. Capraru, M. Simionescu. Immunoliposomes directed toward VCAM - 1 interact specifically with activated endothelial cells - a potential tool for specific drug delivery. *Pharm. Res.*, **22**, 1906-1917 (2005).
4) W. I. Gulewitsch, S. Amiradžibi. Über das Carnosin, eine neue organische Base des Fleischextraktes. *Ber. dt. Chem. Ges.*, **33**, 1902-1903 (1900).
5) D. Ackermann, O. Timpe. K. Poller. Über das Anserin, einen neue Bestandteil der Vogelmuskulatur. *Hoppe-Seyler's Z. physiol. Chem.*, **183**, 1-10 (1929).
6) K. G. Crush. Carnosine and related substances in animal tissues. *Comp. Biochem. Phisiol*., **34**, 3-30 (1970).
7) I. P. Kendrick, H. J. Kim, R. C. Harris, C. K. Kim, V. H. Dang, T. Q. Lam, T. T. Bui. J. A. Wise. The effect of 4 weeks β-alanine supplementation and isokinetic training on carnosine concentrations in type I and II human skeletal muscle fibres. *Eur. J. Appl. Physiol*., **106**, 131–138 (2009).
8) S. L. Stvolinsky, M. L. Kukley, D. Dobrota, M. Matejovicova (Vachova), I. Tkac, A. A. Boldyrev. Carnosine: An Endogenous Neuroprotector in the Ischemic Brain *Cell. Mol. Neurobiol*., **19**, 45-56, (1999).
9) O. I. Aruoma, M. J. Laughton, B. Halliwell. Carnosine, homocarnosine and anserine: could they act as antioxidants in vivo? *Biochem. J.*, **264**, 863-869 (1989).
10) P. Johnson, J. S. Fedyna, A. Schindzielorz, C. M. Smith, P. J. Kasvinsky. Regulation of muscle phosphorylase activity by carnosine and anserine. *Biochem. Biophys. Res. Com*., **109**, 769–775 (1982).
11) G. R. Lenz, A. E. Martell. Metal chelates of some sulfur containing amino acids. *Biochem*., **3**, 745−750 (1964).
12) A. Torreggiani, G. Fini, G. Bottura. Effect of transition metal binding on the tautomeric equilibrium of the carnosine imidazolic ring. *J. Mol. Struct.*, **565−566**, 341−346 (2001).
13) L. J. Hobart, I. Seibel, G. S. Yeargans, N. W. Seidler. Anti-crosslinking properties of carnosine: Significance of histidine. *Life Sci*., **75**, 1379−1389 (2004).
14) V. Checchetto, E. Teardo, L. Carraretto, E. Formentin, E. Bergantino, G. M. Giacometti, I. Szabo. Regulation of photosynthesis by ion channels in cyanobacteria and higher plants. *Biophys. Chem*., **182**, 51–57 (2013).
15) M. Zhong, R. Kawaguchi, M. Kassai, H. Sun. Retina, Retinol, Retinal and the Natural History of Vitamin A as a Light Sensor. *Nutrients*, **4**, 2069-2096 (2012).

16) H. Fliegl, A. Köhn, C. Hättig, R. Ahlrichs. Ab initio calculation of the vibrational and electronic spectra of *trans*- and *cis* azobenzene. *J. Am. Chem. Soc.*, **125**, 9821-9827 (2003).
17) E. Merino, M Ribagorda. Control over molecular motion using the *cis–trans* photoisomerization of the azo group. *Beilstein J. Org. Chem.*, **8**, 1071-1090 (2012).
18) T. Imahori, R. Yamaguchi, S. Kurihara. Azobenzene-Tethered Bis(Trityl Alcohol) as a Photoswitchable Cooperative Acid Catalyst for Morita–Baylis–Hillman Reactions. *Chem. Eur. J.*, **18**, 10802-10807 (2012).
19) B. M. Neilson, C. W. Bielawski. Illuminating Photoswitchable Catalysis. *ACS Catal*., **3**, 1874-1885 (2013).
20) K. Ichimura. Photoalignment of Liquid-Crystal Systems. *Chem. Rev*., **100**, 1847–1873 (2000).
21) A. A. Beharry, G. A. Woolley. Azobenzene photoswitches for biomolecules. *Chem. Soc. Rev*., **40**, 4422-4437 (2011).
22) B. Schierling, A.-J. Noël, W. Wende, L. T. Hien, E. Volkov, E. Kubareva, T. Oretskaya, M. Kokkinidis, A. Römpp, B. Spengler, A. Pingoud. Controlling the enzymatic activity of a restriction enzyme by light. *Proc. Natl. Acad. Sci. USA*, **107**, 1361-1366 (2009).
23) A. Polosukhina, J. Litt, I. Tochitsky, J. Nemargut, Y. Sychev, I. De Kouchkovsky, T. Huang, K. Borges, D. Trauner, R. N. Van Gelder, R. H. Kramer. Photochemical Restoration of Visual Responses in Blind Mice. *Neuron*, **75**, 271-282 (2012).
24) J. M. Kuiper, J. B. F. N. Engberts. H-Aggregation of azobenzene-substituted amphiphiles in vesicular membranes. *Langmuir*, **20**, 1152-1160 (2004).
25) Y. Zhao. Rational design of light-controllable polymer micelles. *Chem. Rec*., **7**, 286-294 (2007).
26) J. Y. Wang, Q. F. Wu, J. P. Li, Q. S. Ren, Y. L. Wang, X. M. Liu. Photo-sensitive liposomes: chemistry and application in drug delivery. *Mini. Rev. Med. Chem.*, **10**, 172-181 (2010).
27) J. N. Israelachvili, D. J. Mitchell, B. W. Ninham. Theory of self-assembly of hydrocarbon amphiphiles into micelles and bilayers. *J. Chem. Soc., Faraday Trans. 2*, **72**, 1525-1568 (1976).

Chapter 8

Summary

Samenvatting

Zusammenfassung

8.1 Summary

Amphiphilc molecules, namely fatty acids, are basic building blocks of each living organism. A large structural variety has been observed in nature allowing the survival of the organism in extreme environments. Thereby, specific modifications can enable life not only at high temperature and pressure differences, but also in toxic media. To overcome the limited availability of these molecules and to understand, study and mimic the function of the in nature occurring fatty acids, organic synthesis is an irreplaceable tool. In this thesis various attempts have been made to synthesize cycloalkane-containing fatty acids and to investigate a new lipid system containing only naturally occurring building blocks.

The first part of my thesis shows different synthetic strategies to obtain non-natural and natural fatty acids exhibiting cycloalkane moieties, such as ladderane units (**Chapter II** and **III**) or a *trans*-cyclopropane ring (**Chapter IV**).
Hence, in **chapter II**, inter- and intramolecular [2+2] photochemical cycloadditions were employed as a tool to obtain molecular structures with fused cyclobutane rings, known as ladderane units. First, for the intermolecular photoreaction the starting material, cyclobutene was successfully synthesized in three synthetic steps reaching an overall yield of 41%. In the next step of this study, different cycloalkenes were employed in the photocatalyzed intermolecular reaction with cyclopentenone to obtain a molecule exhibiting three fused cycloalkane rings. It was found that the ratio of both alkene reactants is crucial for the positive outcome of the photo reaction. The application of alkene and alkenone in a ratio of 2 to 1, respectively, resulted in yields between 54% and 62%. Furthermore, employing X-ray crystallography we demonstrated that both photochemical products exhibiting three fused cycloalkane rings have the *exo*-configuration after having transformed them into the corresponding hydrazone **1** and **2** (Figure 8.1).

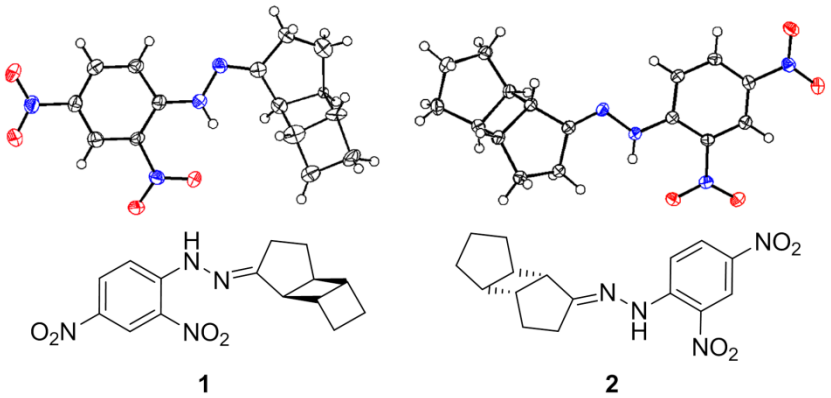

Figure 8.1: Chemical structures of photoproducts **1** and **2** and their corresponding X-ray structures.

In the second part of **chapter II**, we investigated the applicability of the intramolecular cycloaddition using a reusable spacer to obtain ladderane units with three fused cyclobutane rings in only one synthetic step. For this purpose the starting material exhibiting two alkene units and a spacer was synthesized. The spacer, i.e. a pseudo-geminal substituted paracyclophane, was synthesized in nine synthetic steps reaching an overall yield of 50%. Further, the alkene unit exhibiting two conjugated *trans*-double bonds, i.e. 5-phenylpenta-2,4-dienoyl chloride, was obtain in two synthetic steps and attached to the molecular spacer in an amidation reaction yielding the starting material for an intramolecular cycloaddition. First attempts using spacer-alkene constructs for the photochemical reaction resulted most probably in the formation of cyclooctadiene units instead of the desired ladderane units with three cyclobutane rings. Nevertheless, these results suggest that this strategy is applicable for intramolecular cycloadditions and further optimization of the reaction might give access to the desired ladderane unit with three cyclobutane rings.

After the investigation of the inter- and intramolecular cycloaddition in **chapter II**, both photoproducts obtained by the intermolecular photo reaction were successfully employed in **chapter III** as starting materials for the synthesis of fatty acids exhibiting ladderane units. In this regard, two amphiphilic ladderane molecules exhibiting three fused cycloalkane rings have been successfully synthesized employing seven synthetic steps in an overall yield of up to 14.5%. Essential for the success was the optimization of two key steps, i.e. a formylation reaction and a Wittig reaction. Having in mind that ladderane structures allow bacteria to survive in an environment of high temperatures and of a broad range of pH values both obtained ladderane fatty acids will be of use for further studies applying artificial membranes.

While in **chapter III** the work concentrated on the synthesis of fatty acids with fused cycloalkane rings, in **chapter IV** the successful synthesis of the natural product majusculoic acid **3** (Figure 8.2) exhibiting a cyclopropane moiety is demonstrated. In this regard, two total synthesis pathways were identified using cross metathesis and a *Wittig* reaction as key synthetic steps. It needs to be emphasized that majusculoic acid bears synthetically challenging molecular units, which require advanced diastereo- and enantioselective chemistry. Examples are the incorporation of a *trans*-cyclopropane ring and selective introduction of E- and Z- olefins. These exceptional structural features were successfully incorporated in this molecule employing asymmetric catalysis, cross metathesis, a Wittig reaction and double bond isomerization to the more stable isomers. Moreover, the synthesis allowed for the first time the determination of the absolute configuration (*R*,*R*) of the *trans*-cyclopropyl unit of the natural compound.

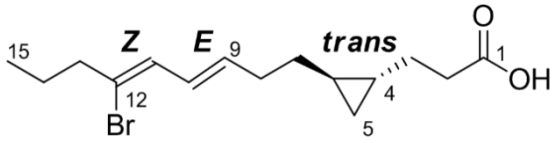

3

Figure 8.2: Chemical structures of the synthesized natural product majusculoic acid **3**.

Having majusculoic acid in hand and having evaluated its total synthesis, this natural product is accessible for future biological studies to allow understanding the mode of action and role of

this compound. It needs to be emphasized that majusculoic acid is of interest to be investigated in more detail, since it shows antifungal activity against *Candida* species. However, biological test were so far restricted due to the limited availability of majusculoic acid.
The second part of my thesis is dealing with the synthesis of a new class of amphiphiles, namely *N*-phosphoamino acids **4** (Figure 8.3), and their application to create artificial membranes for potential drug delivery systems. Thus, in this **chapter V** *N*-phosphoamino acids are introduced as a new class of amphiphiles consisting only of natural building blocks, i.e. amino acids, aliphatic alcohols and phosphonates (Figure 8.3). In this regard, an efficient and fast synthesis was elaborated resulting in 18 new amphiphilic phosphoamidates in just three synthetic steps and isolated overall yields of up to 70%. Also, physical properties of *N*-phosphoamino acids have been studied using nuclear resonance spectroscopy, differential scanning calorimetry and determination of their pK_a-values. Moreover, cryo-TEM was employed to study the aggregation of these amphiphilic compounds. It was found that *N*-phosphoamino acids can form a broad variety of assemblages, such as micelles, vesicles, sheets and ribbons. It was demonstrated that the form of the aggregate is dependent of the size and charge of the amino acid acting as head group of the amphiphile. During this research we successfully showed the relationship between charge, size and shielding effect of the residue of the amino acid on the aggregation of *N*-phosphoamino acids.

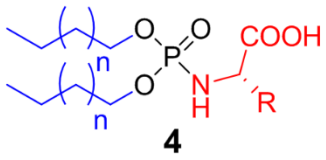

4

Figure 8.3: Chemical structures of amphiphilic *N*-phosphoamino acids **4**. Color code: amino acids (red), aliphatic alcohol (blue) and phosphoric acid (black).

In the next step, the potential applicability of *N*-phosphoamino acids as drug delivery systems was investigated (**Chapter VI**). First, high biocompatibility for these newly introduced amphiphiles was shown by employing MTT (3-(4,5-di**m**ethylt**h**iazol-2-yl)-2,5-diphenyl**t**etrazolium bromide) assays. This experiment revealed high *HeLa* cell viability in presence of *N*-phosphoamino acids carrying aliphatic, aromatic and negatively charged residues at the amino acid head group. It needs to be emphasized that all tested amphiphiles own high biocompatibility using concentrations up to 100 µM allowing full cell viability. The low toxicity of these compounds can be explained by the fact that *N*-phosphoamino acids exhibit only natural occurring building blocks, i.e. amino acid, phosphate and aliphatic alcohol. Also, we demonstrated different potential drug release mechanisms for *N*-phosphoamino acids. The first strategy is based on the protonation of the negatively charged head group of the amphiphile resulting in the loss of the amphiphilic character and the clearance of the liposome under acidic conditions. This behavior suggests a fast drug release during endocytosis. A more interesting release mechanism was observed for *N*-phosphoamino acid carrying small amino acids, i.e. glycine, alanine and beta-alanine, as head group. Employing cryo-TEM and NMR studies it was shown that these *N*-phosphoamino acids degrade by self-activated cleavage of the

amphiphilic tail leading in mono-tailed *N*-phosphoamino acids and resulting in open vesicles observed by cryo-TEM.
Both the high biocompatibility and the potential release mechanism, suggest potential applicability of *N*-phosphoamino acids as drug delivery systems. Therefore, in **chapter VII** we employed these amphiphiles for further modification to demonstrate their facile modulation for their potential optimization as drug delivery systems. First, we established two synthetic strategies giving access to a broad variety of derivatives in only two synthetic steps using *N*-phosphoamino acids or their precursor, i.e. *N*-didodecyl phosphoryl chloride, as starting materials. On the one hand, using the latter hydrophobic compound two amphiphiles and their corresponding methyl esters were obtained exhibiting an azobenzene moiety at the head group. On the other hand, employing *N*-phosphoamino acids as starting material, three amphiphiles and their corresponding methyl esters were successfully synthesized with a dipeptide head group. Employing toxicity studies it was demonstrated that all obtained *N*-phosphoamide derivatives exhibit very good biocompability with IC_{50} up to 100 μM. Furthermore, using cryo-TEM we revealed that *N*-phosphoamides with a dipeptide head group can form a broad variety of aggregates, i.e. vesicle, twisted ribbons, open and end-capped tubes. In contrast to the *N*-phosphoamino acids exhibiting one amino acid at the head group (**Chapter VI**), neither decomposition nor formation of open vesicles was observed for amphiphiles with a dipeptide head group. Hence, we can conclude that a simple modification at the free acid group of *N*-phosphoamino acids leads to higher stability of liposomes formed by these amphiphiles. Finally, the *N*-phosphoamides exhibiting an azobenzene moiety were tested for their ability to act as molecular switches. We demonstrated that all synthesized azobenzene derivatives can undergo a thermal and photo-induced reversible *cis*-*trans* isomerization and the half-life time of their *cis*-isomers was determined ranging from 21 min to 88 min. Moreover, it was shown that several photo-induced isomerization cycles can be performed without decomposition of the synthesized molecular switches.

8.2 Samenvatting

Amfifiele moleculen, vetzuren, zijn de standaard bouwstenen van elk levend organisme. Een grote verscheidenheid in structuren wordt in de natuur gevonden, waardoor het organisme in extreme omstandigheden kan overleven. Daarbij kunnen specifieke modificaties het leven niet alleen mogelijk maken onder grote verschillen in temperatuur en druk, maar ook in toxische media. Om ervoor te zorgen dat de gelimiteerde beschikbaarheid van deze moleculen overwonnen wordt en om de van nature bestaande vetzuren te begrijpen, te bestuderen en te imiteren, is de organische synthese een onvervangbaar middel. In dit proefschrift wordt met behulp van verschillende strategieën getracht om vetzuren te synthetiseren die cycloalkanen bevatten en om een nieuw systeem van lipides te bestuderen die alleen bouwstenen bevat die van nature voorkomen.

Het eerste gedeelte van mijn proefschrift bevat verschillende synthese-strategieën om onnatuurlijke en natuurlijke vetzuren te verkrijgen die cycloalkaan-groepen bevatten, zoals ladderaan-eenheden **(Hoofdstuk II** en **III**) of een trans-cyclopropaan ring (**Hoofdstuk IV**).
In **hoofdstuk II** worden inter- en intramoleculaire [2+2] fotochemische cycloaddities toegepast als strategie om moleculaire structuren te verkrijgen die gefuseerde cyclobutaanringen bevatten, ook bekend als ladderanen. Eerst werd voor de intramoleculaire fotoreactie als startmateriaal cyclobuteen gesynthetiseerd in drie stappen met een totale opbrengst van 41%. In de volgende stap van deze studie werden verschillende cycloalkanen toegepast in de fotokatalytische intermoleculaire reactie met cyclopentenon om een molecuul te vormen met drie gefuseerde cycloalkaanringen. De verhouding tussen de beide alkenen bleek cruciaal te zijn om deze fotoreactie goed te laten verlopen. Het gebruik van de verhouding van alkeen en alkenone van 2 staat tot 1, resulteerde in opbrengsten van 54% en 62%. Ook werd door middel van Röntgen-kristallografie aangetoond dat beide fotochemische producten drie gefuseerde cycloalkaan ringen bevatten met een exo-configuratie nadat ze omgezet waren in de overeenkomstige hydrazonen **1** en **2** (Figuur 8.1).

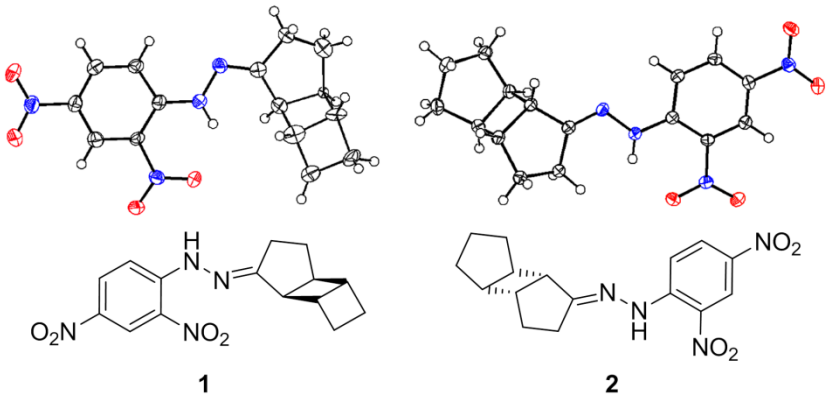

Figuur 8.1: Chemische structuren van producten **1** en **2** van de fotoreacties en de bijbehorende Röntgen structuren.

In het tweede gedeelte van **hoofdstuk II** hebben we de mogelijkheid voor het toepassen van de intramoleculaire cycloadditie van een herbruikbare spacer onderzocht om in slechts één synthetische stap ladderaan-eenheden te verkrijgen met drie gefuseerde cyclobutaan ringen. Met dit als doel werd een startmateriaal gesynthetiseerd met twee alkeen-eenheden en een spacer. De spacer, i. e. een pseudo-geminaal gesubstitueerd paracyclofaan, werd gesynthetiseerd in negen stappen met een totale opbrengst van 50%. De alkeen-eenheid die twee geconjugeerde trans-dubbelen bindingen bevat, i. e. 5-fenylpenta-2,4-dieonyl chloride, werd in twee stappen gesynthetiseerd en gekoppeld aan de moleculaire spacer in een amideringsreactie wat het startmateriaal opleverde voor een intramoleculaire cycloadditiereactie. De eerste pogingen om de spacer-alkeen constructies te gebruiken voor de fotochemische reactie resulteerde hoogst waarschijnlijk in de vorming van cyclooctadieen-eenheden in plaats van de gewenste ladderaan-eenheden met drie gefuseerde cyclobutaanringen. Desalniettemin suggereerden deze resultaten dat deze strategie toepasbaar

is voor intramoleculaire cycloaddities en verder optimalisatie voor intramoleculaire cycloaddities en van de reactiecondities zou kunnen leiden tot de gewenste ladderanen met drie gefuseerde cyclobtuaanringen.
Aan de hand van de studies van inter-en intramoleculaire cycloaddities in **hoofdstuk II** werden beide fotoproducten, die verkregen werden in de intermoleculaire fotoreacties, succesvol toegepast in **hoofstuk III** als startmateriaal voor de synthese van vetzuren die ladderaan-eenheden bevatten. Twee amfifiele laderaanmoleculen met drie gefuseerde cycloalkaanringen werden succesvol gesynthetiseerd in zeven stappen met een totale opbrengst tot 14.5%. Essentieel voor het succes was de optimalisatie van twee belangrijke stappen, i. e. de formyleringsreactie en de Wittig-reactie. Het gegeven dat ladderaan-eenheden bacterieen helpen overleven in een omgeving van hoge temperaturen en een groot scala aan pH-waarden, zal van pas komen voor toekomstige studies van beide verkregen ladderaanvetzuren waarin kunstmatige membranen gebruikt worden. Terwijl in **hoofdstuk III** werd geconcentreerd op het beschrijven van de synthese van vetzuren met gefuseerde cycloalkaan ringen, wordt in **hoofstuk IV** de succesvolle synthese van het natuurproduct majusculoic acid 3 (Figuur 8.2) beschreven, wat een cyclopropaan-eenheid bevat. Twee totaalsynthese-strategieën werden geïdentificeerd met behulp van cross-metathese en een Wittig reactie als voornaamste synthetische stappen. Benadrukt moet worden dat majusculoic acid verschillende synthetisch uitdagende moleculaire eenheden bevat, die geavanceerde diastereo- en enantioselectieve chemie vereisen. Voorbeelden hiervan zijn de introducties van de *trans*-cyclkopropaan ring en de selectieve E- en Z-olefine groepen. Deze exceptionele structurele kenmerken werden succesvol geïncorporeerd door het gebruik van asymmetrische katalyse, cross metathese, een Wittig reactie en isomerisatie van dubbele bindingen naar de stabielere isomeren. Daarbij werd het door deze synthese voor het eerst mogelijk om de absolute configuratie (*R*,*R*) van de *trans*-cyclopropyl groep in het natuurproduct te bepalen.

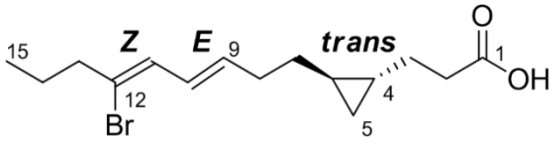

3

Figure 8.2. Chemische structuren van het gesynthetiseerde natuurproduct majusculoic acid **3**.

Met het verkrijgen van majusculoic acid en met de evaluatie van de totaalsynthese is het nu mogelijk om met toekomstige biologische studies de rol en de functie van dit product te bestuderen. Benadrukt moet worden dat het van belang is om deze verder studies naar majusculoic acid uit te voeren, vanwege de antimyotische activiteit tegen *Candida*-soorten. Biologische testen werden tot nu toe beperkt door de gelimiteerde beschikbaarheid van majusculoic acid.
In het tweede gedeelte van dit proefschrift wordt de synthese van een nieuwe klasse van amfifielen, de *N*-fosfo aminozuren **4** (Figuur 8.3), en hun toepassing om artificiële membranen te creëren voor potentiële drug delivery systems behandeld. In **hoofstuk V** worden *N*-fosfo aminozuren geïntroduceerd als een nieuwe klasse van amfifielen bestaande uit natuurlijk bouwstenen, i. e. aminozuren, alifatische alcoholen en fosfonaten (Figuur 8.3). Daarvoor werd

een efficiënte en snelle synthese samengesteld die resulteerde in 18 nieuwe amfifiele fosfo amidaten in slechts drie synthetische stappen en geïsoleerde opbrengsten tot 70%. Ook werden de fysieke eigenschappen van *N*-fosfo aminozuren bestudeerd met behulp van nucleaire resonantie spectroscopie, dynamische differentiecalorimetrie en de bepaling van de pK_a-waarden. Daarbij werd cryo-TEM gebruikt om het aggregatiegedrag van deze amfifiele moleculen te bestuderen. Er werd vastgesteld dat *N*-fosfo aminozuren een breed scala aan assemblages kan vormen, zoals micellen, vesikels, lamellen en linten. Aangetoond werd dat de vorm van het aggregaat afhankelijk is van het formaat en de lading van het aminozuur aan het hoofd van het amfifiel. Gedurende het onderzoek hebben we succesvol de relatie tussen lading, formaat en afscherming van het residu van het aminozuur vastgesteld voor de aggregatie van *N*-fosfo aminozuren.

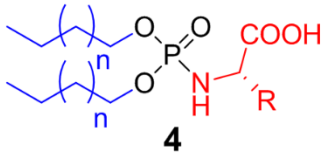

4

Figuur 8.3. Chemische structuren van amfifiele *N*-fosfo aminozuren 4. Kleurcode: aminozuren (rood), alifatisch alcohol (blauw) en fosforzuur (zwart).

In de volgende stap werd de potentiële toepasbaarheid van *N*-fosfo aminozuren als drug delivery system bestudeerd (**Hoofdstuk VI**). Als eerste werd hoge biocompatibiliteit aangetoond voor deze nieuw ontwikkelde amfifielen met gebruik van MTT (3-(4,5-di**m**ethyl**t**hiazol-2-yl)-2,5-difenyl**t**etrazolium bromide) assays. Dit experiment liet hoge levensvatbaarheid van *HeLa* cellen zien in de aanwezigheid van N-fosfo aminozuren die alifatische aromatische en negatief geladen gedeelten bevatten in de kopgroep van het aminozuur. Benadrukt moet worden dat alle geteste amfifielen hoge biocompatibiliteit hebben en dat alle cellen levensvatbaar waren terwijl concentraties tot 100 µM gebruikt werden. De lage toxiciteit van deze stof kan verklaard worden door het feit dat *N*-fosfo aminozuren alleen bouwstenen bevatten die van nature voorkomen, i. e. een aminozuur, een fosfaat en een alifatisch alcohol. Ook werden verschillende potentiële mechanismen van geneesmiddelafgifte voor *N*-fosfo aminozuren gedemonstreerd. De eerste strategie is gebaseerd op de protonering van de negatief geladen kopgroep van het amfifiel welke resulteert in het verlies van het amfifiele karakter en de vrijgave van het liposoom onder zure condities. Dit gedrag suggereert een snelle drug release tijdens endocytose. Een interessanter mechanisme van geneesmiddelafgifte werd geobserveerd voor *N*-fosfo aminozuren die kleine aminozuren bevatten, i. e. glycine, alanine en beta-alanine, als kopgroep. Met cryto-TEM en NMR studies kon worden aangetoond dat deze *N*-fosfo aminozuren degraderen door zelfactiverende afsplitsing van één amfifiele staart, waardoor mono-*N*-fosfo aminozuren gevormd werden die geobserveerd werden met cryo-TEM als open vesikels.
Zowel de hoge biocompatibiliteit als het potentiële mechanisme van geneesmiddelafgifte suggereren de potentiële toepasbaarheid van deze *N*-fosfo aminozuren als drug delivery systems. Derhalve werden deze amfifielen in **hoofdstuk VII** verder gemodificeerd om de gemakkelijke modulatie voor potentiële optimalisatie als drug delivery systems te demonstreren. Eerst werden twee synthetische strategieën samen gesteld om toegang te geven

tot een grote verscheidenheid aan afgeleiden in slechts twee synthetische stappen door *N*-fosfo aminozuren of door hun precursor, i. e. *N*-didodecyl fosforyl chloride, als startmateriaal te gebruiken. Met behulp van het laatst genoemde hydrofobe materiaal werden twee amfifielen en hun corresponderende methyl esters verkregen die een azobenzeen-eenheid bevatten in de kopgroep. Met behulp van de *N*-fosfo aminozuren als startmateriaal werden drie amfifielen en hun corresponderende methyl esters op een succesvolle manier gesynthetiseerd met een dipeptide kopgroep. Toxiciteitsstudies demonstreerden dat alle verkregen *N*-fosfo amide derivaten zeer goede biocompatibiliteit vertoonden met IC_{50} waarden tot 100 μM. Met behulp van cryo-TEM werd duidelijk dat *N*-fosfo amidaten met een dipeptide kopgroep een grote verscheidenheid aan aggregaten kunnen vormen, i. e. vesikels, gedraaide linten, open en gesloten buisjes. In tegenstelling tot de *N*-fosfo aminozuren die een aminozuur in de kopgroep bevatten (**Hoofdstuk VI**), werd voor amfifielen met een dipeptide kopgroep geen decompositie of vorming van open vesikels geobserveerd. Hierdoor kunnen we concluderen dat een simpele modificatie aan de vrije zuurgroep van *N*-fosfo aminozuren leidt tot hogere stabiliteit van liposomen die gevormd worden door deze amfifielen. Als laatste werden de *N*-fosfo amides die een azobenzeen eenheid bevatten getest op hun potentie om te functioneren als moleculaire schakelaars. We hebben aangetoond dat alle gesynthetiseerde azobenzeen derivaten een thermische en fotogeïnduceerde *cis-trans* isomerisatie kunnen ondergaan met een halfwaardetijd tussen de 21 en 88 min. Ook werd aangetoond dat een aantal fotogeïnduceerde isomerisatie-cycli uitgevoerd konden worden zonder dat decompositie van de gesynthetiseerde moleculaire schakelaars plaatsvond.

8.3 Zusammenfassung

Amphiphile Moleküle, wie z.B. Fettsäuren, sind Grundbausteine jedes lebenden Organismus. In der Natur wird eine große strukturelle Vielfalt von Fettsäuren beobachtet, die das Überleben der Organismen unter extremen Bedingungen möglich machen. Dabei wird in der Natur durch gezielte Modifizierung dieser Säuren nicht nur das Leben bei hohen Temperatur- und Druckunterschieden, sondern auch in giftigem Umfeld ermöglicht. Die organische Synthese ist aufgrund des begrenzten Vorkommens dieser Moleküle sowie um die Funktion dieser natürlich vorkommenden Moleküle zu verstehen und zu imitieren ein unerlässliches Werkzeug. In dieser Doktorarbeit werden unterschiedliche Methoden angewendet um Fettsäuren, die Cycloalkane als Bausteine beinhalten, zugänglich zu machen. Weiterhin wird eine neue Klasse an nur aus natürlichen Bausteinen bestehenden Lipiden synthetisiert und untersucht.
Der erste Teil meiner Arbeit befasst sich mit unterschiedlichen synthetischen Strategien zur Synthese von natürlichen sowie unnatürlichen Fettsäuren, die Cycloalkane, wie Cyclobutan (**Kapitel II** und **III**) oder *trans*-Cyclopropan (**Kapitel IV**) beinhalten.
Um Strukturen mit linear verbundenen Cyclobutyleinheiten, auch als Ladderan bezeichnet, zu erhalten, wurden in **Kapitel II** inter- und intramolekulare photochemische [2+2] Cycloadditionen angewendet. Zunächst wurde hierfür das Startmaterial der intermolekularen

Photoreaktion, ein Cyclobuten, in drei Stufen mit einer gesamt Ausbeute von 41% hergestellt. Weiterhin wurde eine Vielfalt an käuflichen Cycloalkenen für diese photokatalysierte Reaktion mit Cyclopentenon verwendet, so dass Strukturen mit drei fusionierten Cycloalkanen erhalten wurden. Dabei wurde festgestellt, dass das Verhältnis beider Startmaterialien zu einander einen großen Einfluss auf die Produktbildung nimmt. Die Anwendung eines zwei zu eins Verhältnisses von Alkan zu Alkenon ergab eine Ausbeute zwischen 54% und 62%. Weiterhin wurden zwei durch die Photoreaktion erhaltene Produkte zu den korrespondierenden Hydrazonen **1** und **2** (Figur 8.1) umgesetzt. Diese fanden wiederum Anwendung in Kristallographiestudien um die *exo*-Konfiguration der drei fusionierten Cycloalkane nach zu weisen.

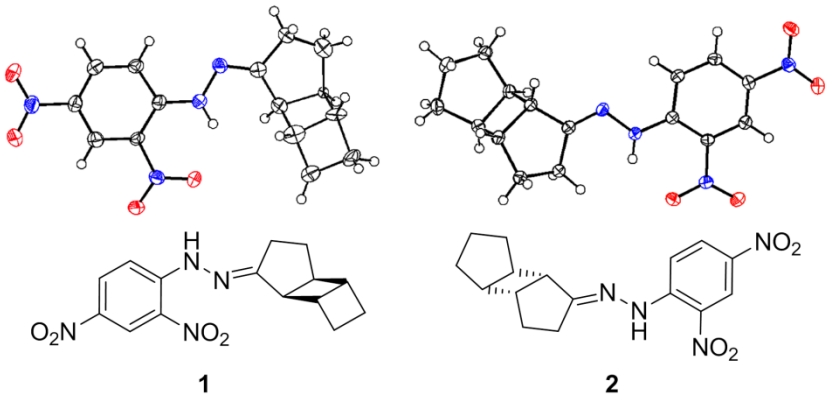

Figur 8.1: Chemische Strukturen der Photoprodukte **1** und **2** sowie die korrespondierenden X-Ray-Strukturen.

In der zweiten Hälfte des **Kapitels II** wurde die Anwendung von intramolekularen Cycloadditionen unter Verwendung eines wiederverwendbaren Linkers untersucht. Ziel dieser Methode war es Moleküle mit drei fusionierten Cyclobutanen durch nur eine synthetische Stufe zu erhalten. Zu diesem Zweck wurde das Startmaterial, das zwei Alkeneinheiten, die durch einen Linker verbunden sind, trägt, hergestellt. Der Linker, ein pseudo-geminal substituierter Paracyclophan, konnte in neun Stufen mit einer Gesamtausbeute von 50% hergestellt werden. Weiterhin wurde die Alkeneinheit, 5-Phenylpenta-2,4-dienoyl Chlorid, die zwei konjugierte *trans*-Doppelbindungen beinhaltet, in zwei Stufen synthetisiert. Zwei Äquivalente dieses Alkens wurden dann in einer Amidierungsreaktion an den Linker gebunden und ergaben das erwünschte Startmaterial der Photoreaktion. Erste Versuche, dieses Molekül in einer intramolekularen Photoreaktion anzuwenden resultierten in der Synthese eines Nebenproduktes, das vermutlich eine Cyclooktadieneinheit anstelle der drei Cyclobuane besaß. Aus dieser Beobachtung lässt sich schließen, dass diese Strategie unter den richtigen Reaktionsbedingungen Anwendung finden kann, um Ladderaneinheiten schnell zugänglich zu machen.
Nachdem im **Kapitel II** die Anwendung der inter- und intramolekularen Photoreaktion gezeigt wurde, wurden zwei der erhaltenen Produkte in **Kapitel III** als Startmaterial für die Synthese von Fettsäuren, die jeweils drei linear fusionierte Cycloalkaneinheit (Ladderaneinheit) tragen,

eingesetzt. Dabei wurden, in einer neunstufigen Synthese, mit einer Gesamtausbeute von bis zu 15%, zwei Fettsäuren, die jeweils eine Ladderaneinheit tragen, erfolgreich synthetisiert. Die Optimierung zweier Schlüsselreaktionen, einer Formylierungs- und einer Wittig-Reaktion, war dabei von großer Bedeutung. Aufgrund der Tatsache, dass natürlich vorkommende, Ladderan tragende Fettsäuren Bakterien das Leben unter hohen Temperaturen und in einem breiten pH-Spektrum ermöglichen, ist es von großem Interesse, weitere Studien unter Verwendung von künstlichen Membranen, die die synthetisierten Fettsäuren beinhalten, durchzuführen.
Während im **Kapitel III** der Schwerpunkt auf der Synthese von Fettsäuren, die Ladderaneinheiten tragen, lag, wurde in **Kapitel IV** die Synthese von einer natürlich vorkommenden, Cyclopropan beinhaltenden Fettsäure, der Majusculoicsäure **3**, berichtet. Hierfür wurden zwei synthetische Strategien unter Verwendung von Cross-Metathese- und *Wittig*-Reaktion als Schlüsselreaktionen verfolgt. An dieser Stelle ist es erwähnenswert, dass die Majusculoicsäure aus synthetischer Sicht mehrere herausfordernde Strukturbausteine besitzt, die die Anwendung von diasterio- und enantioselektiver Synthese benötigten. Unter anderem mussten ein *trans*-Cyclopropanring und eine E- sowie eine Z-Doppelbindung selektiv eingebaut werden. Diese außergewöhnlichen strukturellen Funktionen wurden in das Molekül unter Verwendung von asymmetrischer Katalyse, Cross-Metathese, *Wittig*-Reaktion und einer Doppelbindungs-Isomerisierung erfolgreich eingebaut. Außerdem erlaubte die Synthese zum ersten Mal die Bestimmung der absoluten Konfiguration (*R,R*) des *trans*-Cyclopropanrings der Majusculoicsäure.

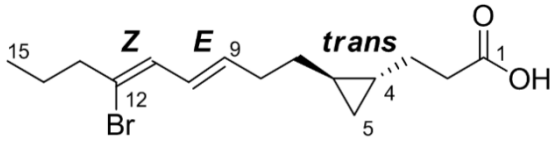

3

Figur 8.2: Chemische Struktur der Majusculoicsäure **3**.

Nachdem die Synthese der Majusculoicsäure erfolgreich etabliert wurde und dieser Naturstoff somit für biologische Studien zugänglich ist, ist es von Großem Interesses dessen Funktion und Wirkungsweise zu verstehen. Dabei sollte erwähnt werden, dass frühere Studien bereits antifungale Aktivität der Säure gegen *Candida*-Gattungen gezeigt haben. Jedoch waren aufgrund der limitierten Erhältlichkeit der natürlichen Säure weitere biologische Studien eingeschränkt.
Der zweite Teil meiner Arbeit befasst sich mit der Synthese einer neuartigen Klasse an Amphiphilen, den *N*-Phosphoaminosäuren **4** (Figur 8.3), und deren Anwendungsmöglichkeiten im Bereich künstlicher Membranen und Medikamenten-transportsysteme. Zu diesem Zweck wurden in **Kapitel V** die *N*-Phosphoaminosäuren, die nur aus natürlich vorkommenden Bausteinen, wie Aminosäuren, aliphatischen Alkoholen und Phosphaten (Figur 8.3) bestehen, vorgestellt. Weiterhin wurde eine effiziente Synthese für *N*-Phosphoaminosäuren, die aus nur drei synthetischen Stufen besteht, berichtet und angewendet, dies ermöglichte in kurzer Zeit die Synthese von 18 unterschiedlichen amphiphilen Phosphoamiden und Gesamtausbeuten von bis zu 70%. In den folgenden Studien wurden die Eigenschaften der *N*-Phosphoaminosäuren durch Kernspinresonanzspektroskopie und dynamische Differenzkalorimetrie bestimmt sowie die

Bestimmung der pK_s-Werte durchgeführt. Außerdem wurden mit Hilfe von cryo-TEM Untersuchungen die durch diese Amphiphile geformten Aggregate studiert. Dabei wurde gezeigt, dass *N*-Phosphoaminosäuren eine Vielfalt an Aggregaten, wie Mizellen, Vesikel, Doppelmembranschichten und Bänder formen können. Weiterhin wurde ein direkter Zusammenhang zwischen der als Kopfgruppe des Amphiphiles verwendeten Aminosäure und den jeweils geformten Aggregaten beobachtet. Dabei spielten die Ladung und Größe des Aminosäurerestes sowie abschirmende Effekte durch diese Reste eine große Rolle.

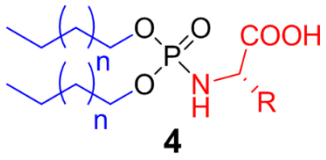

4

Figur 8.3: Chemische Struktur der amphiphilen *N*-Phosphoaminosäure **4**. Farbkod: Aminosäure (rot), aliphatische Alkohole (blau) und Phosphorsäure (schwarz).

In dem darauf folgenden Teil der Arbeit (**Kapitel VI**) wurde die potenzielle Anwendungsmöglichkeit für *N*-Phosphoaminosäuren als Medikamententransportsysteme untersucht. Hierfür wurde die biologische Verträglichkeit dieser neuen Amphiphile unter Anwendung eines MTT-Assays (3-(4,5-Di**m**ethyl**t**hiazol-2-yl)-2,5-diphenyl**t**etrazolium-bromid) getestet. Die für diesen Assay verwendeten *HeLa*-Zellen wiesen eine hohe Überlebensrate in der Gegenwart der *N*-Phosphoaminosäuren, die repräsentativ einen aliphatischen, aromatischen oder negativ geladenen Rest an der Kopfgruppe trugen, auf. Alle getesteten Komponenten zeigten dabei niedrige Toxizität und hohe Biokompatibilität bei Konzentrationen von bis zu 100 µM. Diese niedrige Toxizität war zu erwarten, da alle *N*-Phosphoaminosäuren ausschließlich aus natürlichen Bausteinen, wie Aminosäuren, aliphatischen Alkoholen und Phosphaten, bestehen. Anschließend wurden Untersuchungen durchgeführt, die potenzielle Medikamentenfreisetzungsmechanismen für *N*-Phosphoamino-säuren offenbarten. Dabei handelte es sich bei der ersten Strategie um einen Portionierungsmechanismus, bei dem durch Portionierung der Kopfgruppe der amphiphile Charakter der *N*-Phosphoaminosäure verloren ging und eine Freisetzung des Medikaments in saurem Medium zu beobachten war. Diese Eigenschaft lässt eine Medikamentenfreisetzung während der Endocytose vermuten. Ein weiterer potenzieller Freisetzungsmechanismus wurde für die *N*-Phosphoaminosäuren mit kleinen Aminosäuren, wie Glycin, Alanin und beta-Alanin, als Kopfgruppe beobachtet. Unter Anwendung von cryo-TEM und NMR-Studien konnte gezeigt werden, dass diese Amphiphile durch eine selbstaktivierte Abspaltung einer aliphatischen Kette zu *N*-Phosphoaminosäuren mit nur einer Kette zersetzt wurden und eine Öffnung der Vesikel beobachtet werden konnte.
Sowohl die hohe Biokompatibilität als auch die möglichen Freisetzungsmechanismen legen nahe, das *N*-Phosphoaminosäuren hohes Potenzial im Bereich der Medikamenten-transportsysteme haben. Deshalb wurden in **Kapitel VII** diese Komponenten weiteren Modifikationen unterzogen, um einfache Wege zur Optimierung dieser *N*-Phosphoaminosäuren zu demonstrieren. Zunächst wurden zwei Strategien etabliert, die ausgehend von den im **Kapitel V** synthetisierten *N*-Phosphoaminosäuren bzw. deren Vorstufe, *N*-

Didodecylphosphorylchlorid, und unter Verwendung von zwei einfachen synthetischen Stufen, einen schnellen Zugang zu einer Bandbreite an Derivaten ermöglichten. Einerseits wurden unter Verwendung der *N*-Didodecylphosphorylchlorid zwei neue Amphiphile, die eine Azobenzengruppe als Kopfgruppe tragen, sowie deren korrespondierende Methylester hergestellt. Andererseits wurden unter Verwendung der *N*-Phosphoaminosäuren als Startmaterial drei neue Amphiphile, die ein Dipeptid als Kopfgruppe tragen, sowie deren korrespondierende Methylester erfolgreich hergestellt. Ebenfalls hatten toxizitäts Studien für diese Moleküle eine hohe Biokompatibilität mit IC_{50}-Werten bis zu 100 μM gezeigt. Außerdem wurde durch Verwendung von cryo-TEM gezeigt, dass die Dipeptid tragenden Derivate eine Vielzahl an Aggregaten, wie unter anderem Vesikel, gewundene Bänder, offene und verschlossene Röhren, formen können. Jedoch wurde im Gegensatz zu den *N*-Phosphoaminosäuren, die nur eine Aminosäure als Kopfgruppe (**Kapitel VI**) aufweisen, keine Zersetzung oder Öffnung der Vesikel beobachtet. Somit können wir schlussfolgern, dass eine einfache Modifizierung an der Säuregruppe der *N*-Phosphoaminosäuren zu höherer Stabilität der resultierenden Liposome führen kann. Schließlich wurden die *N*-Phosphoaminosäuren, die eine Azobenzengruppe als Kopfgruppe aufweisen, nach ihrem Vermögen untersucht als molekulare Schalter zu dienen. Dabei wurde gezeigt, dass alle synthetisierten Azobenzen Derivate eine thermisch- sowie photoinduzierte, umkehrbare *cis-trans* Isomerisierung eingehen können und eine Halbwertszeit von 21 bis zu 88 Minuten für das *cis*-Isomer aufweisen. Auch wurde gezeigt, dass mehrere photoinduzierte Isomerisierungszyklen durchgeführt werden können, ohne dass eine Zersetzung des synthetisierten molekularen Schalters zu beobachten war.

Acknowledgments

• Dankzegging •Danksagung

The years I have spent in Groningen have been an irreplaceable experience. I enjoyed not only working in an international environment but also living in one of the nicest cities in the Netherlands. During the last years I have had the opportunity to meet people from all over the world and I am happy that I am able to call many of them friends.

At first, I would like to express my gratitude to my supervisor Prof. Dr. Ben Feringa. Thanks for giving me the opportunity to accomplish my Ph.D. studies in your group. In this regard, I am especially thankful for your encouragement and trust, which helped me to overcome the initial challenges and to finish my studies. During the time in your group at the University of Groningen I gained knowledge, which will be undoubtable helpful during my further scientific career. Besides the professional working environment I was impressed and thankful for your time and suggestions considering private difficulties. Thanks, for all your support and advice!
Furthermore, I would like to thank my co-supervisor Prof. Dr. Adri Minnaard. Your help especially during the first two years of my studies was irreplaceable. I enjoyed working with you and I appreciated to be seen as a member of your group.
Also I like to thank Dr. Anna Hirsch, who has always time and an open door for everyone. Anna I have to thank you for correction of my posters and presentations, and also for listening and giving me advice.
Furthermore, I would like to express my gratitude to Prof. Dr. Sijbren Otto, Prof. Dr. Bert Poolman and Prof. Dr Ernst J. R. Sudhölter, who were part of the reading committee, for reading, correcting and approving the manuscript. I thank you for all your useful comments, which improved my thesis.
For the organization, time and support I would like to thank at this point my paranymphs Dr. Wiktor Szymanski and Dr. Andreas Bastian. Also I like to thank in this regard Claudia Poloni for her support and Anja Huizing for her help with the Dutch summery.

For performing mass analysis and helping with the GC-MS I would like to thank Theodora Tiemersma-Wegman and Monique Smith. Pieter van der Meulen and Wim Kruizinga I like to thank for helping me out during several NMR measurements. Also, my thanks goes to Ebe Schudde for technical support and for helping me with the setup for the photoreactions. For the quick X-Ray analysis I like to thank Auke Meetsma. Finally, I like to thank Wim Velema for

performing MTT-assays, Petra Erne and Marc Stuart for the large quantity of taken cryo-TEM images at the end of my Ph.D. studies. Marc I also like to thank you for all your suggestions and the time you spent correcting my thesis.

Of course, I like to express my thanks to all my colleagues and frinds from the Feringa, Minnaard, Hirsch, Otto, Roelfes, Browne, Harutyunyan and Herrmann groups. Thereby, I like to mention especially all my lab mates of the 'Vyscom lab' (Johannes, Ashoka, Manuel, Felix, Peter F., Thomas J., Cati, Dorus, Simon, Miro), in which I was working the first half of my studies. I will never forget the highly challenging 'lab Olympics'. Furthermore, I like to thank the bioorganic lab, which I joined for the second half of my studies. Wiktor, Wim, Derk Jan, Yange, Claudia, Anja, Anniek and Mickel thanks for the great working atmosphere. Also, I express my gratitude to all members of the asymmetric subgroup for the suggestions and discussions.

Furthermore, I would like to thank Hilda Biemold and Tineke Kalter-Meuken, who are daily performing important work in the background and keep everything going. At this point I like especially to thank Tineke for her help and support during organizing of my defense.

It is also important to me to mention colleagues, neighbors and people, who become friends during the time in Groningen and who made me enjoying the time: Miriam, Salomeh, Esther, Alberto, Matea, Krzysztof, Agnieszka M., Deepak V., Agnieszka G., Jan Willem, René, Jan K., Diego, Stefano and Pavlo. I will especially miss the live music and the BBQs with all of you.
Last but not least, I like to express my thanks to all the family members and friends from Germany who supported me before and during my Ph.D. studies:
Andreas, ohne dich hätte ich diesen wichtigen Schritt in meinem Leben vermutlich nicht angetreten. Ich möchte dir dafür danken, dass du immer an meiner Seite bist und ich mich immer auf dich und deine Hilfe verlassen kann. Dein Verständnis, deine Geduld, dein Zuspruch und vor allem deine Liebe haben mich die letzten Jahre begleitet und sind wie du selbst ein unersetzlicher Teil meines Lebens geworden. Danke, für alles! Ich liebe dich!
Meinen Eltern und meiner Schwester möchte ich danken für die grenzenlose Unterstützung, das Vertrauen und die Liebe, die sie mir entgegen bringen. Insbesondere möchte ich meiner Mutter für ihre selbstlose Liebe danken, die nicht nur mein Leben, sondern auch das von Andreas und meinen Großeltern bereichert. Weiterhin, möchte ich Barbara und Richard meinen Dank aussprechen. Man kann sich keine besseren Schwiegereltern wünschen. Danke, dass ihr mich mit offenen Armen aufgenommen habt und mir das Gefühl gebt ein Teil der Familie zu sein. Auch Christoph und Sylwia möchte ich meinen Dank aussprechen. Es ist nicht selbstverständlich ein Teil einer so großartigen Familie zu sein. Viele schöne und unersetzliche Erinnerungen sind an euch und eure wundervollen Kinder, Dennis und Leon, gebunden. Euch allen danke ich, dass ihr die schönen sowie die schweren Momente des Lebens mit mir und Andreas teilt. Ohne eure regelmäßigen Besuche in Holland hätte etwas Wichtiges gefehlt.